DRH 0423-5

MLM-3540

Light-Weight Radioisotope Heater Unit Final Safety Analysis Report (LWRHU-FSAR)

Volume II: Accident Model Document (AMD)

Ernest W. Johnson

October 1988

MOUND

operated by
EG&G MOUND APPLIED TECHNOLOGIES
P.O. Box 3000, Miamisburg, Ohio 45343-0987

for the
U. S. DEPARTMENT OF ENERGY
Contract No. DE-AC04-88DP43495

DISCLAIMER

MLM--3540-Vol.2

DE89 005495

Light-Weight Radioisotope Heater Unit Final Safety Analysis Report (LWRHU-FSAR)

Volume II: Accident Model Document (AMD)

Ernest W. Johnson

October 1988

MOUND

operated by

EG&G MOUND APPLIED TECHNOLOGIES

P.O. Box 3000, Miamisburg, Ohio 45343-0987

for the

U. S. DEPARTMENT OF ENERGY

Contract No. DE-AC04-88DP43495

TABLE OF CONTENTS

TABLE OF FIGURES

TABLE OF FIGURES (Continued)

LIST OF TABLES

VOLUME II

ACCIDENT MODEL DOCUMENT

1.0 INTRODUCTION

The purposes of this volume of the LWRHU SAR, the Accident Model Document (AMD), are to:

A. identify all malfunctions, both singular and multiple, which can occur during the complete mission profile that could lead to release outside the clad of the radioisotopic material contained therein;

B. provide estimates of occurrence probabilities associated with these various accidents;

C. evaluate the response of the LWRHU (or its components) to the resultant accident environments; and

D. associate the potential event history with test data or analysis to determine the potential interaction of the released radionuclides with the biosphere.

The organization of this AMD follows the format developed in a January 23-24, 1985, meeting at Valley Forge, Pennsylvania (Reference 1). This structure is given in Table II-1.

There have been data supplied from a variety of sources which are used in the formulation of this document. Sources are identified in the specific locations, including appendixes and in the bibliography, and are summarized below:

A. Los Alamos National Laboratory (LANL) - In addition to being the design and fueling/assembly agency, LANL performed the bulk of the environmental safety tests on LWRHU hardware (including helium release);

B. Applied Physics Laboratory - (APL) - This organization was responsible for the analyses of the various situations which must be addressed during reentry events: thermal stress, ablation, peak clad temperature, etc.;

C. General Electric Company (GE) - They are the prime contractor for the radioisotope thermoelectric generator (RTG), including the FSAR for that system, and their methodology for the LWRHU SAR was extensively used, particularly the failure/abort sequence trees (FASTs) and many interpretations of the shuttle details during specific events;

TABLE II-1

VOLUME II: ACCIDENT MODEL DOCUMENT (AMD) FORMAT

1.0 Introduction

Purpose of AMD
Document Organization
Data Acknowledgments

1.1 Mission and Systems Description

- Mission Phases with Timeliness/Events
- LWRHU Design

2.0 Summary of Accident Evaluation

Flowchart
Centaur Domination of Accident Environments Described
Tabulation of Accidents/Consequences by Phase

3.0 Accident Evaluation and Failure Mode Analysis

3.1 Objectives and Approach Sequence Tree Construction
3.2 Mission Accident Evaluation

- Each Phase Addressed Separately
- Each Accident in Each Phase Treated Separately in Entirety

3.2.1 Phase 0-Prelaunch

- Top-Level Event Tree Showing Accidents with Probabilities
- Accidents Defined and Characterized from Initiation to Identification of Source Terms Where Applicable

  - Accident Description
  - Accident Environment Definition
  - Initial LWRHU Response to Explosions
  - Synergistic Effects of Environments
  - Intermediate Events Identified
  - Final Disposition of LWRHU
  - Source Term Characterized

TABLE II-1 (Continued)

All Inputs Positively Identified and Referenced to Appendixes
Minimal Analysis and/or Testing to be Shown or Discussed
- Results to be Presented
- Reference to Details in Appendixes

Repetitious Material Will be Included Where Applicable for Each Accident for Purposes of Completeness and Ease of Readibility and Understanding

o Complete Phase Event Tree

- Presented After All Accidents Are Defined and Characterized

- Accidents and Events Identified by Designators Referenced in Each Accident Evaluation

3.2.2 Phase I - Above Sequence and Content Repeated for Each Subsequent Phase

APPENDIXES: Include all test and analytical data used (and its justification) for all accidents, environments, and LWRHU response modes addressed in the accident evaluations.

A. Accident Definition
B. Accident Environments
C. LWRHU Response to Explosions
D. LWRHU Response to Fragments/Projectiles
E. LWRHU Response to Propellant Fires
F. Spacecraft Reentry Breakup Analysis
G. LWRHU Reentry Response
H. Impact Test Program Results
I. Burial Thermal Analysis
J. Source Term Evaluation

D. Johnson Space Center (JSC) - This NASA office was responsible for providing the shuttle and payload descriptions plus defining the accident environments and probabilities;

E. Jet Propulsion Laboratory (JPL) - This organization provided spacecraft details plus some analyses (release altitude of LWRHUs, for example); and

F. Monsanto Research Corporation (MRC) - In addition to manufacturing all nonradioactive components for the LWRHUs, MRC was responsible for issuing this SAR and for performing some tests and analyses in support of its issuance.

G. EG&G - Mound Applied Technologies (EG&G-MAT) - Effective October 1, 1988, the Mound Plant operations were taken over by EG&G-MAT from MRC. The references in this document are indicative of the timeframe of responsibility.

2.0 SUMMARY OF ACCIDENT EVALUATION

The flowchart sequence of mission phase as a function of success/failure branches is given in Figure 1. This flowchart (referred to as the Top-Level Tree) was provided to MRC by GE (Reference 2) by definition to ensure that the radiological safety input assessment was based on similar ground rules. These top-level trees are separated and addressed in much greater detail in Section 3.0.

The release of plutonia to the environment occurs only in the Phase 5 VEEGA (Venus-Earth-Earth Gravity Assist) encounter with earth during a fly-by as given below:

Branch	Ci(TBq)	Form	Locale	Probability
5A	2935 (109)	Vapor	Upper Atmosphere	5×10^{-9}
5A	155 (5.74)	Particles	Land Surface	5×10^{-9}
5B	250 (9.25)	Vapor	Upper Atmosphere	1×10^{-8}
5B	1906 (70.5)	Pellets	Ocean Bed	1×10^{-8}
5B	644 (23.8)	Pellets	Land Surface	1×10^{-8}
5B	135 (5.00)	Particles	Land Surface	1×10^{-8}

No fuel releases from accidents other than the VEEGA reentries have been identified for LWRHUs.

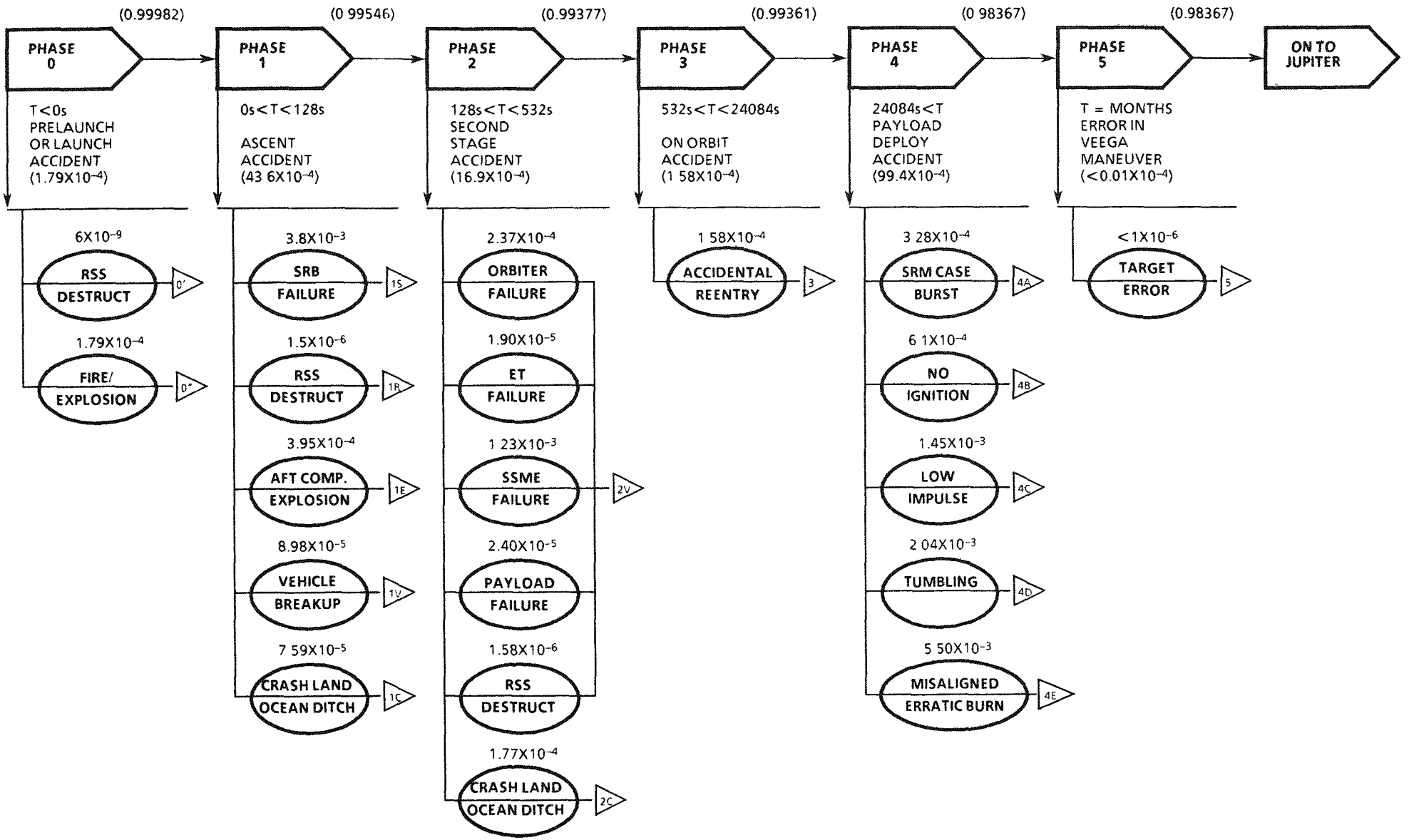

FIGURE 1: The top-level FAST was defined to be the same as the GE-derived FAST for the GPHS RTG. Each phase and branch is delineated in more detail in Figures 3 through 19.

3.0 ACCIDENT EVALUATION ON FAILURE MODE ANALYSIS

3.1 Objectives and Approach (Reference 3)

Heat sources containing plutonia are designed to be capable of controlling the radioactive materials so that, should the material ever reach Earth, the radiological risk would conform to recommended international limits. Because even the most reliable systems pose a finite failure probability, there is the requirement that the accident probability analyses, as well as population dose and health effect analyses, be completed prior to launch.

In general, each nuclear heat source is analyzed with regard to its application to a particular mission. For a given mission, the specific phases (e.g., prelaunch transportation and handling, launch, ascent, and final operation) must be defined so that normal procedures and mission events may be systematically analyzed to determine the results of an abnormal event.

The systematic analysis of each phase begins with an analysis of abort or failure modes with the objective of identifying potential single or multiple malfunctions that can potentially affect the nuclear power source during the complete mission. An explanation of the failure and abort sequence tree, which is a logic diagram used to develop the analysis, is shown in Figure 2. In the case of the launch vehicle, the failure analysis includes the condition of the vehicle after failure and also the occurrence probability for that condition. For each of the vehicle conditions defined in the analysis, a sequence of adverse environments is defined, and this is followed by an evaluation of the response of the nuclear power source to each of the adverse environment sequences. If the analysis of an extreme environment shows that there is a potential for a fuel release, the occurrence probability can be determined from the interrelation of the failure analysis and sequence tree construction. A summary of those initiating systems which could promote the accidents is given in Table II-2.

To evaluate the consequences of these events, the analyst must define the source terms. Within the context of space nuclear safety, a source term is the quantity of fuel which may be uncontrolled. In describing a source term, the analyst must consider its state (e.g., particle-size distribution, chemical form if changed from its original form, and degree of containment) and its location (e.g., at high altitude, on land, or in water; latitude and longitude; or random deposition during reentry from a specified orbit).

Information on the reasons that events occur leading up to the accident itself may be found in NSTS 08116 (Reference 5). The accident environments and probabilities given below were excerpted from NSTS 08116 summaries.

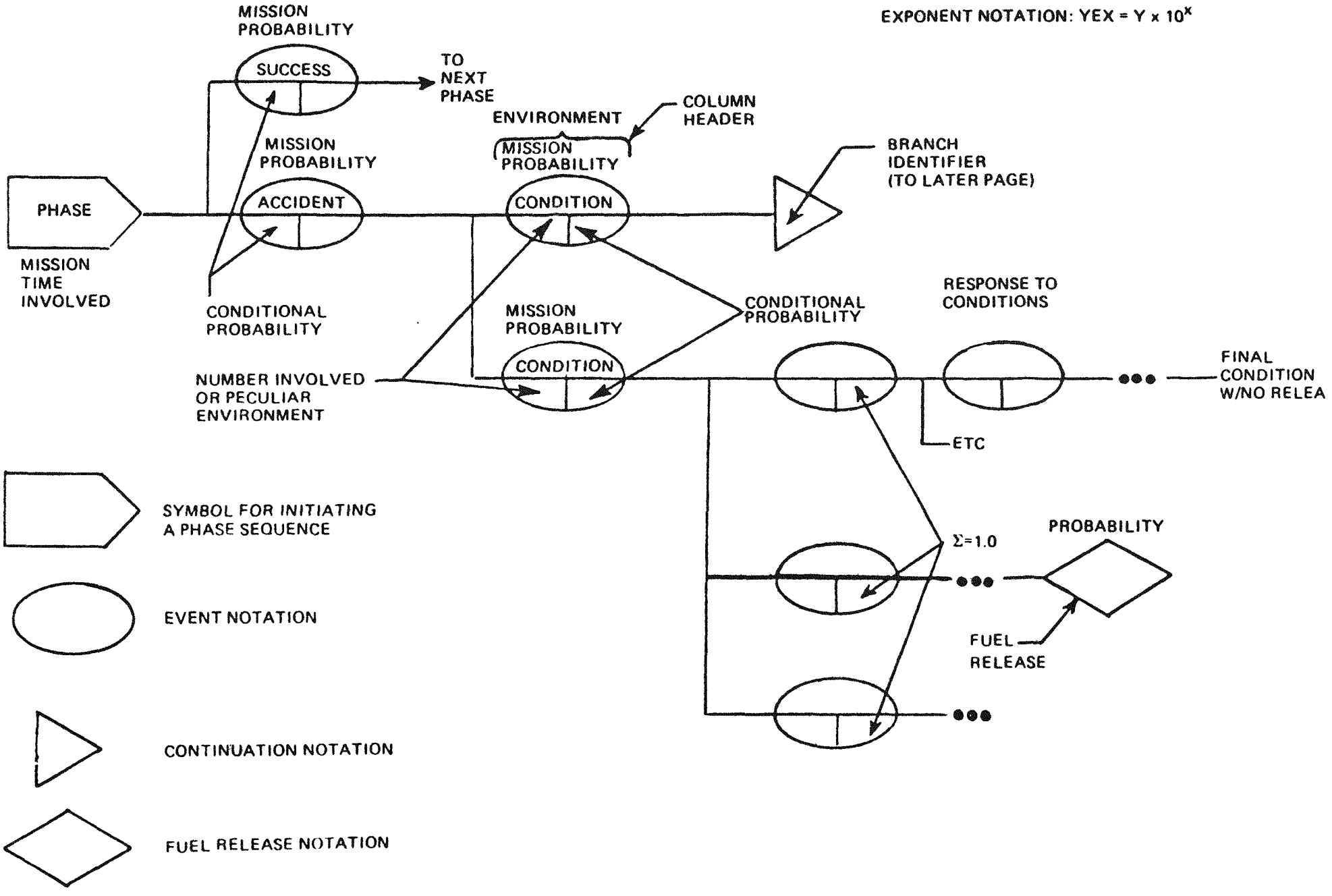

FIGURE 2: The methodology used in constructing the FASTs for this SAR.

TABLE II-2: The potential initiating system(s) which result in the various FASTS branches.

Phase-Branch	Event or Consequence	Possible Initiating System
0'	On-Pad RSS Destruct	Range Safety System (RSS)
0"	Fire/Explosion	Launch Support Equipment, Orbiter, ET*, SRB or SSME
1S	Explosion/Fire/Breakup	SRB Failure
1E	Aft Compartment Explosions	Payload, Orbiter, ET, SRB, or SSME
1V	Vehicle Breakup	Payload, Orbiter, ET, SRB, or SSME
1C	Crash Land/Ocean Ditch	Payload or Orbiter
1R	RSS Destruct	Payload, Orbiter, ET, SRB, SSME, or RSS
2V	In-Flight Breakup	Payload, Orbiter, ET, or SSME
2C	Crash Land/Ocean Ditch	Payload, Orbiter, ET, or SSME
3	Orbiter Reentry	Payload or Orbiter
4	Spacecraft Reentry	Payload
5	VEEGA Reentry	Spacecraft

*ET = External Tank

3.2 Mission Accident Evaluation

3.2.1 Phase 0 (Prelaunch/Launch) - Although separated in time (T) as prelaunch (T - 30,600 s to T - 31 s or from when the cryogenic liquid propellant introduction into the various tanks begin until the launch sequence becomes automatic) and launch (T - 31 s to T - 0 or from the end of prelaunch, through space shuttle main engine (SSME) ignition, solid rocket booster (SRB) ignition, and lift-off), these two mission segments are lumped together in this Phase 0 analysis. Figure 3 is the top-level FAST for Phase 0.

3.2.1.1 Inadvertent Range Safety System (RSS) Destruct

Branch 0' (Figure 4) illustrates the potential pathways to be taken by LWRHUs due to an inadvertent RSS destruct signal being given to the SRBs. The environmental sequence is:

A. SRB fragments could impinge upon exposed LWRHUs at velocities up to 102 m/s. The fragment response of LWRHUs is given in Appendix D and the test data show that no aeroshell or clad failures are expected [some aeroshell deformation and pyrolytic graphite (PG) breakup could occur, however]. The 34 probe LWRHUs are protected by the heavy probe aeroshell and cover so would not incur any damage.

B. After the SRB fragment impacts LWRHU(s), there could be secondary impacts. These would be on the spacecraft or the shuttle bay doors initially and followed by concrete or ground impact. Again, based upon the analyses presented in Appendixes D and H, no gross aeroshell failures nor clad ruptures would be expected as a result of these secondary impacts.

C. A liquid propellant fireball and/or SRB fuel fire would not compromise the LWRHU (even if some aeroshell damage was incurred earlier). Appendix E provides the results of tests and analyses which demonstrate that, at worst, the vent could melt if a 630-s solid fuel fire exposure were encountered. Some clad reaction with the PG could occur but not of a sufficient depth to promote fuel release. The short duration of the liquid propellant fireball would not result in the clad being elevated to a temperature which would result in failure by melting (see Figure E-1).

3.2.1.2 Fire/Explosion

A second environmental scenario which has been identified for the prelaunch phase is that of a fire and/or explosion on the launch pad. Figure 5 shows the Branch 0" that delineates the two potential explosion scenarios followed by fireball and impact environments. The sequence for either explosion branch is as follows:

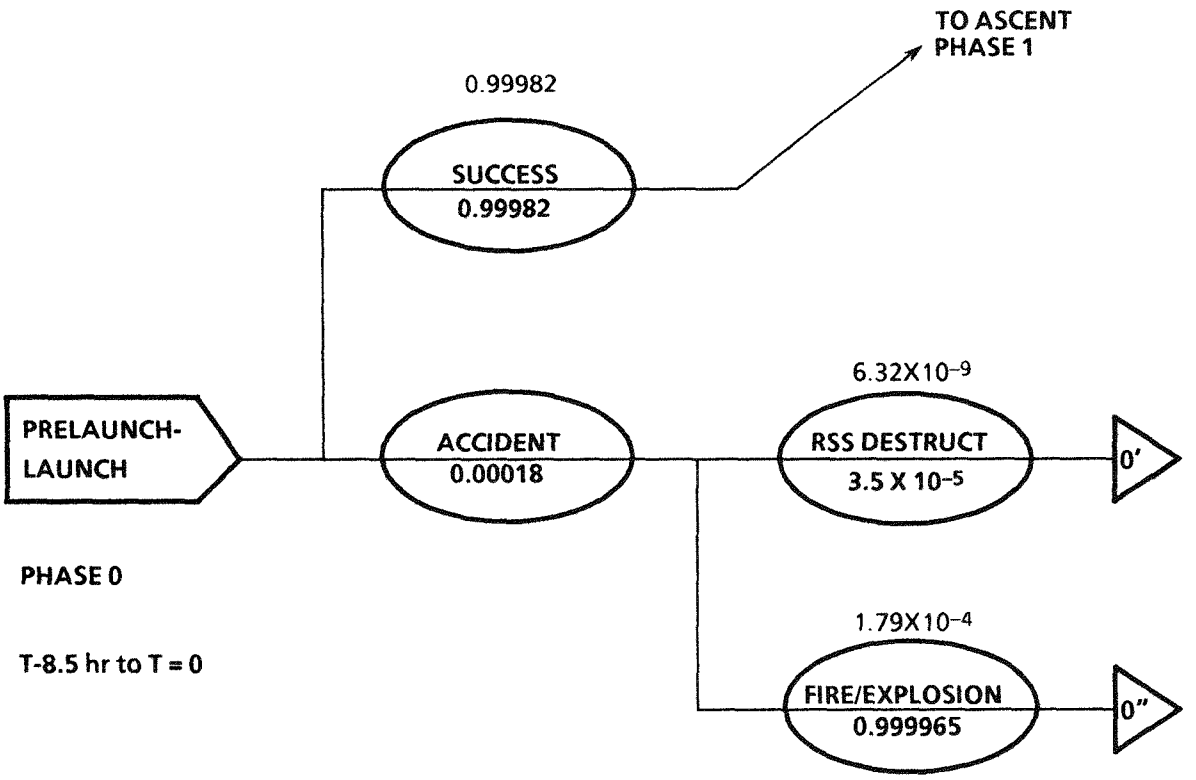

FIGURE 3: The top-level FAST for Phase 0 indicates two potential accident results.

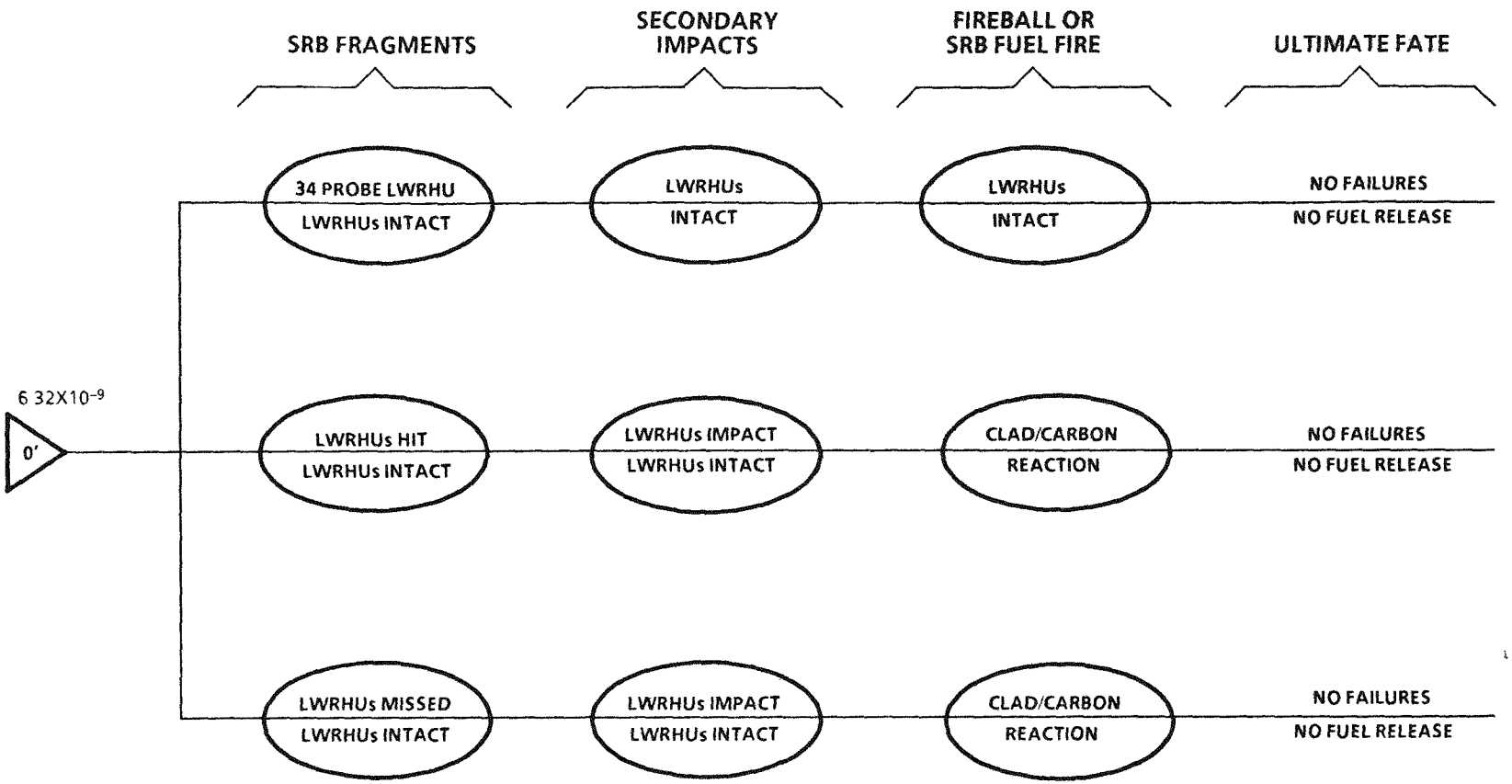

FIGURE 4: Although minor clad distortion and aeroshell damage could result in the 53-102 m/s SRB fragment impact on some LWRHUs, the subsequent ground or RSS* impact followed by either the cryogenic fuel fireball or exposure to a piece of burning SRB fuel would not release fuel. A partial clad-carbon reaction could occur, however.

*RSS = Rotating Service Structure in this instance.

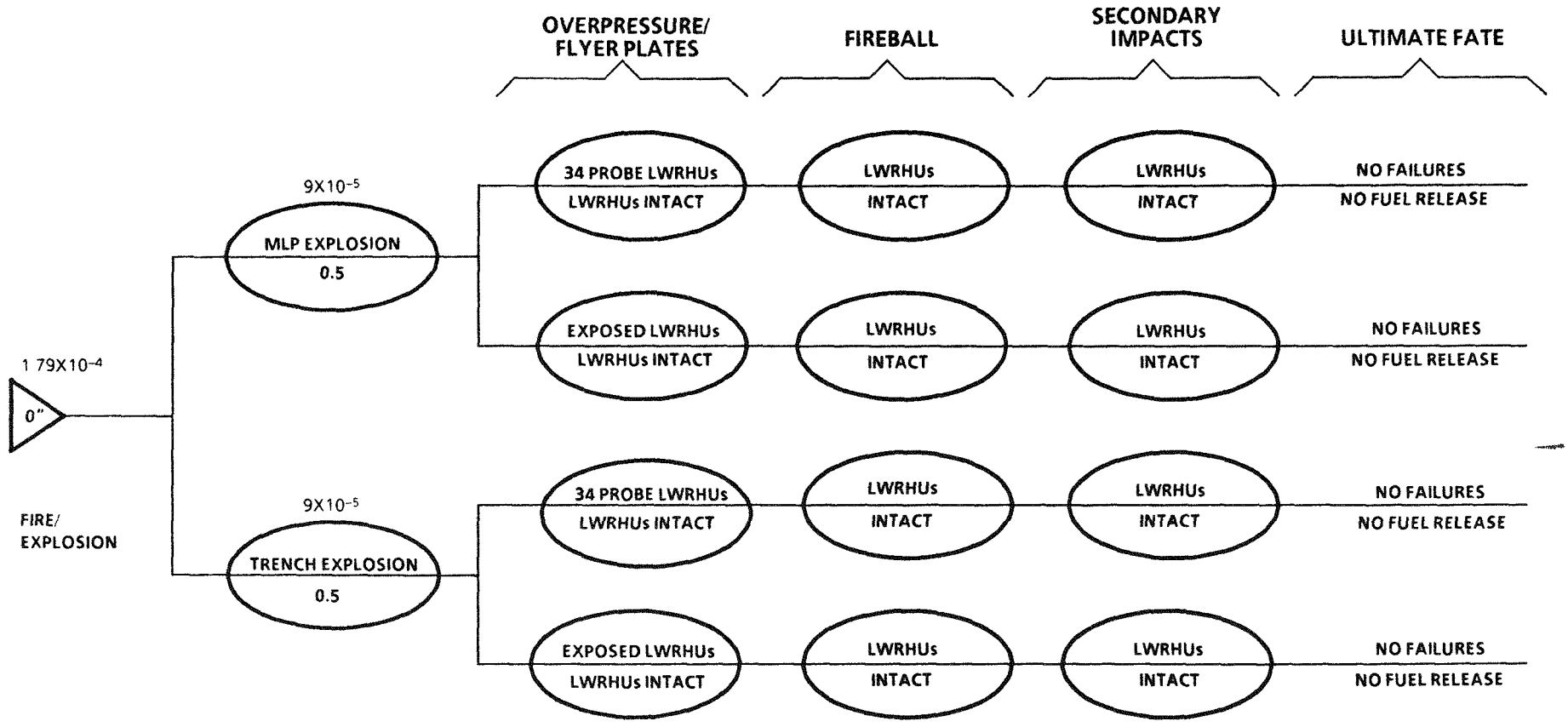

FIGURE 5: Branch 0" of Phase 0 for cryogenic propellant fire and/or explosion indicates that none of the sequential insults would result in a clad failure with fuel release. Note that the FIREBALL and SECONDARY IMPACT could be reversed (depending upon scenario chosen) with same end result.

A. The response of all exposed (excludes the 34 LWRHUs in the probe) LWRHUs to the range of overpressure of both the mobile launch pad (MLP) or flame trench explosion is documented in Appendix C. In essence, no explosion will fail the aeroshell in these blast environments although the LWRHU can require a significant velocity.

B. LWRHUs can encounter projectile/flyer plates generated from spacecraft or shuttle orbiting structures. Appendix D covers these collision scenario effects. Essentially all encountered velocities are well below the threshold for aeroshell failure so subsequent events will be met with an intact LWRHU (although the PGs could be cracked).

C. The exposed LWRHUs could be subjected to the ensuing liquid propellant fireball. The effect of such a fireball on LWRHUs is discussed in Appendix E. No clad failures or fuel releases are anticipated as a result of this environment as the temperature reached by the clad is not of sufficient magnitude to melt the materials. Exposure of the LWRHUs to burning SRB fuel is thought to be a nonproblem as the LWRHUs would be expelled in a direction away from the SRBs.

D. Secondary impacts (concrete or sand) would be assessed as in 3.2.1.1, B. No failures or fuel releases would be experinced as a result of this event.

3.2.2 Phase I (Ascent)

Phase 1 for the FAST analysis begins at lift-off (T = 0) and ends at T = 128 s when the SRBs are separated from the ET. As may be noted in Figures 6 through 13 and Table II-2, this phase of the Galileo Mission contains the majority of failures and greatest variety of consequences that can befall the LWRHUs aboard the spacecraft. The phase begins at the launch pad and, under normal circumstances, terminates at an altitude of about 45 km. During this time, the launch configuration accelerates from a velocity of 0 m/s to 1200 m/s. Figure 6 provides the top FAST for the Phase I (Ascent) portion of the Galileo Mission. The subbranches are delineated in the following paragraphs.

3.2.2.1 SRB Failures

The 1S Branch represents that portion of the Ascent Phase accidents which are driven by SRB failures (Figure 7). This type of accident is further broken into four subbranches as defined in the following paragraphs.

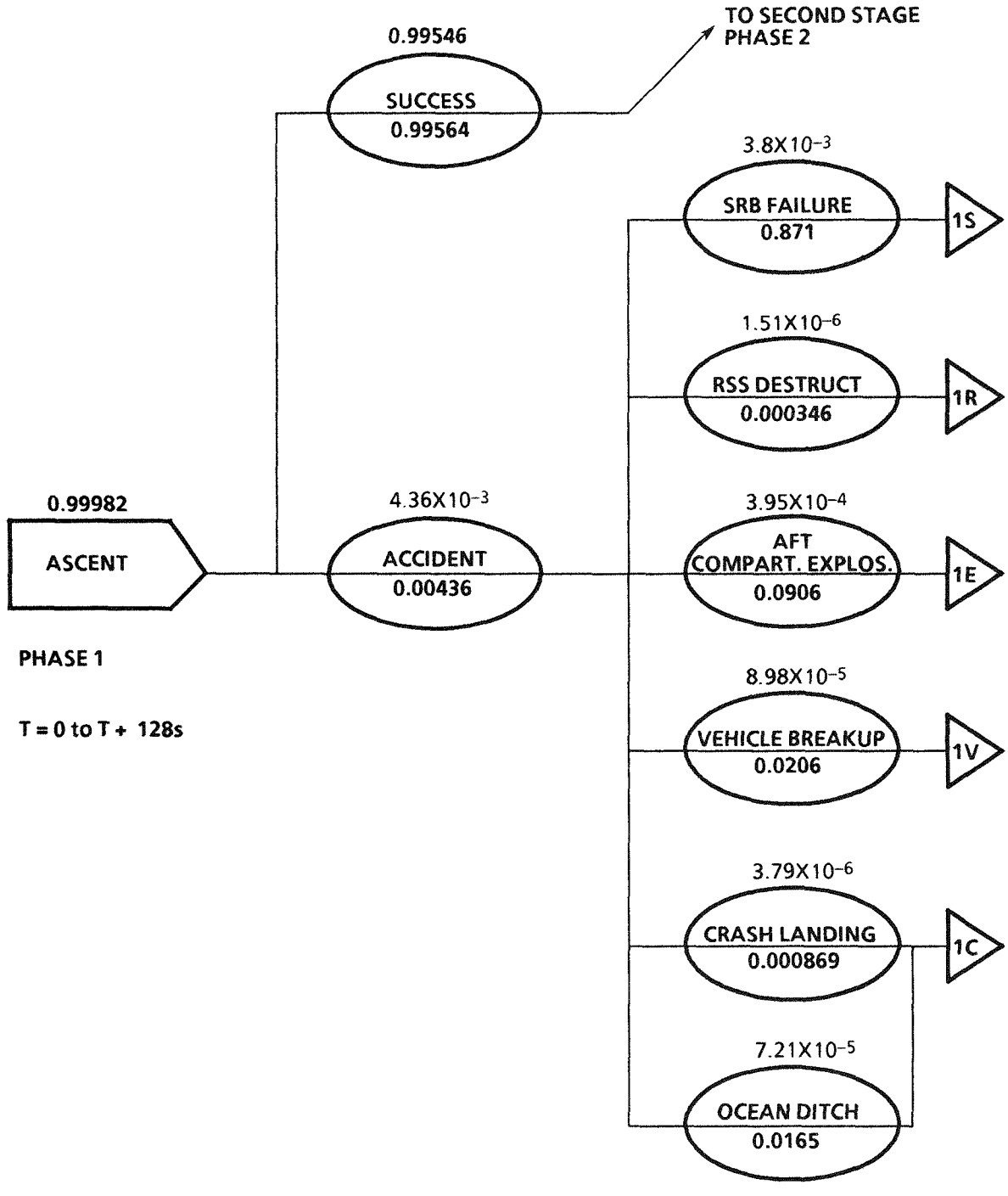

FIGURE 6: The Phase 1 top-level FAST identifies a variety of accidents which could result in adverse environments for the LWRHUs.

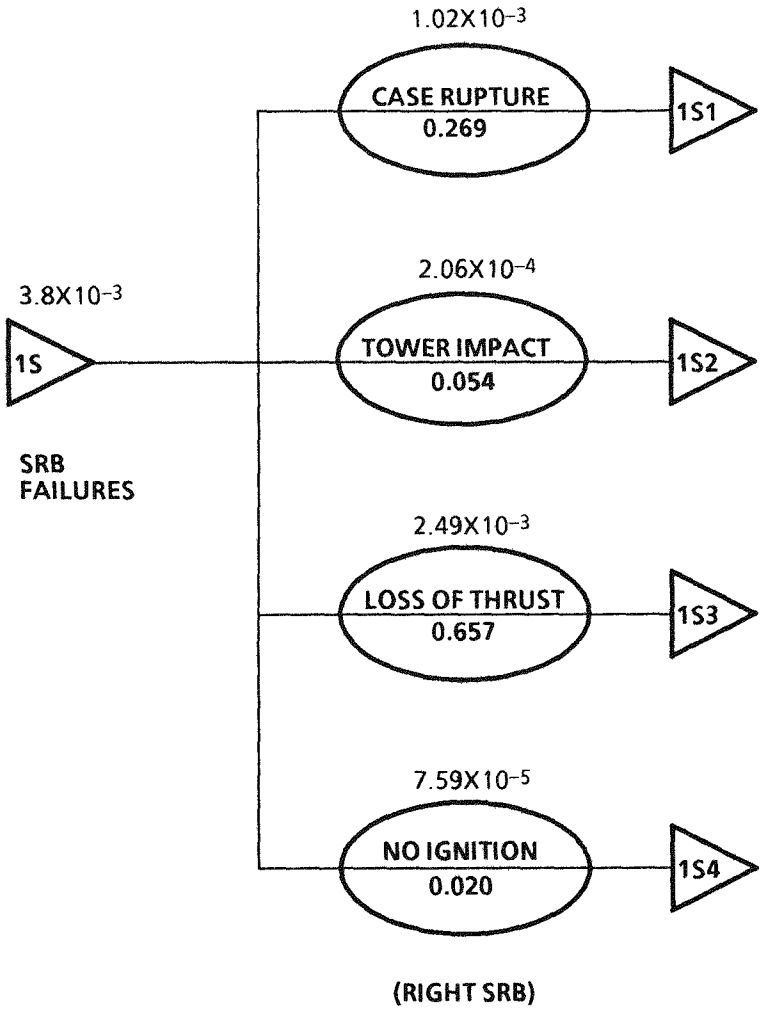

FIGURE 7: The 1S branch of Phase 1 is broken into four subbranches of specifically defined environmental conditions.

3.2.2.1.1 SRB Case Rupture (T + 10 to T + 120 s)

Figure 8 illustrates the subbranch 1S1 FAST for the SRB Case Rupture. In this schematic, the 34 LWRHUs contained within the heavy protective shield of the probe are noted to be unaffected throughout the accident environments. The balance (95 LWRHUs) are subjected to two different SRB fragment velocity environments:

A. From T + 10 to T + 105 s, the SRB fragment velocity maxima are lower than those in the following 15 s (see Appendix D). Even the highest velocity SRB fragment, should it strike an LWRHU, would not result in removal of the aeroshell from about the clad although PG fracturing would occur. The subsequent earth or water impact would be the damaged but intact LWRHU at the terminal velocity of 46 m/s.

B. From T + 105 to T + 120 s, SRB fragments can attain considerably higher velocities. These velocities could result in removal of the aeroshell and result in some clad distortion but no breaches (see Appendix D). In this assessment, an average of 16 LWRHUs are protected and thus will impact as integral LWRHUs; the 79 remaining would impact the water or land as deformed but integral clads at an impact velocity of 49 m/s (Appendix H).

As the SRB internal pressure decreases very rapidly after 120 s, no case ruptures are defined for the final 8 s of Phase 1. In all cases above, no clad failures which release plutonia are expected as a consequence of an SRB fragment hit followed by LWRHU (whole or bare clad) earth or water surface impact.

3.2.2.1.2 Tower Impact (T < 2s)

One of the consequences of an SRB malfunction during the first 2 s of flight is a tower impact which causes failure of the ET, releasing the cryogenic propellants onto the MLP or into the flame trench where they mix and explode. Figure 9 gives the 1S2 subbranch FAST for this event. The consequences of the two types of on-pad explosions were discussed earlier in Section 3.2.1.2 for Phase 0" Fuel Explosion. As in this earlier addressing of these types of accidents, no aeroshell removal is expected and no fuel releases due to clad failure would result.

3.2.2.1.3 Loss of Thrust (T + 10 to T + 128 s)

The FAST dealing with the loss of thrust type of accident (subbranch 1S3) is shown in Figure 10. Again, the 34 LWRHUs that are inside the probe are protected from ruinous environments. The 95 exposed LWRHUs could experience a vapor cloud explosion for the first 20 s of the period; Appendix C provides rationale which indicates that aeroshell removal would not occur in this event. The final 98 seconds of this FAST branch results in vehicle breakup, but the LWRHUs are not affected and would impact water or land intact.

As all impacts (water or land) are of LWRHUs at terminal velocity (46 m/s), no clad failures which result in release of plutonia are foreseen.

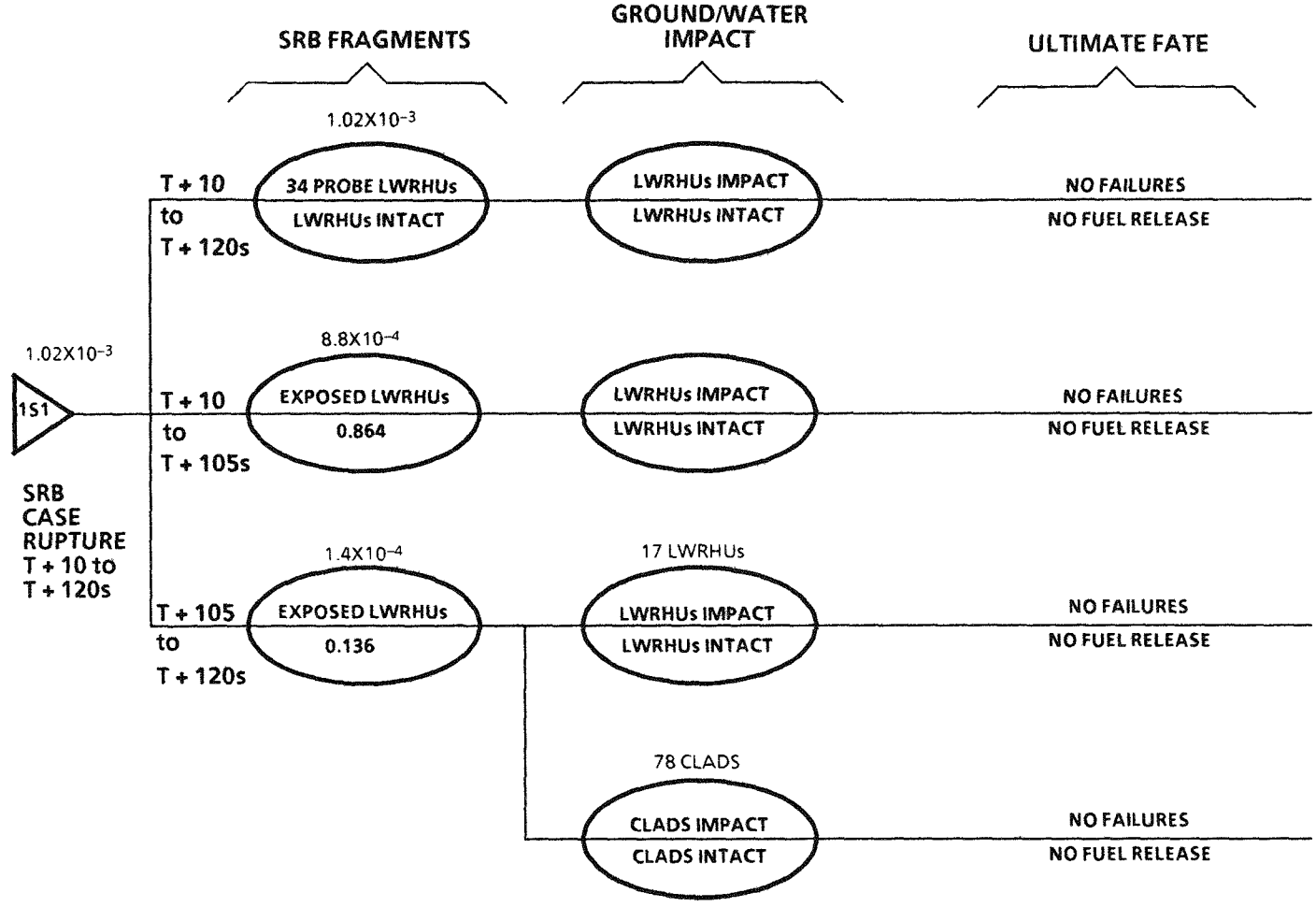

FIGURE 8: Subbranch 1S1 shows that late in the phase, the exposed LWRHUs can lose the graphites with subsequent ground/ocean impact. Fireball/SRB fuel exposure consequence is nil as the minimum occurence altitude is 200 m (short exposure times).

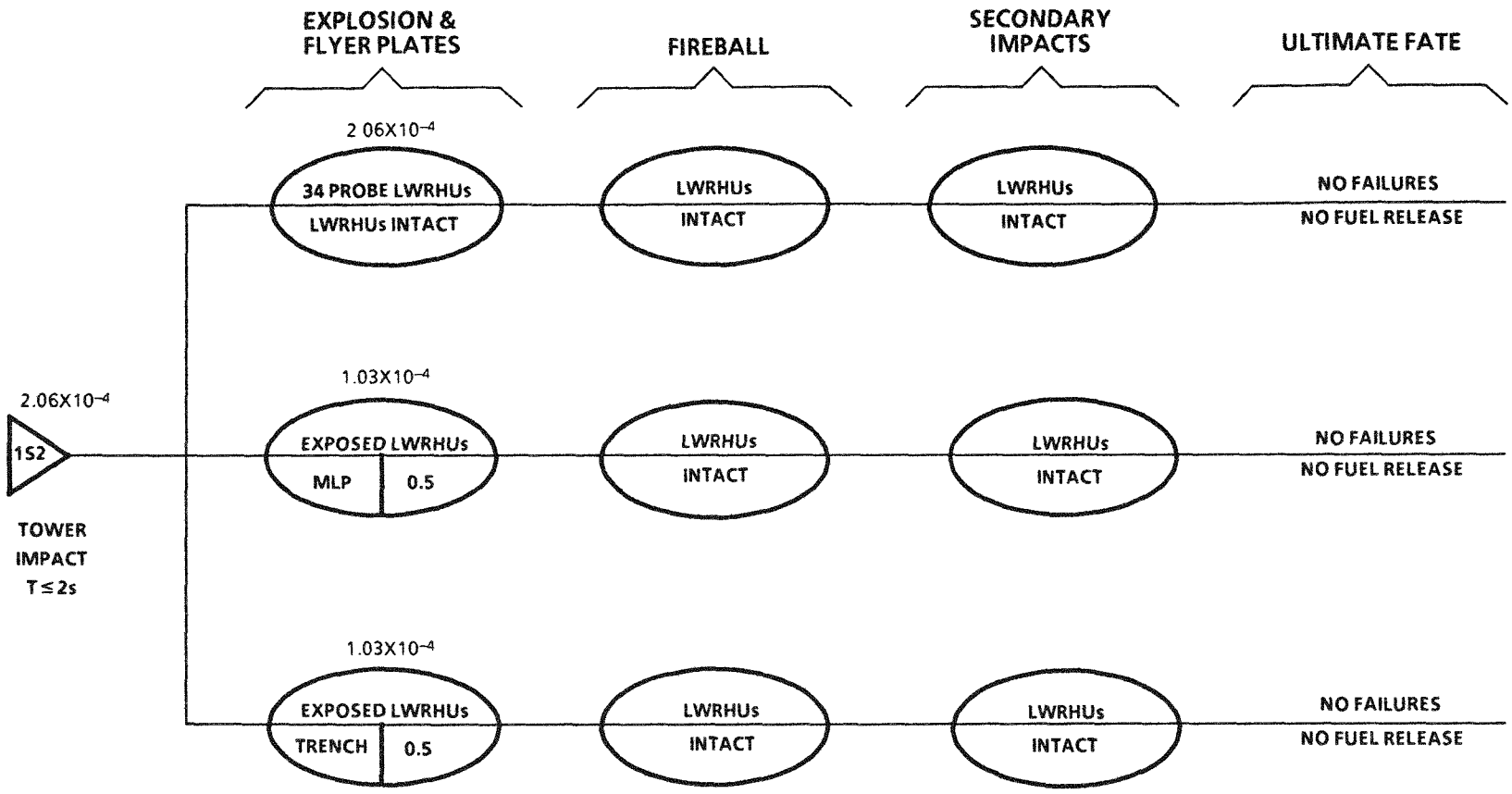

FIGURE 9: The fact that the LWRHU aeroshell remains about the clad in all scenarios relevant to subbranch 1S2 results in there being no clad failures nor fuel releases.

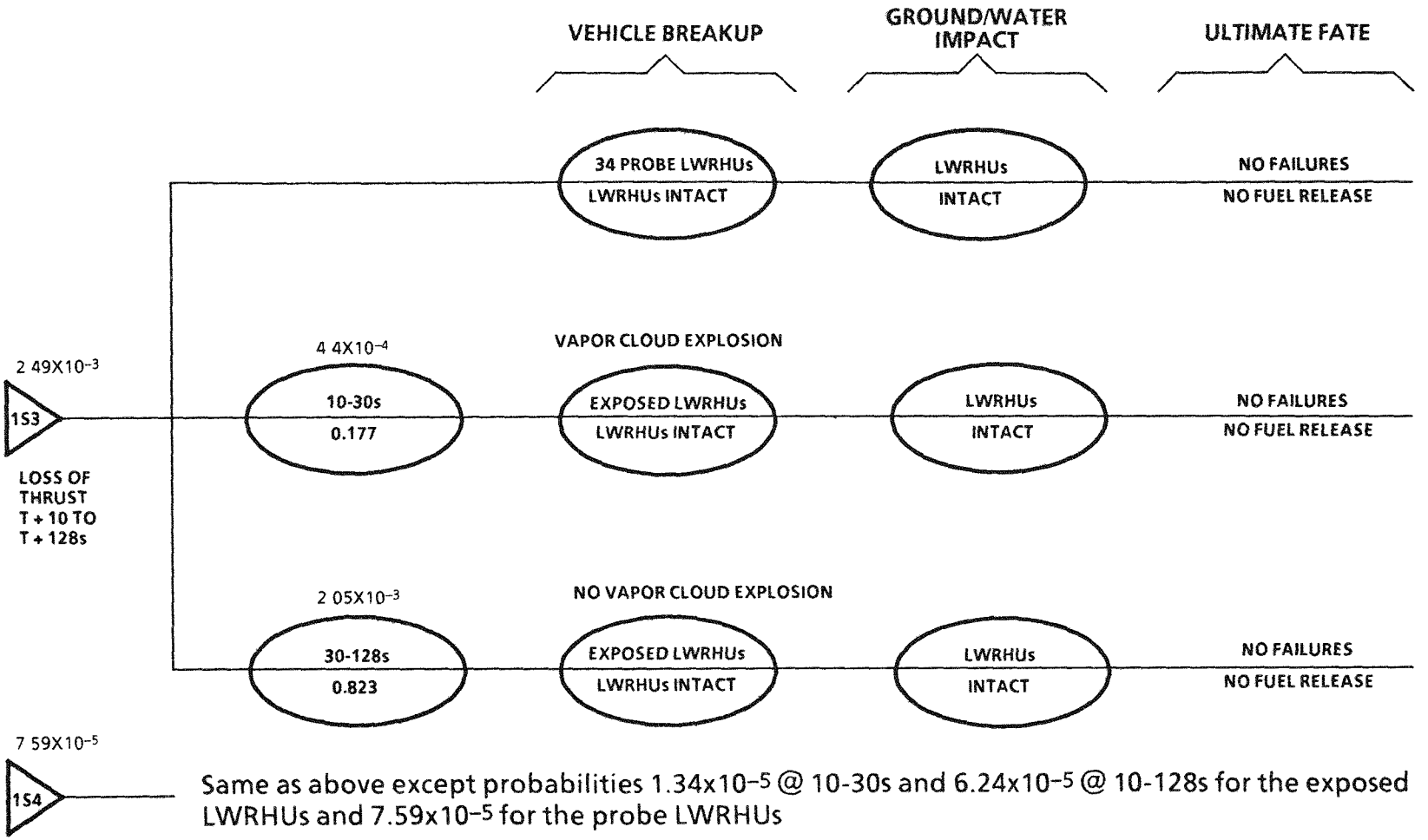

FIGURE 10: The 1S3 subbranch loss-of-thrust failures do not result in environments severe enough to fail the LWRHU; no fuel releases are thus identified. Subbranch 1S4 has the same structure and is thus not redrawn.

3.2.2.1.4 No Ignition

The FAST for subbranch 1S4 (No Ignition) is also defined in Figure 10. Its structure is the same as 1S3 although the probabilities are different. As in 1S3, the LWRHUs remain intact through water or land impact. The clads do not breach, so plutonia is not released in the 1S4 FAST.

3.2.2.2 Aft Compartment Explosion

The FAST which addresses the consequences of an aft compartment explosion (Branch 1E) is given in Figure 11. After separating out the 34 probe LWRHUs which are protected by the heavy probe aeroshell, the exposed LWRHUs can be subjected to three distinct sequences of environments:

A. T = 0 to T = 10 s: This early ascent event is close enough to the MLP that the explosion overpressure/flyer plate/fireball/secondary impact is identical to the Phase 0" MLP event discussed earlier in 3.2.1.2.

B. T = 0 to T = 30 s: The next time increment changes the MLP explosion to a vapor cloud event and removes the potential for a fire/fireball environment. This scenario is identical to the middle line of 1S3 (Figure 10) and is described in 3.2.2.1.3.

C. T = 30 to T = 128 s: The final time increment results in only a terminal velocity impact of the intact LWRHU; this is described in 3.2.2.1.3 also.

In all of the above segments, the LWRHU remains intact (although some PG insulator breakup can occur) and the clad suffers no breaches throughout the various environmental exposures. Therefore, no plutonia fuel releases are defined as a result of the various accident sequences associated with aft compartment explosions during the Phase 1 ascent.

3.2.2.3 Vehicle Breakup

The FAST for Branch 1V (vehicle breakup) is given in Figure 12. As the caption on this figures implies, the sequential events are identical to those for 1E as described in 3.2.2.2 except for the addition of a flame trench explosion in the first 10 s. The sequence of environments which follows the flame trench explosion was addressed previously in 3.2.1.2. The events outlined in 1V do not result in LWRHU aeroshell removal nor clad breaching. Therefore, no plutonia would be released to the environment from LWRHUs as a consequence of vehicle breakup during Phase 1 ascent.

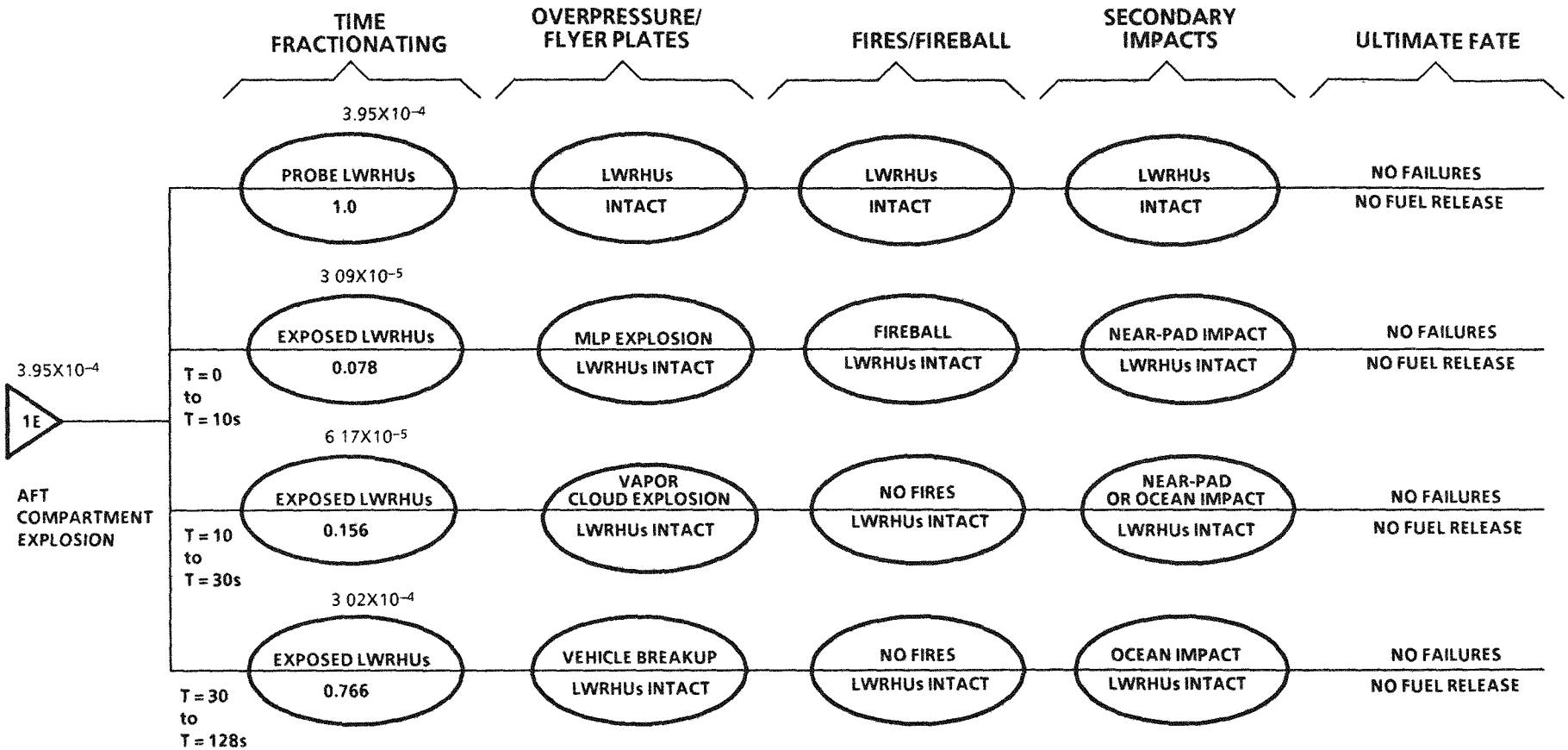

FIGURE 11: Three distinct environments can occur during Phase 1E (Aft Compartment Explosion) depending upon when in the 128-s phase the malfunction occurs.

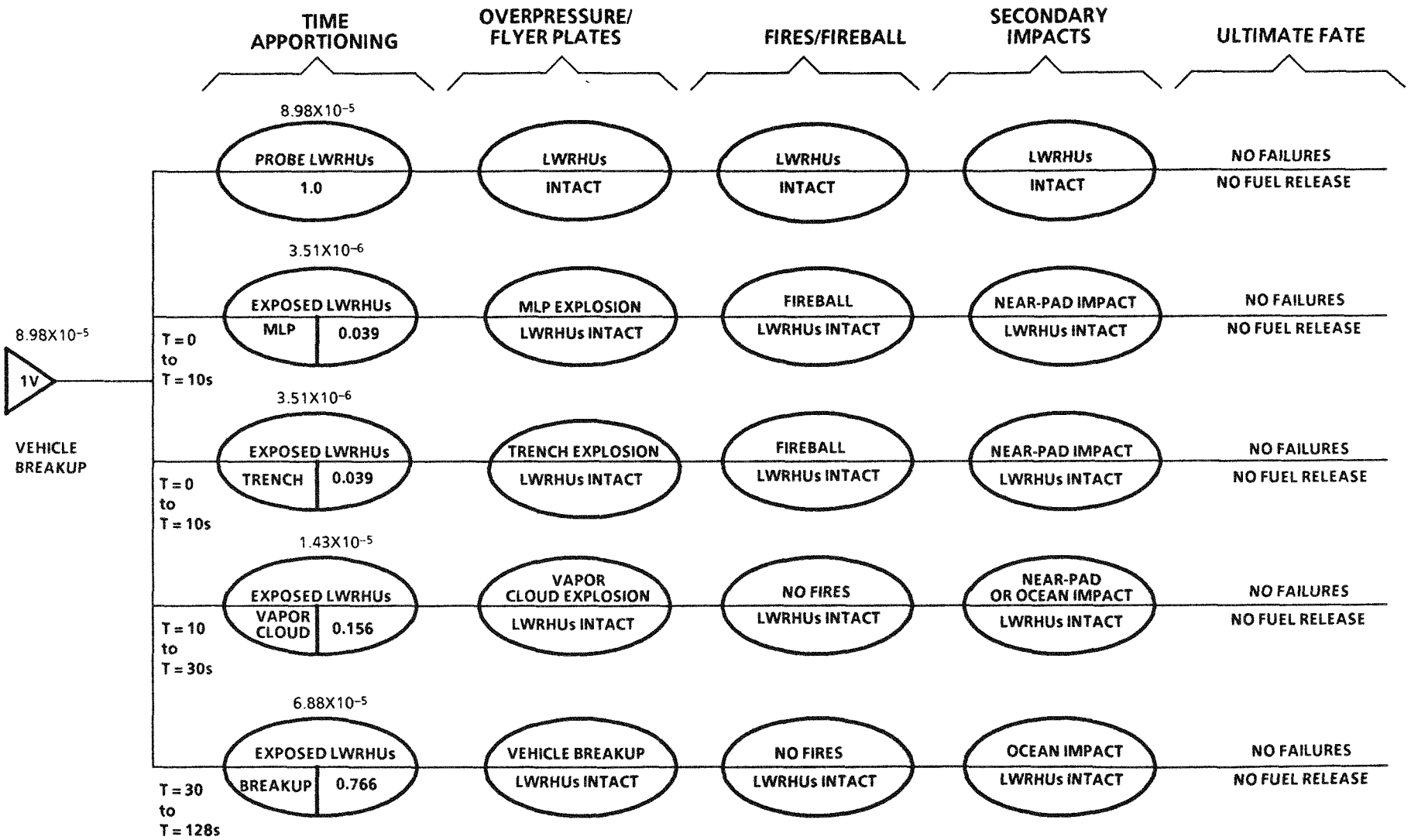

FIGURE 12: Branch 1V (Vehicle Breakup) is very similar to the previous branch (1E) in consequences; the addition of a subbranch for the trench explosion is the major difference.

3.2.2.4 Crash Landing and Ocean Ditch

The branch 1C FAST for the events which follow a crash landing or ocean ditch of the orbiter is shown in Figure 13. The ditch/crash itself is performed at a velocity of 103 m/s or less, so no rough landings/ditches would cause aeroshell failures. The potential post-touchdown explosion/flyer plate environment is addressed in Appendixes C (2.4) and D (5.0) and assumes aft compartment fragments. The secondary impacts of the resultant intact LWRHUs would not remove the aeroshells nor fail the clads of the 95 exposed LWRHUs. Therefore, no plutonia is expected to occur as a result of a crash landing or ocean ditch due to the landing/ditch itself or a possible subsequent explosion.

3.2.2.5 RSS Destruct

Figure 13 also indicates that the FAST for 1R (RSS Destruct) exists but that it parallels 1S1 (Section 3.2.2.1, Figure 8) in environment and consequences. The employment of the range destruct during Phase 1 could result in removal of the aeroshell in numerous exposed LWRHUs but, as indicated in 3.2.2.1, no clad breaches which would release plutonia fuel would be expected.

3.2.3 Phase 2 (Second Stage)

Phase 2 begins at T + 128 s after the release of the two SRBs from the ET and continues to T + 532 s at which time the SSMEs are shut down and the orbiter separates from the ET. The top-level FAST for Phase 2 is given in the Figure 14. Although there are numerous events which can result in an accident situation, the consequences are only two: vehicle breakup and crash landing/ocean ditch. These two events are addressed below:

3.2.3.1 Vehicle Breakup

The FAST for the Phase 2 vehicle breakup branch (2V) is shown in Figure 15. As a vapor cloud explosion does not occur at this high an altitude at the high velocities, the overpressure/flyer plate environment is benign (mainly aerodynamic) and would not result in aeroshell removal from the exposed LWRHUs. In later portions of this phase, reentry heating can occur. A reentry during this phase would result in thermal responses equal to or less than experienced during orbital decay, so the LWRHUs would remain integral after the thermal pulse. Details of reentry and thermal stress considerations are detailed in Appendix G.

Following a fall with or without the reentry heat pulse, LWRHUs will impact either ground or water surface(s). As the aeroshells are still intact, the normal impact responses discussed in Appendix H would occur with the LWRHUs remaining in an unfailed condition. Therefore, after vehicle breakup in Phase 2, no release of plutonia to the environment as a result of failed clads is expected.

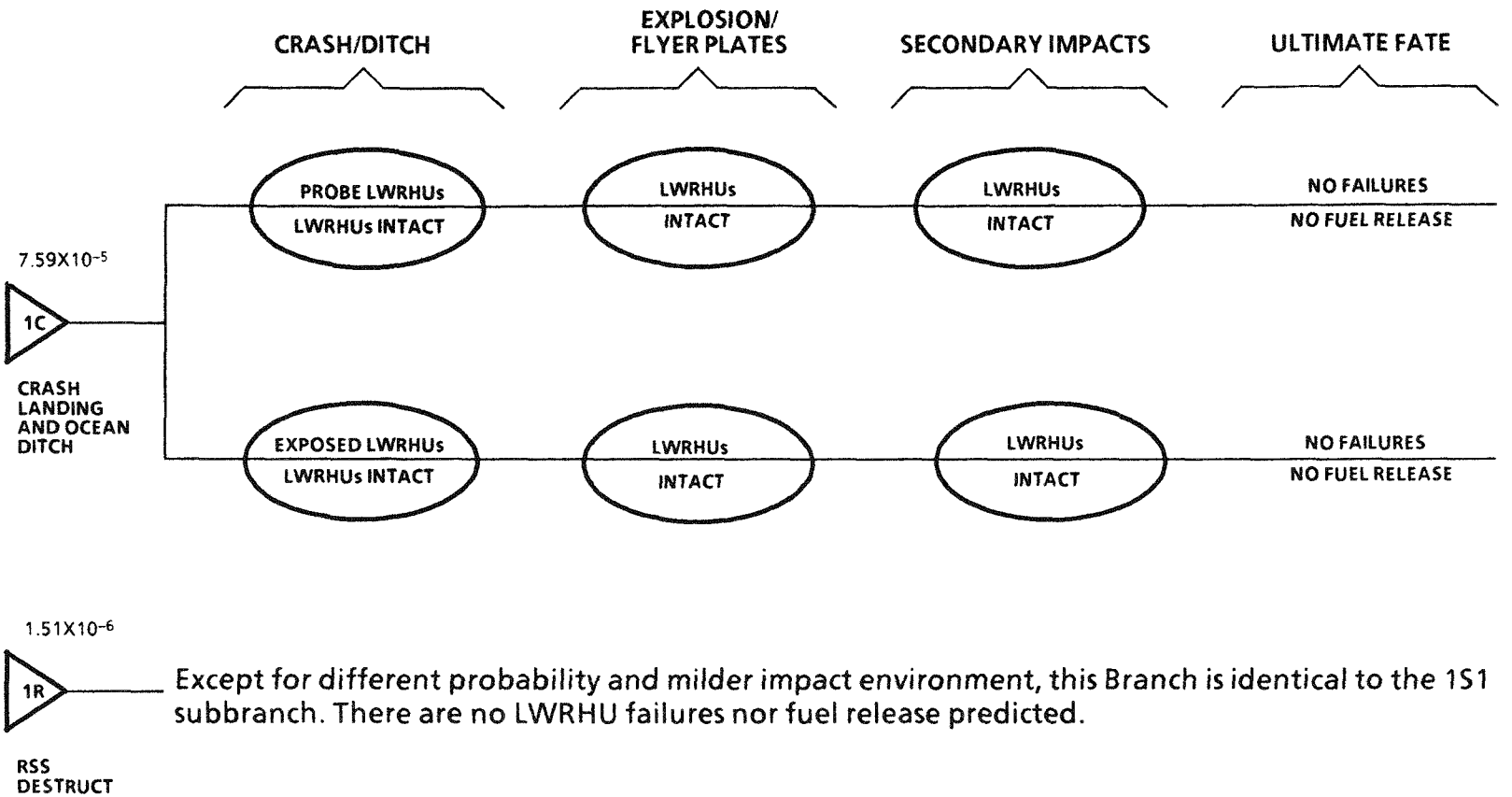

FIGURE 13: Branches 1C and 1R predict no failures nor fuel releases from the LWRHUs should the postulated accidents occur.

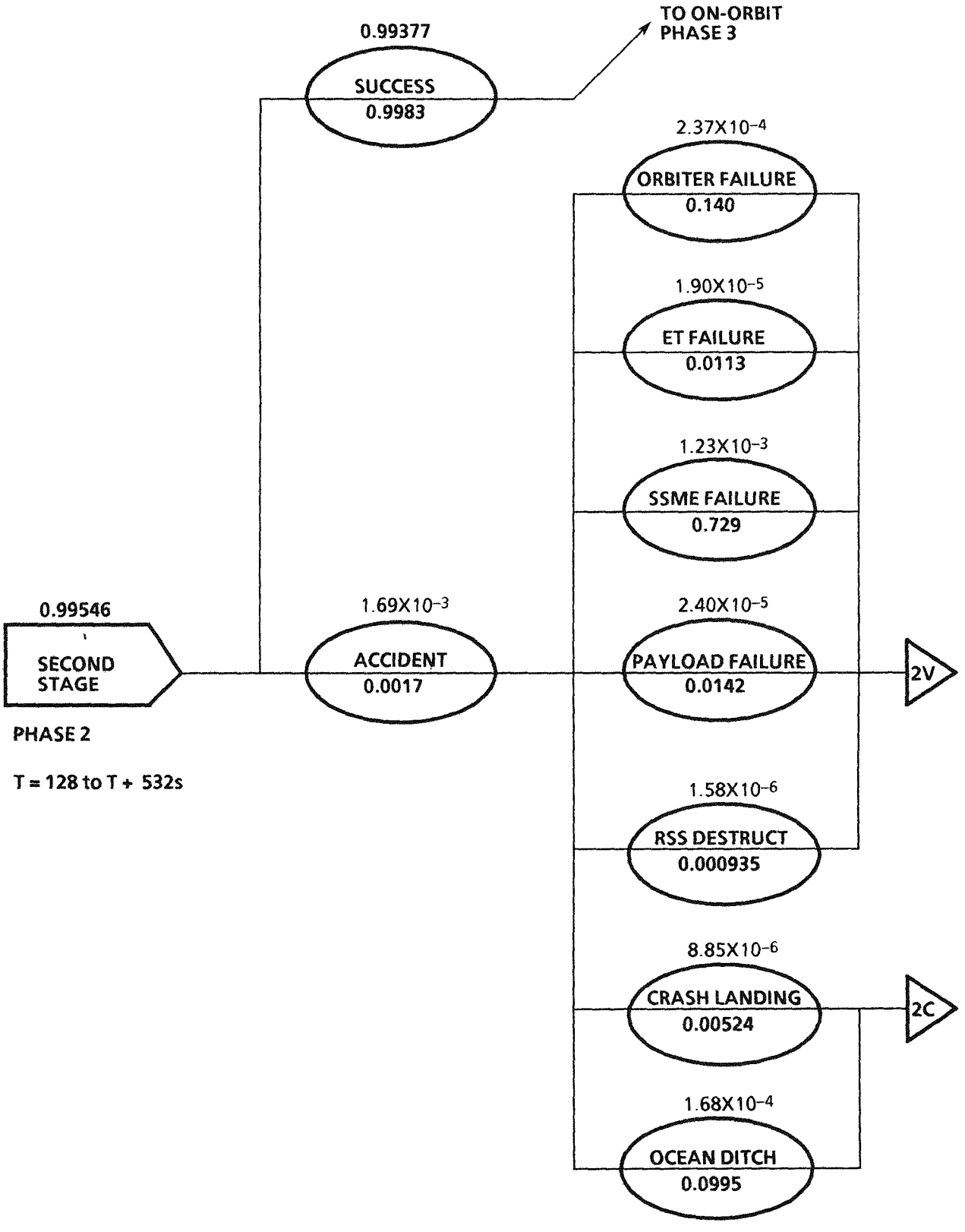

FIGURE 14: Although several initiating accident causes can occur in Phase 2, only two subbranches result from these various start conditions.

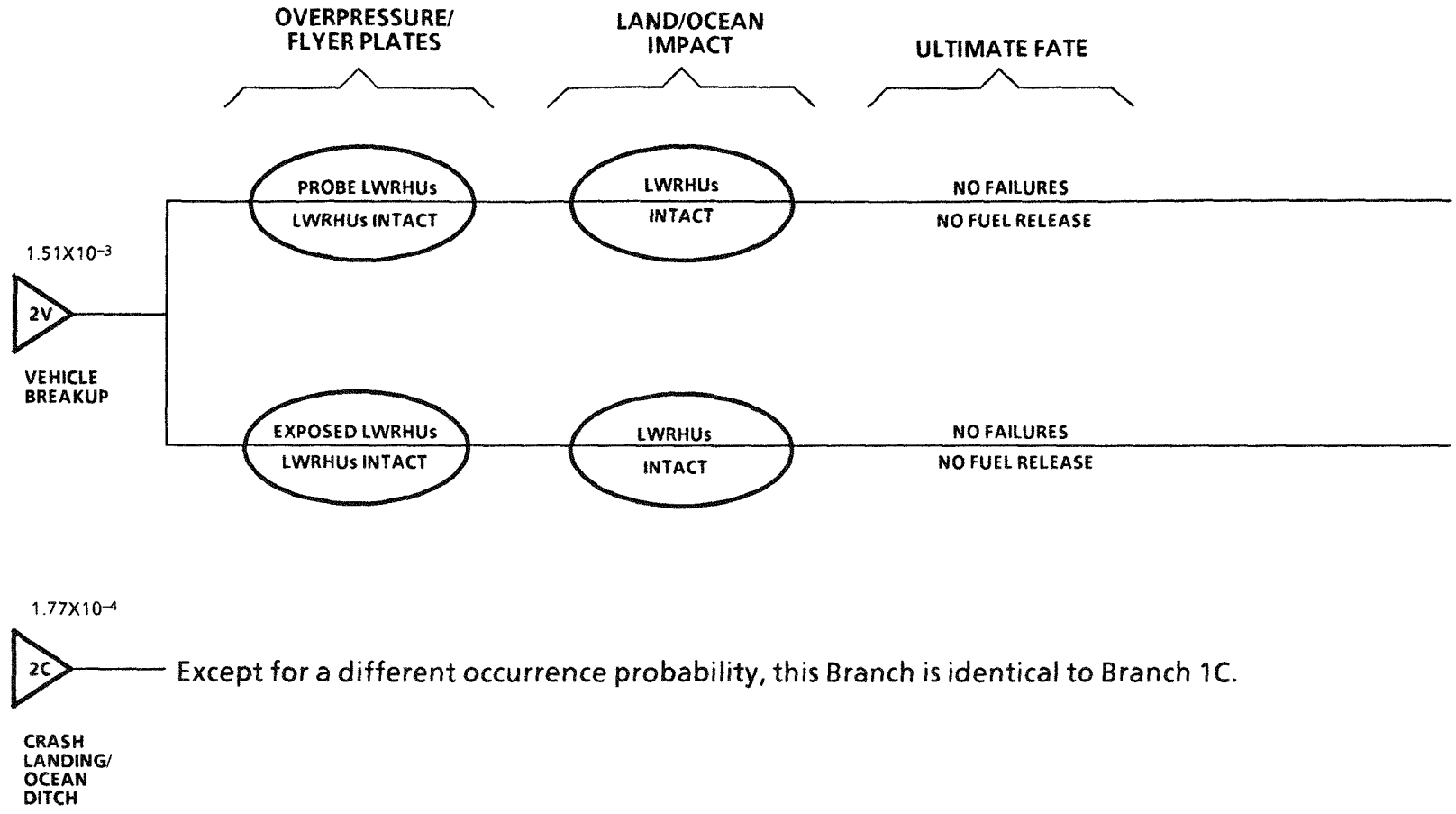

FIGURE 15: The two defined non-success environments in the second phase indicate no LWRHU failures nor any fuel release.

3.2.3.2 Crash Landing/Ocean Ditch

The 2C Branch addresses the crash landing/ocean ditch; this is indicated in Figure 15 but not redrawn as it is identical, except for the occurrence probability, to the 1C Branch (Figure 13). In summary, no LWRHU failures would be expected for these accident scenarios and no plutonia fuel would be released.

3.2.4 Phase 3 (On Orbit)

The on-orbit or Phase 3 of this assessment begins after the ET/orbiter separation (T + 532 s) and end upon the deployment of the spacecraft at T + 24084 s. Any malfunction which results in the orbiter reentry and breakup will result in orbital decay reentry of the LWRHUs.

The sequence of orbital reentry (LWRHUs remaining intact as described in Appendix G) and impact (LWRHUs remaining intact, although deformed, as noted in Appendix H) would not cause LWRHU clad failure and thus not result in a release of plutonia to the environment. Figure 16 provides the FAST for this phase.

3.2.5 Phase 4 (Payload Deploy)

The single FAST for the accidents which could occur and result in the release of LWRHUs during Phase 4 is shown in Figure 17. This phase begins at T + 24084 s and is of indeterminate length. All accidents would occur as a result of an inertial upper stage (IUS) failure followed by the LWRHUs undergoing reentry, then impact.

Appendix G addresses the various earth-orbit reentry responses by LWRHUs. Any such reentry would result in the LWRHU retaining its integrity (some ablation would occur, of course) and the clad would not attain a temperature high enough to melt nor degrade its metallurgical properties. Terminal velocity impacts would not fail the clad, as tests described in Appendix H conclude. Therefore, any accidents during Phase 4 which result in the reentry and subsequent earth surface impact of an LWRHU would not release plutonia fuel.

3.2.6 Phase 5 (VEEGA Maneuver)

In the Galileo Mission, in order to attain the velocity to reach Jupiter, there will be two Earth fly-bys (VEEGA stands for Venus-Earth-Earth Gravity Assist). In normal cases, these fly-bys miss the Earth's upper atmosphere by a few hundred kilometers. A misdirected approach, although deemed improbable, could result in the spacecraft entering the Earth's atmosphere, breaking up, and releasing the exposed LWRHUs to a severe reentry pulse. The FAST for this event is given in Figures 18 through 20.

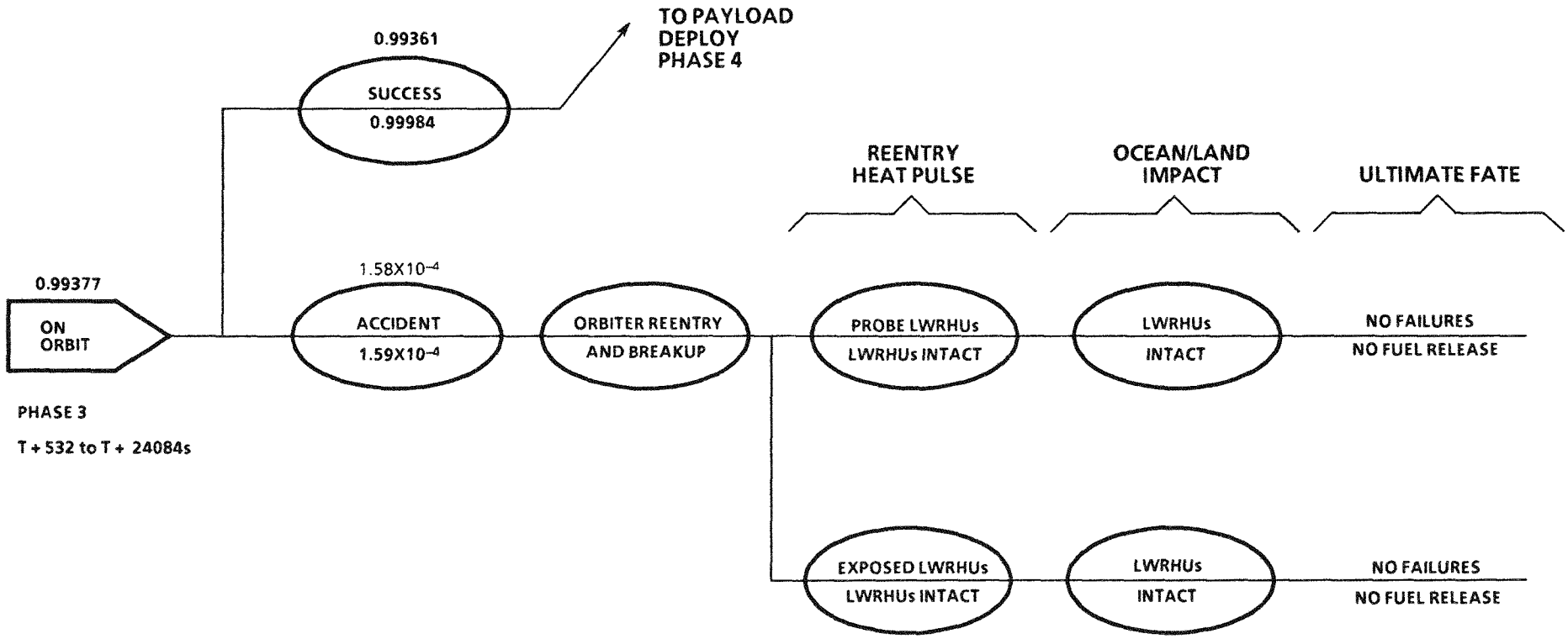

FIGURE 16: A single orbital reentry followed by earth/water impact is the effect of a Phase 3 on orbit accident.

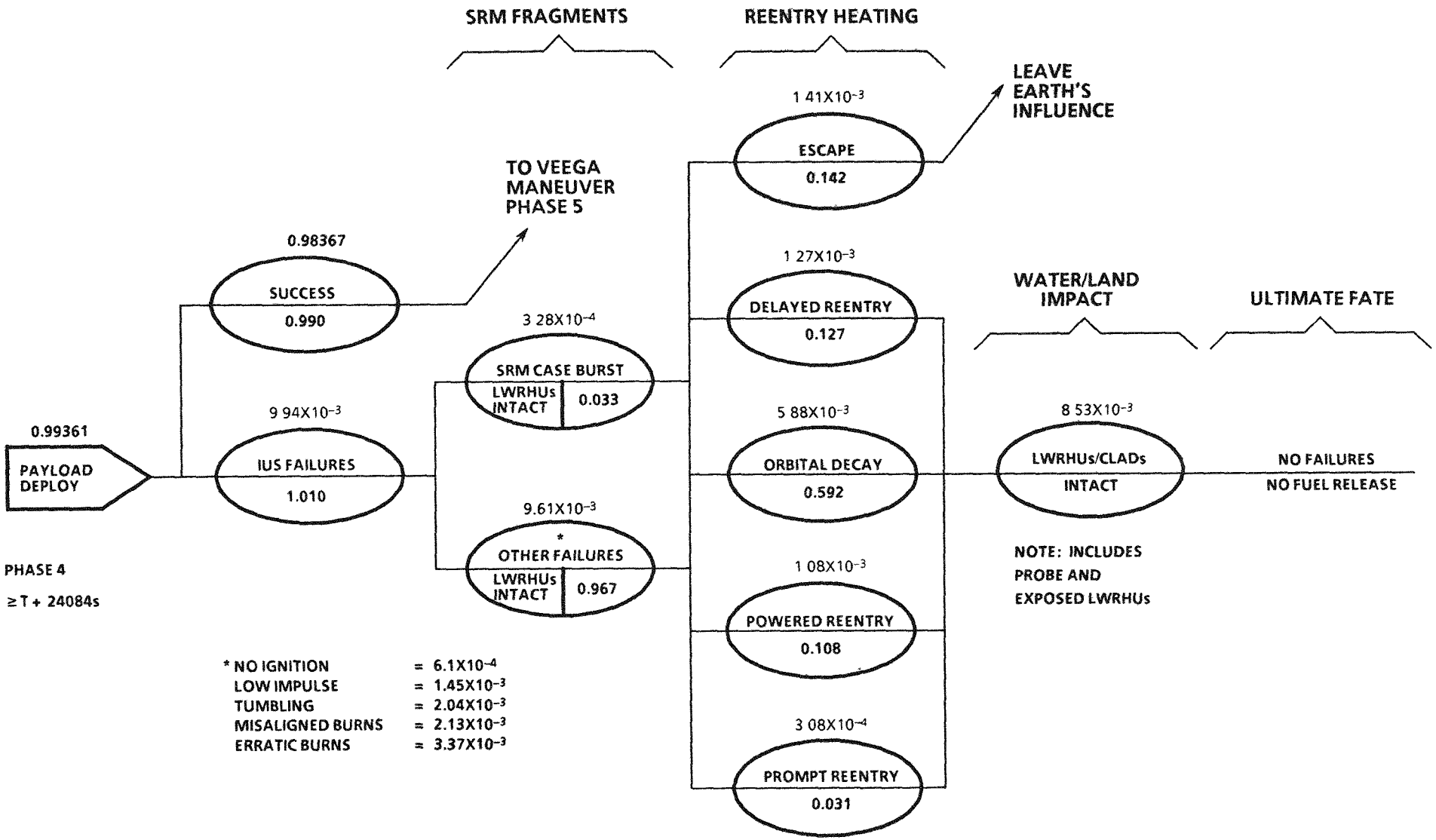

FIGURE 17: As no non-VEEGA reentry will result in clad melting or aeroshell failure, Phase 4 accidents would not result in fuel release based on the terminal velocity impact tests performed.

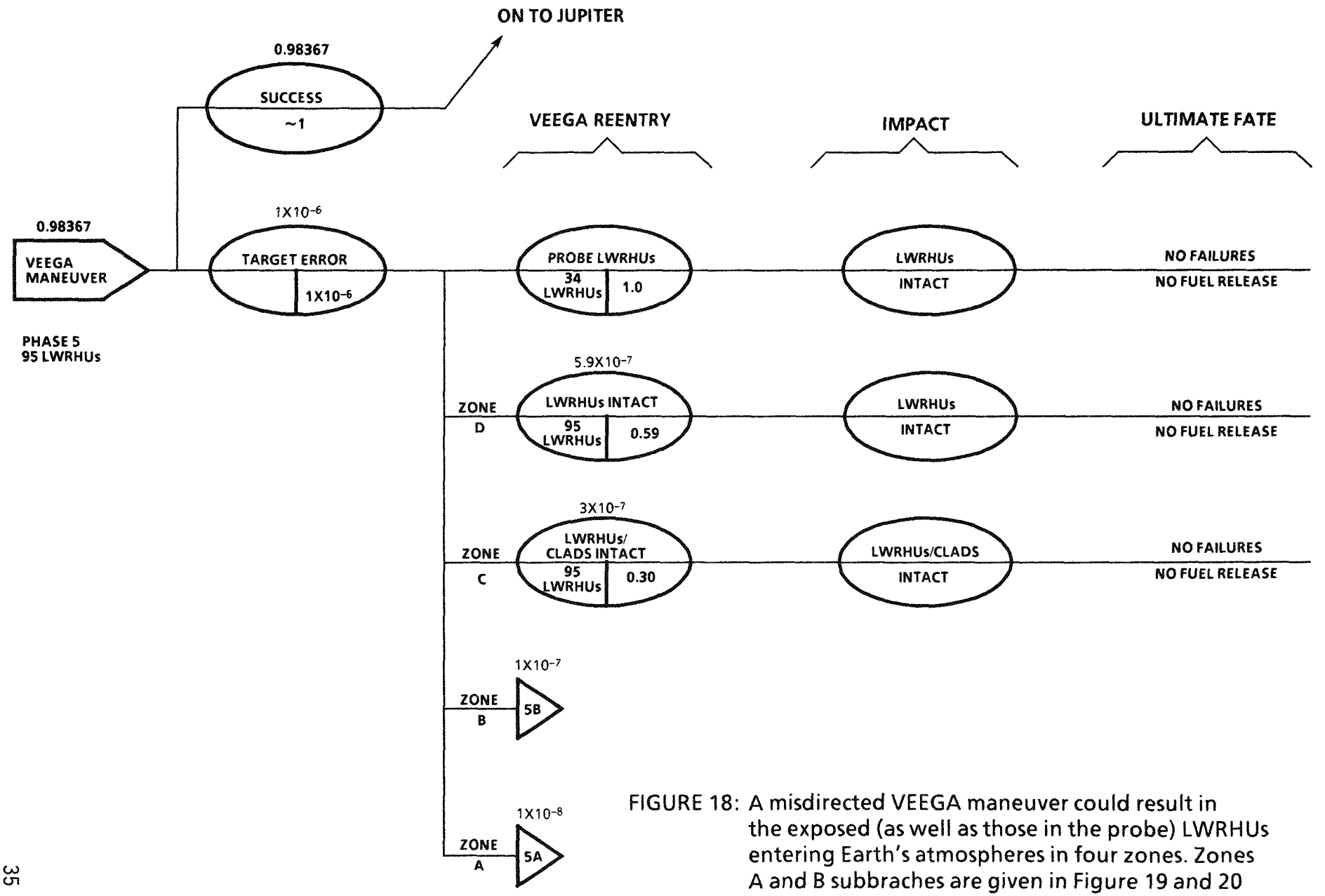

FIGURE 18: A misdirected VEEGA maneuver could result in the exposed (as well as those in the probe) LWRHUs entering Earth's atmospheres in four zones. Zones A and B subbraches are given in Figure 19 and 20 and identify plutonia fuel releases.

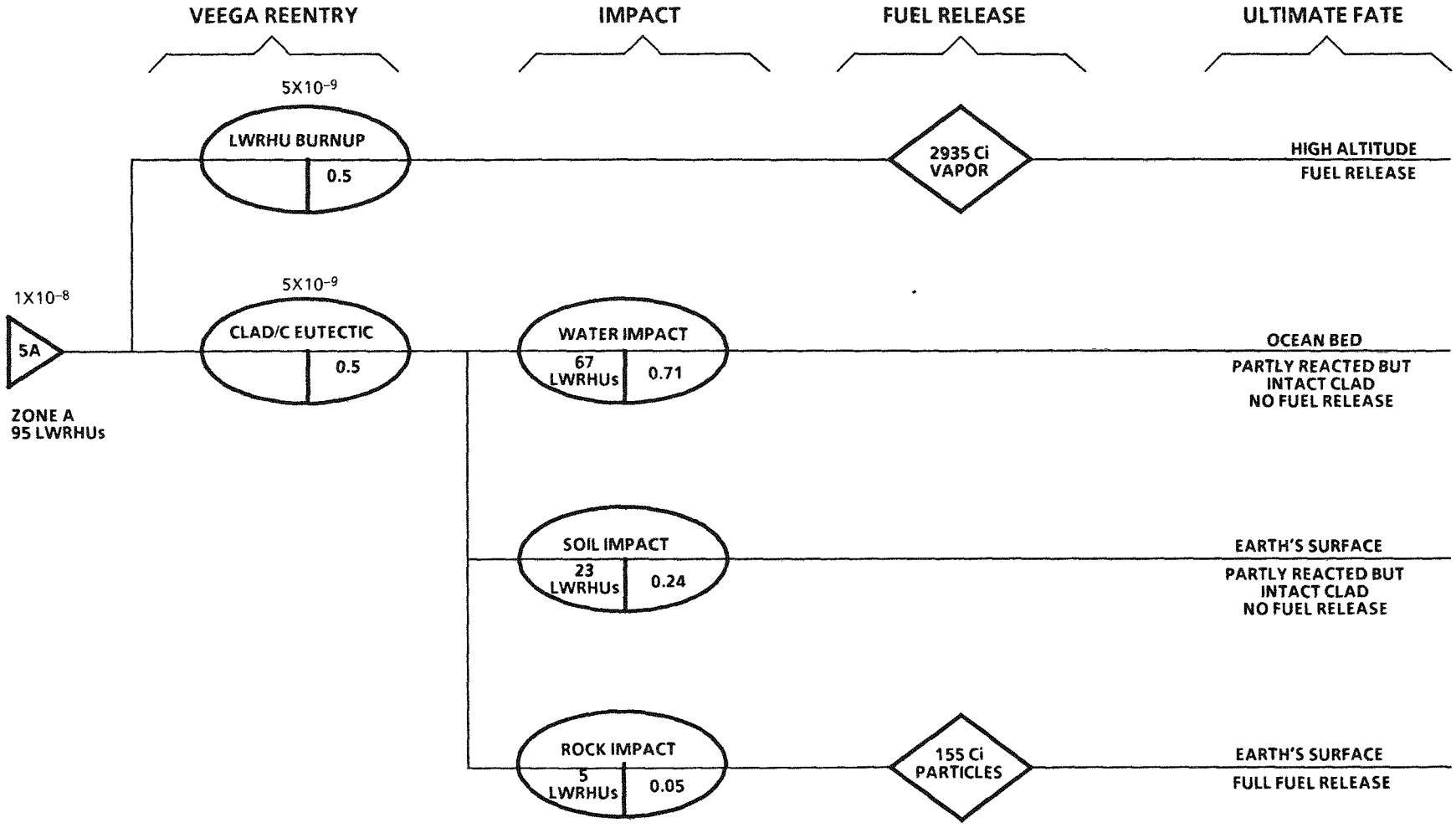

FIGURE 19: The shallow-angle VEEGA reentry (Zone A) indicates a 50% probability of complete burnup of the 95 LWRHUs not in the probe. As the clad-carbon eutectic temperature is approached in the other 50% of the time, a hard surface impact may result in the release of plutonia.

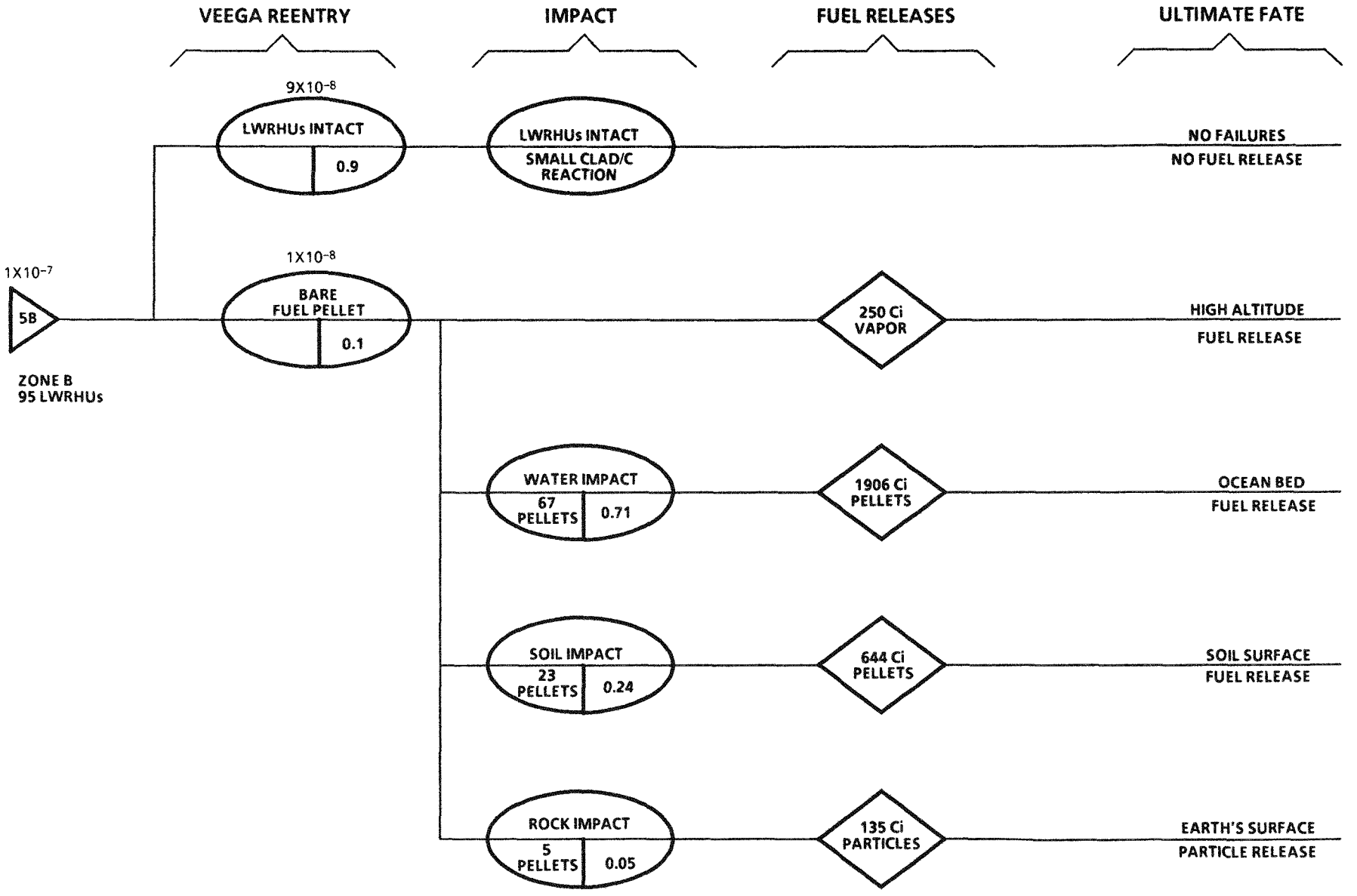

FIGURE 20: The uncertainty split for Zone 5B indicates that there is a 10% probability that bare fuel pellets would reenter, partially evaporate, and impact upon the Earth's surface.

As in previous assessments, the 34 LWRHUs within the probe are considered to be protected; the probe aeroshell is designed to enter Jupiter's atmosphere at a considerably higher velocity so it should withstand Earth's environment even though the chemistries of the environments are different. Appendix F addresses spacecraft breakup (which should be very rapid here) so the LWRHUs are released early in the aerothermal realm. The LWRHUs would assume a side-on stable (tilted at 40°) configuration to provide the maximum cross sectional area (Reference 4) regardless of orientation or spin state upon entering Earth's upper atmosphere. All 95 LWRHUs not in the probe are assumed to acquire this altitude for all four zones analyzed.

Appendix G addresses the VEEGA zonal responses of the LWRHUs. These zonal responses are a function of the reentry angle (γ) and are summarized as follows:

A. Zone A - This zone is for very shallow reentry angles - 4 to 7.5 degrees. This prolonged high heat pulse will fail the aeroshell 50% of the time and the released fuel pellet will completely vaporize at high altitudes. For the other 50% of the time, the aeroshell will ablate less than 100% through and the integral unit will incur Earth impact. The clad has undergone some eutectic formation with the inner PG sleeve and the vent might have melted (it is pure platinum rather than Pt-40% Rh). The FAST for Phase 5A is shown in Figure 19.

B. Zone B - At somewhat steeper angles bracketed by 7.5 to 20 degrees, the aeroshell will fail 10% of the time but remains integral with only minor clad-PG reaction the rest of the time (See Figure 20). As outlined in Appendix G, approximately 8.5% of the plutonia will be deposited as a gas in the upper atmosphere with the pellet (now 91.5% of its original mass) impacting Earth's surface in those that do fail.

   Figure 20 also details the pellet impact fate. Ocean and soil impacts by the fuel pellets would result in no further comminution of the pellets. In the 0.05 time fraction where the impact involves rocks or other hard surfaces, generation of particles upon impact would result. As no studies of bare LWRHU fuel impacts have been performed, it was assumed that the particulate spectrum is identical to other similar velocity impacts (Appendix H).

   It should be pointed out that the chance of five fuel pellets striking a surface which would comminute those pellets is the most probable assuming random partitioning. Other values are possible, of course. The probability of all 95 randomly striking a rock surface would be $(0.05)^{95}$ or in the order of 10^{-124}.

C. Zone C - At reentry angles from 20 to 40 degrees, the aeroshell 100% ablation value is reached so late in the heat pulse that the clad does not receive sufficient energy to melt. Therefore, the unfailed clad impacts the Earth's surface at a velocity of 49 m/s but only 2% of the time. This velocity is insufficient to cause clad failure and release of plutonia (see Appendix H).

D. Zone D - Over the region 40 to 90 degrees, the steep reentry does not fail the aeroshell nor melt the clad (Appendix G). Therefore, the integral LWRHU will impact the Earth's surface with no resultant clad breaches and no release of plutonia to the environment.

In summary, this event provides the only scenario severe enough to promote the release of plutonia, based upon the analyses and tests documented in the Appendixes which immediately follow this section.

The long-term consequences of released fuel are considered in the Volume III Nuclear Risk Analysis Document.

4.0 LONG-TERM CONSIDERATIONS

The FASTs described in the previous sections all terminated at the point where the LWRHU finally came to rest or was dispersed. Obviously there can be subsequent long-term potentials for releases should the LWRHUs not be recovered (which is likely!). Appendix I addresses this point and concludes that the releases from unfailed clads are negligible and these are not considered as releases in this study.

5.0 REFERENCES

1. Verbal Presentation, C. T. Bradshaw, Valley Forge, Pennsylvania (January 23, 1985).

2. Private Communication, C. T. Bradshaw/E. W. Johnson, March 29, 1988.

3. Space Shuttle Data for Planetary Mission Radioisotope Thermoelectric Generator (RTG) Safety Analysis, NSTS-08116.

4. Telecon, E. W. Johnson/Eugene Shoemaker, August 23, 1988.

APPENDIX A: ACCIDENT DEFINITION
APPENDIX B: ACCIDENT ENVIRONMENTS

(These two required appendixes have been combined to provide continuity in this FSAR.)

1.0 INTRODUCTION

The body of the Accident Model Document addressed the overall rationale and consequences should LWRHUs be subjected to the various accident environments which could result should the shuttle or spacecraft encounter malfunctions. These assessments combined the probabilities for the defined accident condition with the released quantity (if any) of plutonia fuel. In these appendixes, the response(s) of the LWRHUs to the various failure-generated environments will be addressed.

The potential accidents as a function of phase and initiating event were presented earlier in Section 3.1 and shown in a tabular manner in Table II-2.

2.0 ENVIRONMENTS

Appendixes C through I include analyses and test data assessment to evaluate the behavior of LWRHUs in response to the various events. These are broken down by defined appendixes in Table II-1 and are briefly described as follows:

C. LWRHU Response to Explosions - Cryogenic propellant and compressed gas containers can result in shock overpressure environments which could adversely affect LWRHUs.

D. LWRHU Response to Fragments/Projectiles - Fragments may be generated by SRB failure, by intervening material being accelerated by a cryogenic propellant explosion or by rupturing gas vessel walls. As the debris has a wide range of areal density and velocity, the response of an LWRHU to this accident category will also be quite varied.

E. LWRHU Response to Propellant Fires - Fireballs and fires of both cryogenic and solid rocket fuels origin can produce thermal environments of a severity which dictates that LWRHUs likely to encounter them be assessed as to their viability in those environments.

F. Spacecraft Reentry Breakup Analysis - The point at which LWRHUs are released from the spacecraft structure in the event of an accidental reentry is another defined response for these plutonia-containing devices.

G. LWRHU Reentry Response - Upon approaching orbit, on orbit, or in the event of a VEEGA malfunction, LWRHUs could be subjected to aerothermal heating environments of varying severities. The response of an LWRHU as a function of reentry angle, velocity, orientation, etc., is addressed for orbital and VEEGA reentries.

H. Impact Test Program Results - The encounter with Earth's surface, either as a bare clad or as an integral LWRHU, is addressed in this Appendix.

I. Burial Thermal Analysis - This one-page assessment of a worst-case earth burial of an LWRHU addresses this requirement.

The last defined Appendix (J) is titled "Source Term Evaluation". As the FASTs in the body of the AMD identify only high altitude vapor and Earth surface pellet or particle releases, this will be a very brief summary appendix. Appendix L is included in an attempt to provide some range of uncertainties to the numerical results given in the previous appendixes.

APPENDIX C

LWRHU RESPONSE TO EXPLOSIONS

1.0 LWRHU ANALYSES AND TESTS

The LWRHU response to the overpressure is that, in general, the aeroshell will be stripped from the clad at overpressures >3.9 MPa (570 psi) for end-on and >5.5 MPa (800 psi) for side-on orientation of the assembly with respect to overpressure direction (Reference 1). Large overpressure conditions per se do not fail the clad. Some slight deformation was noted on clads from assemblies tested to 12.75 MPa (1850 psi) (Reference 2).

The method used to calculate these two estimated failure thresholds is given in Teledyne Energy Systems Report No. TES-3203, F. A. Schumann, June 3, 1985 (Reference 1). Dr. Schumann employed the following methodology:

1. Define pressure-time characteristics on the aeroshell on the two orientations.

2. Determine the response amplification or maximum dynamic load factor (a function of pulse shape and duration and aeroshell period).

3. Compare the pressure-stress relationship with material capability and thus the initiation of fractures.

4. Associate this with the static overpressure that would result in failure initiation.

The two failure threshold values were 3.9 MPa (570 psi) for a shock wave impinging upon the closed end of the LWRHU aeroshell and 5.5 MPa (800 psi) for the aeroshell being struck side-on with the shock.

After this analysis was performed, two LWRHU test assemblies were subjected to a 429 psi/2.96 MPa overpressure and 2.1 psi s/15.4 kPa s static impulse test performed by LANL. The results (Reference 3) verify that this analysis has credence (even though slightly lower than the desired overpressure level) in that damage to the two LWRHUs in the test was minimal. Figure C-1 illustrates the conditions of the "end-on" exposed assembly (LRF-131, on the left-hand side of the three photomacrographs in Figure C-1) and the "side-on" item (LRF-167, to the right of LRF-131 in the three pictures). Although some pyrolytic graphite insulation breakup is noted (especially on the inner sleeve in LRF-167), the material did not move physically from its intended location during the test exposure.

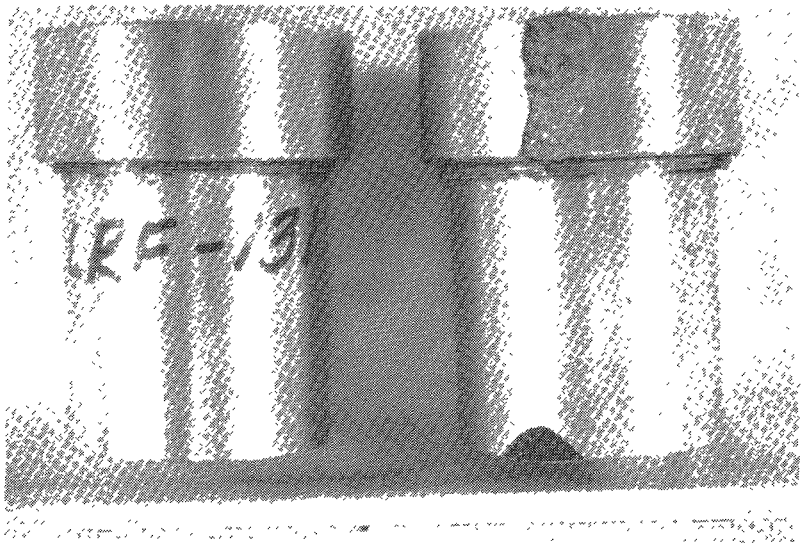

As-tested cans,
side view.

1.3X

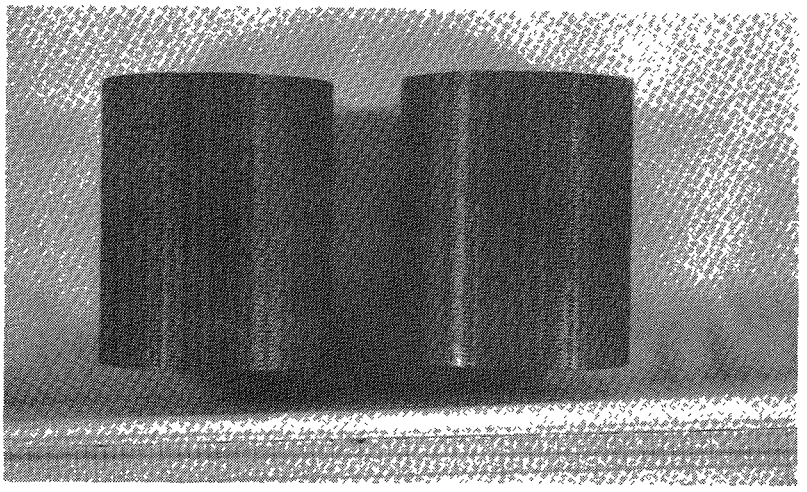

As-removed aeroshells

1.3X

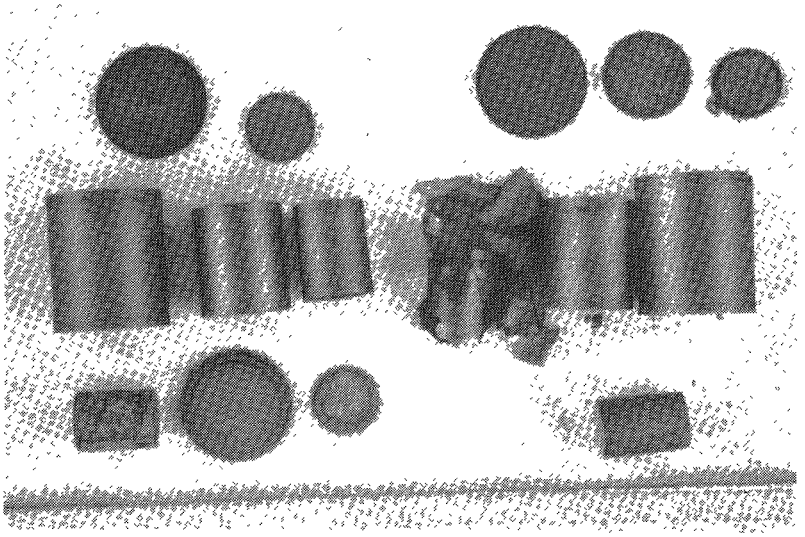

Disassembled internals

0.9X

FIGURE C-1: Disassembly stages of LRF-131 (end-on) and LRF-167 (side-on) 2.96 MPa overpressure test analyses (small Divisions = mm).

The significantly greater inner sleeve damage in LRF-167 is quite likely due to the hits incurred sometime during the test; these are evident on the can in the top photograph.

2.0 ET PROPELLANT EXPLOSION SCENARIOS

NASA, in Reference 4, has defined the parameters associated with hypothetical explosion environments which could be encountered by radioisotope heat sources aboard the space shuttle. These parameters are defined in Section 4.0 of Reference 4 and are summarized as follows:

A. Static Overpressure, MPa, abbreviated as ΔP_s,
B. Static Overpressure Impulse, kPa·s, abbreviated as I_s,
C. Dynamic Pressure, MPa, abbreviated as P_D
D. Peak Reflected Pressure, MPa, abbreviated as P_R, and
E. Dynamic Pressure Impulse, kPa·s, abbreviated as I_D.

2.1 On-Pad (SRB Failure Initiated or Tower Impact)

A hypothetical condition has been defined by NASA (Reference 4, Section 4) whereby ET propellant (liquid oxygen/liquid hydrogen or LOX/LH_2) would spill, collect on the MLP or flame trench, become mixed and subsequently explode. The location of the RTGs (and the assumed location of the LWRHUs) above the surface of this mixed propellant pool during a normal launch is shown in Figure C-2.

The initiating event for this sort of accident assumes an SRB failure which grossly fails the ET or that the ET comes into contact with the tower and suffers a gross rupture. Either will result in the rapid release of cryogenic propellants, mixing of these propellants as they fall onto the MLP or flame trench, and then exploding.

Tables 4.1 and 4.2 of Reference 4 provide the levels of variables (overpressures and impulses) at various distances from the surface of the pools. Table C-1 lists only the most severe defined cases as a function of height above the pool surface. As the LWRHU has been tested and shown to remain essentially intact at static overpressures greater than those listed, the LWRHU aeroshell will remain intact about the clad for subsequent accident environments which could be encountered.

2.2 ET Propellant Aft Compartment

It is conceivable that the cryogenic propellant feed lines from the ET to the SSMEs could rupture due to a smaller explosion, and the LOX/LH_2 collect in the aft (engine) area of the orbiter and mix in a scenario not unlike that described in 2.1 above. As the amount of liquid which could collect there is limited, the resulting blast levels are less as can be noted in the third part of Table C-1.

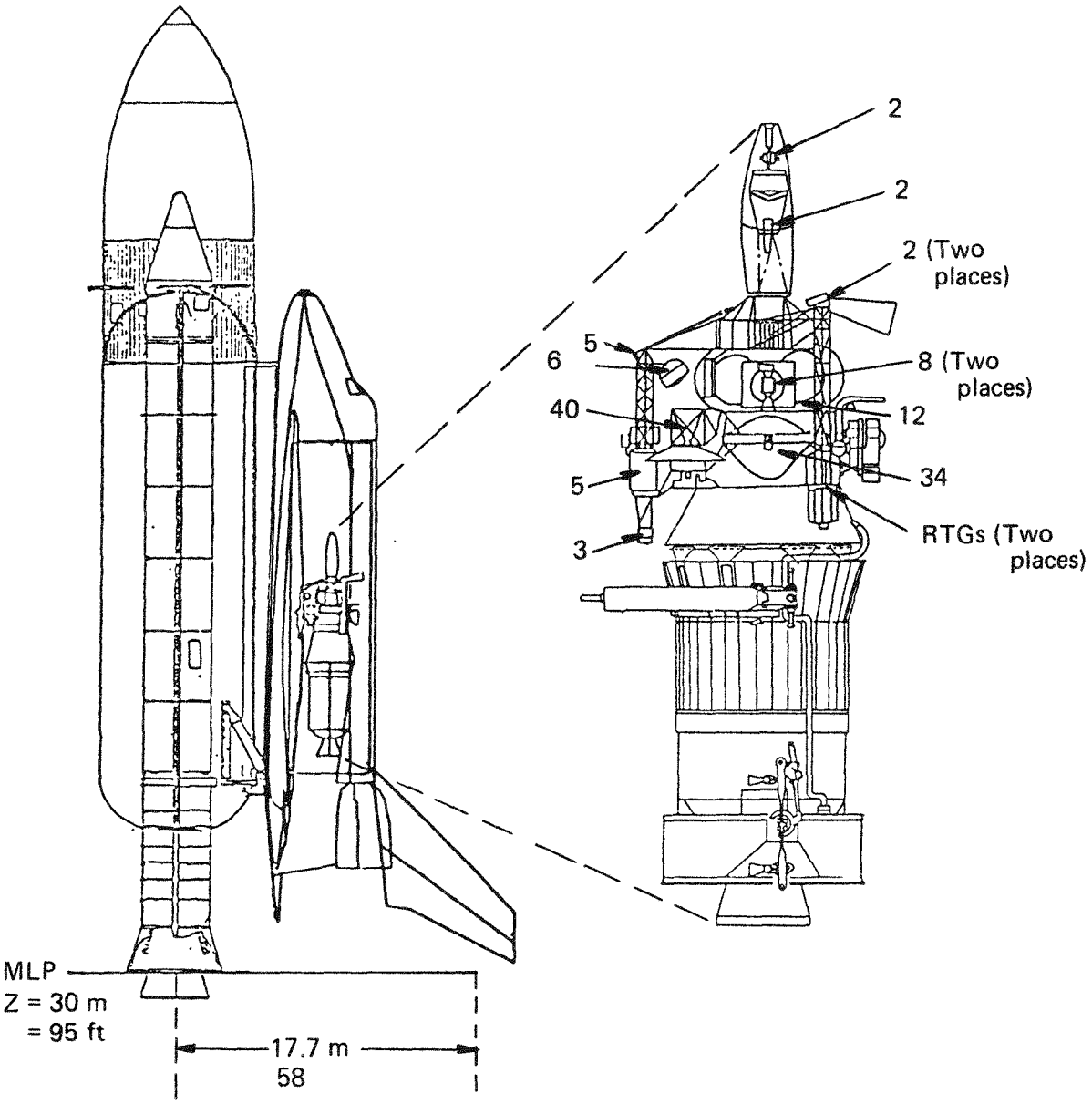

FIGURE C-2: The T=0 configuration for the Galileo Spacecraft, MLP, pad and flame trench.

Table C-1: Worst-case (0.1 percentile) blast levels for MLP, trench and aft compartment explosions

HEIGHT (m)	PS (MPa)	P_D (MPa)	P_R (MPa)	I_s (kPa·s)	I_D (kPa·s)
		MLP EXPLOSIONS, 0.1 PERCENTILE			
6.1	2.41	3.61	16.60	12.6	4.1
9.1	2.22	3.48	15.09	12.8	5.7
12.2	1.40	2.19	8.61	13.3	4.8
16.8	1.06	1.50	6.12	10.7	5.0
21.3	0.89	1.38	4.89	11.9	5.2
30.5	0.63	0.81	3.18	10.6	5.4
		TRENCH EXPLOSIONS, 0.1 PERCENTILE			
33.5	1.12	1.63	6.57	28.9	10.7
39.6	1.03	1.59	5.86	37.4	20.7
45.7	0.94	1.59	5.13	35.2	18.3
61.0	0.85	1.29	5.65	31.7	14.5
88.4	0.60	0.76	2.96	27.2	15.0
		AFT COMPARTMENT EXPLOSION, 0.1 PERCENTILE			
6.1	1.21	2.05	7.17	4.6	2.0
9.1	0.81	1.19	4.32	4.2	2.1
12.2	0.61	0.83	3.00	4.1	2.1
16.8	0.58	0.77	2.82	3.7	2.7

The low overpressure levels would not fail the LWRHU aeroshells nor would the low impulses generate a velocity sufficient to fail a LWRHU even if it hit the tower (possible only in the first few seconds).

2.3 ET Propellant In-Flight

A massive structural failure of the ET during flight (similar to Challenger 51-L) can result in a mid-air detonation of the released and mixed cryogenic propellants. As may be noted in Table C-2, these blast levels are not sufficient to cause clad nor aeroshell failure. It should be noted that these values are valid for only 10 s < time < 30 s. For METs 30 s < Time < MECO, the threat of a cryogenic explosion at these high altitudes is "considered to be nil" per Reference 4, Section 4.2.2.

2.4 Other Explosions

Reference 4 in Section 4.3 identifies a number of in-bay explosions which could occur as the result of a fire or crash. Those significant items are:

a. Orbital Maneuvering Subsystem (OMS) contains monomethyl hydrazine (MMH) at nominally 1.94 MPa.

b. Galileo Retropropulsion Module (RPM) contains MMH at 2.07 MPa (but only 0.34 at launch).

c. The IUS contains a tank of hydrazine (2.86 MPa) for the Reaction Control Subsystem (RCS).

d. The Galileo RPM also has two helium tanks at 19.7 MPa internal pressure.

e. The Power Reactants Storage and Distribution Subsystem (PRSDS) has 355 kg of LOX <7.24 MPa and 42 kg of LH_2 < 2.31 MPa.

The explosion variables presented by these various events are presented in Table C-2 (middle set). These levels are considerably lower than the minimum value to remove the aeroshell (3.93 MPa static overpressure) so the LWRHU will not be damaged other than pyrolytic graphite break-up and minor distortion. The velocity imparted to a LWRHU will also be low (worst case is the PRSDS event which would result in an LWRHU velocity of 54 m/s) so secondary impacts or other events would not result in clad failure or fuel release.

Table C-2: Summary of vapor cloud and major shuttle bay explosions.

IN-FLIGHT ET EXPLOSIONS, 10s < MET < 30s (TABLE 4.4, REFERENCE 4)

DISTANCE FROM COE, m	PS (MPa)	P_D (MPa)	P_R (MPa)	I_s (kPa·s)	I_D (kPa·s)
80.2	2.05	0.84	13.73	22.3	11.0
80.8	1.81	0.98	11.82	22.2	11.7
88.7	0.94	1.25	5.23	17.2	11.5
120.7	0.43	0.42	1.96	10.2	9.9

OTHER EXPLOSION SOURCES (LAST COLUMN = SOURCE)

	(kPa)	(kPa)	(kPa)	(Pa·s)	(Pa·s)	
8.81	20.7	1.45	146	44	2	OMS
1.58	31.0	3.24	166	13	1	RPM (MMH)
2.44	36.5	4.48	185	25	2	IUS (N_2H_4)
1.86	97.9	29.6	377	41	9	RPM (He)
7.10	951	215	5350	2480	6205	PRSDS

CRASH-LANDING PRSDS EXPLOSION ENVIRONMENT

	(MPa)	(MPa)	(MPa)	(kPa·s)	(kPa·s)
--	2.05	0.84	13.73	22.3	11.0

A crash of the orbiter could result in an added condition of a spill/mixed PRSDS propellant explosion. This event would have properties similar to the in-cloud vapor explosion; these variables are given in the final portion of Table C-2. This explosion level would result in the LWRHU exiting the area with a velocity of 394 m/s (1290 ft/s). This seems unlikely as the propellant available is only 42 kg LH_2 and 355 kg LOX.

3.0 LWRHU VELOCITIES AS A RESULT OF EXPLOSIONS

The velocity of an isolated LWRHU upon the passing of an explosion front can be calculated by using techniques described in Reference 5. The first task is to determine the duration of the static overpressure pulse via Equation 4 and the behavior of this parameter (P_s) as a function of time, t(plotting or use of Equation 5). Equations 6 and 7 are used to determine ρ_g (gas phase density in the passing of the shock wave) and V_g(the overpressure front velocity). For this case, assuming that γ= 1.40, ρo = 1.205 kg/m^3, a_o = 335 m/s, and P_o = 0.101 MPa, then:

$$\rho_g = \frac{2\gamma P_o + (\gamma+1) P_s}{2\gamma P_o + (\gamma-1) P_s} \cdot \rho_o = \left\{\frac{1 + 8.486\ P_s}{1 + 1.414\ P_s}\right\} \quad 1.205 \text{ kg/m}^3$$

$$\text{and } V_g = a_o P_s \left\{\frac{2}{\gamma P_o [(\gamma+1) P_s + 2\gamma P_o]}\right\}^{\frac{1}{2}} = 335\ P_s\ [0.020\ (8.486 P_s + 1)]^{-\frac{1}{2}} \text{ m/s}$$

By choosing small time increments, once can numerically integrate Equation 2 in Reference 5:

$$V - V_o = \frac{1}{2} \frac{C_D A}{m} \int_o^t \rho_g\ (V_g - V)^2\ dt,$$

and for small (0.0005 s) time intervals

$$V - V_o \sim 5.95 \times 10^{-6}\ \rho_g\ (V_g - V)^2$$

where V = LWRHU velocity at the end of the time increment,
V_o = LWRHU velocity at end of previous time increment, and
$m/C_D A$ = ballistic coefficient for LWRHU (42.0 kg m^{-2}).

The calculations were performed using LOTUS 123 software, the equations are as below:

B7: (F3) [W15] +H$7*D7*(C7-E7)^2,

C7: (F3) [W15] 335*A7*@SQRT(1/(0.02* (8.487*A7+1)))

D7: (F3) [W15] 1.205* ((1+8.487*A7)/(1+1.414*A7)), and

E7: (F2) [W15] ((2*H$7*D7*C7+1)

-+@SQRT((2*H$7*D7*C7+1)^2-4*H$7*D7*(H$7*D7C7^2+B6)))/(2*H$7*D7)

In the above, A7 = P_s, B7 = V-V_o, C7 = V_g, D7 = ρ_g, and E7 = V.

4.0 RESULTS AND CONCLUSIONS

4.1 Aeroshell Integrity

Based upon previous analysis and experiments, the aeroshell will not fail during any of the defined explosions which could be encountered during a shuttle mission. A summary plot of the shapes of the various overpressure histories illustrates that the expected environments are well below the calculated failure threshold and LANL tested values (Figure C-3).

4.2 LWRHU Velocity

Velocities imparted to an unfailed LWRHU as shown in Figure C-4 for the nearest defined distances for the MLP, trench and aft compartment explosions are shown as a function of the conditional probability for that resultant velocity. These values will be used in the following appendixes to assess impact and fragment encounter scenarios.

5.0 REFERENCE

1. Schumann, F. A., Study of the Blast Overpressure Capability for the RHU Heat Shield, TES-3203, Teledyne Energy Systems (June 3, 1985).

2. Tate, R. E., and Land, C. C., Environmental Safety Analysis Tests on the Light-Weight Radioisotope Heater Unit, LA-10352-MS, Los Alamos National Laboratory (May 1985).

3. Informal MRC Report, Letter, E. W. Johnson/G. L. Bennett, August 8, 1985.

4. Space Shuttle Data for Planetary Mission Radioisotope Thermoelectric Generator (RTG) Safety Analysis, NSTS 08116.

5. Hill, D., Subroutine "DIVEL" to Estimate the Velocity Imported to a Projectile by the Dynamic Component of a Blast Wave, GE-PIR-6779 (April 7, 1988).

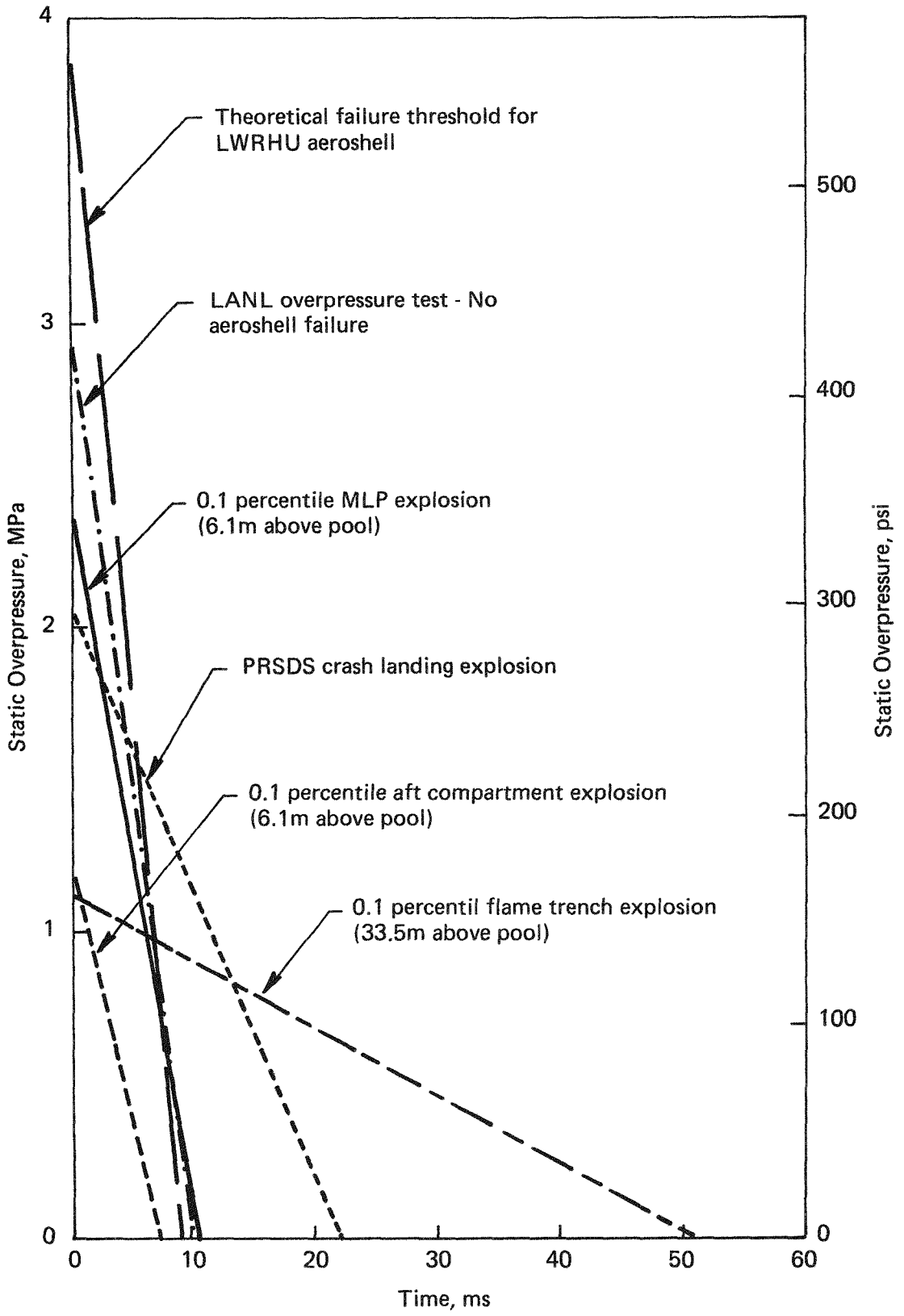

Figure C-3: Overpressure-time curves are shown above for the various defined scenarios and from the test and analyses performed on hardware.

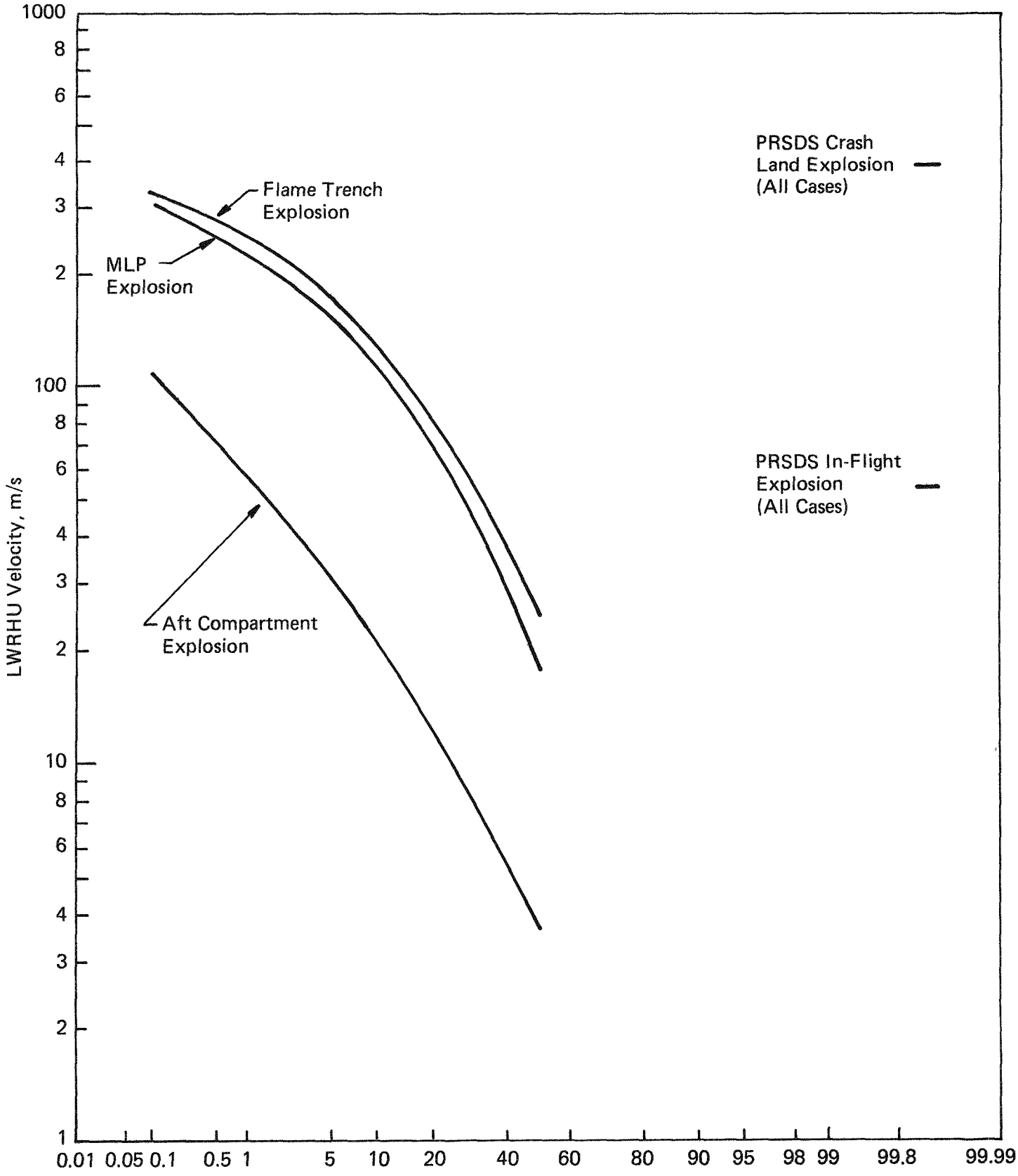

Figure C-4: LWRHU velocities as a function of explosion level probability are given above for the three variable level events plus the two PRSDS events which are the "worst case" one-time environments.

APPENDIX D

LWRHU RESPONSE TO FRAGMENTS AND PROJECTILES

1.0 INTRODUCTION

Potential propellant explosions or structural failure of those bodies that have elevated internal pressures can result in the generation of a variety of high velocity debris which could encounter LWRHUs aboard the Galileo spacecraft. Reference 1 (NSTS 08116) cites the various sources of these moving structures and provides data regarding areal density, velocity, rotation, direction, etc. These fragment sources are summarized as follows:

A. SRB fragments, including case pieces, joint fragments and clevis pins,

B. Fragments generated as a result of the explosion of the ET contents,

C. Aerodynamic breakup, and

D. Other pressurized structures.

This appendix will address the consequences of these fragments or projectiles striking an LWRHU.

2.0 TEST DATA

Throughout the LWRHU development and production programs, testing of impact characteristics has been performed. Post-production special engineering tests were also done to address changing guidelines as to environmental severity or type of encounters which could be expected to occur. The relevant test conditions and results are summarized in Sections 2.1 and 2.2.

2.1 Intact LWRHU

2.1.1 SRB Fragments

Three LWRHU engineering test items were subjected to SRB fragment impact performed by LANL. Two of the numerous sled tests performed at SNLA involved LWRHU test items; Table D-1 provides the testing variables and summarizes the test article condition.

Test LFT-ENG-2 (117 m/s SRB fragment velocity) caused aeroshell deformation and breakup, but the FWPF remained about their clads (Figures D-1 and D-2). The clads were deformed, but no metal failures were noted nor was any urania found outside the clads.

Test LFT-2 (212 m/s SRB fragment velocity) resulted in the fuel clad being removed from the housing and graphite (Figures D-4 and D-5). The clad was undoubtedly released at impact and traveled about 26 m thereafter, sustaining a few abrasions during this time but no release of the urania fuel simulant.

TABLE D-1: LWRHU-SRB FRAGMENT IMPACT DETAILS

CLAD NUMBER	130	131	366
TEST NUMBER	LFT-ENG-2	LFT-ENG-2	LFT-2
DATE RUN	2-10-88	2-10-88	5-18-88
SRB PLATE SIZE WEIGHT MATERIAL	1.42 m x 1.42 m x 13 mm D-6 ac STEEL	1.42 m x 1.42 m x 13 mm D-6 ac STEEL	1.42 m x 1.42 m x 12 mm D-6 ac STEEL
VELOCITY	117 m/s	117 m/s	212 m/s
TEMPERATURE	15°C	15°C	20°C
ORIENTATION	90° (SIDE ON)	45°	90° (SIDE ON)
EXTERNAL VIEWS	SEE FIGURE D-1	SEE FIGURE D-2	SEE FIGURE D-4
CLAD CONDITION	SEE FIGURE D-3	SEE FIGURE D-3	SEE FIGURE D-5
CLAD DISTORTION*	1.107	1.046	1.214

*Maximum diameter divided by minimum diameter after impact (average of three determinations at three locations along the clad length).

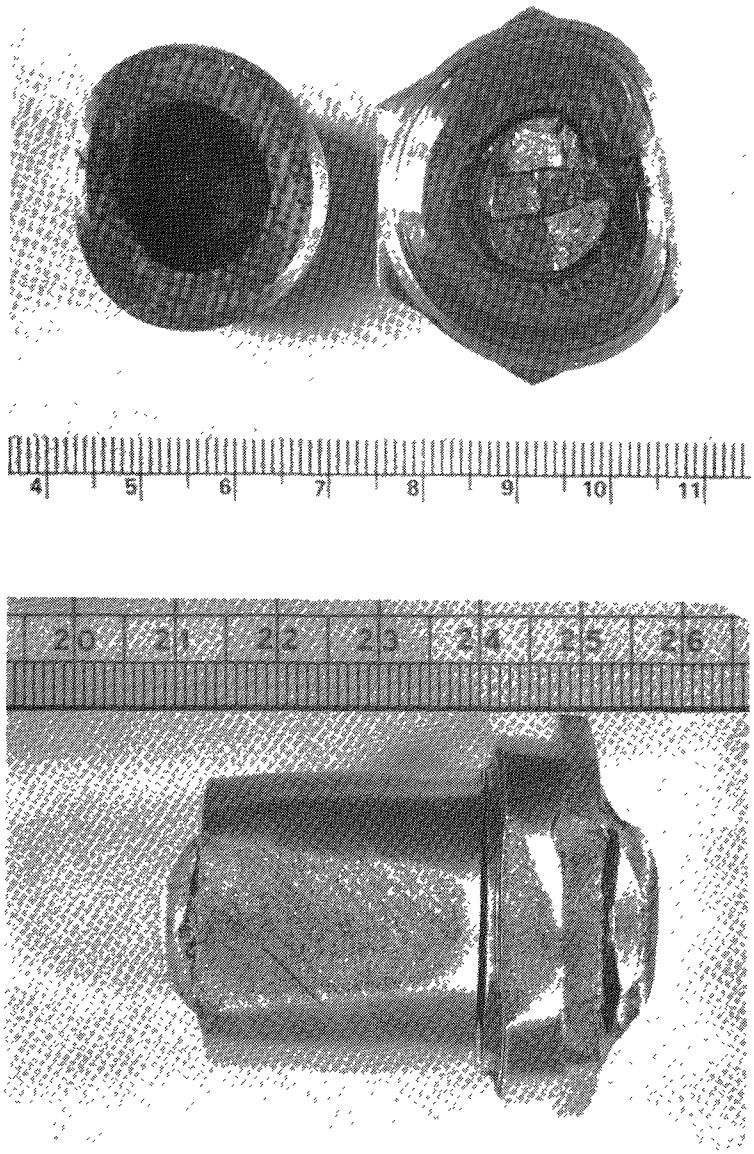

Figure D-1: The 117 m/s SRB fragment impact at 90° did not release the LWRHU components from the can (small divisions = mm).

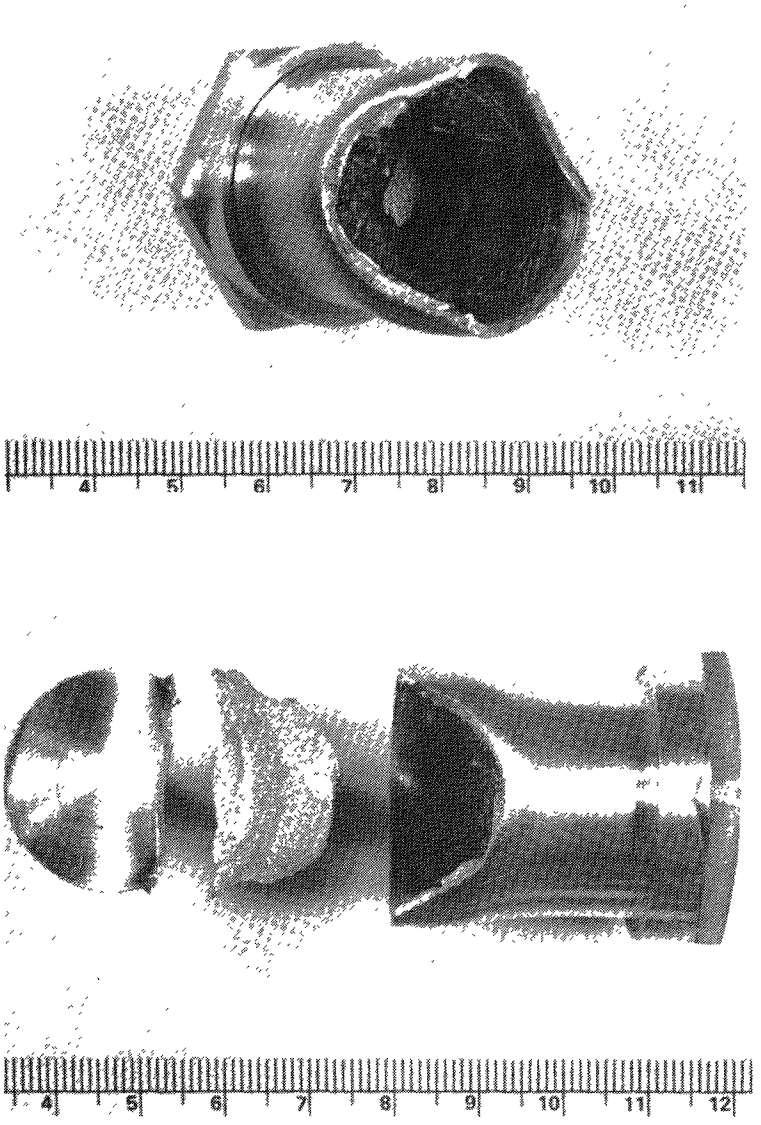

Figure D-2: The 117 m/s SRB fragment on the LWRHU that was oriented at 45° resulted in more can and graphite damage (small divisions = mm).

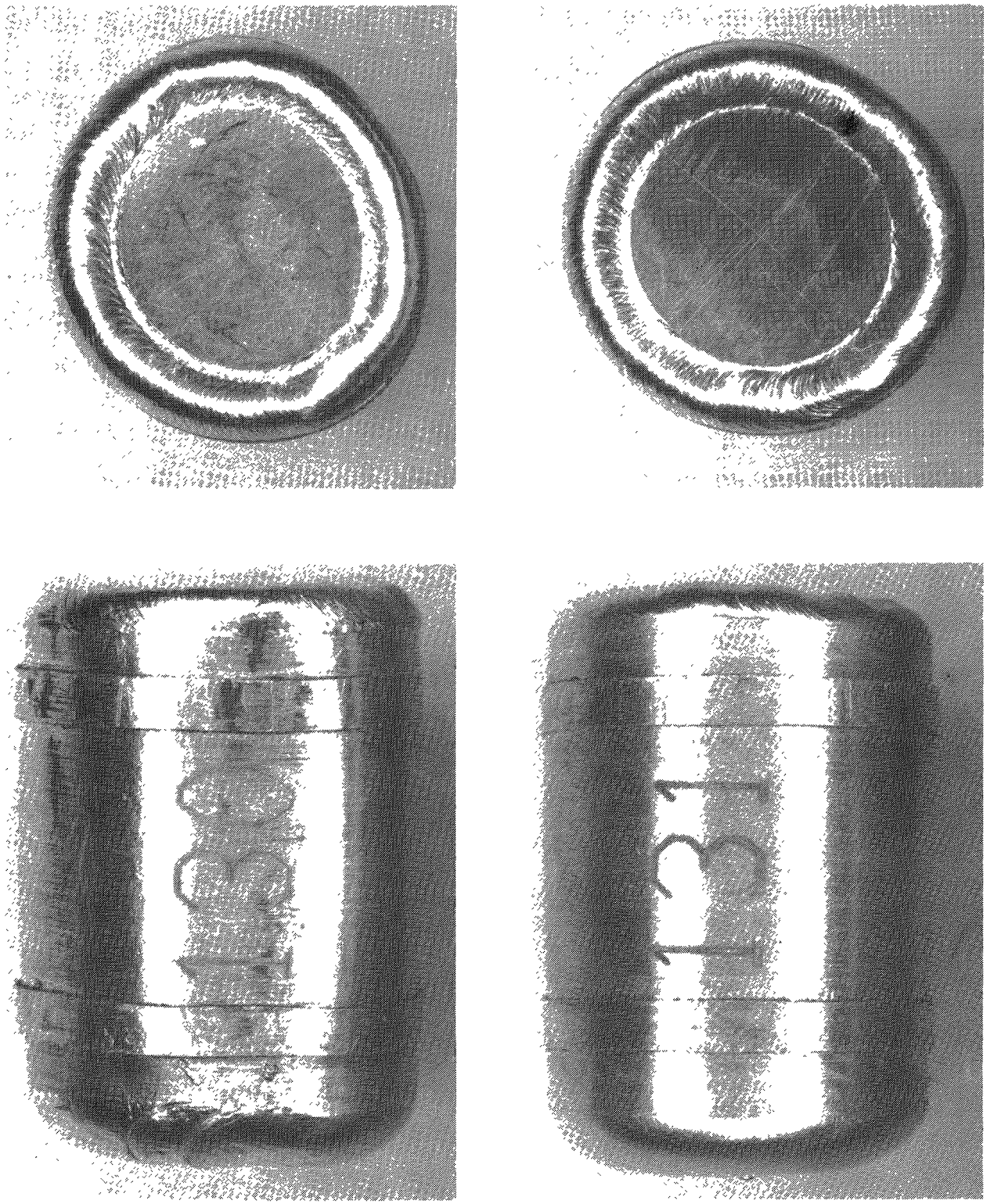

Figure D-3: Minimal distortion was noted in the two LWRHU Clads that were hit at 117 m/s by the SRB plate (divisions = mm).

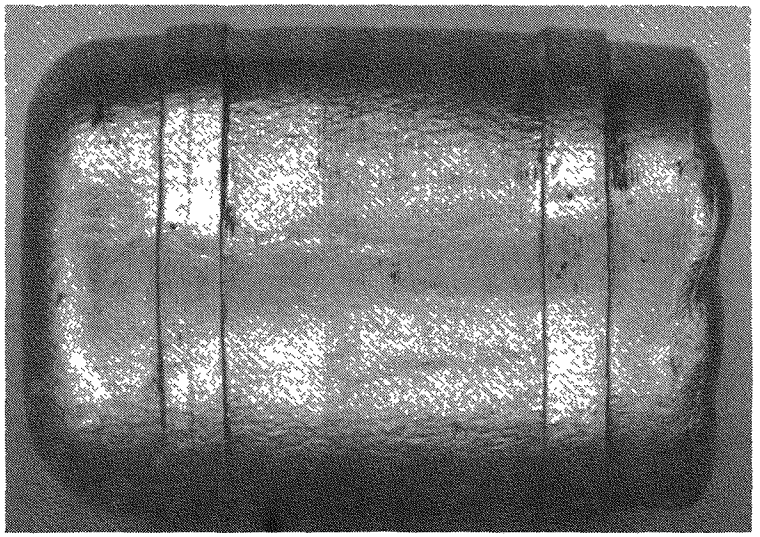

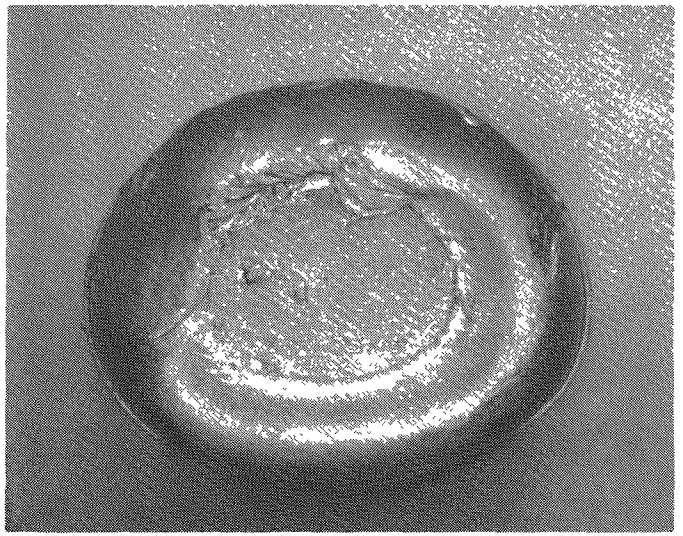

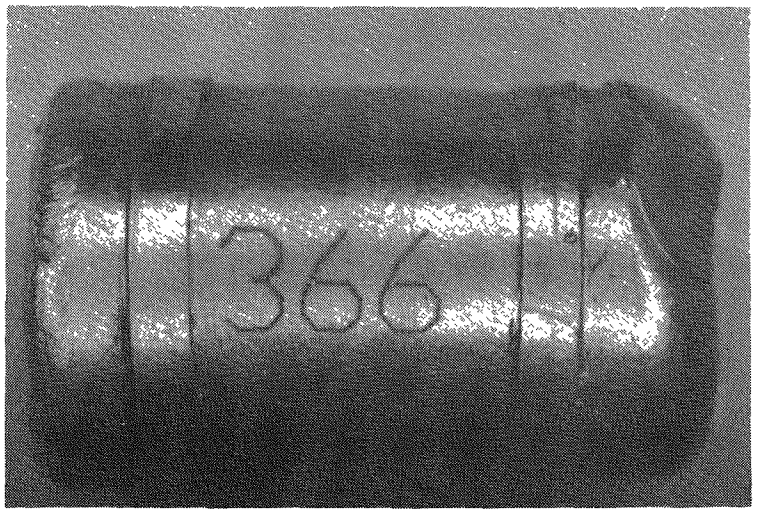

Figure D-4: LWRHU Clad 366 after being subjected to the 212 m/s SRB fragment impact test, 90° (side-on) orientation, fully-assembled LWRHU test item (divisions = mm):
Upper Left: Impact Face
Left: Side View (90° to Impact Face)
Above: End-on View

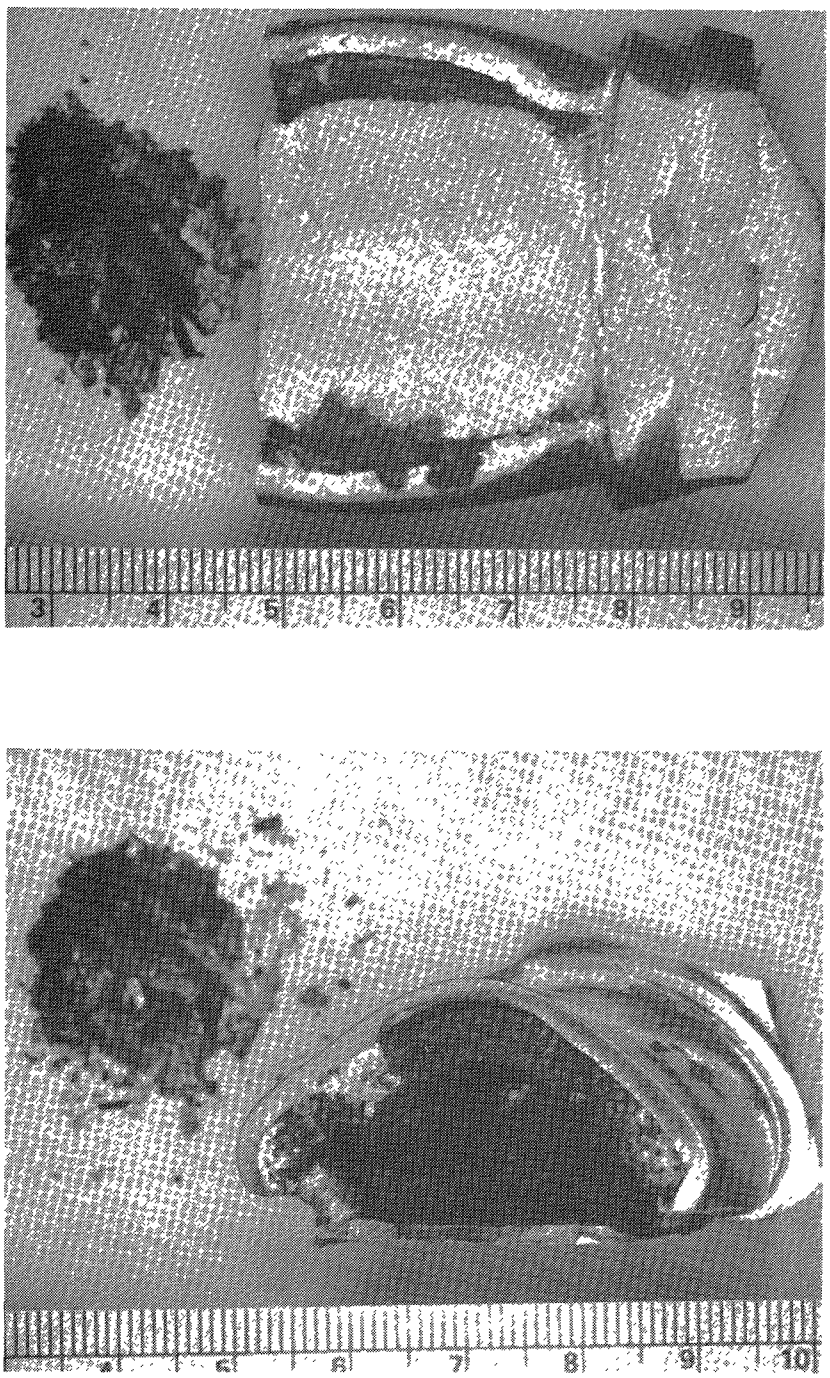

Figure D-5: The aluminum housing containing Clad 366 was considerably deformed and failed after being struck by the 212 m/s SRB fragment. Debris to the left is remains of the PG Sleeves; numbers are one cm apart.

2.1.2 Bullet-like Fragments

LANL, in Reference 2, performed a number of tests whereby 18 g Al 2219-T87 slugs, 13 mm diameter by 50 mm long, were fired point blank into test LWRHUs (urania fueled) positioned in a simulated magnetometer ring. The results of these tests are summarized as follows:

LWRHU NUMBER	BULLET VELOCITY, m/s	RESULTS
009	289	Clad deformed, not breached
005	661	Clad deformed, not breached
008	773	Unit not hit
018	775	Clad not recovered, no U found
169	757	Clad deformed, not breached
003	940	Clad failed, U by chemistry
013	908	Clad failed, U by chemistry

From these data, an LWRHU will withstand bullet-type hits of up to 775 m/s with no plutonia release. Above this velocity, failure and fuel release would occur.

2.1.3 Normal LWRHU Impacts

Plutonia-fueled LWRHUs were impact-tested at post re-entry terminal velocity by LANL. Appendix H describes those tests and the results. In summary, 49 m/s against an essentially unyielding surface at varying impact angles does not fail the clad nor release fuel.

2.2 Bare LWRHU Clad

Studies performed show that the only case where a free clad would exist is after an encounter with a high velocity SRB fragment which could remove the protective graphites. Tests delineating LWRHU clad responses to impacts are given below.

2.2.1 Flat-on (90°) Tests

LANL (Reference 3) performed some engineering impact tests using bare clads impinging upon a flat steel surface. Although significant distortions were noted, impacts at 48, 105, and 128 m/s did not result in clad failure nor fuel release.

2.2.2 Aluminum Flyer Plates

MRC (Reference 4) performed flat-on and 45° impacts of bare LWRHU clads with 6061 aluminum flyer plates 3.7 mm thick at 1100 m/s. No failures were noted in the three specimens thus tested. These tests included secondary impacts on a heavy (11 mm thick) aluminum plate, which was the shuttle floor flyer plate reference. These three impacts at approximately 330 m/s and at various angles resulted in significant added distortion to the clads, but with no failures or release of the urania simulant fuel.

2.2.3 Heavy Steel Structure Impacts

MRC (Reference 4) also performed higher velocity impacts of bare clads on 12-mm thick structural steel plates that were designed to determine whether expected maximum velocities would result in failures or fuel release:

1. An end-on impact onto the plate, oriented perpendicular to the trajectory, resulted in the LWRHU clad being imbedded in the plate with about 2 mm protruding above the plane of the plate after a 607 m/s impact. No loose urania contamination was noted, although the clad appeared to have failed.

2. An impact on such a steel plate oriented at 45° to the flight path of the LWRHU clad (V = 593 m/s) resulted in total release of the urania simulant. This was the fifth high-velocity encounter with other materials for this test unit, however.

3.0 SRB CASE FRAGMENT IMPACTS

Many of the LWRHUs are subject to being struck by SRB case wall fragments, joint fragments and clevis pins in the case of an SRB case rupture. Reference 1 addresses the postulated SRB environment in great detail in Chapter 5. For the case of the LWRHUs, this complexity was beyond the scope of the authorized study so use was made of Tables 5.7 through 5.10 of Reference 1. These tables provide summary ranges and correction factors which are applicable to LWRHU "hits".

3.1 Geometrical Considerations

As stated above, Reference 1 defines the nature of SRB fragments, including the geometrics required in order to have an LWRHU struck by an SRB fragment. Figures D-6, D-7, and D-8 show the LWRHU-case impact cases:

Figure D-6: This sketch shows that for times less than 105 s, the eight most aft LWRHUs could be struck by case fragments from Cylinder #5. All other LWRHUs would be in the Cylinder #6 fragment field.

Figure D-7: At MET>105 s and applicable to all joint and clevis pin debris, Cylinders #5 and #6 case fragments could hit virtually any LWRHU. The #7 Cylinder case segment's potential flight path could include the RTG boom, plasma wave subsystem (PWS) and low gain antenna (LGA-2) LWRHUs.

As to joint debris, the #5/#6 field includes all except the four most forward LWRHUs; the #6/#7 field includes only these four plus the LWRHUs on the RTG boom(s).

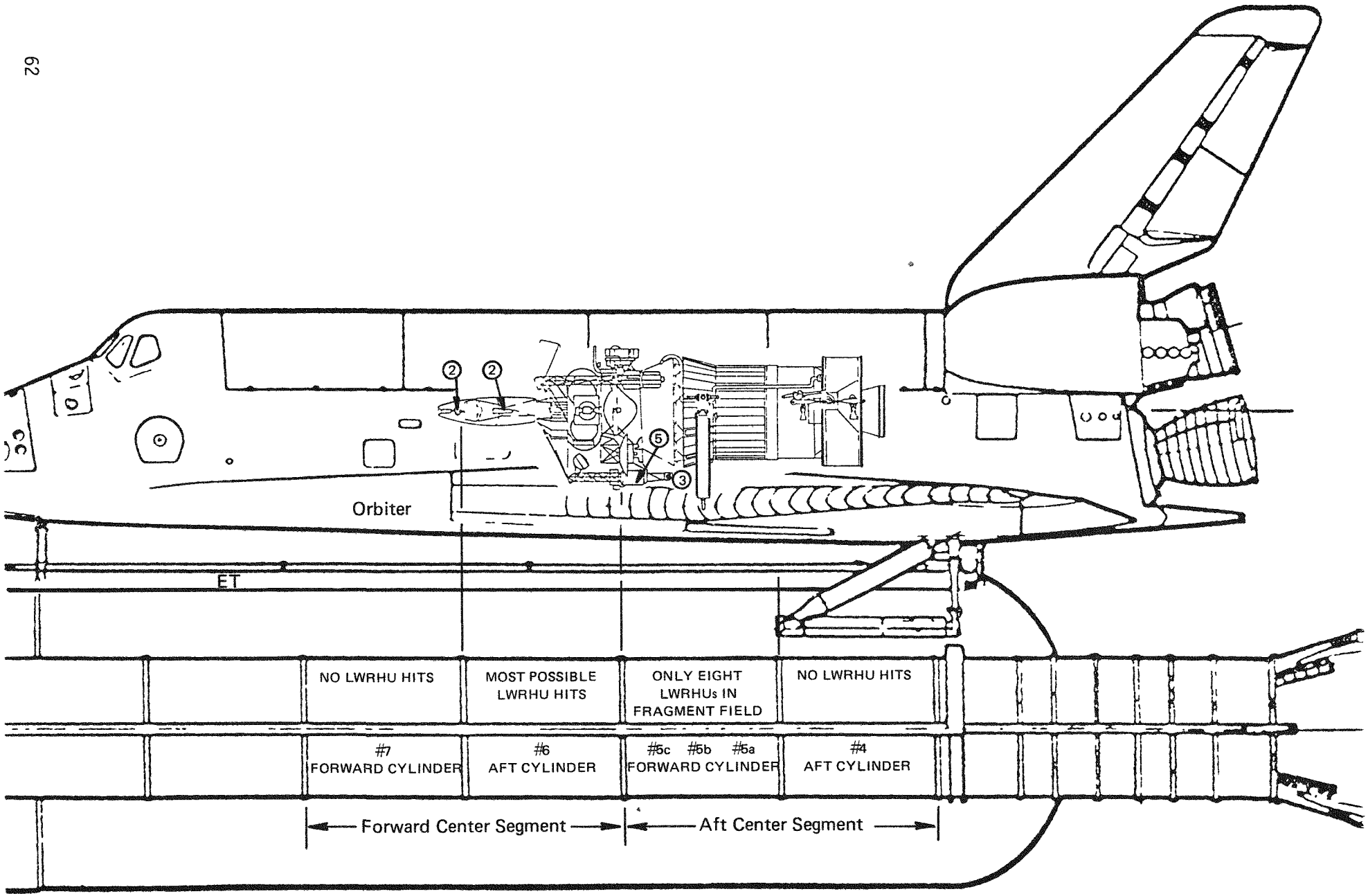

Figure D-6: At MET <105s, SRB cylinders 5 and 6 provide the fragment field for hitting LWRHUs.

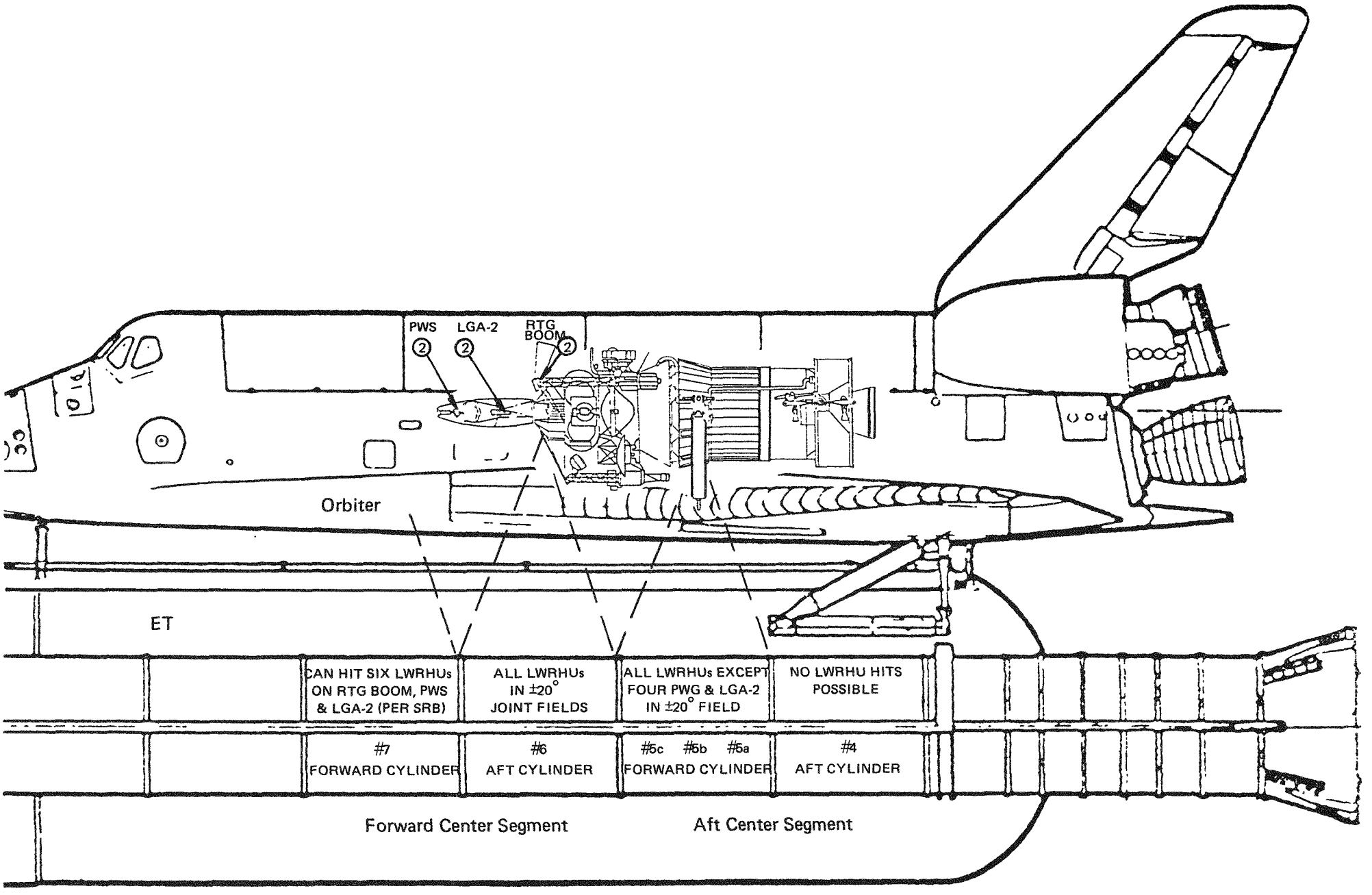

Figure D-7: SRB cylinders 5 and 6 provide most of the fragment field for LWRHUs; cylinder 7 can intercept the six most forward LWRHUs (per SRB) at MET > 105s. Possible joint and clevis pin trajections are applicable from this drawing also.

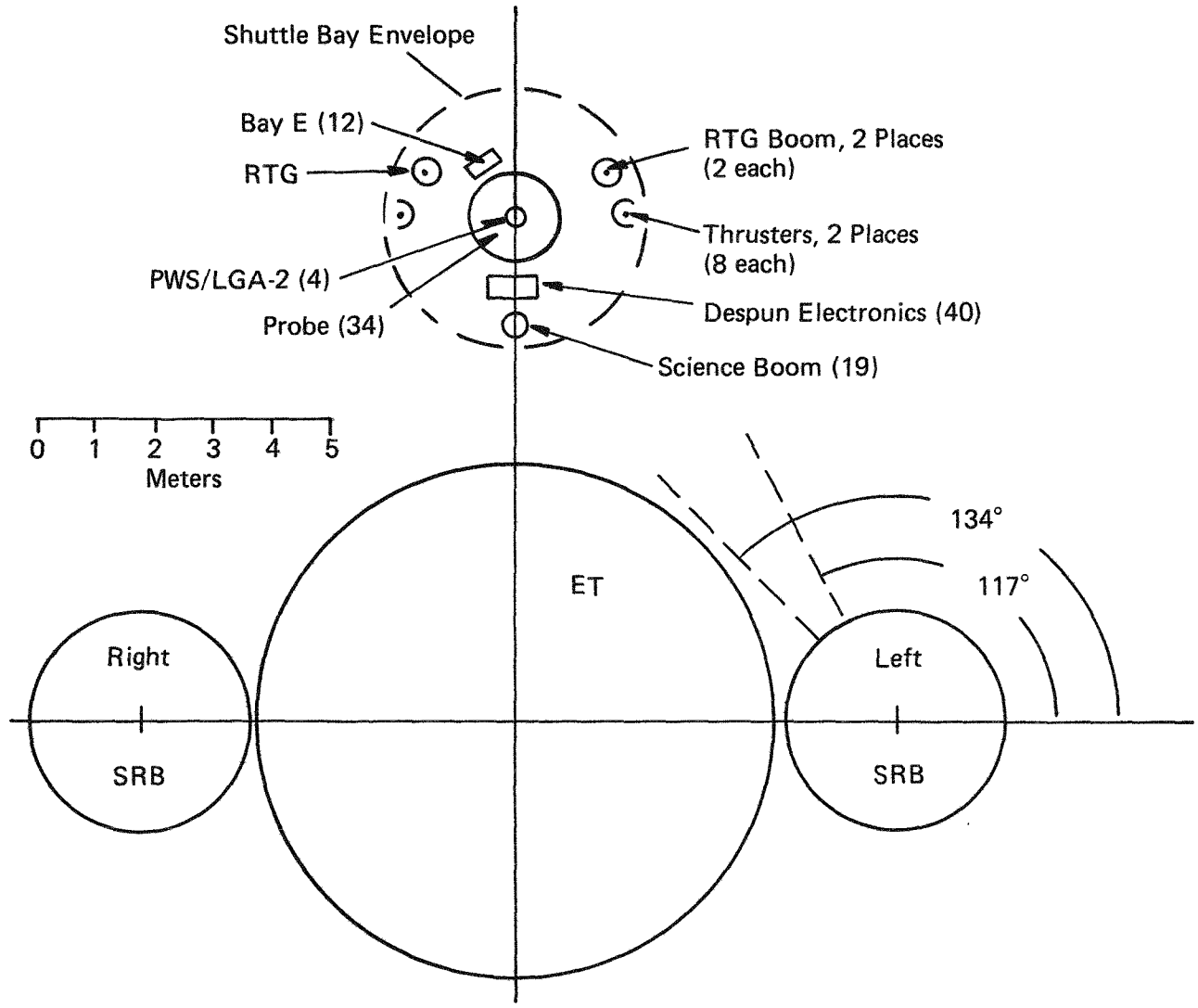

Figure D-8: The axial configuration of LWRHUs with respect to potential SRB fragment hits shows potential hit angles ranging from 117° to 134°.

Figure D-8: The arrangement of LWRHUs from an axial standpoint shows the paths that a fragment must traverse in order to hit an LWRHU. Not shown (as it varies along the length) is the fact that all paths must pass through the oribiter wing/floor structure prior to striking a LWRHU.

It is assumed that LWRHUs that are protected by intervening spacecraft structure will not be affected by fragments originating from the opposite SRB. Table D-2 gives the summary. In all cases, the massive aeroshell protection afforded by the probe makes all LWRHUs within the body immune to SRB fragment impacts.

3.2 SRB Case Impact Conditions

As indicated earlier in 3.0 above, a sophisticated assessment of populations, cross sections, and other variables was not done to assess the effect on the LWRHU of an impinging SRB fragment. Instead, the maximum velocities that are defined to be possible were calculated, hits are assumed and consequences traced from there. This is possible as the LWRHU withstands the SRB fragment environment as may be noted in Section 2.1.1 and Table D-3.

For the first 105 s, SRB fragment impacts on LWRHU(s) would result in some graphite damage and clad deformation as the defined fragment maximum velocity of 102 m/s is well below the tested velocity of 117 m/s. The LWRHU would be expelled from the shuttle bay along an approximately 125^{o} line from the failed SRB. The range could be up to a few hundred meters (depending upon the orientation, altitude and velocity of the shuttle) at low altitudes and the units would be widely dispersed should the SRB failure result in fragment hits late in the first 105 s.

For the period 105 s < MET < 120 s, the failure of any cylinder could result in fragments with velocities which could remove the protective graphites as illustrated in the 212 m/s SRB fragment test (Table D-1). This would result in a bare clad falling to earth or water from altitudes on the order of 36 km (which should allow plenty of time to reach terminal velocity prior to surface impact).

In none of these potential SRB fragment and impact scenarios is the LWRHU clad expected to fail or release plutonia to the environs based on the test information generated to define this interaction.

4.0 SRB JOINT AND CLEVIS PINS

Using methods described in Section 5.2.2.3 of Reference 1, the velocities of SRB joint fragments and clevis pins were determined. The two joints which could provide this debris to the LWRHUs are the 5/6 and 6/7 cylinder joints (See Figure D-7).

TABLE D-2: TRAJECTORIES REQUIRED FOR SRB SEGMENTS TO INTERCEPT LWRHUs ARE LISTED BELOW

RIGHT RTG BOOM (2)	117^{o}	PROTECTED
RIGHT THRUSTERS (8)	117^{o}	PROTECTED
BAY E (12)	122^{o}	PROTECTED
PWS/LGA-2 (4)	126^{o}	126^{o}
DESPUN ELECTRONICS (40)	130^{o}	130^{o}
SCIENCE BOOM (19)	134^{o}	134^{o}
LEFT THRUSTER (8)	PROTECTED	117^{o}
LEFT RTG BOOM (2)	PROTECTED	117^{o}
PROBE (34)	PROTECTED	PROTECTED

TABLE D-3: THE LAST COLUMN OF THIS TABLE GIVES THE RANGE OF THE MAXIMUM SRB FRAGMENT VELOCITIES AS A FUNCTION OF MET

MET,s	V, m/s	0.8x1.07V, m/s[a]	WITH SPIN ADD-ONS, m/s[b]
0-20	38-105	33-90	51-102
20-70	38-90	33-84	51-98
70-105	52-104	45-89	62-98
105-120	76-137*	65-117*	81-122*
	116-218+	109-205+	126-207+

*CYLINDERS #5 AND #7
+CYLINDER #6

[a]The 0.8 term is the factor for wing attenuation as all SRB case fragments must pass through the wing/floor structure of the orbiter (This is 0.88 for the final cylinder 6 value.) The term 1.07 is the maximum factor due to the assumption that the cylinder that failed is the origin of the fragment.

[b]Based on plot given in Figure D-9. It was assumed that the spin rate was reduced by 25% due to striking of intervening material in all instances. For the last line, a factor of 19.3/11.0 was used to increase the tip velocity per 5.2.2.2.c in Reference 1. Note that these are maximum velocity of centroid velocity plus fragment tip velocity.

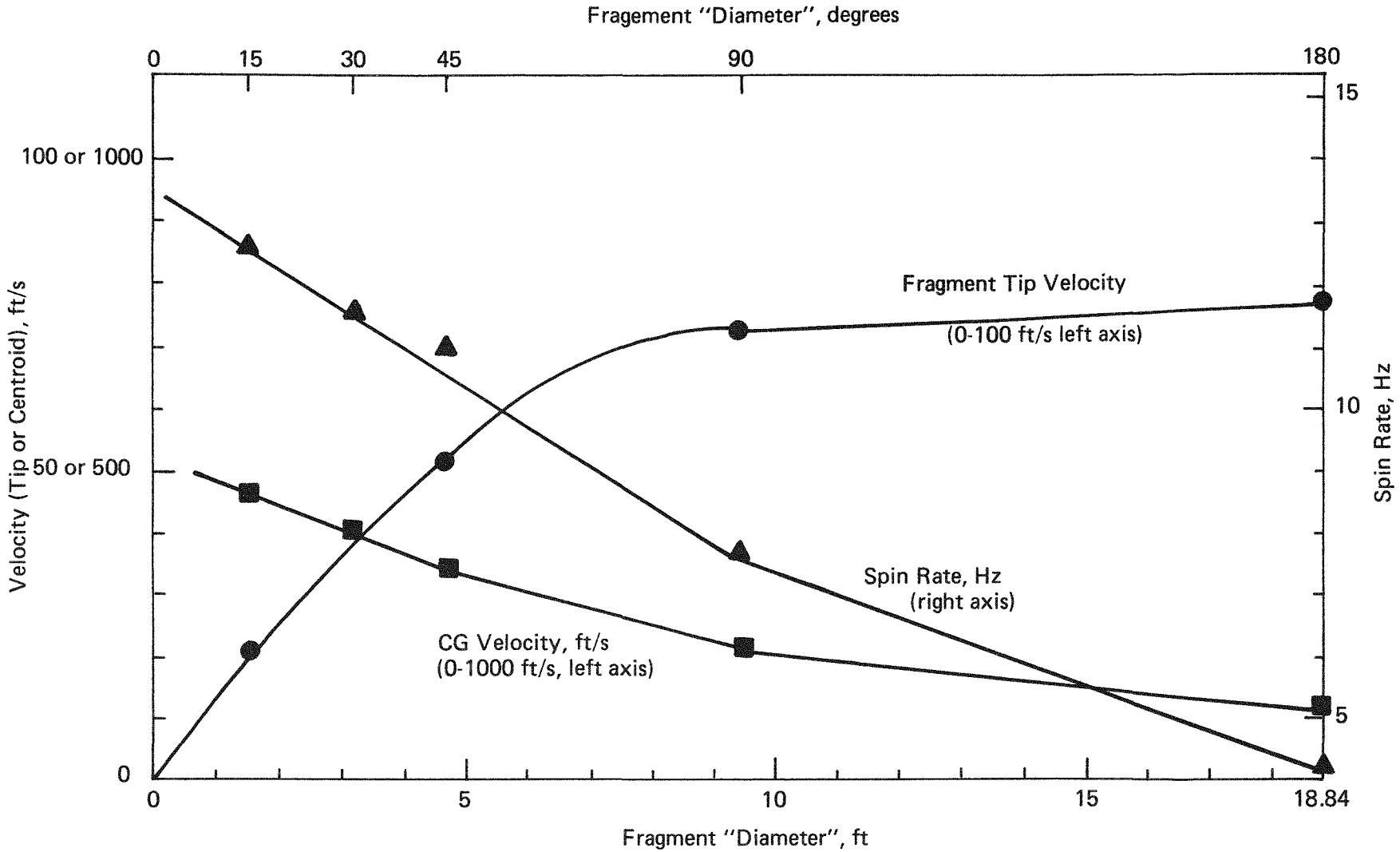

Figure D-9: The behavior of SRB fragment center of gravity (CG) and tip velocities is plotted.

For the joint segments (0.3 to 1.5 m or 1 to 5 ft in length), it can be seen that all must pass through the wing or floor prior to impacting an LWRHU. The maximum velocity is calculated as:

V = (Reference Velocity) (Wing Hit Reduction) (1 to 1.35) + Spin.

Therefore, for the first 105 s, the joint fragment velocity into a LWRHU would range from 51 to 115 m/s. This would result in LWRHUs incurring aeroshell damage and clad deformation but the unit would remain intact for subsequent impacts.

For the mission elapsed time (MET) period 105 s < MET < 120 s, the joint fragment velocity range would be between 81 and 238 m/s. This latter value exceeds by 12% the maximum LWRHU/SRB fragment test point. Based upon the two tests at 117 and 212 m/s and bare clad impacts at velocities to 128 m/s with no failure, it is unlikely that this highest joint fragment impact velocity would result in clad failure, although the graphites would be removed.

[Estimations were made on the unfailed clad deformations (mm) of side-on impacts reported by LANL in Reference 3. The four estimations from Figure 16 in Reference 3 are the following, the last two being repeats from Table D-1):

48 m/s (bare): $\frac{17.3}{16.0} = 1.08$

105 ms (bare): $\frac{17.0}{12.0} = 1.42$

128 m/s (bare): $\frac{18.8}{11.5} = 1.63$

105 m/s (LWRHU): $\frac{19.0}{18.0} = 1.06$

117 m/s (LWRHU): $= 1.11$

212 m/s (LWRHU): $= 1.21$

When plotted as a function of velocity squared (V^2), Figure D-10 results. By a short extrapolation to the 238 m/s velocity ($V^2 = 56694$ m^2 s^{-2}), it may be noted that the graphite-protected clad deformation is well within bare clad non-failure limits.]

The clevis pins would have the same velocity characteristics as the joint fragments per Reference 1, Section 5.2.2.2. The above rationale for joint fragments would apply for these smaller items. Also, by noting the test results for high velocity bullets impinging upon LWRHU test items (Section 2.1.2 above), small aluminum slugs of virtually the same mass and dimensions as the clevis pins did not cause clad failure even at velocities as high as 775 m/s.

Clevis pins at 0 < MET < 105 s could damage the aeroshell and deform the clad but the LWRHU would remain intact. At 105 < MET < 120 s, aeroshell destruction with clad deformation would occur at the higher clevis pin velocities.

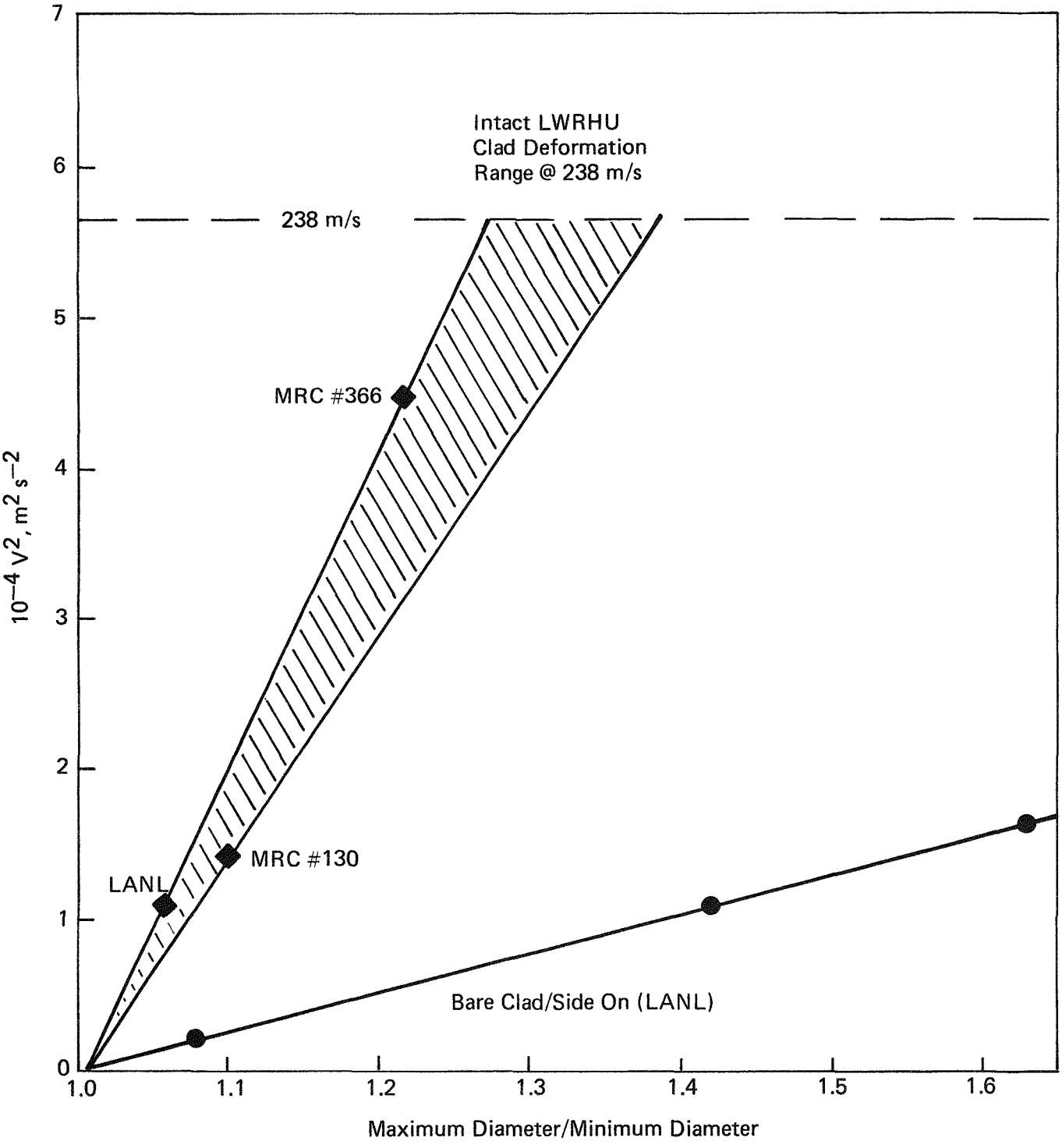

Figure D-10: A measure of aeroshell protection equivalency to the clad during impacts may be estimated by plotting clad deformation versus velocity squared (energy).

5.0 ET PROPELLENT EXPLOSION-GENERATED DEBRIS

During the launch of the space shuttle, it is possible to spill and ignite the cryogenic propellants contained in the ET (see Appendix C, earlier). In addition to the blast wave, shuttle components may be accelerated and impact with LWRHUs on the Galileo spacecraft. The following two sections address the two categories of debris as defined in Chapter 5 of Reference 1.

5.1 Flyer plates are aluminum plates with an areal density of 0.024 pounds per square inch (psi) (or about 6.2 mm thick plates). For up to 30^{o} tilt of the spacecraft in the area of the launch pad, the maximum flyer plate velocities for the four accident conditions as well as the LWRHU and net velocities are as follows:

SCENARIO	FLYER PLATES $\Phi = 30^{o}$ m/s	LWRHU m/s	Δ V m/s
On Pad	362	303	59
In Trench	268	328	60
Aft Compartment	233	107	126
In-Flight	236	$\sim$ 200	$\sim$ 36

The light-weight flyer plate impact velocities are well below any LWRHU failure thresholds, either bare clad or intact. A strike by a flyer plate will result in the LWRHU following essentially the same flight path as the flyer plate field/explosion front. Thus, although the aeroshell could be damaged, the LWRHUs would remain intact and the clad unbreached (although perhaps somewhat deformed).

[Aluminum plate/LWRHU clad interactions at velocities up to 1100 m/s resulted in no fuel release; see Section 2.2.2 for this summary].

5.2 Shrapnel

Reference 1, in Tables 5.17 through 5.24, lists a number of potential shrapnel velocities for the various accident scenarios. The highest value noted was 233 m/s (In-Trench Explosion, 130 ft/40 m height, 0.1 percentile at $\Phi = 0$). This is well below the highest velocity case cited in the previous section, so the conclusion is that the LWRHU will behave as defined above.

6.0 REFERENCES

1. Space Shuttle Data for Plantetary Mission Radioisotope Thermoelectric Generator (RTG) Safety Analysis, NSTS-08116.

2. Tate, R. E., and Land, C. C., Environmental Safety Analysis Tests on the Light-Weight Radioisotope Heater Unit, LA-10352-MS, Los Alamos National Laboratory (May 1985).

3. Tate, R. E., The Light Weight Radioisotope Heater Unit (LWRHU): A Technical Description of the Reference Design, LA 9078-MS, Los Alamos National Laboratory (January 1982).

4. Johnson, E. W., Cryogenic Explosion Environment Modeling and Testing of Space Shuttle and Light-Weight Radioisotope Heater Unit Interactions, MLM-3303, Monsanto Research Corporation (October 1985).

APPENDIX E

LWRHU RESPONSE TO PROPELLANT FIRES

1. SRB PROPELLANT FIRES

1.1 Test Results

In order to define the behavior of an LWRHU in the proximity of an SRB fuel fire, LANL subjected a test LWRHU 5 mm from the uninhibited edge of a 0.9 x 0.9 x 0.9 m cube of burning UPT-3001 solid rocket propellant. As the other surfaces were inhibited, only the side to which the test LWRHU was exposed burned; the burn lasted for 630 s. The flame temperature of 2060°C reached out to at least 1.8 m.

The LANL narrative describing the condition is as follows (Reference 1):

> "After the fire test, the aeroshell of the test unit was intact. The surface that faced the fire was somewhat eroded and encrusted with propellant fire products. The aeroshell surface in contact with the sand bed was partially covered with a layer of fused sand. No α-activity was detected on the exterior of the unit after the fire exposure. When the unit was disassembled, the outer and middle pyrolytic graphite insulator bodies were found to be unchanged.
>
> However, the inner insulator body had reacted with the Pt-Rh fuel capsule, presumably forming a Pt/Rh-C eutectic. The temperatures reported for the Pt-C eutectics are 1705 and 1694°C. The Pt vent frit has disappeared and the capsule wall thickness has been reduced in places to 0.41 mm (0.016 in.), which is 40% of its original thickness. There is, in addition, some evidence of a reaction between the UO_2 fuel simulant and the inner surface of the fuel capsule. Obviously, the integrity of the unit has been greatly reduced by exposure to the 10.5-min. propellant fire. Yet the outer graphite components of the unit provided sufficient containment capability so that gross fuel dispersal would not occur if the unit were handled with reasonable care after a fire exposure."

Although it may be noted in Appendix D that some damage would be incurred by the aeroshell should it be struck by SRB fragments, all test results of the launch pad area impact sort indicate that the aeroshell will remain about the clad. The aeroshell damage could result in some added platinum-rhodium/carbon eutectic formation (slightly less thermal protection) but the end result should be as per the final sentence from the LANL observation in the preceding paragraph.

1.2 Event Scenarios

1.2.1 SRB Case Rupture - Section 3.2 of Appendix D addressed the fate of an LWRHU upon being struck by an SRB case fragment. In summary, except for high altitudes where MET > 105 s, the fragments would result in damaged but still integral LWRHUs.

It should be pointed out that in the late stages (MET > 105 s) there is a potential of stripping the aeroshell from the clad, but that the probability of this bare clad encountering a piece of burning fuel is zero (high altitude, little propellant remaining and significant dispersion). Therefore, there is no fuel release(s) identified as a result of SRB propellant fires after SRB case rupture dispersal of the LWRHUs.

1.2.2 SRB Joint and Clevis Pins - Section 4.0 of Appendix D indicates that hits on LWRHUs due to SRB joint segments or clevis pins would damage the graphites but not strip the aeroshell from the clad. The effects (no releases) would be as discussed in 1.2.1 above.

1.2.3 ET Explosion-Generated Debris - Both flyer plates and shrapnel accelerated during an ET trench or MLP explosion result in a damaged but integral LWRHU aeroshell as the relative velocities of encounters are quite low (Section 5.1 and 5.2, Appendix D). Therefore, regardless of how the SRB fuel would encounter an LWRHU, no failure to the extent of releasing plutonia would occur.

2.0 ET FIREBALL

The large quantity of liquid cryogenic propellant inventory contained in the external tank (ET) could result in the generation of a fireball. Reference 2 in Section 7.0 addresses this phenomenon; Figure E-1 provides a pictorial representation of those data. (The "Thermochemical Model" (TM) is considerably hotter than the "Experimental Upper Bound" (EUB) curves for temperature and heat flux. Both are included in this analysis.)

The LWRHUs would be integral after the overpressure and/or fragments immediately proceeding this fireball (See Appendixes C and D). The lowest clad temperature curve (EUB) was taken from Reference 3. The estimation of the clad temperature response to the more severe TM condition was based on high flux reentry curves (Reference 4) with the clad responses shown as a function of time.

From this plot, it may be noted that even if the LWRHU remains in the post-fireball fire, the maximum temperature of the clad will approach 1370 K (approximately 1100 ^{o}C) after the one-half hour duration of this fire. The Pt-30Rh/carbon eutectic of 2033 K and melting point of 2183 K for this alloy indicate good margin of safety even during this long post-fireball fire. Therefore, no fuel would be expected to migrate outside the clad during (or after) this event.

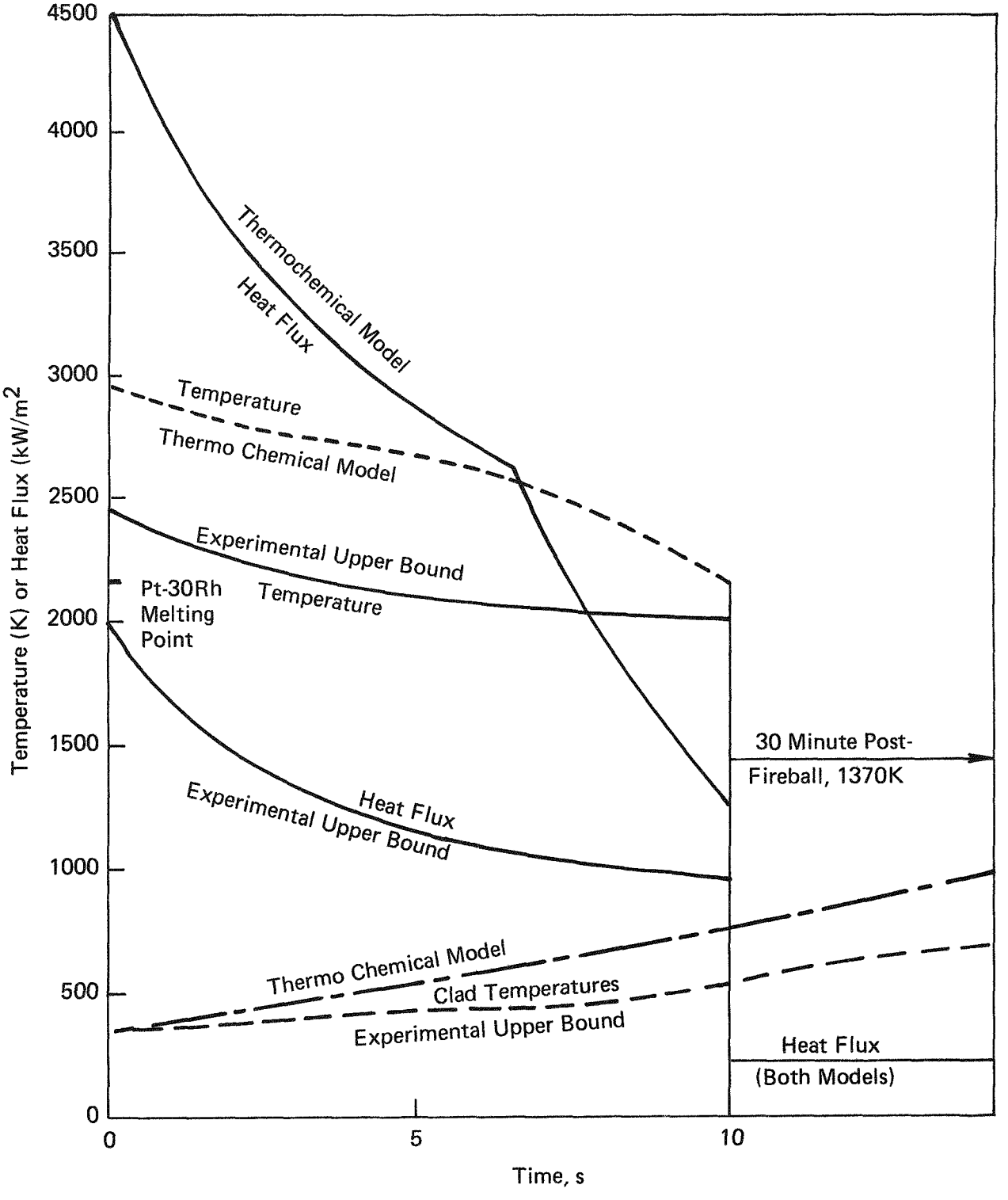

Figure E-1: Variables associated with a liquid propellant fireball at the launch pad are shown above as a function of time.

The fireball chemical environs is not expected to degrade significantly the carbon aeroshell or the PG insulators. Note that there is an excess of 2.7X hydrogen to oxygen in the ET on a molar basis. This generally reducing atmosphere should further allay any concerns regarding the loss of carbon components during the 10-s fireball due to oxidation.

3.0 ORBITER FIREBALLS

Reference 2 also defines the behavior of the fireball arising from the liquid cryogenic propellants carried aboard the orbiter. In essence, the behavior is identical to that shown for an ET event save that the fireball duration is only 5 s whereas the ET event is 10 s long. The adverse consequence of an event such as this is less than for the ET event, so further elaboration is unnecessary; throughout the overpressure/fragment/secondary report/fireball sequence, the LWRHU remains intact (some damage to carbons could result, however) and no fuel releases are expected.

4.0 OTHER CONSIDERATIONS

Reference 3 addressed the potential reaction(s) of the exposed clad with materials in the vicinity of the launch pad. As the aeroshell is expected to remain about the clad in these revised (from 1984) scenarios, clad compromise due to chemical reactions during the fireball or post-fireball fire would not occur.

Note that the probability of exposure of LWRHUs to the cryogenic explosion overpressure disappears after MET > 30 s. In all likelihood, the exposure of LWRHUs to a fireball would be negligible after MET > 10 s.

5.0 REFERENCES

1. Tate, R. E., and Land, C. C., Environmental Safety Analysis Tests on The Light Weight Radioisotope Heater Unit (LWRHU), LA-10352-MS, Los Alamos National Laboratory (May, 1985).

2. Space Shuttle Data for Planetary Mission Radioisotope Thermoelectric Generator (RTG) Safety Analysis, NSTS 08116.

3. Johnson, E. W., Light-Weight Radioisotope Heater Unit Safety Analysis Report (LWRHU-SAR), Volume II Accident Model Document, MLM-3293, Monsanto Research Corporation (October, 1985).

4. Draft LWRHU VEEGA Reentry Response, the Johns Hopkins University Applied Physics Laboratory (May, 1988).

APPENDIX F

SPACECRAFT REENTRY BREAKUP ANALYSIS*

1.0 INTRODUCTION

This appendix reports the result of a JPL study of release of the LWRHUs (Light-Weight Radioisotope Heater Units) carried on the Galileo spacecraft during accidental Earth reentry. The study has two parts: (1) to identify the LWRHU most likely to be released first (out of over 100 on board) during a "minimum gamma" reentry, and (2) to evaluate the release point (altitude, speed, and flight path angle).

The LWRHUs have been designed with ablative heat shield and impact absorbing features appropriate for surviving Earth reentry. The early release trajectory determined here will be used in subsequent analyses, by others, of the entry ablation and ground impact.

This appendix is essentially the same as Appendix F in the October 1985 LWRHU-SAR. Verbal communications with JPL have indicated that the differences in upper stage or mission profile would not perturb the conclusions. Some changes, mainly in the quantities and locations of LWRHUs on the spacecraft, have been made; conclusions have been altered, however.

2.0 CHOICE OF TRAJECTORY

The minimum gamma reentry trajectory is the case where the spacecraft enters the atmosphere at parabolic speed at a path angle such that it will later skip up to the entry altitude before again descending. It is known from prior experience that this trajectory gives the largest time-integrated aeroheating and thus the greatest ablation of heat shield during the entry. Thus, the LWRHU which is released first on a minimum gamma trajectory is to be considered as incurring the greatest ablation.

3.0 RELEASE: BREAKUP CASE 2

The entry conditions for the Galileo spacecraft on the minimum gamma trajectory have been described in References 2 and 3 (called Case 2). In this entry case, considered to result from a misdirected IUS burn, the fully deployed spacecraft enters the Earth's atmosphere at 400 kft altitude at parabolic speed (36 kft/s). An entry angle of 5^{o} was adopted as approximating that for skip-up. Two subcases were considered: (1) a nonspinning spacecraft in the aerodynamic trim condition, in which the magnetometer boom trails and the spacecraft axis makes an angle of attack of about 70^{o}; and (2) a spinning spacecraft (3 rpm) with axis almost vertical; i.e., at an angle of attack of about 90^{o}. It was noted that Subcase (2) is more likely than (1), since it requires only a single malfunction (misdirected IUS burn), whereas Subcase (1) requires a second failure (absence of spin).

*Reference 1, A. D. McRonald

A similar situation arises in the present LWRHU analysis: a particular nonspin fixed attitude favors the very early release of a particular LWRHU, while the more likely spinning subcase gives a later release.

4.0 CHOICE OF LWRHU FOR EARLY RELEASE

The first step in the LWRHU analysis was to identify LWRHUs that, from their location and method of mounting, would likely be released from the spacecraft early in the entry, essentially by aeroheating. The minimum gamma trajectory is characterized by a substantial level of aeroheating (up to tens of $Btu/ft^2/s$ for the spacecraft) over a period of tens of seconds in the entry heat pulse, combined with the relatively low aerodynamic force (stagnation pressure of a few pounds per square foot).

One difficulty in identifying an LWRHU likely to experience early release is the large number of LWRHUs carried; the spacecraft has 129 of these, distributed over about 16 locations (see Figure F-1). Of these, 34 are inside the Jovian probe and are assumed to remain so during the entry. Of the remaining 95 on the rest of the spacecraft, 52 are mounted, typically in groups of three, in aluminum cans secured by mounting brackets on the outside of two large outrigger electronic units (boxes): 12 are located on three faces of Bay E, and 40 are on two opposite faces of the Despun Electronics. Figure F-1 shows a schematic of the spacecraft. Because these 52 LWRHUs are mounted close to the outside face of a relatively large unit (and below an outer multilayer thermal blanket, as all are), the heating rate is relatively low (varies as the inverse square root of body size); and they are unlikely to be released early.

The choice of the first release is then narrowed to five items: (1) inboard magnetometer; (2) outboard magnetometer; (3) PWS (Plasma Wave Subsystem); (4) LBA (Linear Boom Actuator), and (5) Science Boom Hinge Cable. After detailed consideration of each location, manner of mounting, thermal insulation, etc., it became evident that the most likely candidate for early release was Item (2), the group of three LWRHUs mounted in individual aluminum cylindrical cans attached via brackets to a thick aluminum cross plate at the outboard end of the magnetometer boom. The three cans are grouped around the central magnetometer, which is encased in a thermal blanket. An outer blanket is fitted over the whole assembly and kept in place by means of the stand-off isolation loops.

5.0 RELEASE OF THE LWRHUs

Following a similar approach to that taken in analyzing the RTG release (References 1 and 2), two subcases were analyzed: (1) with the spacecraft fixed in an attitude giving maximum aeroheating of the outboard magnetometer RHUs, and (2) with the spacecraft spinning with its axis at 90° to the flow. Subcase (1) represents the earliest possible release, and Subcase (2) a more realistic early release.

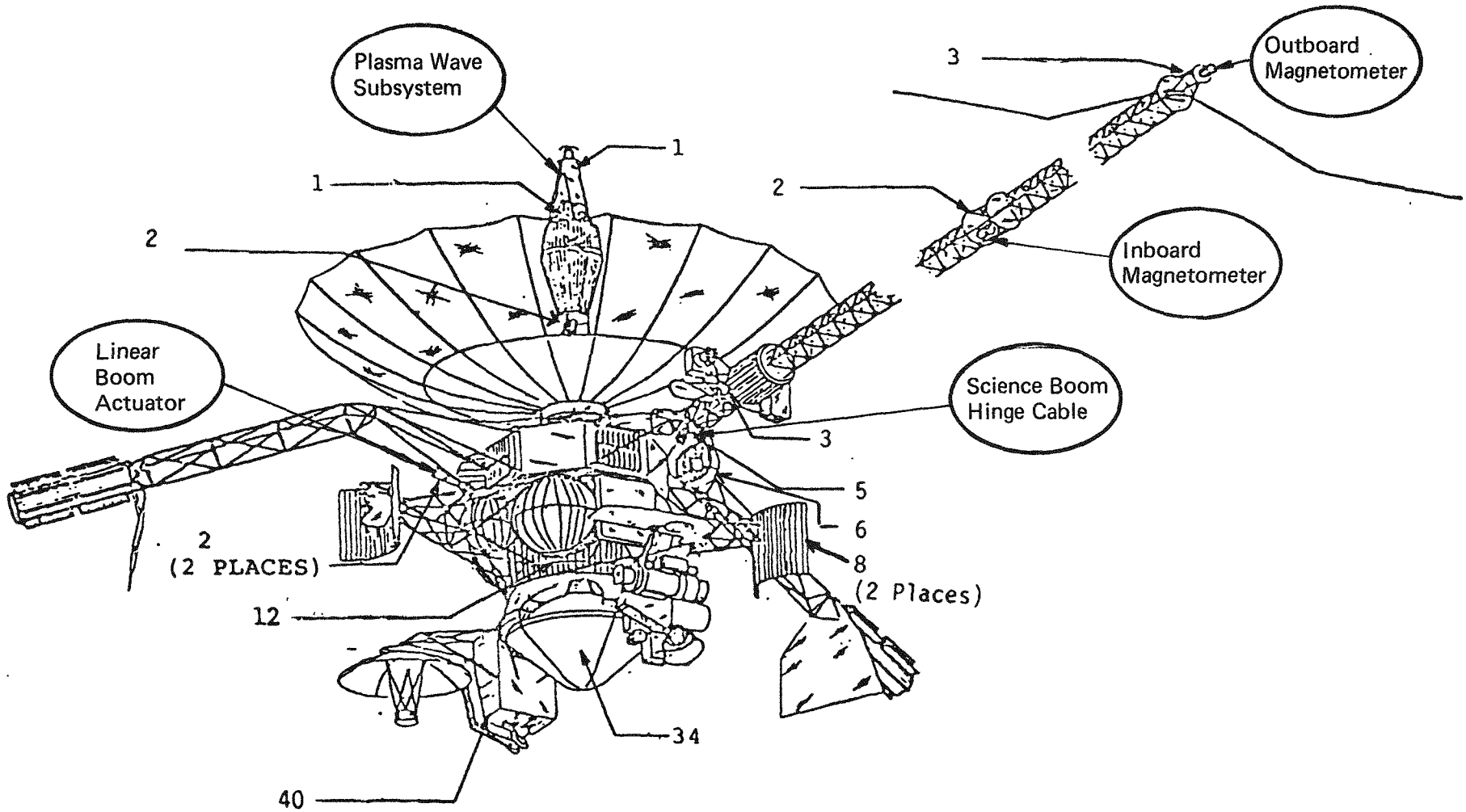

FIGURE F-1: The five locations of LWRHUs which were assessed for earliest release are identified above. The three located on the outboard magnetometer (upper right) are the first to be released in a reentry event.

The aeroheating at the LWRHU site was evaluated for both subcases. There is first free-molecular heating of the "top hat" thermal blanket covering all three LWRHUs and the magnetometer sensor. At about 15 s in Subcase (1) and 17 s in Subcase (2), the blanket fails and heating of the LWRHU cans begins. At about 25 s, the conditions become a continuum. In Subcase (1), the tops of the LWRHU cans are heated, while in Subcase (2), the heating is cyclic, due to the spacecraft spin (period 19 s). At about 32 s in Subcase (1), the top of the LWRHU can begins to melt, and this represents the earliest time for release of any of the LWRHUs. The corresponding point in Subcase (2) occurs at 44 s. We note that ejection of the LWRHU capsule is more positive in Subcase (2), due to centrifugal force impacted by the spin. As has been mentioned, the spin case is more likely on the single-point failure basis and, in addition, gives more positive ejection of the capsule.

The corresponding altitude Z, inertial velocity V, and inertial flight path angle values at LWRHU release for the two subcases are:

(1) earliest: Z = 315 kft; V = 36069 ft/s; $\gamma = -3.481^{o}$;
(2) early probable: Z = 290 kft; V = 36072 ft/s; $\gamma = -2.909^{o}$.

6.0 FAILURE OF THE MAGNETOMETER BOOM

It is appropriate to check that the magnetometer boom will stay intact at least until the LWRHUs on the outboard end are released. The boom is of light fiberglass rod construction, covered with multilayer insulation. In Subcase (1), the hypothesis is that the end plate faces the flow, and thus the boom runners are seen at a glancing angle. Calculations indicate that the boom blanket will fail before 32 s but that the fiberglass longerons will be intact at this time (LWRHU release).

In Subcase (2), the spacecraft rotates with its axis at 90^{o} to the flow, so that the magnetometer boom is exposed cylically to the flow. It is calculated that the boom blanket and the fiberglass longerons will fail by about 40 s, but the electrical wires will be intact, and the outboard unit will continue to rotate for the moment as if the boom structure were there. Thus, in both subcases, the thermal response of the boom will not affect the LWRHU release times stated above.

7.0 SUMMARY AND CONCLUSIONS

This analysis has identified a group of three LWRHUs, mounted in individual aluminum cans on the outboard magnetometer boom of the Galileo spacecraft, as likely to be released first during accidental Earth reentry of the spacecraft on the minimum gamma trajectory.

Thermal response calculations of the aeroheating absorbed first by the thermal blanket and then by the LWRHU mounting cans give the following release points:

(1) earliest (spacecraft in fixed attitude most favorable to early release): release at 315 kft altitude, velocity 36069 ft/s, path angle -3.481°;

(2) early probable (spinning spacecraft, axis 90° to flow): release at 290 kft altitude, velocity 36072 ft/s, path angle -2.909°.

With regard to initial conditions or entry ablation studies, it is recommended that appropriate assumptions are: at release, the LWRHUs have incurred no significant prior aeroheating, have no significant body rotation rate, and have no preferred initial attitude. However, one cannot exclude the possibility of small initial rotation rates and of various attitudes; and appropriate assumptions should be made where relevant.

8. REFERENCES

1. McRonald, A. D., "Release Conditions of the LWRHUs" Galileo Breakup Analysis," 3547-GLL-83-121 (November 8, 1983).

2. McRonald, A. D., "Release Conditions of the Two RTG's, Galileo Breakup Case 2: Shallow Entry of the Deployed Spacecraft," IOM 3547-GLL-82-102 (July 1, 1982).

3. McRonald, A. D., "Review of the Heat Source Module Release Conditions, Galileo Entry Breakup Cases 1 and 2", IOM 3547-GLL-82-180 (November 22, 1982).

4. Space Shuttle Mission Data for Planetary Mission Radioisotope Thermoelectric Generator (RTG) Safety Analysis, NSTS-08116.

APPENDIX G

LWRHU REENTRY RESPONSE

1.0 INTRODUCTION

The LWRHU has been designed to survive unplanned orbital reentry incidents, should abort condition(s) be encountered during phases of the mission which would result in these reentry events. The principal concerns based on the design are:

A. Ensure that the most severe reentry condition would result in the maintaining of an integral clad through the heat pulse.

B. Ensure that excessive ablation of the aeroshell does not occur which could adversely affect the overall thermal distribution and subsequent clad response.

C. Ensure that even with "worst-case" thermal input, the aeroshell does not incur thermal stress failure which could compromise the clad integrity.

These considerations have been addressed in analyses peculiar to the LWRHU system by APL who provided the draft of this appendix (ANSP-L-829, RL-85-045). Subsequent to this earlier SAR, the Galileo mission was altered to include the VEEGA trajectory which in turn opened the possibility of a superorbital reentry. Reentry analyses and some additional thermal stress assessments were performed by APL to address these newly-defined accident scenarios.

2.0 THERMAL RESPONSES OF THE Pt-30Rh

One of the potential reentry failure modes for the LWRHU is overheating of the Pt-30Rh clad to the extent that the material reaches its carbon eutectic. The carbon eutectic of Pt-30Rh is 1730°C. Because of the uncertainty of the flight attitude of the cylinder, the reentry performance was evaluated assuming, in one case, end-stable and, in a second case, side-stable hypersonic flight. The analysis of two different flight attitudes was accommodated through the use of two separate multidimensional thermal models.

2.1 End-Stable Thermal Analysis of Maximum Clad Temperature

The thermal analysis of the LWRHU in the end-on attitude concentrated on the γ^* (maximum thermal response) trajectory. The initial conditions for the trajectory are $\gamma = -4.75^{\circ}$, V = 11 km/s, and h = 122 km (altitude). It was assumed for the analysis that helium was released from the fuel at the time estimated by LANL, and that it first filled the gap between the fuel and the clad and later filled the gaps outside the fuel clad. The thermal model that was used for the end-on thermal response calculations used 762 nodes: the nodal locations are sketched in Figure G-1.

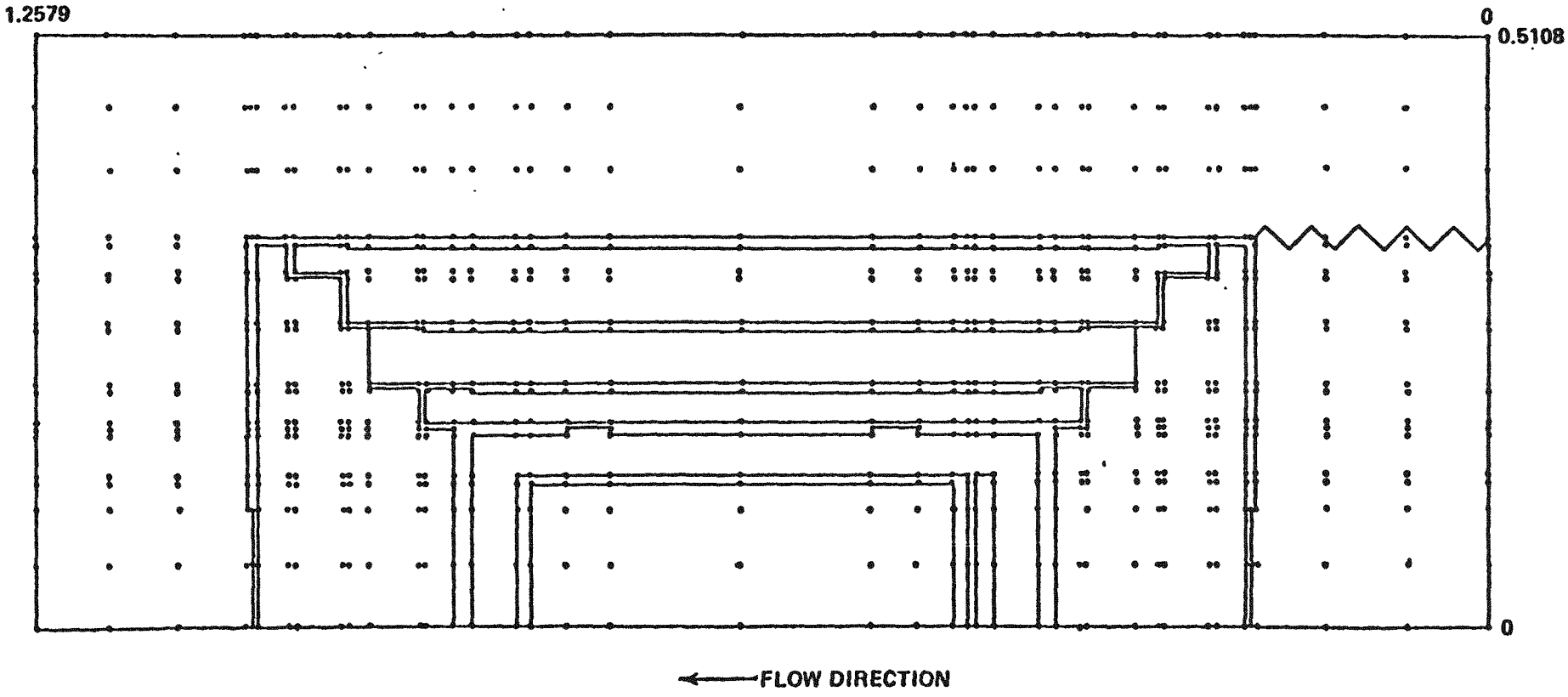

FIGURE G-1: Sketch of the end-on LWRHU thermal model which shows the 762 nodal points. Dimensions are in inches in this particular drawing.

The internal thermal contact between adjacent parts was specified in accordance with the following table:

Contact Conductance G = 1000 Btu/ft^2 hrR (5680 W/m^2 · K)
plus radiation

- aeroshell/outer sleeve standoffs - radial
- aeroshell/insulator plugs - radial
- aeroshell standoff/insulation plug - axial
- aeroshell end cap standoff/insulation plug - axial

Contact Conductance, G = 500 Btu/ft^2 hrR (2840 W/m^2 · K)
plus radiation

- outer sleeve/middle sleeve standoffs - radial
- middle sleeve/inner sleeve standoffs - radial
- outer sleeve (lower segment)/forward insulation plugs - axial
- middle sleeve/forward and aft insulation plugs - axial
- inner sleeve/clad standoffs - radial
- clad weld bead/forward insulation plug - axial
- fuel/clad - radial
- fuel/shim - axial

Contact Conductance, G = 2000 Btu/ft^2 hrR (11360 W/m^2 · K)
plus radiation

- shim/clad (force fit) - radial

The helium was assumed to release from the fuel when the clad temperature reached 860°C. At this time, the open fuel/clad interfaces were assumed to fill with helium instantaneously and thereby supplement interface radiation with gaseous conduction. When the clad temperature reached 1150°C, the helium was assumed to be released from the clad and into the gaps between the clad and graphite parts. Here again, gaseous conduction at all open interface interior to the aeroshell was assumed to occur instantaneously.

The convective heating (q) boundary conditions over the windward-end face and side surface are described by Figure G-2. The side heating distribution was taken to be the mid-range values defined by the bounds shown in this figure. The heating rate level over the leeward end face was a uniform distribution defined at 5% of the stagnation level.

The results of the end-on reentry analysis are summarized by the clad response shown in Figure G-3. This figure shows the results of two calculations. For the calculation denoted by the solid line, it was assumed that the vacuum was maintained within the gaps throughout the flight period, thereby restricting the heat transfer at this interface to radiation only.

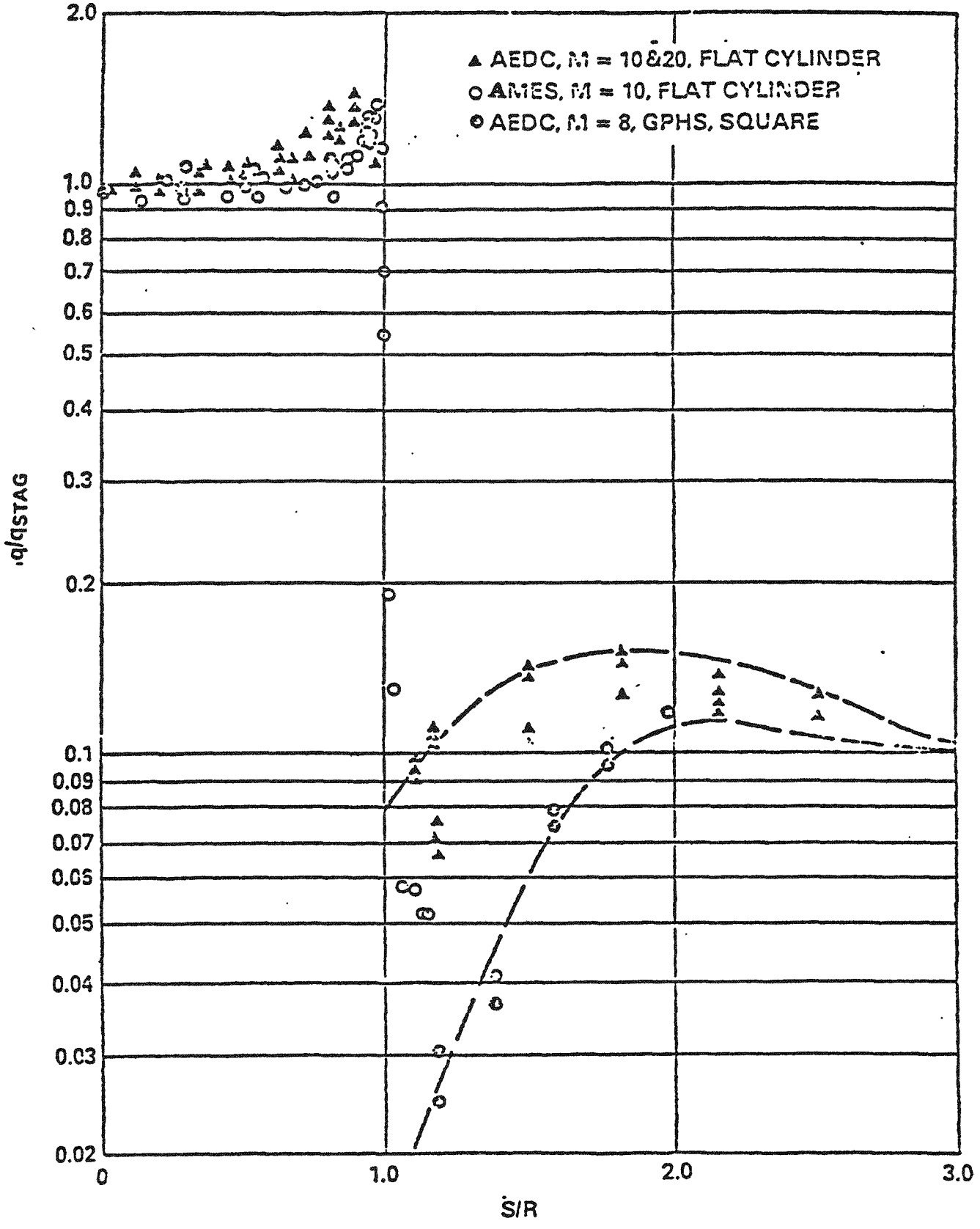

FIGURE G-2: The plots above describe the heating boundary conditions used in the APL analyses.

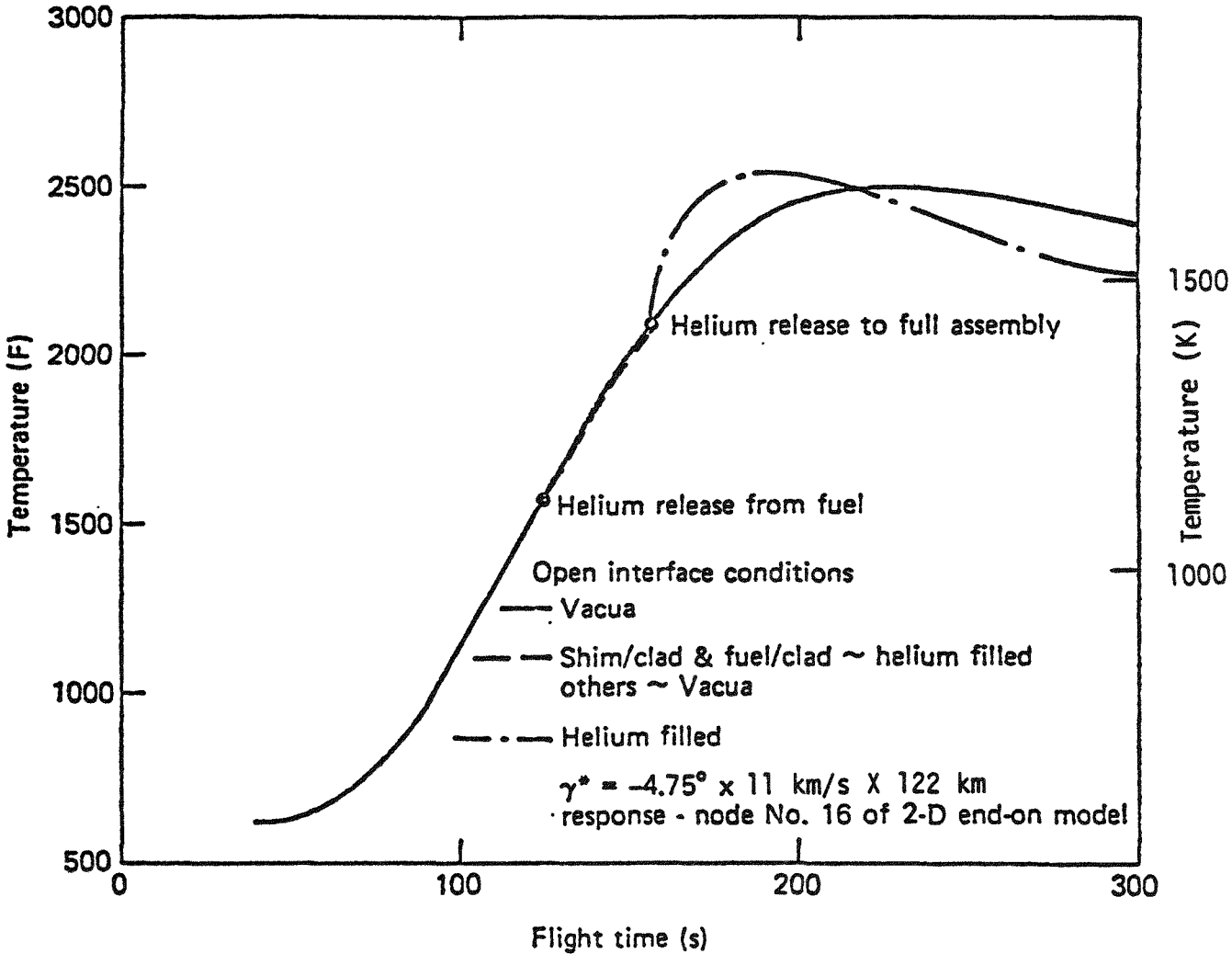

FIGURE G-3: LWRHU standoff design clad response to γ^* reentry (40.3 g) in an end-on stable attitude.

The dashed lines show the change in the temperature that results when helium is released from the fuel and flows into the gaps as described above. The helium is released from the fuel and flows into the gaps as described above. The helium release to the fuel assembly is an important event, resulting in a peak clad temperature slightly greater than predicted, should the gaps remain evacuated. The peak clad temperature is 1400°C, substantially below the clad eutectic of 1730°C. More details of these calculations are available in Reference 2.

2.2 Side-Stable Thermal Analysis of Maximum Clad Temperature

The thermal analysis of the LWRHU in the side-stable attitude also concentrated on the trajectory that produces maximum thermal response of the clad. The trajectory initial conditions for the side-stable γ are slightly different from those for the end-stable case. For the side-stable situation, the inertial flight path angle is $\gamma = -4.80°$, the velocity is 11 km/s, and the initial altitude is 122 km. As was the case with the end-stable analysis, it was assumed that helium was released from the fuel and filled the gap between the fuel and the clad when the clad temperature reached 860°C. The helium was assumed to be released into the remaining gaps in the assembly when the clad temperature reached 1150°.

The thermal model that was used for the side-stable thermal response calculations used 460 nodes. The nodal locations are sketched in Figure G-4. It was assumed that the thermal contact conductance between the Fine-Weave Pierced fabric and the pyrolytic graphite insulators had a value of 1000 Btu/ft^2 hr R (5680 W/m^2 K) and that the thermal contact conductance between the pyrolytic graphite insulators had a value of 500 Btu/ft^2 hr R (2840 W/m^2 K). The hypersonic convective heat transfer distribution around the circumference of the cylinder is described by Figure G-5. It was assumed that the heat transfer coefficient on the end of the LWRHU is 10%.

3.0 CLAD IMPACT TEMPERATURE

The temperature of the clad at the time of impact with the earth can be an important factor in determining the survivability of the clad. Owing to the porous nature of the FWPF aeroshell, a proper estimate of the impact temperature must account for the passage of ambient gases into and out of the gaps. The gases that need to be considered are the helium that has been generated by the fuel decay and the ambient air. The amount of these gases in the gaps and the degree of rarefaction of the gases dictate the amount of heat conductions across the gaps and, therefore, the thermal response. The computation of the diffusion of the gases adds significantly to the computational time within the thermal response program and so a two-dimensional thermal model was used to provide the estimate of the impact temperature. The details of the calculation are provided in Reference 3. The results of the calculation are described in Figure G-6. This figure shows both the helium mass fraction in the gaps and the thermal response of the LWRHU. At the beginning of reentry, it is assumed that there is a small quantity of helium present in the gaps; this helium diffuses through the FWPF aeroshell and escapes to space early in the reentry. Later, as the fuel is heated, the helium is released from the lat-

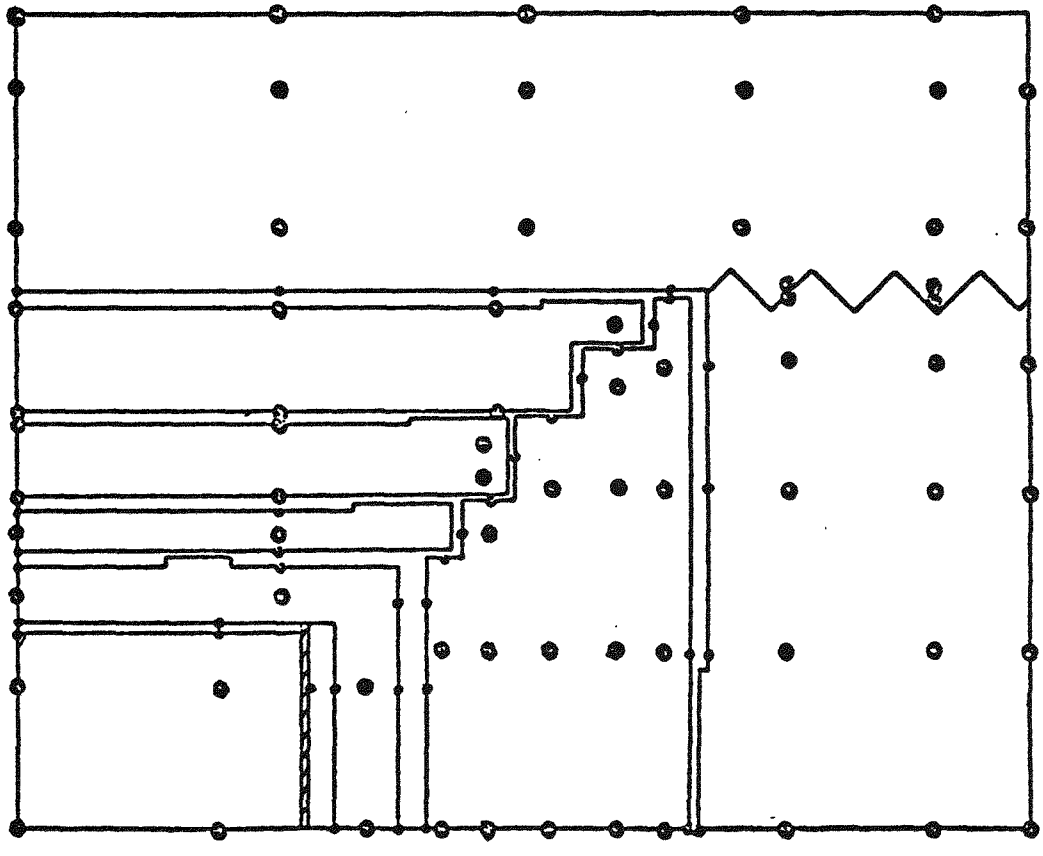

FIGURE G-4: Sketch of the LWRHU side-stable 3D configuration showing some of the nodal locations.

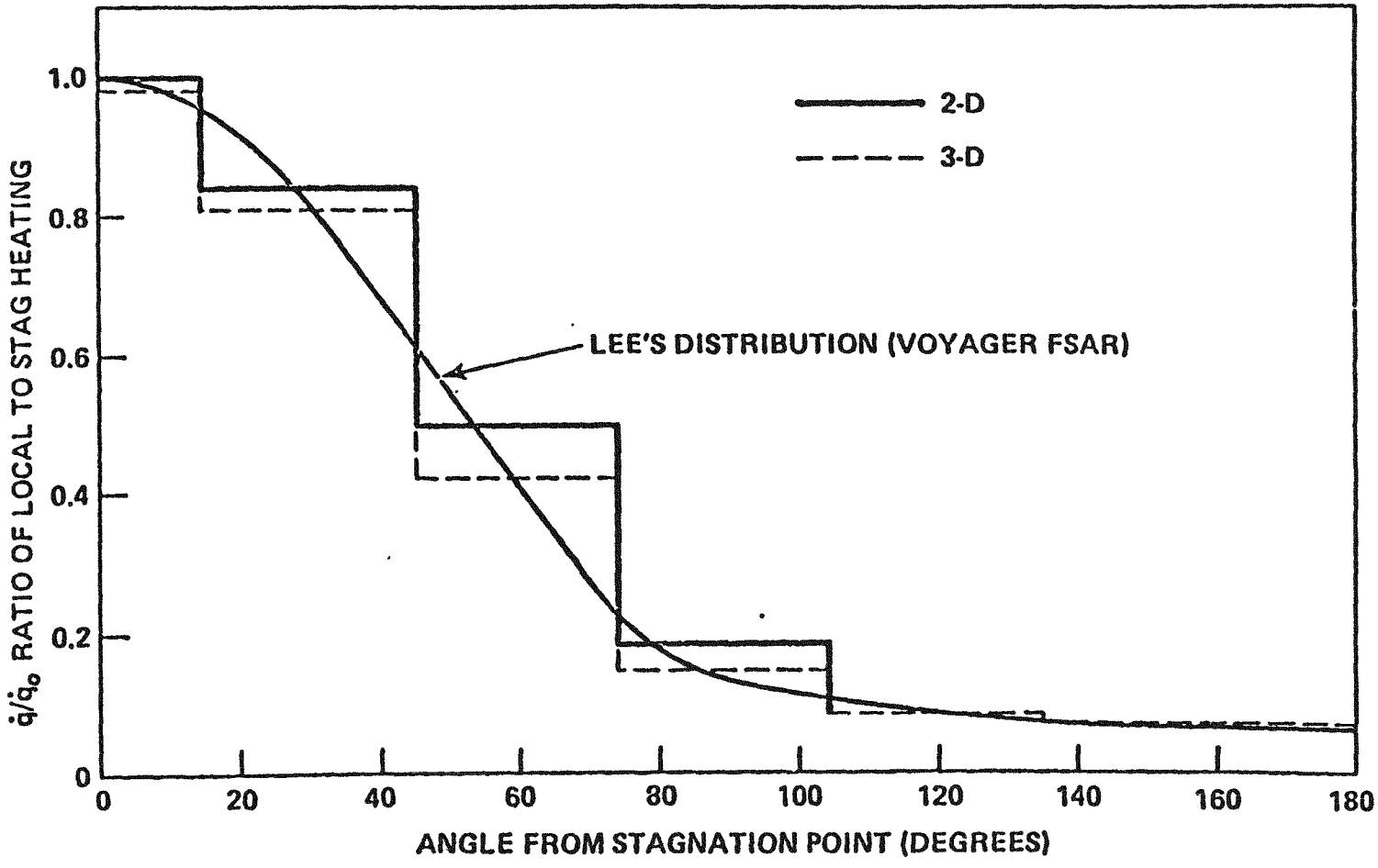

FIGURE G-5: Heat transfer distribution around a circular cylinder.

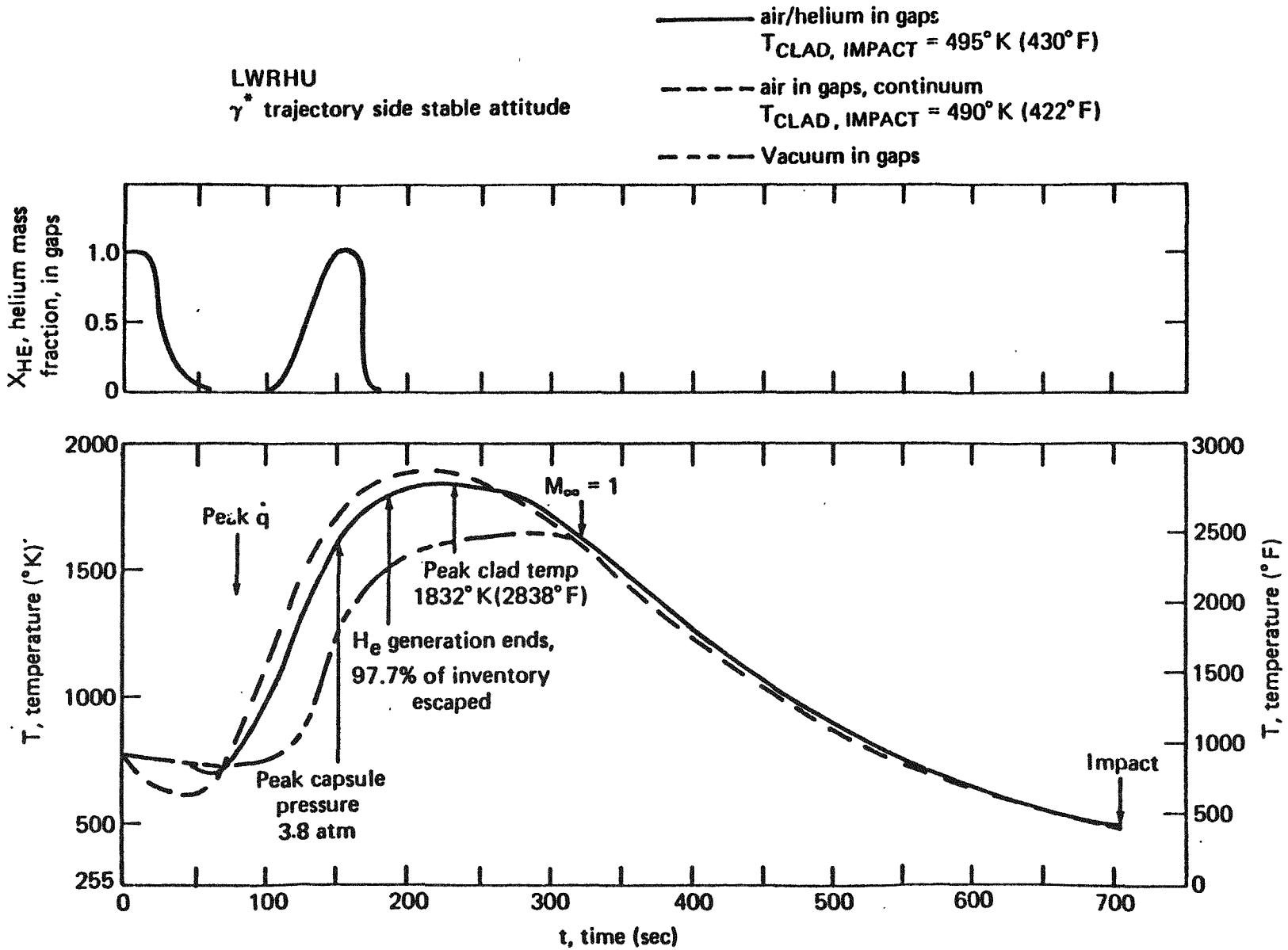

FIGURE G-6: Helium mass fraction in gaps and clad thermal response.

tice, so that by about 150 s into the reentry, the helium concentration in the gaps has peaked, and the helium mass fraction in the gaps has reached nearly 100%. As time increases, the helium escapes and is replaced by air. The temperature at the time of impact is not much different from that which would have been predicted had air been present in the gaps at a continuum pressure level throughout the reentry period. The clad temperature at the time of impact is estimated to be 220°C, a value sufficiently low that LANL expects the impact characteristics to remain similar to those that have been tested at room temperature.

4.0 ABLATION OF THE LWRHU FWPF AEROSHELL

The ablation of the LWRHU aeroshell was estimated for both side-stable and end-stable reentry trajectories. Each of the two cases was evaluated based on the appropriate γ^* trajectory with the conservative assumption that the LWRHU aeroshell was exposed to the reentry environment at a 122-km altitude. In fact, the RHUs are either enclosed in aluminum housings or protected for some period of time by the probe.

It is estimated that the recession will total 40 to 45% of the wall thickness for a side-stable reentry. A profile of the LWRHU aeroshell with an outline of the predicted recession is sketched in Figure G-7.

5.0 THERMAL STRESS OF THE LWRHU FWPF AEROSHELL

The aeroshell of the LWRHU is constructed from FWPF material that was developed by the Air Force as a thermal stress resistant material suitable for use as a reentry body nose tip. Techniques for analyzing the structural behavior of composite materials subjected to thermal load are only now evolving; until better analysis techniques are developed, it is necessary to analyze structures that use this material by using the same analysis techniques that were developed for bulk materials. The analysis program used to evaluate the stress (γ) in the LWRHU aeroshell is SAAS III. Of several stress-strain material models available in SAAS III, three were finally chosen for use with FWPF:

1. Orthotropic - elastic properties
2. Orthotropic - elastic/plastic properties
3. Orthotropic - elastic/plastic, different properties in tension and compression.

These material models are listed in order of increasing complexity and were correspondingly applied as more refined analyses were undertaken.

It was assumed for the stress analysis that the inertial flight path angle was -90^{o}, the initial velocity was 11 km/s and the release altitude was 122 km. Calculations were performed for both an end-stable and a side-stable flight attitude of the cylinder. The initial temperature of the LWRHU was assumed to be $90^{o}C$ ($200^{o}F$) for the end-stable trajectories and $540^{o}C$ (1000^{o}) for the side stable trajectories. The lower of the two temperatures more nearly approximates the steady-state temperature, but the side-stable stress computations were completed before the steady-state values were available. It was assumed that the LWRHUs were released from the spacecraft either at the time of initial entry into the atmosphere (122 km) or at the time of the peak convective heat pulse. For all side stable reentry situations, plane stress and zero stress resultant boundary conditions using elastic material properties were applied. Axisymmetric boundary conditions with elastic material properties were applied to the end-stable reentry conditions. In both the side- and the end-stable orientation, more refined calculations were subsequently made by assuming that plastic yielding in the aeroshell can occur, and that the Prandtl-Reuss flow rules incorporated into the SASS III finite element routine accurately represent this behavior. The elastic-plastic option, combined with defining different material properties in tension and compression, provided the most comprehensive model of each reentry situation. For the end-stable reentry profile, it was unsure whether gap closure in the threaded connection between aeroshell barrel and end cap was maintained. Because of this, a gap solution was obtained by using the special program modification to SAAS III, SASS GAPS.

The end-stable solutions utilize a single quarter section barrel/end cap finite element grid assuming axisymmetry. The boundary conditions are shown in Figure G-8. The threaded region between the aeroshell barrel wall and the end cap was modeled in two ways: (a) the barrel wall and end cap were considered to be a monolithic structure, or (b) gaps will form between the two pieces. The first assumption represents the structure most accurately if the graphite glue that seals the barrel and the end cap maintains its integrity, while the second assumption suggests that the glue will have structurally failed. The results are tabulated in Tables G-1 and G-2.

The minimum margin of safety in tension is 2.1 and in compression is 1.4, where the compressive margin is based on the stress at 1% strain. In fact, the material will strain to at least 5%, and perhaps more; and so the compressive margin is even greater than the value reported.

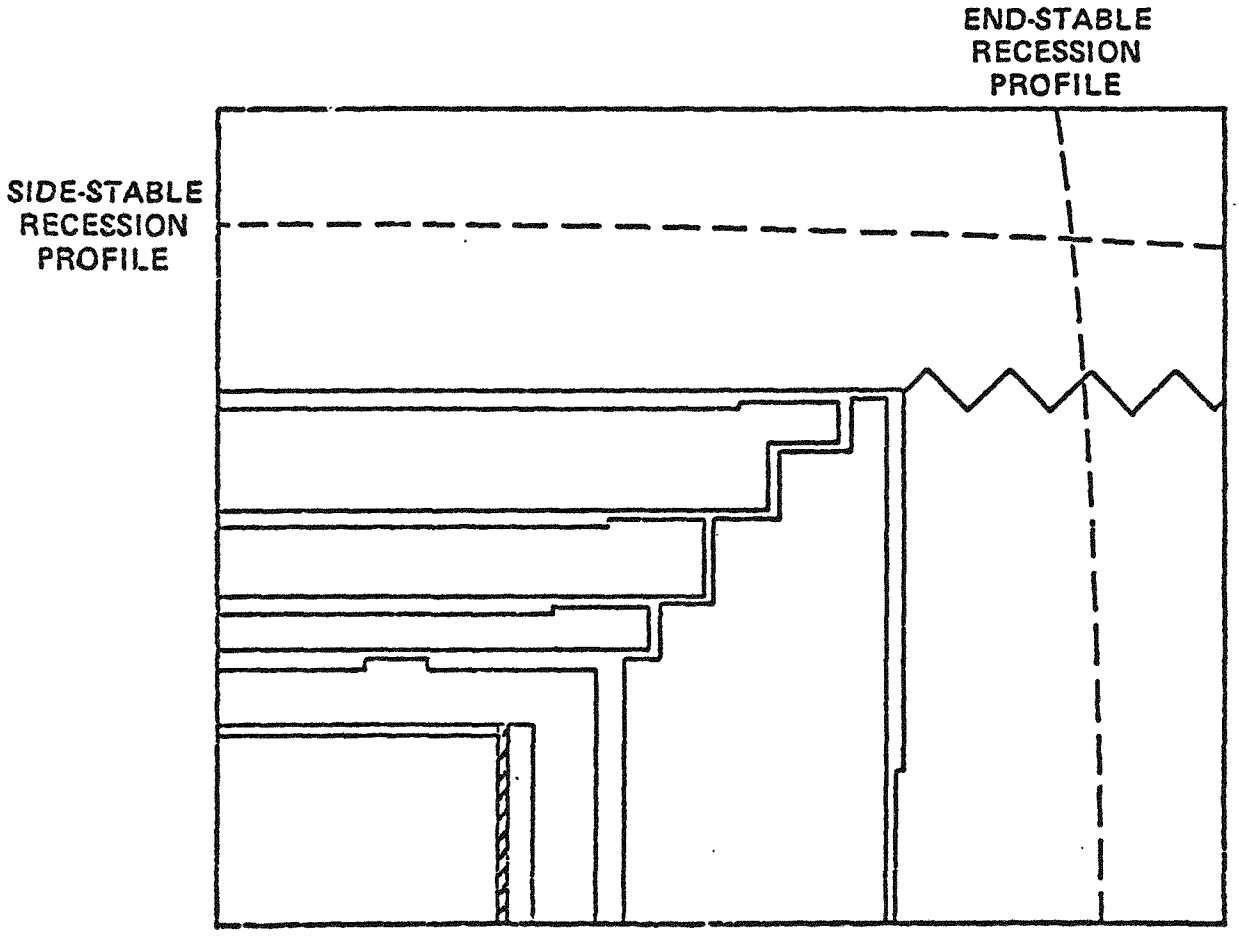

FIGURE G-7: LWRHU recession profiles γ^* trajectory - nominal heating.

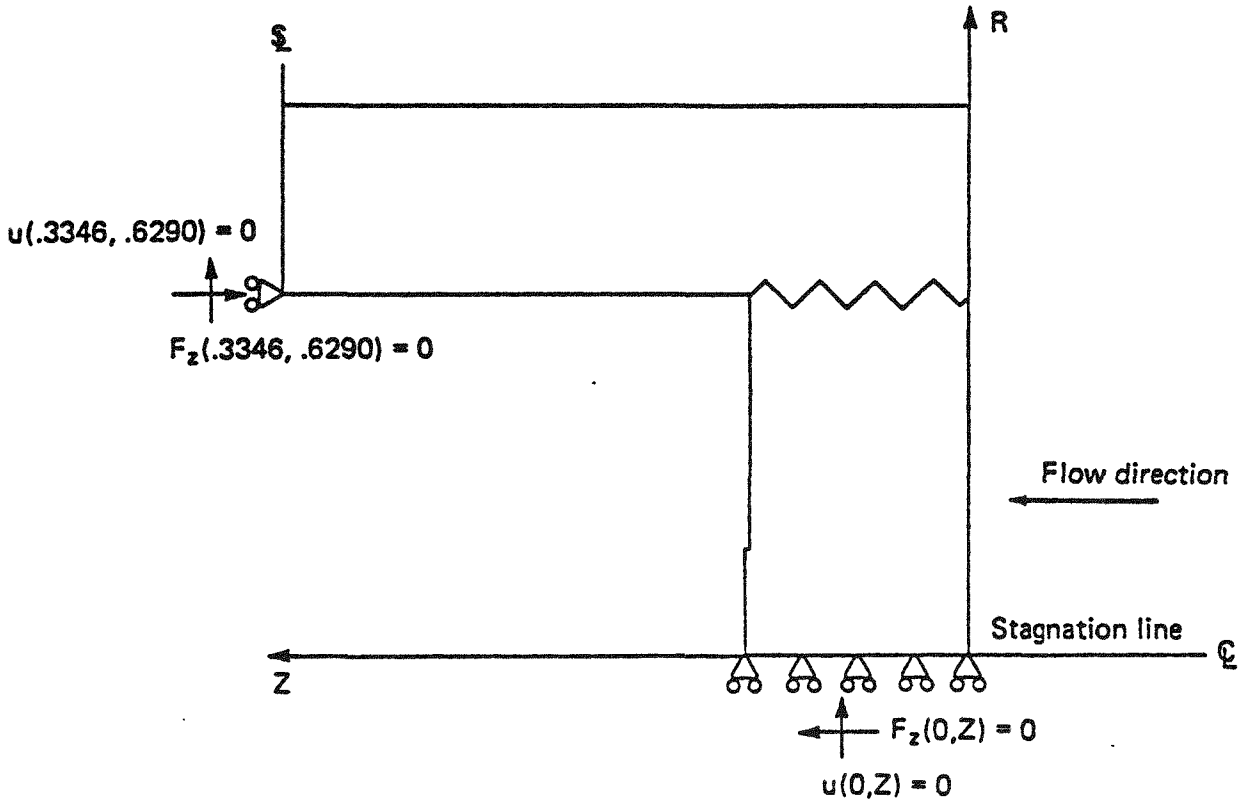

FIGURE G-8: Boundary conditions - end-stable models.

Table G-1: LWRHU End-On Summary Table - Zero Heat Pulse Release

Release @ time = 0.0 s
Calculations @ time = 7.29 s

		IN-PLANE						AXIAL						
	Boundary Condition - Material Model	Ele. #	R (in)	Z (in)	Temp. (°F)	σ_{Max} (σ_T or σ_R)	σ_{ULT} (psi)	S.F.	Ele #	R (in.)	Z (in)	Temp. (°F)	σ_{max} (σ_Z)	σ_{ULT} (psi)	S.F.
Max. Tens.	Axisymmetric-Elastic/T	49*	.3346	.2186	3508	11670 (σ_T)	25000	2.1	37*	.3346	.2859	3045	8177	24300	3.0
	Axisymmetric-EP/TC	49*	.3346	.2186	3508	11666 (σ_T)	25000	2.1	37*	.3346	.2859	3045	8194	24300	3.0
	Axisymmetric-Elastic/GAPS	43*	.3346	.2522	3177	9401 (σ_T)	26000	2.8	37*	.3346	.2859	3045	6264	24300	3.9
Max. Comp.	Axisymmetric-Elastic/T	6**	.5018	.5997	2615	-6122 (σ_T)	22500	3.7	42**	.5018	.2859	3351	-11338	20500	1.8
	Axisymmetric-EP/TC	6**	.5018	.5997	2615	-6076 (σ_T)	22500	3.7	42**	.5018	.2859	3351	-11048	20500	1.8
	Axisymmetric-Elastic/GAPS	6**	.5018	.5997	2615	-5348 (σ_T)	22500	4.2	42**	.5018	.2859	3351	-8106	20500	2.5

* extrapolated values to inner surface of aeroshell
** extrapolated values to outer surface of aeroshell

Table G-2: LWRHU End-On Summary Table - Peak Heat Pulse Release

Release @ time - 7.0 s
Calculations @ time - 7.11 s

	Boundary Condition - Material Model	IN-PLANE Ele. #	R (in)	Z (in)	Temp. (°F)	σ_{max} (σ_T or σ_R)	σ_{ULT} (psi)	S.F.	AXIAL Ele. #	R (in)	Z (in)	Temp. (°F)	σ_{max} (σ_Z)	σ_{ULT} (psi)	S.F.
Max. Tens.	Axisymmetric-Elastic/T	141	.027	.086	1204	6063 (σ_R)	27400	4.5	49*	.3346	.2186	398	4951	23200	4.7
	Axisymmetric-EP/TC	141	.027	.086	1204	6062 (σ_R)	27400	4.5	49*	.3346	.2186	398	4965	23200	4.7
	Axisymmetric-Elastic/GAPS	NO GAP CLOSURE							NO GAP CLOSURE						
Max. Comp.	Axisymmetric-Elastic/T	90**	.5018	.018	3864	-20159 (σ_T)	28000	1.4	72**	.5018	.118	1296	-7998	16000	2.0
	Axisymmetric-EP/TC	90**	.5018	.018	3864	-19615 (σ_T)	28000	1.4	72**	.5018	.118	1296	-7834	16000	2.0
	Axisymmetric-Elastic/GAPS	NO GAP CLOSURE							NO GAP CLOSURE						

* extrapolated values to inner surface of aeroshell
** extrapolated values to outer surface of aeroshell

Table G-3: LWRHU Side-On Summary Table - Zero Heat Pulse Release

Release @ time = 0.0 sec.
Calculations @ time = 7.4 sec.

			IN-PLANE							AXIAL						
	Boundary Conditions - Material Model	Model	Ele. #	R (in)	θ (deg)	Temp. (°F)	σ_{HOOP} (psi)	σ_{ULT} (psi)	S.F.	Ele. #	R (in)	θ (deg)	Temp. (°F)	σ_{T} (psi)	σ_{ULT} (psi)	S.F.
Max. Tension	Plane Stress-Elastic/T	1	86*	.3346	175	1963	6016	28800	4.8							
	SRBC-Elastic/T	2	351*	.3346	177.5	1954	7639	28700	3.8	171*	.3346	87.5	3258	17692	24000	1.4
	SRBC-EP/TC	2	351*	.3346	177.5	1954	7365	28700	3.9	181*	.3346	92.5	3082	15908	24000	1.5
Max. Comp.	Plane Stress-Elastic/T	1	75**	.5015	145	2313	-3341	21000	6.3							
	SRBC-Elastic/T	2	290**	.5015	142.5	2354	-3578	21500	6.0	350**	.5016	172.5	2156	-17789	18500	1.04
	SRBC-EP/TC	2	290**	.5015	142.5	2354	-3168	21500	6.8	350**	.5016	172.5	2156	-12167	18500	1.5

* extrapolated to inner surfaces of aeroshell
** extrapolated to outer surfaces of aeroshell

Table G-4: LWRHU Side-On Summary Table - Peak Heat Pulse Release

Release ⊕ time = 6.96 s
Calculations ③ time = 7.31 s

	Boundary Conditions - Material Model	Model	IN-PLANE Ele. #	R (in.)	θ (deg)	Temp. (°F)	σ_{HOOP} (psi)	σ_{ULT} (psi)	S.F.	AXIAL Ele. #	R (in.)	θ (deg)	Temp. (°F)	σ_{T} (psi)	σ_{ULT} (psi)	S.F.
Max. Tens.	Plane Stress-Elastic/T	1	1*	.3346	2.5	1926	5342	28700	5.4							
	SRBC-Elastic/T	2	21*	.3346	12.5	1985	4428	28900	6.8	1*	.3346	2.5	1954	11842	24300	2.0
	SRBC-Elastic/TC	2	151*	.3346	77.5	1423	5224	27800	5.3	1*	.3346	2.5	1954	10616	24300	2.3
	SRBC-EP/TC	2	151*	.3346	77.5	1423	4851	27000	5.7	1*	.3346	2.5	1954	9946	24300	2.4
Max. Comp.	Plane Stress-Elastic/T	1	5**	.5097	5	4893	-9600	-22800	2.4							
	SRBC-Elastic/T	2	30**	.5098	12.5	4883	-8555	-22700	2.6	30**	.5098	12.5	4883	-27040	-20101	.74
	SRBC-Elastic/TC	2	30**	.5098	12.5	4883	-12240	-22700	1.8	30**	.5098	12.5	4883	-24264	-20100	.83
	SRBC-EP/TC	2	30**	.5098	12.5	4883	-10074	-22700	2.2	50**	.5099	22.5	4589	-17937	-23500	1.3

* extrapolated values to inner surface of aeroshell
** extrapolated values to outer surface of aeroshell

The side-stable solutions were determined by using a coarse-grid, plane-stress solution and noting the time and position of maximum equivalent stress. Final solutions were then obtained by applying the various planar options to the fine-mesh model. The results of the side-stable stress analysis are shown in Tables G-3 and G-4. The most realistic of the stress models is the one using the stress resultant boundary conditions with elastic/plastic material properties that differ in tension and compression. Other boundary conditions and material models (which are less expensive to use) were used for preliminary calculations. The minimum margin in tension is 1.5 for the stress resultant boundary conditions with elastic/plastic material properties that differ in tension and compression. For the same assumptions on boundary conditions, the compressive margin is conservatively stated based on the stress corresponding to a 1% strain. Additional details of the stress analysis are available in Reference 4.

6.0 AEROSHELL INTACT/PG BROKEN REENTRY CASE

During the approach to orbit or in on-orbit situations, there are explosion source within the shuttle bay that could result in the aeroshell not being damaged but the PG insulators could be cracked (see Appendix C, 2.4). In view of the uncertainty surrounding the LWRHU's degree of compaction, prediction of the assembly's reentry thermal response was executed by an approximate technique rather than an elaborate 3-D simulation. The LWRHU's state of compaction was represented by the severe condition of all the assembly's interfaces being closed in perfect thermal contact.

The approximate technique is a 1-D thermal analog which is based on the rationale shown in Figure G-9. The quivalent heating distribution is hallmarked by the heating conversion factors developed in Figure G-10 for the free-molecular and continuum density regimes. The analog showed excellent performance in correlating prior 2-D and 3-D design studies as well as current 2-D studies involving changes in interface heat transfer conditions and reentry reference heating profiles.

Clad melt is the reentry failure mode of concern for the on-orbit explosion scenario. The 1-D analog's prediction of clad thermal response for an orbital decay reentry, given by Figure G-11, indicates a melt temperature margin of 370^{o}F (164^{o}C). This margin, in conjunction with the severe representation of the interfaces' thermal state, indicates that the clad melt failure mode is very unlikely for an orbital decay return with damaged PGs (Reference 5).

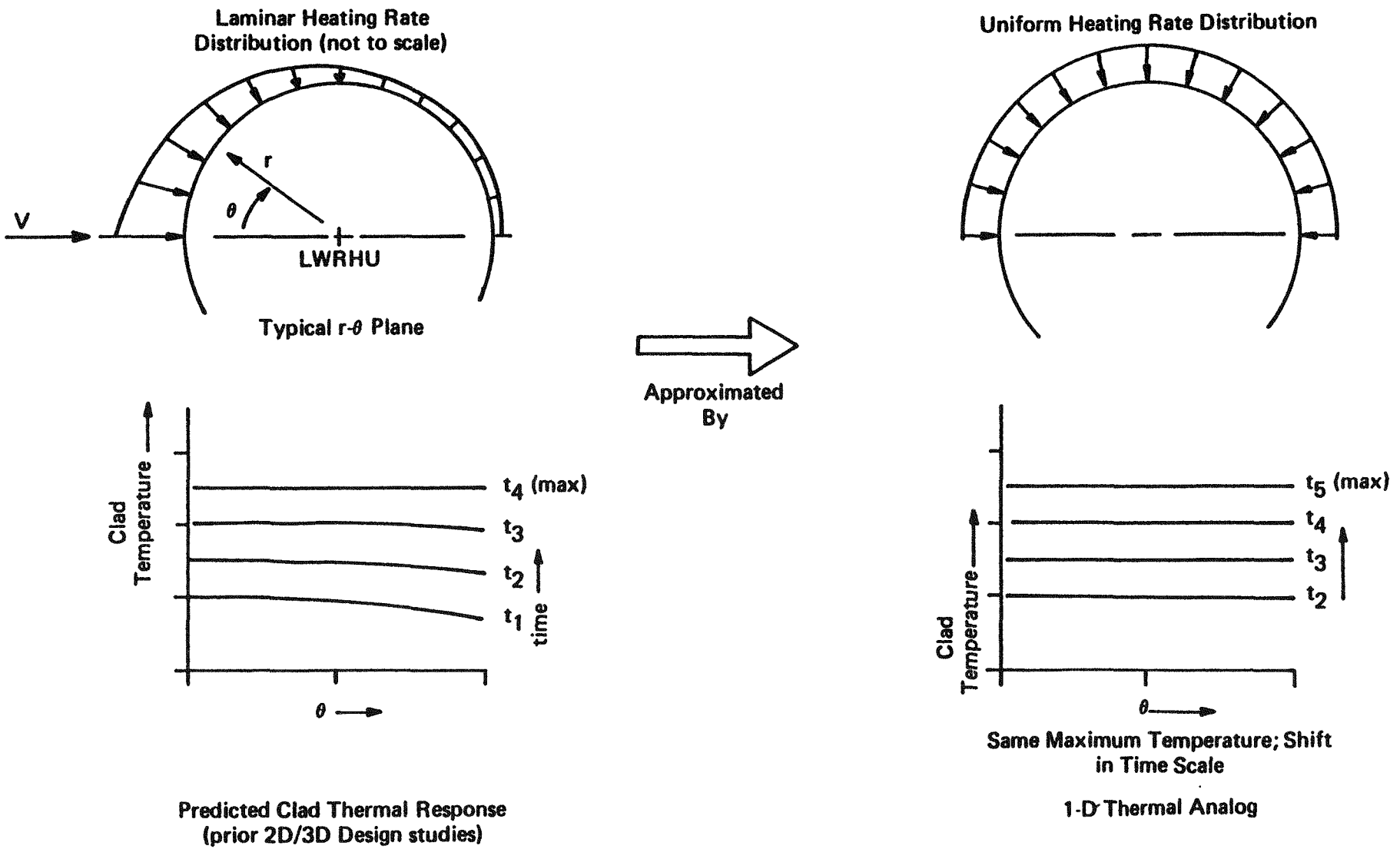

FIGURE G-9: Rationale for 1-D thermal analog.

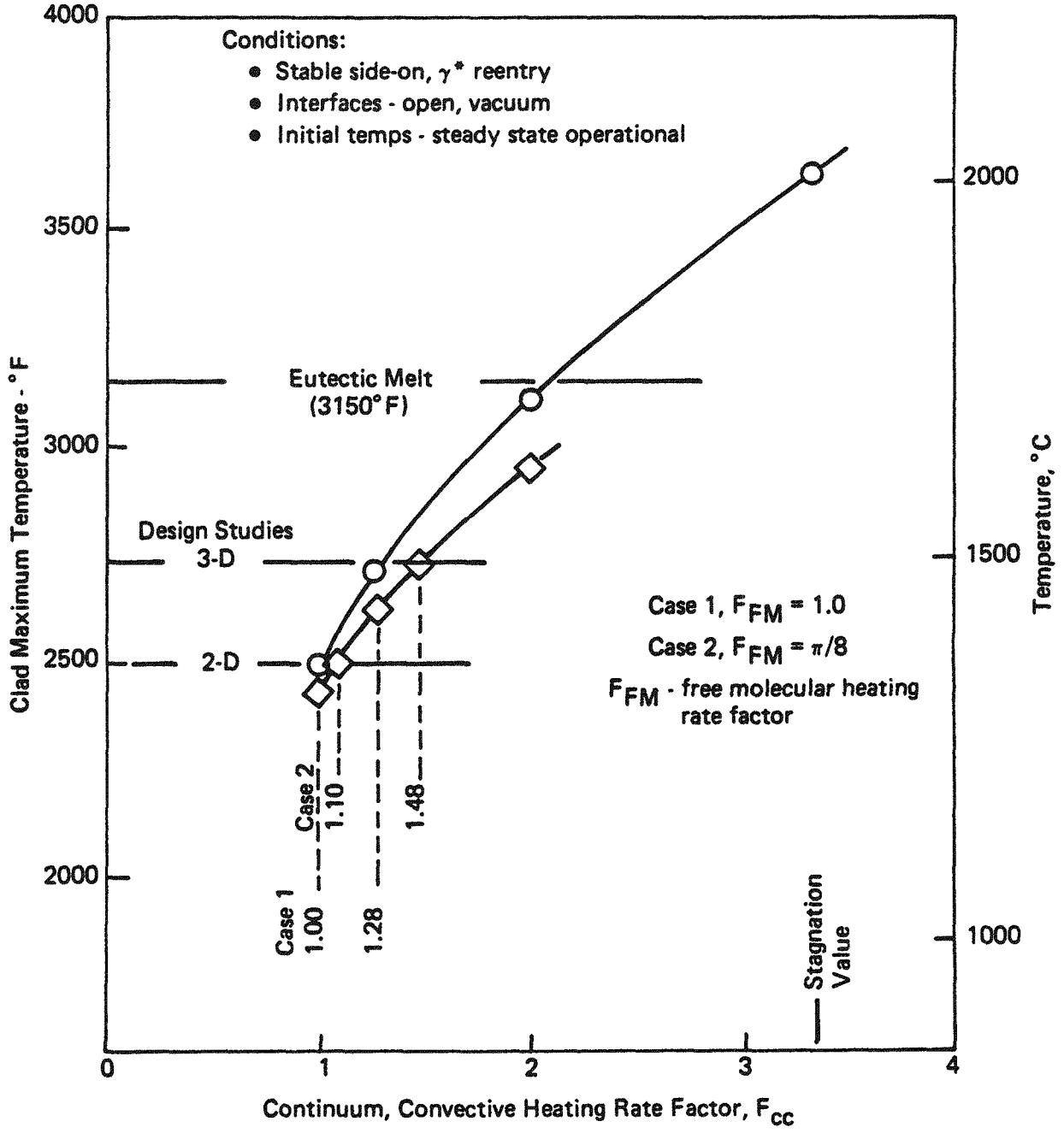

FIGURE G-10: Development of heating rate factors for 1-D thermal analog (correlation of clad peak temperatures - prior design studies).

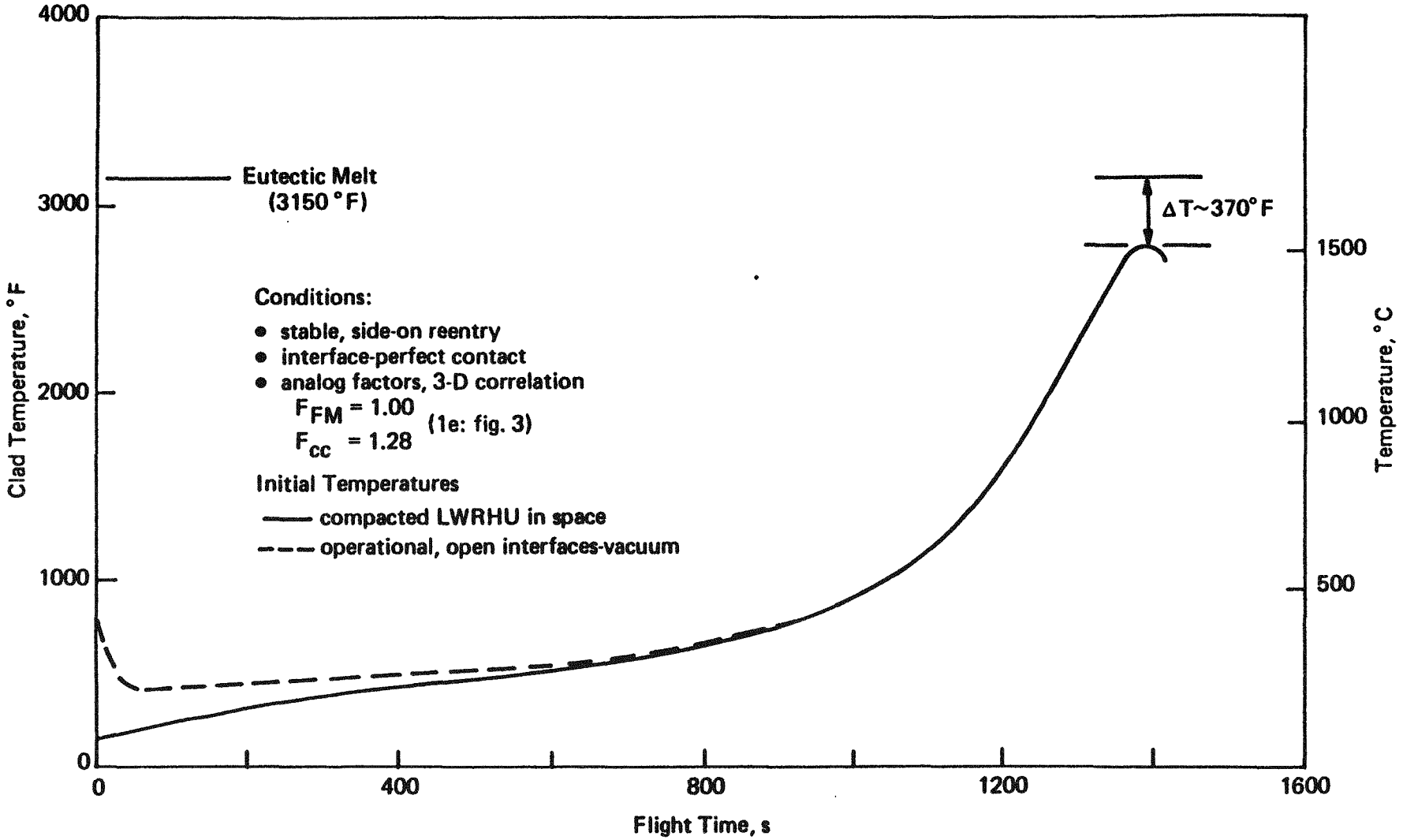

FIGURE G-11: Approximate production of clad maximum temperature; compacted LWRHU - orbital decay reentry; 1-D thermal analog predictor with Case 1 factors.

7.0 SUPERORBITAL (VEEGA) REENTRY RESPONSES

In the safety program effort associated with the Galileo Mission, The Johns Hopkins University/Applied Physics Laboratory (JHU/APL) has been charged by the Department of Energy (DOE) with the primary responsibility of assessing the survivability of the LWRHU in an inadvertent entry into the earth's atmosphere. This section constitutes the JHU/APL contribution to VEEGA portion of the FSAR for the LWRHU (Reference 6).

The mission profile for Galileo includes launch by the Space Shuttle into low earth orbit and subsequent boost into the VEEGA trajectory. This mission profile results in a broad spectrum of possible reentry scenarios, ranging in severity from orbital decay to the very high speed VEEGA reentries. The VEEGA trajectory involves two passes through the earth's gravity field, both of which have some small probability ($\sim 10^{-6}$) of accidental reentry. Detailed analyses of typical reentry scenarios, other than VEEGA, were provided earlier in this appendix. The more severe VEEGA trajectory is the subject of most of this section.

The Galileo/VEEGA earth reentry breakup analysis conducted by the JPL (Reference 7), provided the basis for the initial velocity and altitude conditions selected for the LWHRU analysis. Subsequent detail on altitude-gamma reentry combinations was provided in Reference B, and used to generate the altitude-gamma-velocity charts (Reference 9) used by APL in the reentry analyses.

APL chose to examine the expected initial velocity conditions (46,750 fps, inertial frame) and the midrange altitude versus flight path angle variation corresponding to this velocity as shown in Figure G-12. The first evaluations were restricted to initial flight path angles of -90, -50 and -10 degrees (Reference 10). The -90^{o} case provides representative thermal response behavior for steep reentries to support thermal stress evaluations. The -10^{o} case provides representative thermal and ablation response behavior for shallow reentries where thermal and ablation failure events are more likely to occur.

The orbital and super-orbital (escape velocity conditions) reentry modes were addressed in Reference 11. For the present analyses, the VEEGA entry modes are emphasized. A discussion of the other scenarios is given in Section 7.5.

7.1 Aerodynamics

The LWRHU and LWRHU component aerodynamics used as inputs to the 3DOF trajectory simulation consist of the drag coefficient,

$$C_D = \frac{\text{drag (lbs)}}{1/2\ \rho\ V^2 S}$$

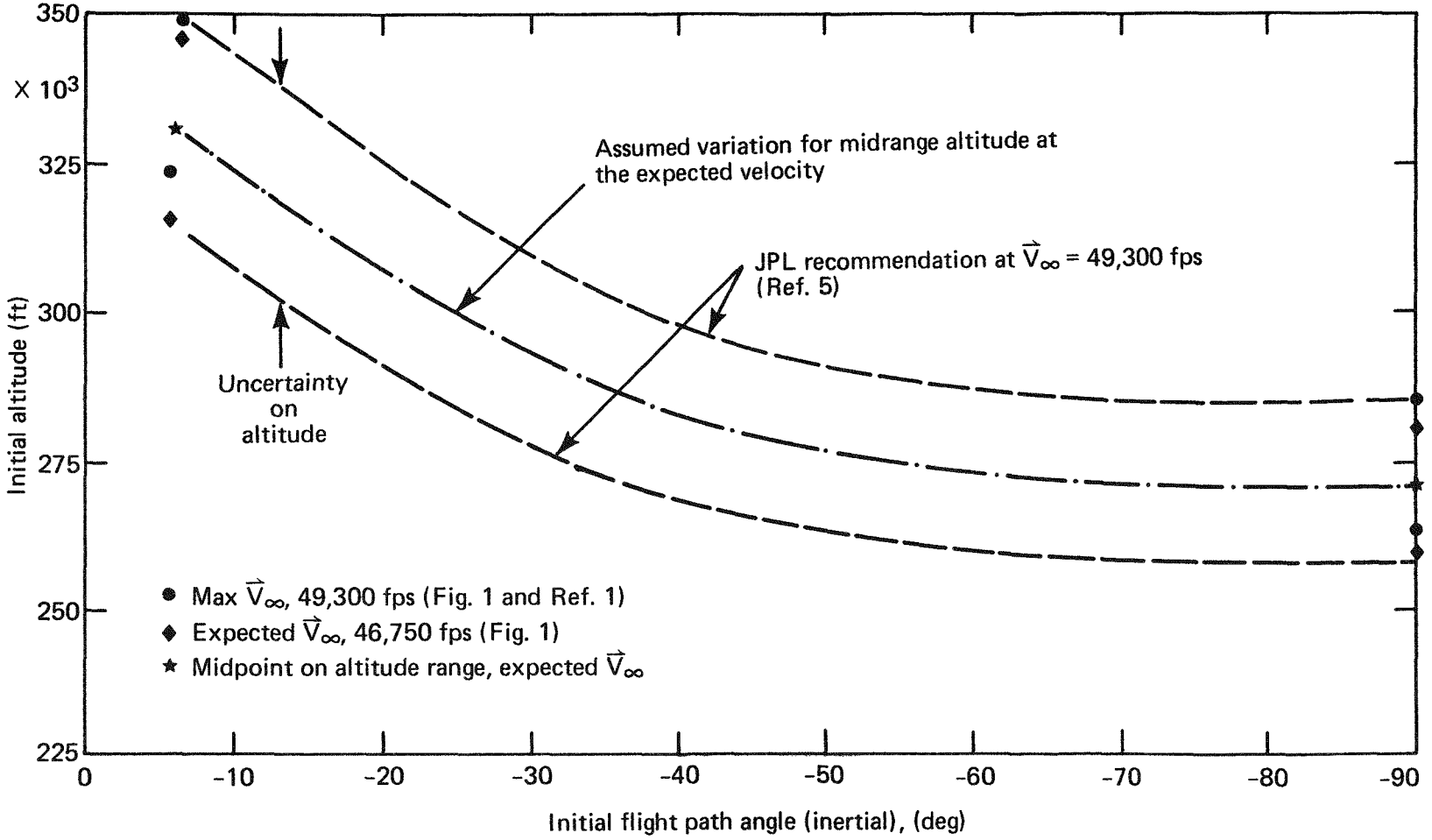

Figure G-12: **Variation of initial altitude versus flight path angle for maximum and expected initial velocities for discrete GPHS module and LWRHU reentries; Galileo-VEEGA mission profile (from Ref. 5).**

where

ρ = density in slugs/ft^2

V = velocity in ft/sec

S = the reference area in ft^2.

These are given as either a function of Mach number and altitude or as a function of Mach number in the continuum flow regime and a bridging function for interpolating between continuum and free molecule flow. A constant value of angle of attack is assumed. Side-on and end-on orientations have been selected for LWRHU thermal and thermal stress analysis. The aerodynamic estimates used as inputs to the 3DOF simulation (Reference 12) are given in Table G-5 for these orientations. Since aerodynamic data for cylinders of these low fineness ratios ($\sim$1.2) are very sparse (especially in the free molecule regime), these aerodynamic estimates are based on a variety of data found on blunt bodies - disks, plates and some cylinders.

The drag coefficient at terminal velocity conditions of the LWRHU, and the terminal velocity were estimated (Reference 13), in support of impact tests performed by LANL as shown in Table G-6. The cross-flow drag (and consequently terminal velocity) is highly dependent on the wall temperature. The transition from cold wall drag to hot wall drag is dependent on Reynolds' number and surface roughness. The expected ranges in these parameters for the LWRHU are such that either cold or hot values are possible in Table G-6.

The drag coefficients for the side-on orientation of the LWRHU clad/fuel assembly and for the fuel pellet were assumed to be the same as for the LWRHU, except that the reference areas are appropriate for these components viz: 0.001074 ft^2 for the clad/fuel assembly and 0.000583 ft^2 for the fuel pellet. The estimated terminal velocities at sea level are 162 ft/sec for the clad assembly and 119 ft/sec for the fuel pellet. For the end-on orientations the terminal velocities are about the same as for the side-on orientation.

7.2 Thermal Analysis

7.2.1 Assumptions -

7.2.1.1 Initial Reentry Conditions and Analysis Guidelines - The analysis guidelines are listed in Table G-7 for the network of VEEGA reentry analyses. The initial primary reentry conditions for all LWRHU assemblies are as given in Section 7.0. These primary reentry evaluation cases were supplemented in the thermal analyses by evaluations at -4.5 and -30 degrees to further define LWHRU response behavior over the entire VEEGA V-γ map.

Table G-5: Estimated Drag Coefficients for Lightweight Radioisotope Heater Unit

A. End-on

M	C_{D_C}
0	1.0
0.8	1.2
1.0	1.4
1.5	1.8
2.0	1.9
10.0	1.9

$C_{DFM} = 2.95$

Equivalent sphere radius, $R_s = 0.147$ ft

Exponent E_D in Matting's Bridging Equation: $E_D = 2.20$

Reference area: $S = \frac{\pi D^2}{4} = \frac{\pi (1.0216)^2/144}{4}$

$S = 0.00569$ ft^2

B. Side-on (taken from 3DOF inputs 10/12/79)

CD	Altitude (ft)
1.200000	0.0
1.200000	100000.00
1.240000	200000.00
1.320000	230000.00
1.330000	235000.00
1.370000	250000.00
1.620000	300000.00
2.049999	350000.00
2.099999	400000.00

Low Mach No. Table Switch when M < 0.9 or when altitude < 100000.0

CD	Mach
0.554000	0.0
0.554000	0.50
1.259999	0.60
2.000000	0.90
2.099999	1.00
2.000000	1.10
1.699999	1.30
1.370000	1.50
1.259999	1.80
1.240000	2.00
1.209999	2.30
1.200000	2.50
1.200000	40.00

$S = \frac{1.2579 \times 1.0216}{144}$

$= 0.008924$ ft^2

Table G-6: Estimated Drag Coefficients and Terminal Velocity for LWRHU.

A. Drag Coefficient, C_D

	Axial	Crossflow	Average	
S = 0.00567 ft^2	1.0	0.7865	0.89	Cold
		1.121	1.06	Hot

B. V_{term}: ft/sec (m/sec)

	Axial		Crossflow		Average		
	Sea Level	10K ft	Sea Level	10K ft	Sea Level	10K ft	
W = 0.08886#	115 (35)	134 (41)	129 (39)	151 (46)	122 (37)	142 (43)	Cold
			108 (33)	126 (38)	112 (34)	130 (40)	Hot

Table G-7: Guidelines for LWRHU Reentry Evaluation Process

GALILEO/VEEGA

A. INITIAL REENTRY CONDITIONS:

JPL BREAKUP STUDY FOR GPHS

VELOCITY: 46,750 FPS (EXPECTED)

ALTITUDE: MIDPOINT ON UNCERTAINTY RANGE

GAMMA: -10, -50, -90 DEGREES

B. REENTRY CONFIGURATION:

SEQUENTIAL BREAKUP

LWRHU ASSEMBLY → CLAD/FUEL ASSEMBLY → FUEL PELLET

NO FUEL PARTICLES OR FRAGMENTS

C. REENTRY ORIENTATION:

ALL CONFIGURATIONS: PRIORITY: 2-D SIDE-ON

SECONDARY: 2-D END-ON

D. FAILURE CRITERIA:

SUBJECTIVE: RECOGNITION OF UNCERTAINTIES

ABLATION: 50% AEROSHELL WALL

CLAD MELT: W/INSULATION: EUTECTIC - 300°F

W/O INSULATION: EUTECTIC - 500°F

E. BREAKUP CRITERIA:

AEROSHELL: INCIPIENT PENETRATION AT 50% WALL, STAGNATION REGION

CLAD: INCIPIENT MELT, STAGNATION REGION

7.2.1.2. Reentry Configurations - This study considered simplified three stage sequential break-up scenario consisting of (a) a full LWRHU assembly followed by (b) an instantaneous breakup and release of the clad fuel assembly followed finally by (c) instantaneous breakup and release of an integral fuel pellet should failure events occur during the course of reentry. Neither fractured segments of the pellet nor particle fines, possibly produced during assembly or the prior phases of the mission, have been considered as discrete reentry bodies upon a clad failure event.

7.2.1.3 - Reentry Orientation - Each of the reentry configurations discussed above can ideally assume three orientations: side-on stable, end-on stable and tumbling. In truth, however, reentry orientation is a dynamic, stochastic process dependent upon applied forces and moments resulting from structural breakup and release. Consequently, given a reentry environment that leads to a complete breakup sequence, and that further includes all orientation permutations, 27 cases would be required to analyze a single reentry condition. Multiplying this potential requirement by four or five initial reentry conditions, as considered in this study, demonstrates the need to choose specific reentry orientations for analysis.

The primary orientation assumed for the LWRHU assembly and subsequent breakup configurations was a sustained side-on stable attitude from initial reentry through to impact. A preferred (or stable) reentry orientation is a hotter condition than a dynamic, tumbling mode and, of the two idealistic stable attitudes, previous design studies indicate a side-on orientation will more likely produce a clad melt event. Of all the in-flight failure modes, the clad melt event bears the greatest significance since it nearly always results in fuel release (if not during flight, then ultimately at impact).

Limited cases of LWRHU reentries for an idealized end-on stable orientation were also examined. Clad/fuel assembly and fuel pellet reentry analyses need to be conducted to examine the effect of orientation on melting.

7.2.1.4 Failure Criteria for Ablation and Thermal Response - The threshold failure criteria used in this study to identify ablation and clad melt failure events (Table G-7) are an attempt to recognize the uncertainties that affect analyses for high energy reentries such as the VEEGA family. These criteria are subjective, relying on engineering intuition rather than hard statistical analyses. In most cases, statistics are simply not available for the numerous environmental and response variables that determine these failure modes.

Two criteria are specified for the melt failure. The threshold failure temperature for those members protected by insulation is the platinum- carbon eutectic temperature minus 300°F. This corresponds to (3660-300°) = 3360°R for the LWRHU's Pt30Rh member. For non-insulated members, the threshold is lowered by 500°F (or 3160°R for the Pt30Rh clad) since there will now be greater sensitivity via direct exposure to environmental uncertainties.

On the probability of melt failure, the farther a response variable such as 'aeroshell recession' or 'clad temperature' is predicted to exceed the failure threshold, the greater the probability of failure.

7.2.1.5 Breakup Criteria - In this study, the failure thresholds for both the ablation and melt failure modes at the side-on stagnation location were chosen to identify an instantaneous catastrophic failure for either the LWRHU or clad/fuel assemblies with resulting instantaneous release of its contents. Fuel pellet melting is also initiated at the threshold of the 500°F uncertainty band for all locations on the pellet. However, the issue for bare fuel reentry is not one of failure identification but rather determination of the pellet's melt mass fraction during entry.

7.2.2 Methodology: Side-on Analyses

7.2.2.1 Zonal Approach for VEEGA Reentry Safety Evaluation - A zonal approach over the VEEGA reentry V-γ map was selected for the evaluation of reentry performance (Figure G-13). Five discrete zones ranging from Zone A for shallow reentries (that are critical to both the aeroshell ablation and clad melt failure modes) to Zone E for steep reentries (which are critical to aeroshell thermal stresses) were defined.

The strategy was formulated for the side-on analysis but the general approach is applicable to any orientation.

The boundaries of the zones are given by the dashed lines with the overall map defined by the escape condition as the left extremum and the vertical entry as the right extremum. Within each zone are, shown by a solid line, the primary reentry evaluation condition for the side-on LWRHU assembly. The supplemental evaluation conditions were conducted to provide a more definitive response description over the entire reentry map. The response behavior of a side-on LWRHU determined for a particular reentry condition in a zone is taken to be representative for the entire zone (i.e., from -70 to -90°). For example, the LWRHU response predicted for the -50° reentry is representative of Zone D (from -40 to -70°) and so on.

This zonal map indicates that resolution on response behavior increases with decreasing flight path angle. In Zone E, this resolution is a relatively coarse 20° on flight path angle since environmental sensitivity to initial flight path angle is low in this region of the map. The resolution has sharpened to 10° in Zone C and becomes even finer in A and B where environmental sensitivities to flight path angle are large.

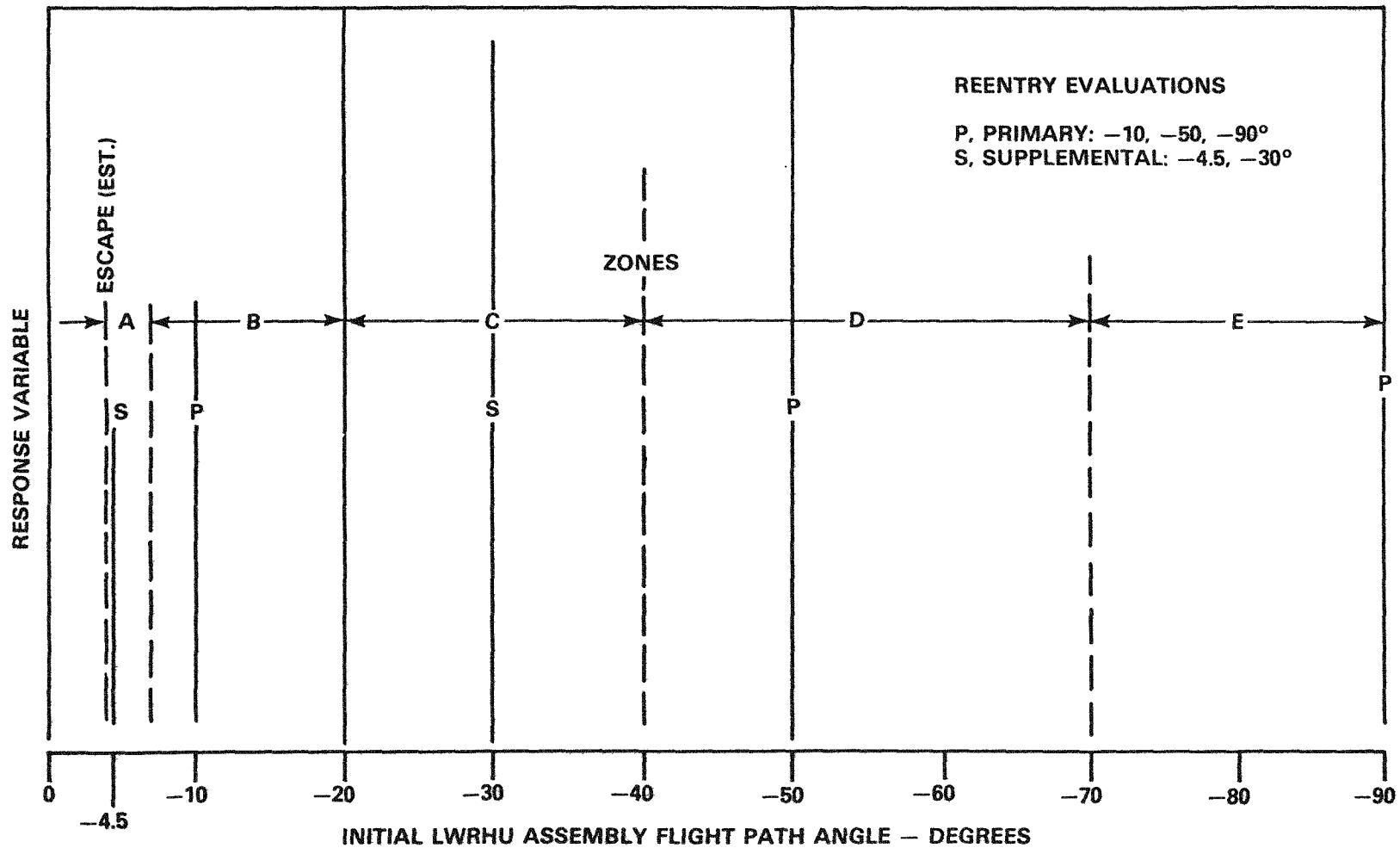

Figure G-13: Zonal evaluation of LWRHU reentry performance for Galileo/VEEGA; side-on stable LWRHU assembly reentry configuration.

From the three degree of freedom (3DOF) trajectory analyses for the side-on orientation, it was determined that the LWRHU would exit in an escape trajectory for initial flight path angles, γ, of -4.0^{o} or less; it would be captured on the second pass for $\gamma = -4.25^{o}$; and it would be captured on its initial pass for $\gamma = -4.50^{o}$. This demonstrates the sensitivity to flight path angle in defining, for the side-on LWRHU, the various classes of reentries. The escape boundary (-4.125^{o}) and the multiple pass boundary (-4.375^{o}?) were taken to be the mid-values based on the cases examined in the trajectory analyses.

7.2.2.2 Reentry Trajectory Analyses - Side-On Stable LWRHU - Since idealized side-on stable orientations were assumed for the LWRHU assembly as well as for subsequent breakup configurations throughout reentry, trajectory analyses were restricted to three degree of freedom flight dynamics as opposed to more complicated 6DOF simulations. The 3DOF code used in these analyses has been documented in Reference 14.

Table G-8 provides the initial conditions for the side-on LWRHU corresponding to Zones A through E defined for the VEEGA reentry map. As previously discussed in Section I, these initial conditions were obtained from the JPL breakup study conducted for the Galileo spacecraft to identify GPHS module release events. This table also states other conditions specified for the analyses. It is emphasized that the trajectory analyses do not contain ablation coupling effects in terms of either changing weight (i.e., mass loss) or changing aerodynamics (via shape change) as a function of reentry flight time. This omission is due to limitations in the available trajectory and heat transfer computational codes at APL.

Figure G-14 shows the representative trajectory profiles over the hypersonic heat pulse period for each of the zones of the Galileo-VEEGA reentry map. There is a remarkable insensitivity of the trajectory track and hence reentry environment to flight path angle in Zones C through E. Flight path sensitivity becomes more evident in travelling from Zone C to Zone B. The totally different character of the Zone A profile is typical of minimum gamma trajectories for prompt reentries that show an intermediate peak in altitude prior to final descent to impact. This type of reentry results in a prolonged convective heat pulse and therefore represent severe environments for evaluating the ablation and thermal response failure modes as will be indicated in the next section. The critical or design minimum gamma would be one in which the track peaks at or close to 400,000 feet (i.e., the edge of the sensible atmosphere) prior to final descent. As will be noted later, the heat pulse flight period for all zones terminate at an altitude of about 100,000 feet or greater. Note that the location of the maximum convective heating rate for the various zones covers a wide range on altitude (approximately 150K to 250K ft) but a narrow band on velocity (38K to 40K fps).

Table G-8: GALILEO-VEEGA Reentry Trajectory Analyses Conditions, Assumptions and Limitations

A. Initial Conditions (inertial frame):

VARIABLE	A	B	C	D	E
Velocity (fps)	46,750	→	→	→	→
Flight path (deg)	-4.5	-10.0	-30.0	-50.0	-90.0
Altitude (ft)	330,700	324,000	293,500	277,000	271,000
Azimuth (deg)	90.0	→	→	→	→
Latitude (deg)	0.1	→	→	→	→
Longitude (deg)	0.1	→	→	→	→

B. Other Conditions and Assumptions:

Atmosphere: 1962 Standard

Earth Model:

Oblate with polar radius: 20,855,100 ft

equatorial radius: 20,925,530 ft

Rotating at $0.72921146 \times 10^{-4}$ radians/second

Boundary Layer is asumed to be laminar.

C. Computer Code Limitations:

No ablation coupling effects on weight or aerodynamics

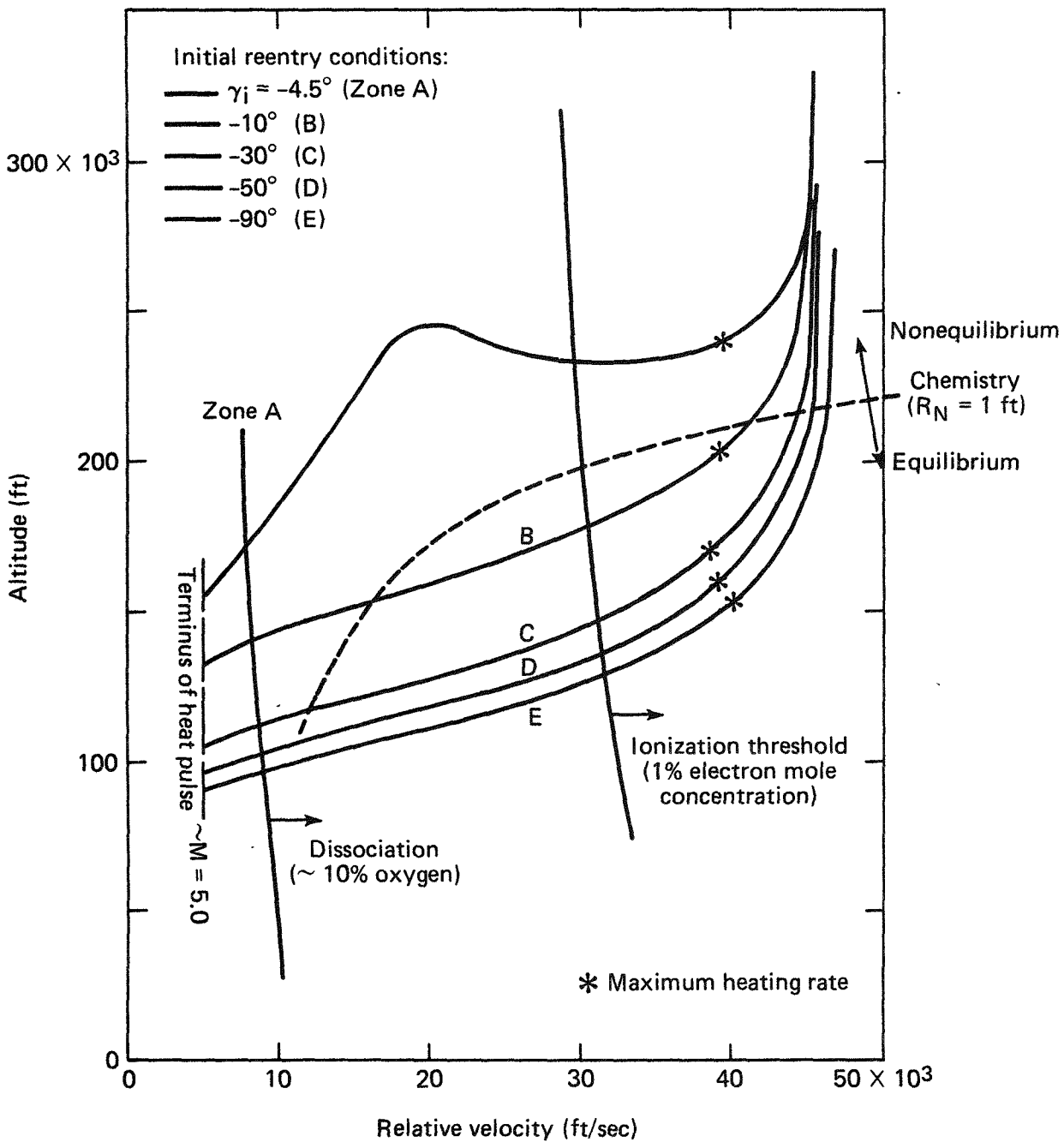

Figure G-14: **Aerothermodynamic regimes for the Galileo/VEEGA zonal reentries; side-on stable LWRHU configuration.**

7.2.2.3 Engineering Methods and Correlations - Due to the high energies of the VEEGA reentries, the aerothermodynamics for the LWRHU are complicated by the addition of shock layer radiation as a mode of heat transfer. Furthermore, both the radiative and convective modes are influenced by chemistry effects that further complicate the reentry environments. This is illustrated in Figure G-14 which shows thresholds for both the dissociation and ionization (and therefore radiating) processes as well as the kinetic threshold as overlays on the trajectory tracks for the various zones of the Galileo-VEEGA reentry map. These thresholds are very approximate but serve to illustrate the various aerothermodynamic regimes encountered by a side-on LWRHU reentry. It is also indicated in Figure G-14, that nonequilibrium chemistry is probably a consideration in the maximum heating region for most of the reentry zones. This has implications regarding both the radiative and convective heat transfer modes as will be discussed later.

An extensive description of the assumptions for the reentry analysis is provided in Reference 15. The reference sources for the theory, experimental data, code user's manuals and other background data are also cited in this reference.

7.2.2.4 Summary of Zonal Environments - Side-on LWRHU Reentry Configuration - The 3DOF trajectory analyses provide aerodynamic and aerothermodynamic histories in addition to the basic position, velocity and acceleration data. Galileo-VEEGA reentry environments for side-on LWRHU flight conditions which were generated using the 3DOF simulation are given in Table G-9 for each of the five zones in this study.

Table G-9 displays the typical environmental trends of increasing heating rates, (item 1) decreasing heat pulse periods (item 4) and decreasing time integrated heat loads (items 2,3,) with increasing flight path angle (i.e., from Zone A to Zone E). The high energy VEEGA reentries invoke an additional heating mode (shock layer radiation) in establishing thermal environments. However, the LWRHU reentry thermal environment remains convectively dominant. Therefore, the omission of the radiation blockage effect (due to ablation products) in this study is not consequential for this reentry safety evaluation except perhaps for very abbreviated flight periods in the steeper reentry zones.

As Mach 5 is essentially the terminus for the hypersonic heat pulse period, it is shown by comparison from this table that the heat load (item 3) is essentially equivalent to the total heat load (item 2). Therefore, failure events leading to atmospheric release of fuel will likely occur at or before the Mach 5 condition and at sufficiently high altitudes ($\geq$ 90,000 feet) to be subject to global dispersion.

Table G-9: Galileo-VEEGA Reentry Environmental Parameters - LWRHU Side-On Stable Attitude

Reentry Parameters	Reentry Zones[1] A (-4.5°)	B (-10°)	C (-30°)	D (-50°)	E (-90°)
1. Max stag. heating rate (Btu $ft^{-2}sec^{-1}$)					
(a) convective[2]	1528.0	3018.3	5387.0	6869.5	8382.1
(b) radiative[3]	11.5	91.5	553.9	1054.3	1781.1
(c) flight time, sec	36.0	16.2	5.4	3.4	2.6
2. Total heat load (Btu ft^{-2})					
(a) convective	106614.0	48830.0	28539.0	23436.0	21729.0
(b) radiative	346.0	643.0	1208.0	1584.0	2097.0
3. Heat load to M=5					
(a) convective	106439.0	48719.0	28488.0	23394.0	21693.0
(b) radiative	346.0	643.0	1208.0	1584.0	2097.0
(c) altitude at M=5	154938.0	133020.0	105128.0	95501.0	89830.0
4. Flight time (sec)					
(a) hypersonic (M>5)	265.8	41.4	12.6	7.9	6.1
(b) supersonic ($5 \geq M \geq 1$)	52.3	36.5	15.6	6.6	5.0
(c) subsonic (M<1)	382.0	385.5	360.6	348.1	336.3

Table G-9 (Continued): Galileo-VEEGA Reentry Environmental Parameters - LWRHU Side-On Stable Attitude

Reentry Parameters	Reentry Zones A (-4.5°)	B (-10°)	C (-30°)	D (-50°)	E (-90°)
5. Max stag pressure (atm)					
(a) value	0.079	0.499	1.777	2.888	3.959
(b) fight time, sec	47.0	22.1	7.4	4.6	3.5
6. Max deceleration					
(a) value (gees)	11.5	67.4	237.2	348.2	525.5
(b) flight time, sec	47.0	22.0	7.4	4.6	3.5
7. Impact velocity, fps	123.5	123.5	123.5	123.5	124.4

Notes:

1. each zone represented by singular reentry as specified by initial flight path angle in parentheses.

2. stagnation convective heating rates and heat loads based on transformed values from a reference one-foot body sphere to the side-on LWRHU using hypersonic stagnation velocity gradient parameters.

3. stagnation radiative heating rates and heat loads based on an effective spherical radius that provides an equivalent adiabatic shock standoff distance as the side-on LWRHU.

Other parameters generated by the 3DOF trajectory code are pertinent to structural environment during flight, viz: maximum stagnation pressure and maximum deceleration (Table G-9, items 5,6). Whereas stagnation pressures are moderate ($\leq$4 atmospheres) over the entire reentry map, the decelerations have a wide range over the various zones.

A rough indication of the impact environment is given by impact velocity (item 7) and subsonic flight periods (item 4) for the various zones. For the full LWRHU assembly, all zones essentially acquire terminal (or equilibrium) velocity of about 125 fps at impact. A long subsonic flight period, which constitutes over 96% of the total flight time for the steeper zones, suggests an extended cooling period to lower the clad's temperatures without incurrence of brittleness, improve its strength and thereby improve its impact performance.

7.2.3 Thermal Models

7.2.3.1 Thermal and Ablation Response Considerations - In determining the LWRHU assembly's thermal and ablation response, two basic modelling requirements need to be considered. The first is one of modelling the LWRHU's structural configuration in variables appropriate for solving the general thermal diffusion partial differential equation. The second modelling requirement is one of simulating the ablation processes operating at the LWHRU aeroshell's external surface.

7.2.3.1.1 LWRHU Thermal Models - Solutions to the thermal diffusion equation must be done numerically since, for reentry problems such as the VEEGA scenarios, the equation itself is highly nonlinear and the required boundary conditions are nonlinear in both time and space. A numerical approach requires subdividing the various structural components into discrete elements or nodes with each of their center of mass being a spatial location for a calculated temperature history as the solution marches in time along the reentry trajectory. Each node is characterized by a thermal capacitance and thermal conductance (connecting adjacent nodes) wherein the total composite is termed the thermal network. The two-dimensional (2-D) thermal network for the LWRHU assembly considered in the side-on analyses is shown in Figure G15-a and represents a cross-sectional view in cylindrical coordinates (R, R) taken at the mid-plane of the assembly. The second thermal model is the side-on clad/fuel assembly reentry configuration (Figure G-15b) that would result from either an ablation or thermal stress failure of the LWRHU aeroshell. The third model considered was the 2-D side-on fuel pellet configuration (Figure G-15c) that would result from a clad melt failure.

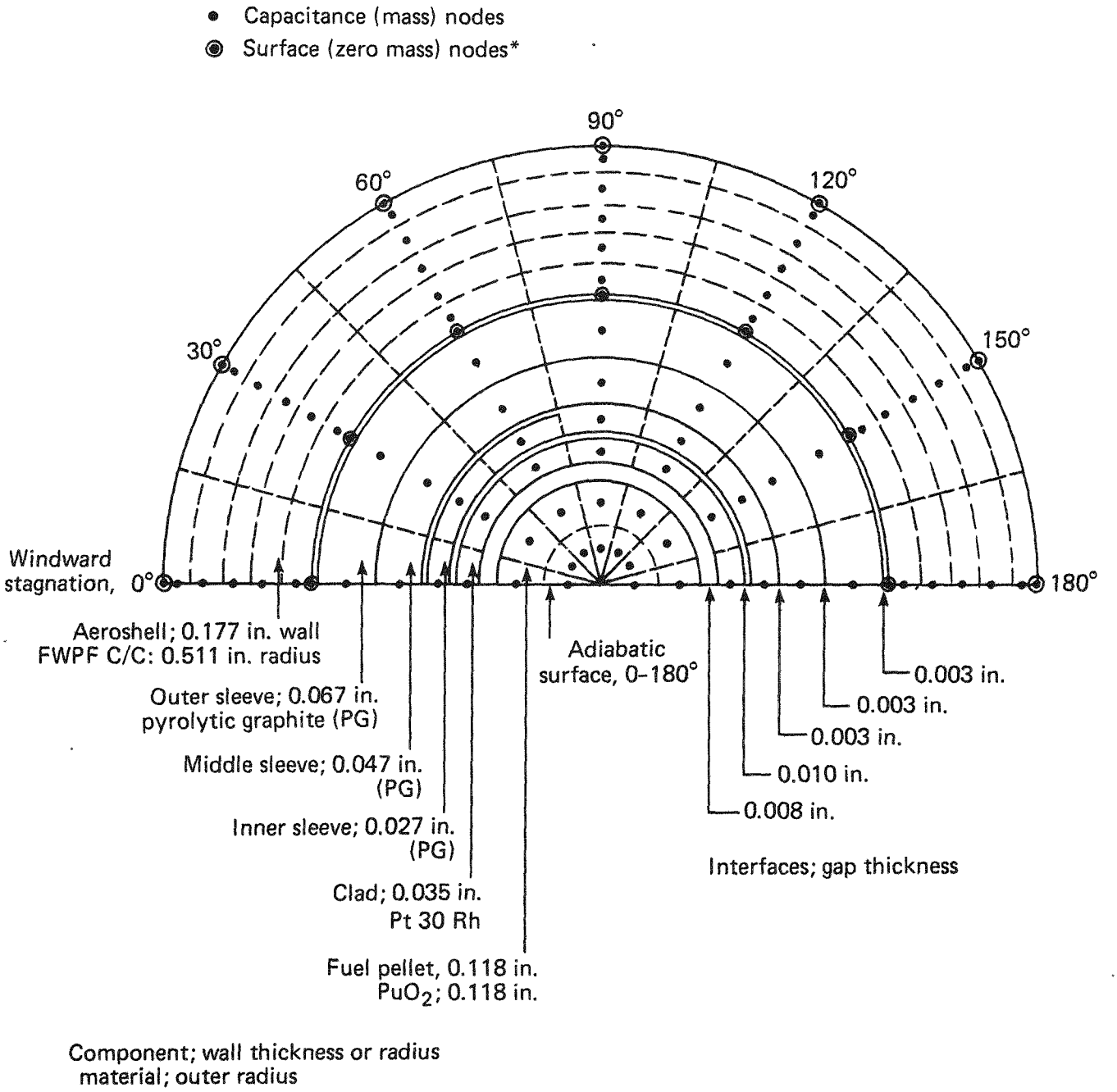

Figure G-15a: **2-D thermal model for side-on LWRHU assembly; mid-span cross section (not to scale).**

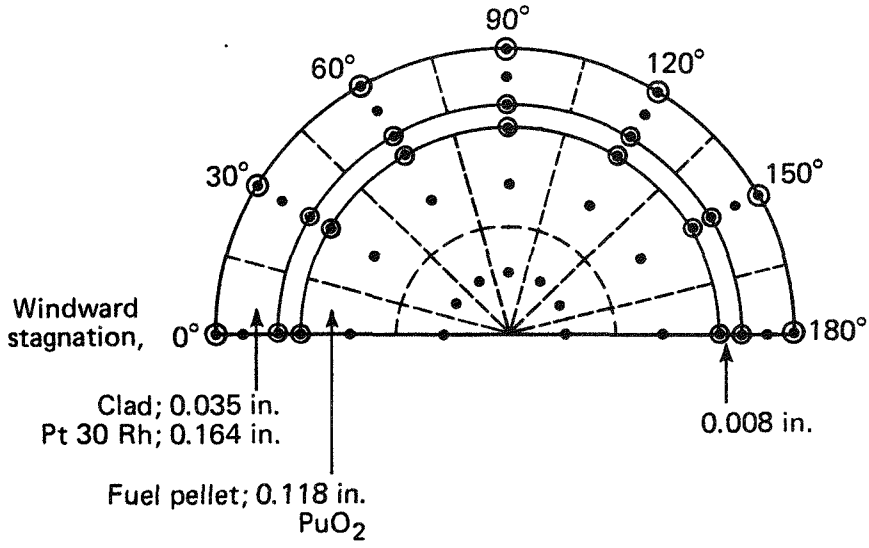

Note: model extracted directly from LWRHU assembly model; refer to Fig. 17a for details.

Figure G-15b: **2-D thermal model for side-on clad/fuel assembly (not to scale).**

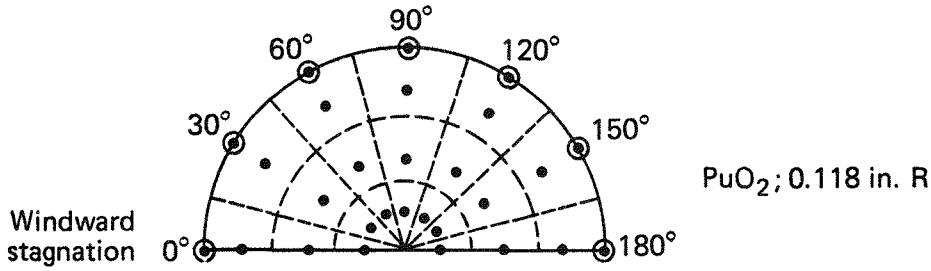

Figure G-15c: **2-D thermal model for side-on fuel pellet (not to scale).**

7.2.3.1.1.1 Interface Heat Transfer - The modes of heat transfer that are typically considered at an internal interface are thermal radiation, gaseous conduction and solid conduction. The first two will be operative for interfaces that have a gap between components and the latter for interfaces with components in intimate contact. In some instances (e.g., high altitude flight), only radiation exchange will be considered as a heat transfer mode. Forced or natural convection models historically have not been considered as an additional heat transfer mechanism in reentry safety analyses.

Prior reentry design studies for parking orbit related scenarios considered vacuum gaps that eventually became filled with helium due to helium release from the plutonia fuel. Release was somewhat arbitrarily related to threshold temperature levels specified for the clad member (Appendix G, Reference 11). A more sophisticated model for the fuel's helium release along with considerations of gas infiltration and extraction through the LWRHU aeroshell's permeable wall provided a clad thermal response that was closely approximated by use of a one atmosphere air-fill in the gaps from initial reentry to impact (Appendix G, Reference 6). The simpler air-fill model was chosen for the VEEGA side-on thermal models to expedite the study. Gaseous conduction is calculated from the fundamental Fourier heat conduction law. Thermal radiation across the interface gaps considers a radiation exchange factor based on parallel plate geometry and limits radiation to just the opposing set of nodes due to the small sizes of the gaps. The gap sizes are shown in Figure 15 and have been assumed to be uniform circumferentially and constant with time.

7.2.3.1.1.2 Boundary Conditions - The numerical solution of the diffusion equation requires an initial value of the LWRHU's temperature distribution and two boundary conditions for each spatial independent variable. The initial temperature distribution is generally taken to be the steady state operating temperature in space which is a strong function of the packaging configuration. As an expedient, it was assumed in this study that all the Galileo units possess the same initial steady state temperature based on direct exposure to space.

Adiabatic (or insulated) surfaces were assumed. This results from the intrinsic symmetry of the problem (Figures G-15a, b, and c).

From considerations of energy balance at all internal and external surfaces for the LWRHU's various components, Figure G-16, the following boundary conditions were specified:

Solid heat conduction $\left(\begin{matrix}\text{to surface}\\ \text{from}\end{matrix}\right)$ equals

gaseous heat conduction plus radiation $\left(\begin{matrix}\text{from surface}\\ \text{to}\end{matrix}\right)$

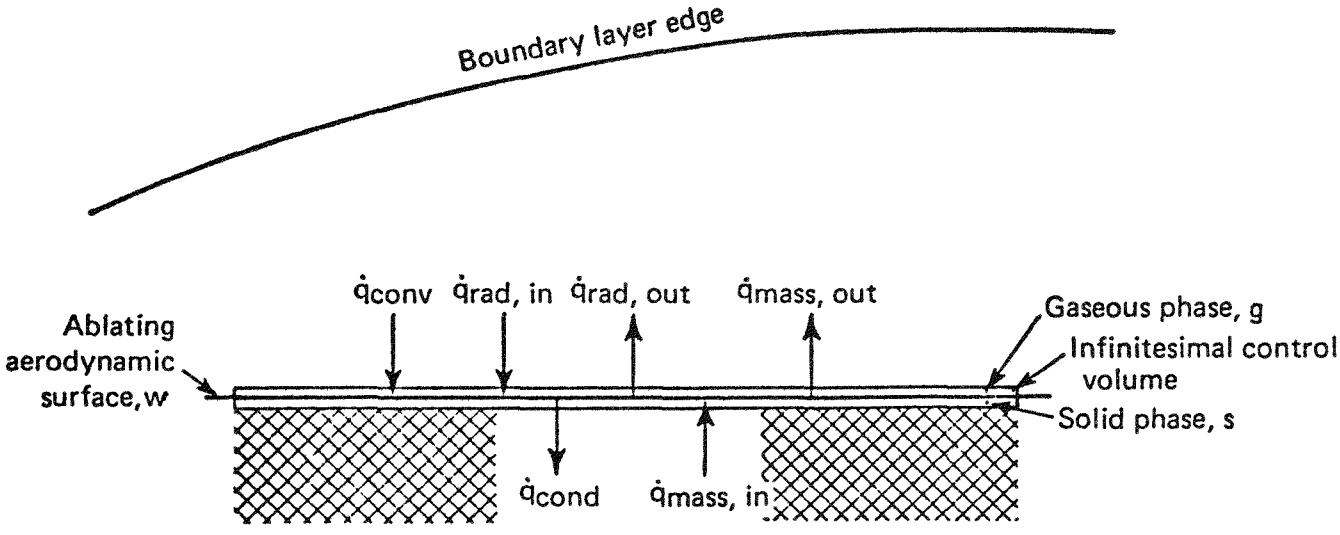

Boundary condition: $\sum_i \dot{q}_i = 0$ where

- $\dot{q}_{conv}$ = Boundary layer convective transfer comprised of gaseous conduction transfer $(-k_{t_g}\partial T/\partial r)_{g,\, r=w}$ and diffusion transfer $\rho \sum_i D_{ij} H_i (\partial k_i/\partial r)_{r=w}$
- $\dot{q}_{rad,\, in}$ = Shock layer radiative transfer
- $\dot{q}_{rad,\, out}$ = Surface emissive transfer, $\sigma \epsilon_h T_w^4$
- $\dot{q}_{cond}$ = Solid conduction (Fourier) transfer, $-k_{t_s} (\partial T/\partial r)_{s,\, r=w}$
- $\dot{q}_{mass,\, in}$ = Mass flux transfer-solid phase, $\dot{m} H_{w_s}$
- $\dot{q}_{mass,\, out}$ = Mass flux transfer-gaseous phase, $\dot{m} H_{w_g}$

} Energy transfer due to thermochemical ablation

Figure G-16: **Surface energy balance — reentry thermal analysis.**

The external (or aerodynamic) surfaces' energy balance is the major requisite of the reentry solution by coupling the reentry environment to the structural response of the reentry body. The energy term coupling the environment to the structural response is the solid conduction term, $\dot{q}$(cond).

7.2.3.1.2 Ablation Models - Carbon-Carbon Material - Figure G17 shows the surface mass balance considered in ablation modelling of carbon-carbon materials. For this study, mass loss due to mechanical ablation (e.g., aerodynamic shear loads) was not considered and represents a major uncertainty in addressing the LWRHU's ablation failure mode. This uncertainty, along with other uncertainties in modelling discussed in various sections of this report, constitute the rationale for the use of a 50% wall thickness failure criterion. Arc jet ablation tests for the LWRHU that are in progress (see Section 7.4) may provide insight for evaluating this ablation term; however, test results were not available in time to influence this study. Furthermore, the tests will not reproduce the pressure/temperature extremes predicted for VEEGA reentry.

Three primary thermochemical ablation processes are considered. These are (in the direction of increasing surface temperature): rate limited (kinetic) oxidation, diffusion oxidation, and sublimation. In this study, the 'moderate' rate limited mass loss schedule shown in Figure G-18, was used along with related reaction energies corresponding to the relationships provided by Hunter (Reference 16) for a glowing combustion process. This process is defined by the reaction:

$$O_2\ (g) + 2C(s) \rightarrow 2CO(g).$$

The diffusion limited oxidation plateau is also based on carbon monoxide as a product of reaction and represents the limiting solid carbon consumption rate for an oxidation process. As the name implies, this limit is imposed when reaction rates become so fast that oxygen (oxidizer) consumption becomes controlled by the time it takes oxygen to diffuse across the boundary layer to feed the reaction.

The sublimation model is based on equilibrium thermochemistry for 16 species including the important carbon vapor molecules C_1 through C_5 which take on increasingly dominant concentrations as temperatures increase in this regime. This C_1 - C_5 JANAF model showed a good correlation of the experimental sublimation mass loss data of Lundell-Dickey (Reference 17). It has been demonstrated that an equilibrium model will result in higher predicted mass loss rates than a more realistic nonequilibrium vaporization model (Reference 18). Further background on the APL ablation models can be obtained from References 16 and 19.

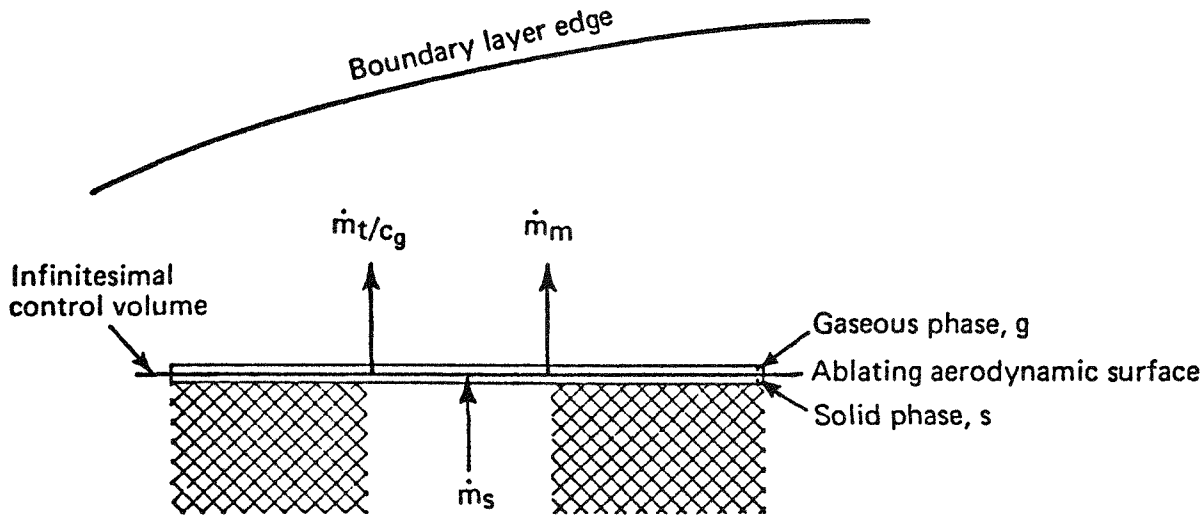

Boundary condition: $\sum_i \dot{m}_i = 0$

- $\dot{m}_s$ ~ Mass flux due to ablation, solid phase
- $\dot{m}_{t/c_g}$ ~ Mass flux due to thermochemical ablation, gaseous phase
- $\dot{m}_m$ ~ Mass flux due to mechanical ablation, solid phase

Figure G-17: **Surface mass balance — reentry thermal analysis.**

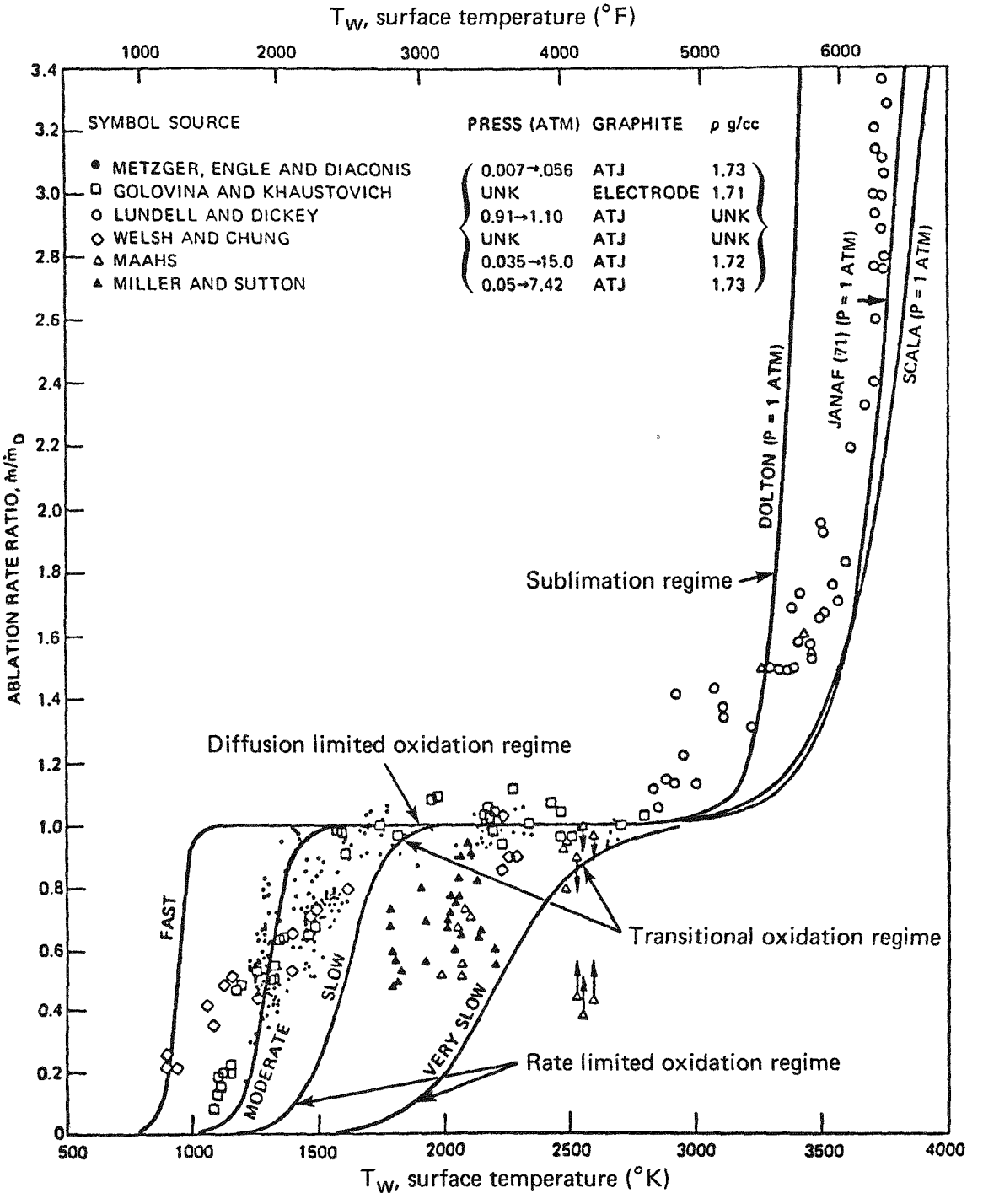

Figure G-18: **Thermochemical ablation regimes for graphite.**

7.2.3.1.3 Ablation Models: Clad and Fuel - For those reentries yielding sequential breakup configurations of, initially, the clad/fuel assembly followed by a bare fuel pellet, the ablation response is more complicated than for the LWRHU carbon-carbon aeroshell because of melting and vaporization. Both the melt and vaporization fronts represent moving boundaries with the velocities being a function of the thermal environment and the heat of formation of the material in undergoing phase transformation. Further modelling complications arise as the melt layer grows in thickness due to interaction of aerodynamic loading.

The computational capability to address the reentry melt problem is not available at APL, therefore the melting event for the clad/fuel assembly and the bare fuel configurations could be addressed only in the most simplistic terms. A simple thermal response analyses was conducted for both configurations which included conditions of (1) a chemically inert surface (2) no shape change effects and (3) no mass removal due to vaporization and mechanical erosion. An approximate approach to account for heat of fusion was attempted for bare fuel reentries by lumping this heat into the material's specific heat property schedule at a temperature level of (T_{melt}-500°F) in conformance with the criteria of Table G-7.

Further perspectives on the fuel reentry problem are available in References 20 and 21.

7.2.3.1.4 Material Properties - Determination of the thermal response of a reentry structure requires specification of the thermodynamic property (specific heat) and the transport property (thermal conductivity) for all materials involved in the design. In addition to these properties, the solution of the surface energy balance requires information on the thermal radiation properties, absorptivity and emissivity, to determine absorbed shock layer radiation and surface re- radiation. Additionally, these properties are required to determine radiation transfer at the internal interfaces.

The material properties used in this analysis for the various components are the same as used in earlier design studies except for the fuel. The selected fuel properties for the side-on studies are the result of a more recent property survey (Reference 22). Due to insufficient information on absorptivity, particularly at the higher temperatures, this property was assumed equal to the more readily available hemispherical emissivity for all materials.

The latent heat of fusion for the clad alloy, Pt30Rh, was determined by using the heats of the constituent elements (Reference 23) times the respective weight fraction for the alloy. The resulting value is a moderate 57.5 Btu/lb. On the other hand, the latent heat for PuO2 is about twice as high at 112.0 Btu/lb (Reference 22). It was incorporated into the specific heat schedule over a five degree band.

7.2.4 Results of Analysis - Side-on Stable LWRHU Response Behavior

7.2.4.1 Reentry Configuration: Side-On LWRHU Assembly - Restricting attention to just the ablation and thermal failure modes, the important response variables become (a) aeroshell stagnation recession, (b) clad maximum stagnation temperature and (c) clad impact temperature. The initial step in this serial evaluation was to conduct reentry thermal analyses for all VEEGA reentry zones to allow comparisons of the response variables against the specified failure criteria. Zones C through E reentries were investigated entirely through to impact whereas, in anticipation of ablation failure events, evaluation for Zones A and B were shortened to just the hypersonic heat pulse (i.e., to Mach 5.0).

The aeroshell's stagnation ablation response for the various zones is given in Figure G-19. The response shows a correspondence to total heat load (Table G-9) as expected. Recessions greater than 50% are indicated for Zone A, B, and C if the analysis is continued through the heat pulse. The recession values in these Zones correspond to approximately 100%, 70%, and 60% recession, respectively. However, under the terms of ablation criterion of Table G-7, aeroshell failure is deemed to occur when 50% recession occurs which for Zones A, B, and C is before the end of the heat pulse. Zones D and E are just below the failure threshold. The extent that the total recession predictions exceed the 50% wall failure threshold provides at least a qualitative sense of the probability of encountering an aeroshell ablation failure event. From this perspective, Zone A indicates a very high probability of occurrence based on the specified criteria for this study. The failure probability of occurrence for Zone B, etc., will become progressively lower with increasing flight path angle.

Table G-10 provides zonal information on the maximum clad temperature obtained in the analysis at the stagnation location and clad impact temperatures. For a complete side-on LWRHU assembly reentry configuration, only Zone A decisively indicates the occurrence of a clad melt failure event although Zone B is only marginally below the failure threshold. The clad impact temperatures for Zones C to E range from 1160 to 1210^{o}R and are well above the ductility transition temperature for the Pt30Rh clad material. Consequently, the only bearing these temperatures might have on clad impact performance is possible strength degradation. This consideration should be factored into any review of available LWHRU experimental impact data.

When combining the information provided in Figure G-19 and Table G-10, it is indicated from these reentry analyses that the ablation failure event will precede the clad melt event for prompt reentries in Zone A.

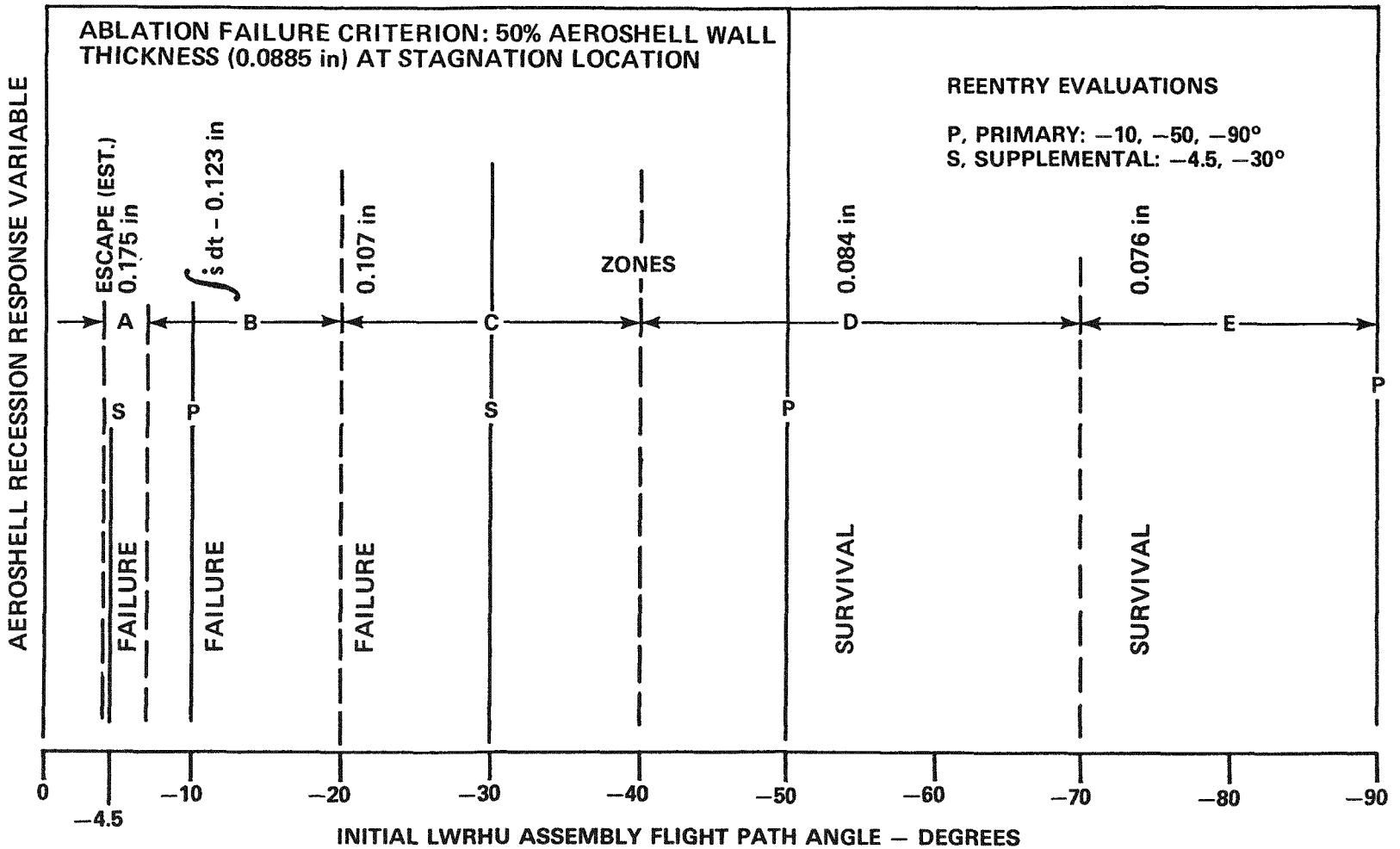

Figure G-19: Aeroshell total stagnation recession predictions; side-on stable LWRHU assembly reentry configuration.

TABLE G-10: GALILEO/VEEGA
THERMAL AND ABLATION RESULTS FOR
LWRHU ASSEMBLY REENTRY CONFIGURATION SIDE-ON STABLE

	REENTRY RESPONSE VARIABLE			REENTRY FAILURE MODE		
ZONE	MAXIMUM RECESSION, IN[a]	MAXIMUM CLAD TEMP. °F[a]	IMPACT CLAD TEMP °F[b]	ABLATION[c]	MELT[d]	IMPACT[e]
A	0.175	3161. (130 SEC)	-	YES	YES	
B	0.123	2174. (90 SEC)	-	YES	NO	NO
C	0.107	1747. (80 SEC)	694.	YES	NO	NO
D	0.084	1644 (80 SEC)	733.	NO	NO	NO
E	0.076	1596 (80 SEC)	746.	NO	NO	NO

(a) stagnation location
(b) impact velocity, all zones: approx. 125 fps (no ablation effect on ballistic coef)
(c) recession ≥ 50% wall thickness ≥ 0.0885 inches
(d) temperature ≥ carbon eutectic - 300 F ≥ 2900 F
(e) ductility/brittleness transition.
(f) time for reentry heat initiation that maximum temperature is attained.

7.2.4.2 Reentry Configurations: Side-on Stable Clad/Fuel Assembly - With the ablation failure and structural breakup criteria specified in Table G-7, the release conditions for an intact clad/fuel assembly are as given in Table G-11. These release conditions offer further insight on LWRHU sequential breakup patterns for the VEEGA environments. The high release velocities for both Zones A and B indicate a considerable reserve of energy remaining for these reentries such that the occurrence of clad melt, fuel release and subsequent fuel melt events are strong possibilities. The occurrence of these events for Zone A is further reinforced by observing that the clad temperature at release is just slightly below the melt failure threshold. On the other hand, the very low release velocity for Zone C indicates that the thermal environment for reentries in this zone has been largely expended and the clad, even at its low release temperature, will experience cool down and survival for the remaining portion of flight.

Using the information in Table G-11 as initial reentry conditions, 3DOF trajectory analyses were conducted for Zones A through C followed by reentry thermal analyses for Zones A and B. The thermal response results are also given in Table G-11. In conformance with the observations discussed earlier on available reentry energy at the clad/fuel assembly release conditions, clad melt failures do occur very shortly after release for Zone A or B. Very little of the available energy in these zones is expended arriving at this state. However, in Zone C, the 3DOF trajectory information indicated that any released side-on clad/fuel assemblies will survive reentry and impact at about 160 fps. Reentry thermal analyses were not conducted for Zone C; however, considering the long cool down flight period (i.e., 288 seconds) and the fact that the clad is directly exposed to the environment, it is estimated that clad impact temperatures will likely be in the range of local ambient to 560°R for this zone.

7.2.4.3 Bare Fuel Pellet Side-on Reentries - The fuel pellet release conditions for Zones A and B are governed by the clad melt event at the stagnation region for the clad/fuel assembly reentry configuration (Table G-11). The melt event included the clad's heat of fusion effect. The pellet release conditions are given in Table G-12 and indicate very little degradation in the reentry energies (i.e. velocities) from the earlier release conditions for the clad/fuel assembly (Table G-11). The high initial velocity for Zone A reentries indicates the fuel pellet will be subjected to a severe environment and likely experience significant melting. Zone B also indicates sufficient residual energy to cause fuel melting.

Table G-11: Galileo/VEEGA Reentry Release Conditions Clad/Fuel Assembly

VARIABLES	ZONE A	ZONE B	ZONE C
Velocity, fps	28,720	19,896	1,241
Altitude, ft	234,419	159,323	93,732
Flight path angle, deg	+0.32	-8.69	-37.04
Clad temperature, F	2415	1074	1095
Fuel temperature, F	1526-1594	920-928	958-966

Table G-12: Galileo-VEEGA Reentry Release Conditions for the Bare Fuel Pellet

VARIABLE	ZONE A	ZONE B
Velocity, fps	28688	19547
Altitude, ft	234457	158359
Flight path angle, deg	+0.325	-8.70
Fuel* temperature,	1619-1638	933-988
Fuel temperature	1538	924-928
Inner array, °F		

*Refer to Figure G-15c thermal model

The fuel reentry analyses was restricted to acquiring a rough approximation for the mass fraction of the pellet that melts for the two VEEGA zones of interest. Using the conditions of Table G-12, trajectory and thermal analyses were conducted for side-on pellet reentries. Computational capabilities were not available to fully analyze the fuel reentry problem. A simple thermal response analysis was conducted which approximated the heat of fusion effect but did not account for any shape change effects nor mass loss due to vaporization or mechanical erosion of the melt layer.

Melt predictions for the pellet using this simplified approach indicated a 14% mass loss in Zone B and 42% in Zone A. The fuel reentry analyses included sensitivity studies in which (a) base heating levels were increased to 10% stagnation levels and (b) the fuel's emissivity was decreased to 0.8. These changes had no effect on the Zone B baseline results and only a minor influence on the Zone A mass fraction. Sensitivity to other variables, such as the fuel's thermal conductivity, lead to uncertainties on melt fractions. It is not unreasonable to think that melt fractions could increase to 75% in Zone A and 42% in Zone B if one could adequately model shape change effects and mechanical erosion and had better information on melt layer thermal properties. The results from this study indicate that radiological source terms resulting from the melt layer will very likely be released at high altitude.

7.2.5 End-on Analysis

7.2.5.1 3DOF Trajectory and Other Input Parameters - The LWRHU end-on reentry stagnation heat transfer environment for the Galileo VEEGA trajectory was computed using the 3DOF code (Reference 14). Two initial flight path angles were chosen for analysis - a steep (-90^{o}) and a shallow (-10^{o}) angle reentry. These cases are the extreme condition under which thermal stress failure and thermal/ablation failures may occur.

The stagnation heating rates for the LWRHU end-on reentries were computed using a reference sphere and a convective heat transfer conversion factor (FC) = 2.4. This factor was determined by taking the ratio of stagnation velocity gradients and assuming the end-on LWRHU geometry to be a flat faced cylinder. Velocities greater than Mach 5.0 are also assumed; this exists during most of the heat pulse. For the stagnation radiative heating rates, the factor is unity because the LWRHU geometry was already considered when installing the tables into 3DOF.

Stagnation heating rates at the shallow and steep flight path angles for a Galileo VEEGA reentry are illustrated in Figure G-20.

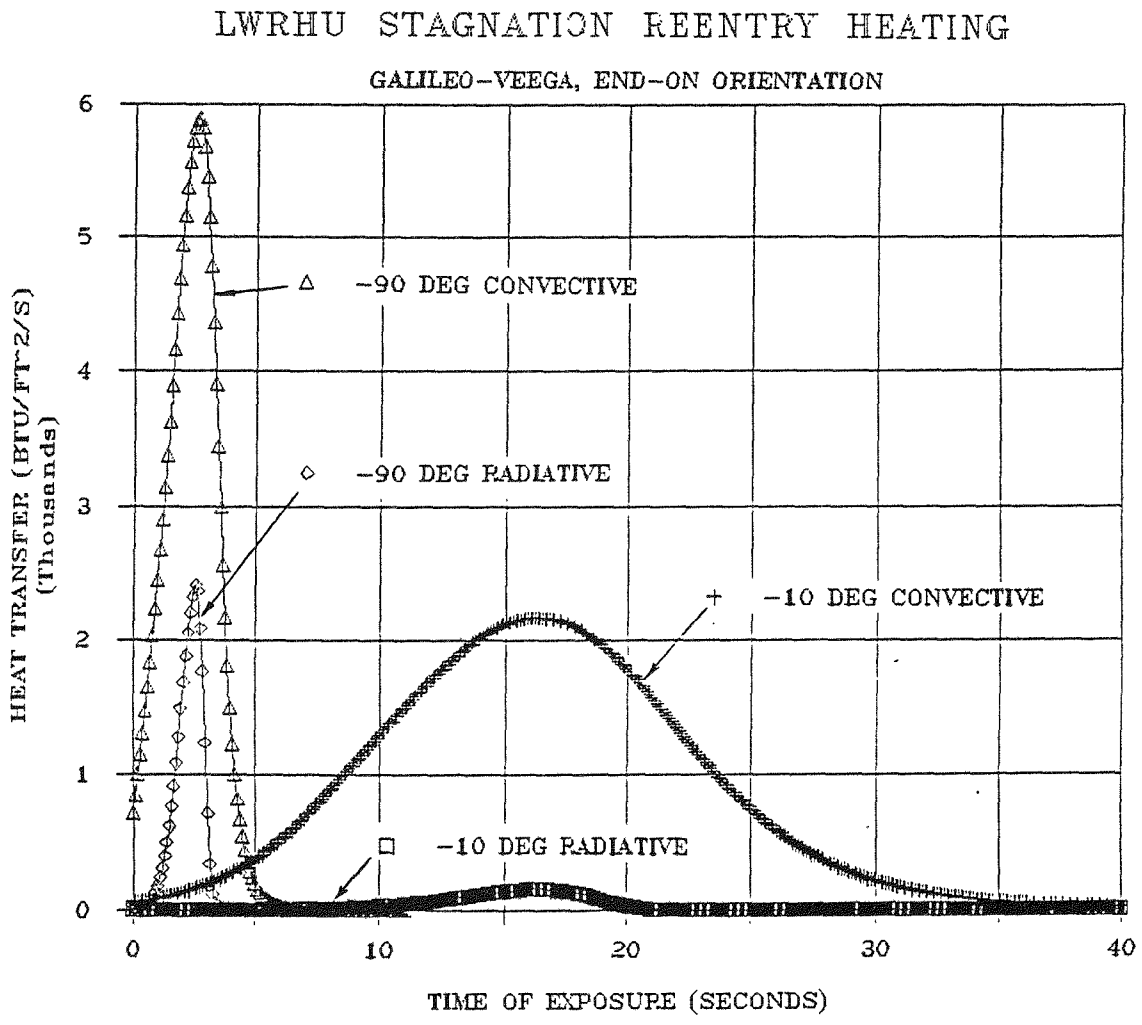

Figure G-20: **LWRHU stagnation reentry heating.**

7.2.5.2 2-D End-on Thermal Analysis

7.2.5.2.1 Summary and Conclusions - A thermal/ablation study was performed for the LWRHU in an end- on reentry attitude for reentry angles of -10^{o} and -90^{o}. A shallow reentry with a flight path angle of -10^{o} was selected for assessing the possibility of clad melt and aeroshell ablation failures due to the high heat loads generated. A steep reentry with flight path angle of -90^{o} was selected for a thermal stress evaluation because it creates high thermal gradients.

The results of the thermal/ablation analyses for the end-on VEEGA reentry of the LWRHU indicate that the aeroshell and clad will survive reentry in the cases examined. The maximum aeroshell end-face ablation was predicted to be below the 50% ablation criteria for aeroshell failure for these cases. Extrapolation of these results to the most shallow flight path angles implies that the 50% ablation criteria may be exceeded at these angles. The peak clad temperature was predicted to be slightly above $2460^{o}R$, which is substantially below the eutectic temperature of Pt30Rh.

7.2.5.2.2 Thermal Model - The thermal/ablation analysis of the LWRHU in the end-on reentry configuration was performed using the JHU/APL SHTPE ablation code (Reference 24). The analytical assumptions are for the most part consistent with those used in the LWRHU side-on analysis. Assumptions that are specific to the end- on geometry are described below. The LWRHU end-on geometry was represented by a two-dimensional 762 node thermal network as shown in Figure G-1. It is identical to the network that was used for the analysis in Reference 25. The model includes representations of the aeroshell and end-cap, all of the internal sleeves, and the cladded fuel pellet. The end-cap holes and the crack around the (fastened) end-cap were not represented by this model. The internal contact conductances between adjacent components were specified according to the analysis in Reference 25. The open fuel/clad gaps were assumed to be helium filled and the end gaps in the aeroshell assembly were modeled as vacuums.

The release of helium from the fuel to the gaps in the aeroshell assembly was not included in this study. This assumption tends to increase the temperature levels of the aeroshell and suppress the temperature rise of the clad. However, based on the results from Reference 25, it is expected that helium in the aeroshell gaps will mainly affect the temperature rate of change of the clad and slightly affect the magnitude (i.e., it will slightly increase the peak clad temperature).

The stagnation heating rate history from the 3DOF computer program provided the boundary conditions for the LWRHU model. The radiation heating rates were applied over the entire windward end-face and were assumed to be equal to the stagnation rate. The convective heating rates were also applied over the entire LWRHU by using the distribution from Reference 25, and the conversion factor used in the 3DOF trajectory. The side heating distribution was taken to be the midrange values of the Reference 25 data and the leeward end-face heating was taken to be uniformly distributed at 5% of the stagnation value.

7.2.5.2.3 Results - The results of the 2-D thermal/ablation analysis are reported below for the Pt30RH clad and the LWRHU aeroshell using the Galileo VEEGA reentry environment. The criterion that is being used for clad melt failure is a clad temperature near the eutectic temperature of Pt30Rh (3660-300°R). The criterion for ablation failures is 50% ablation through the aeroshell.

7.2.5.2.3.1 Aeroshell and Clad Temperatures - The aeroshell and clad temperature histories for the steep and shallow reentry are presented in Figures G-21 and G-22, respectively. The aeroshell temperature drives the clad temperature. The observable trend is that for the steep reentry, the clad temperatures will approach a peak value between 1460-2460°R beyond 29 seconds since the aeroshell driving temperature is declining from 2460°R at 29 seconds. For the shallow reentry (Figure G-22), the trend is that the clad temperatures will peak at approximately 2460°R. In both cases, the peak clad temperature is expected to be below the eutectic temperature of Pt30Rh by a margin of 500° to 1000°R.

7.2.5.2.3.2 Aeroshell Ablation - The ablation profiles for the steep and shallow reentries are shown in Figures G-23 and G-24. Using the 50% ablation criterion for aeroshell failure, the results indicate that the LWRHU aeroshell will probably survive in an end-on orientation for these VEEGA reentry environments. At the aeroshell end-cap where the aeroshell thickness is least (0.2018"), the maximum recession is less than forty percent (40%). This occurs at the perimeter of the end-cap for the shallow angle (-10°) reentry condition.

7.2.6 Comparison of Side-on and End-on Reentry Ablation Response - The -10° and -90° end-on reentries that were investigated for thermal, ablation and thermal stress response represent Zones B and E on the Galileo VEEGA reentry map. The predicted maximum recession in terms of percent aeroshell wall thickness is shown in Figure G-25 for Zones B and E for both the side-on and end-on reentry orientations. The side-on percentages are based on the maximum recession values presented in Figure G-19 and the end-on percentages from the data of Figures G-23 and G-24.

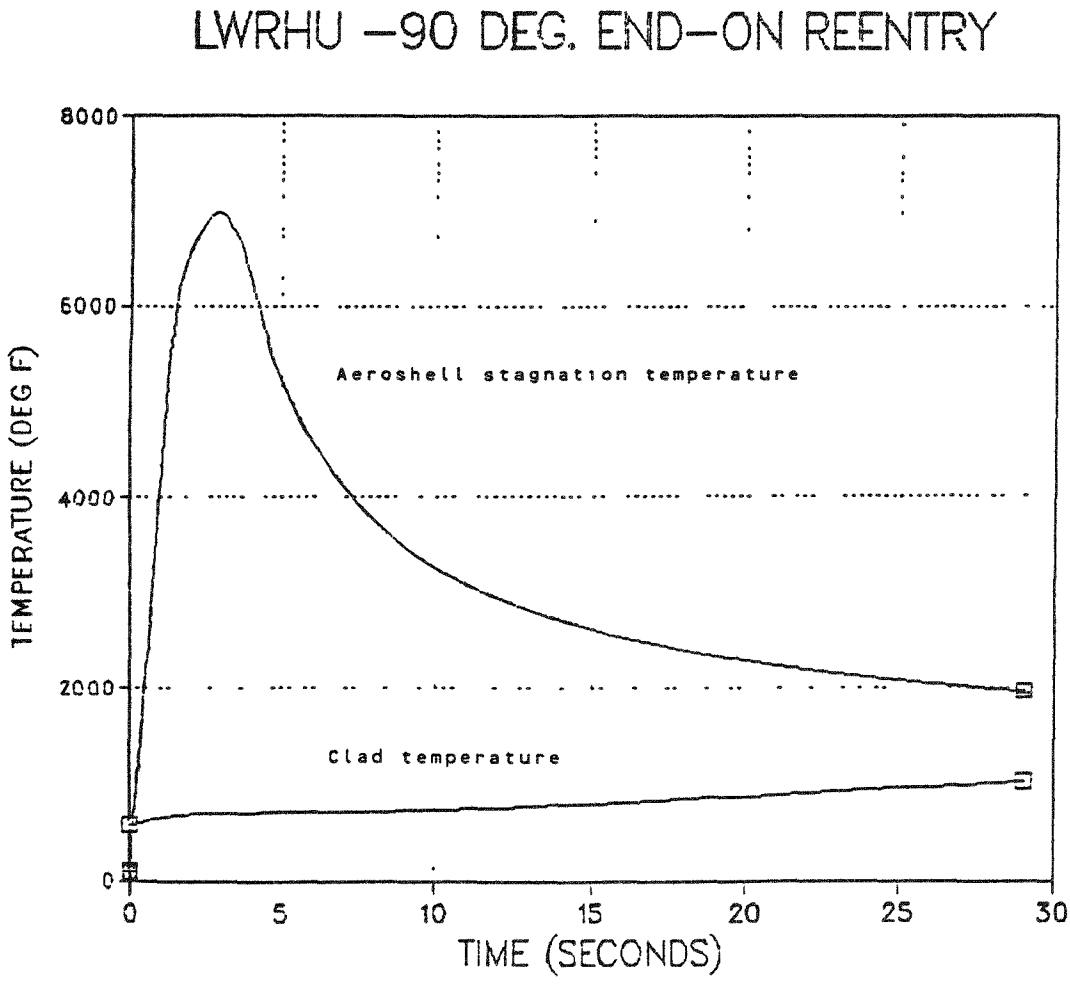

Figure G-21: **LWRHU aeroshell windward end-face and clad temperature response. Galileo-VEEGA steep (-90°) end-on reentry orientation.**

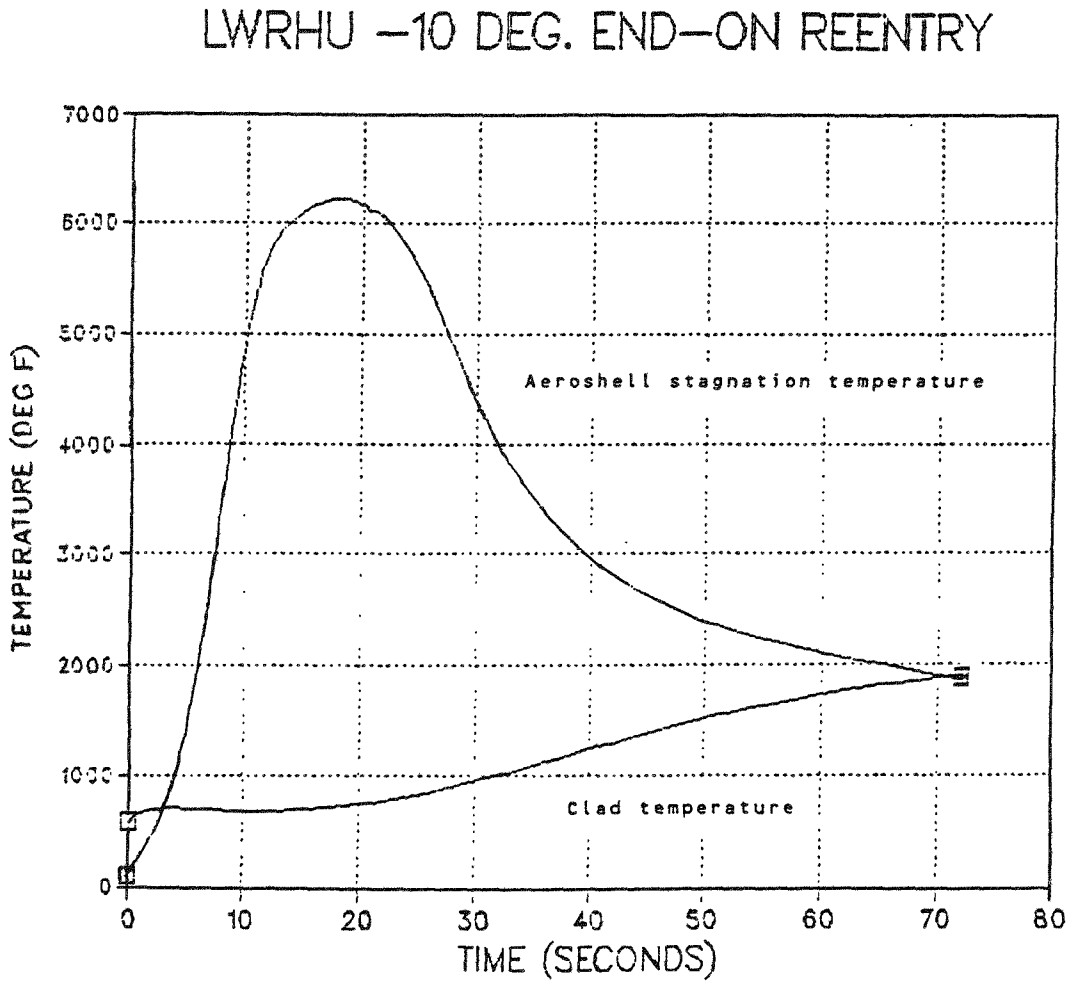

Figure G-22: **LWRHU aeroshell windward end-face and clad temperature response. Galileo-VEEGA shallow (-10°) end-on reentry orientation.**

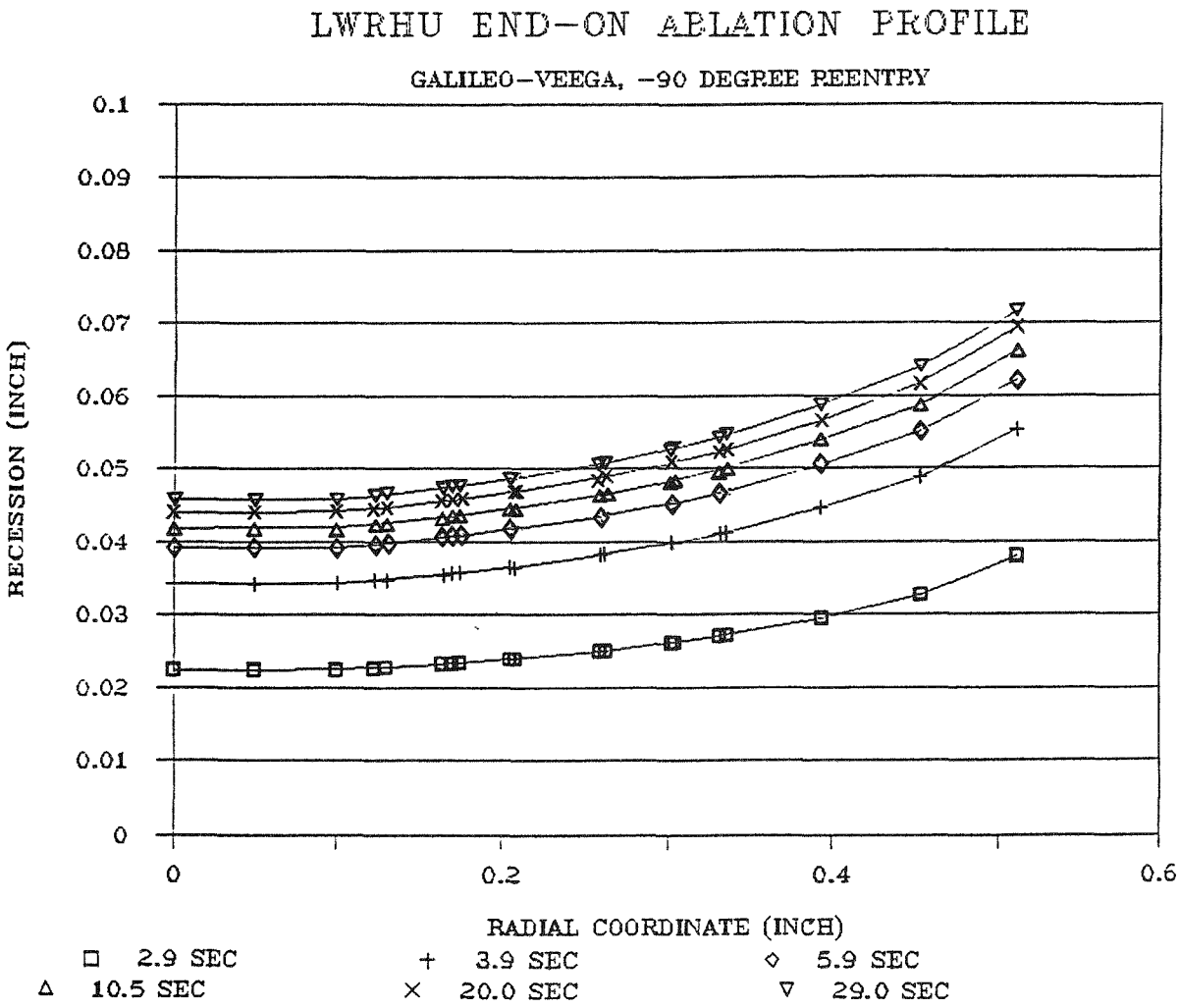

Figure G-23: **LWRHU end-on ablation profile Galileo-VEEGA, -90° reentry.**

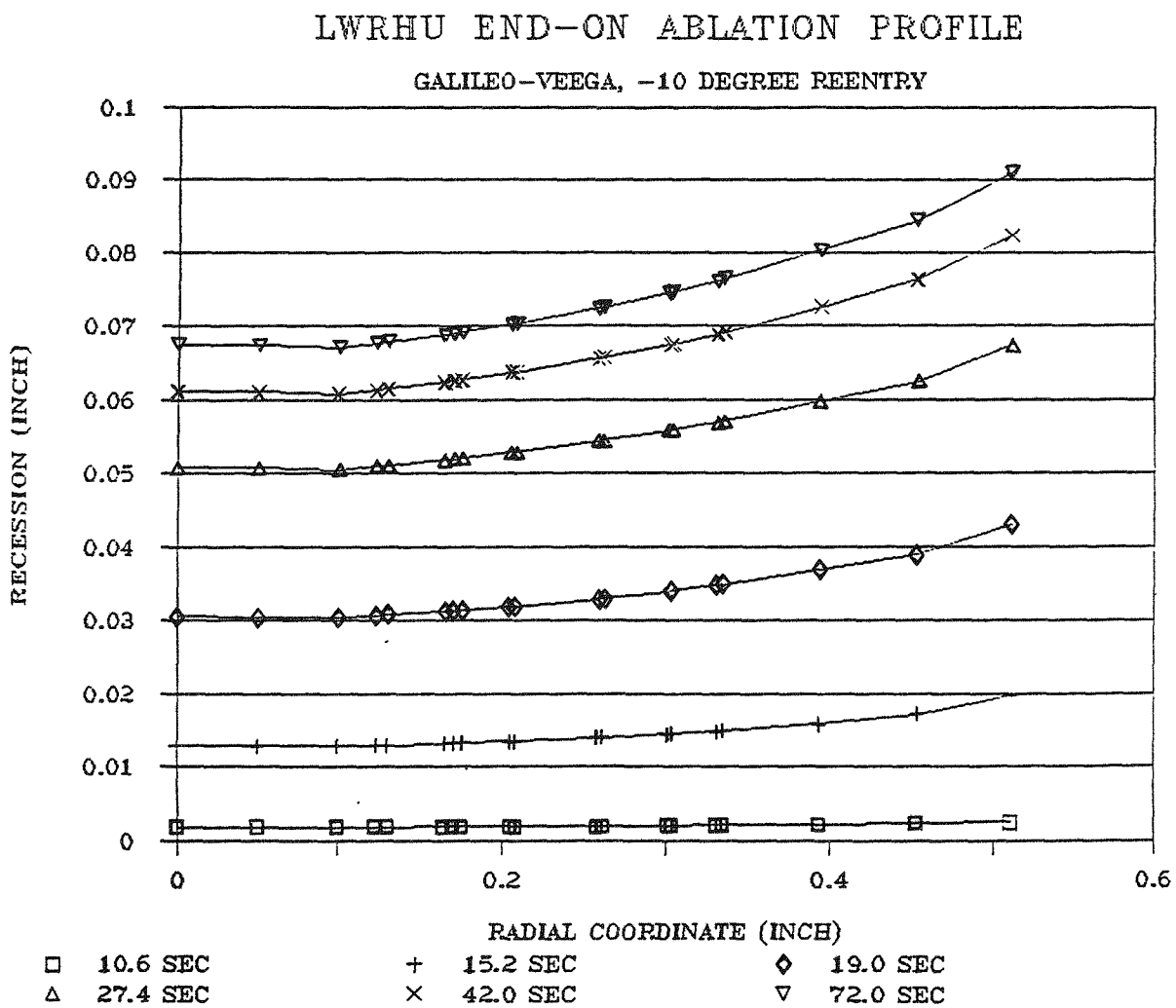

Figure G-24: **LWRHU end-on ablation profile Galileo-VEEGA, -10° reentry.**

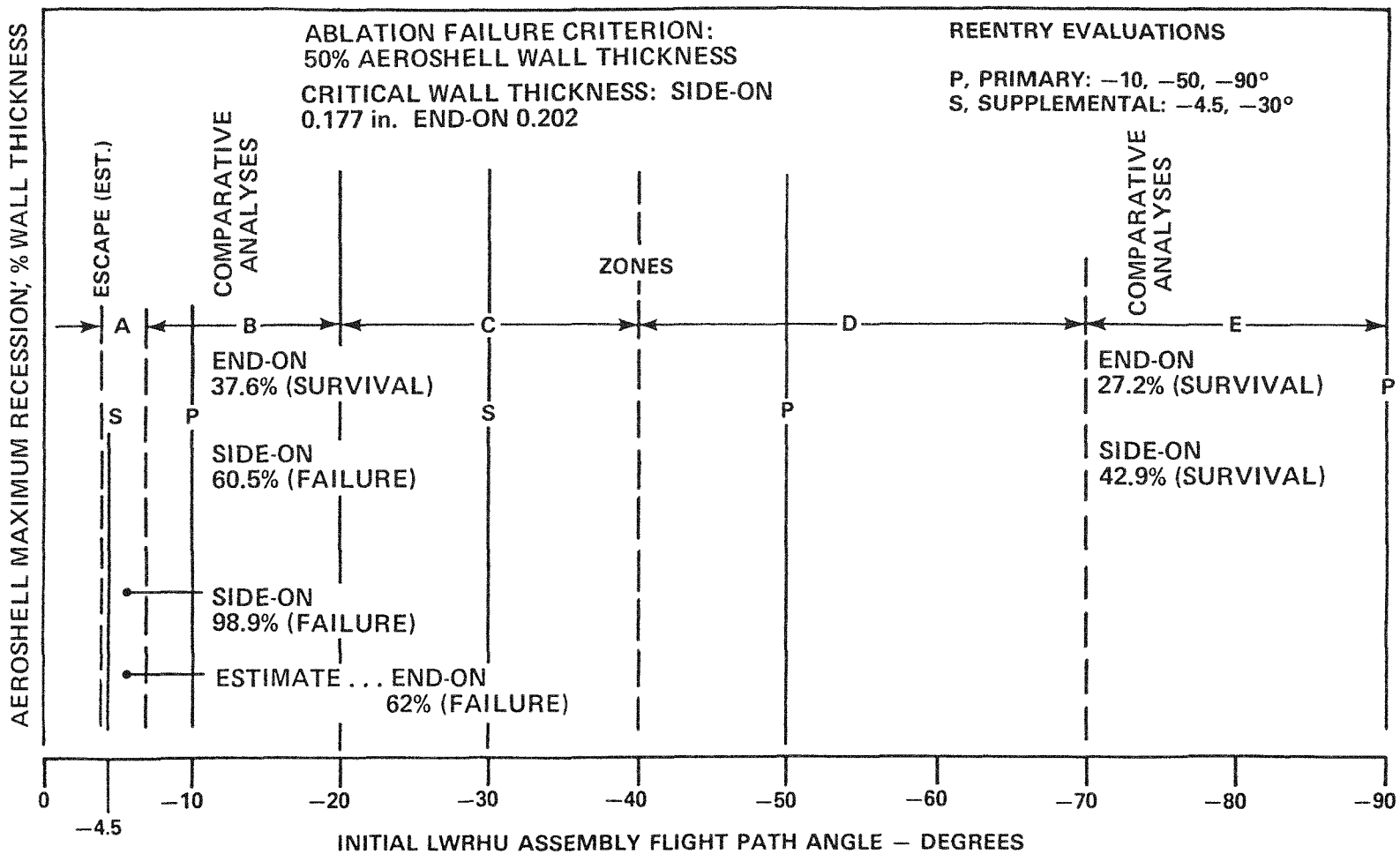

FIGURE G-25: Comparison of the aeroshell maximum recession predictions for side-on and end-on LWRHU assembly reentry configurations.

Comparison of the recessions for these two zones indicates that the end- on attitude produces a milder ablation response and that it will survive across the VEEGA map from Zone B to E. For both Zones B and E, the end-on recession was about 63% of the side-on values. Using this proportion in Zone A, it is estimated that end-on reentries in this zone will exceed the 50% wall failure criterion as noted in Figure G-25. Furthermore, there appears to be sufficient excess over the 50% recession level to anticipate fuel release and some melting for the Zone A end-on reentries. Assuming the released fuel pellet reenters side-on, a rough approximation of the melt fraction for Zone A will be the range quoted in Zone B for the side-on analysis 14% to 42%. Further sequential reentry analyses for the end-on study are required to confirm this estimate. Other failure scenarios where (1) prolonged subsonic oxidation induces a heat shield ablation failure and releases a previously melted clad with liberated fuel fragments or (2) a fuel pellet experiences a high altitude release and either partially or fully survives reentry except for fuel particles that may be aerodynamically scrubbed from the pellet's surface. These events could possibly lead to lower altitude source terms.

In the shallow angle reentries which have a side-on stable orientation another scenario for failure is that in which the aeroshell is assumed not to come apart even through burnthrough occurs. For this scenario the following impact configurations may be possible in the reentry zones defined in this study as: Zone A (reentry angle $\gamma \leq |7^{o}|$); Zone B ($|7^{o}| \leq \gamma \leq |20^{o}|$); and, Zone C ($|20^{o}| \leq \gamma \leq |40^{o}|$).

Zone A: Full LWRHU assembly with aeroshell burnthrough on windward surfaces leading to direct exposure of underlying PG sleeves, extensive melting and resolidification of clad.

Zone B: Full LWRHU assembly with partial burnthrough of aeroshell at the ends with direct exposure of underlying PG insulator end plug, possibly partial clad melting and resolidification in the near end regions.

Zone C: Full LWRHU assembly with partially ablated aeroshell clad assembly intact.

In assessing the radiological risk, both failure scenarios (ablation leading to release of the fuel pellet an containment of a melted clad) was considered as possible.

7.3 Thermo-structural Analysis

7.3.1 Summary and Conclusions - Side-on stable two-dimensional and end-on stable two-dimensional axisymmetric thermo-structural analyses were conducted for the Galileo VEEGA reentry configurations. These analyses were conducted using the computer code "Stress Analysis of Axisymmetric Solids" (SAAS III) utilizing ablation and thermal information from the SHTP and SHTP-E thermal analyses codes. PDA- PATRAN software on the Apollo computer system was used for pre- and post- processing of the finite element input data and the results.

For the most severe thermo-structural case (side-on stable configuration and the steep gamma angle low altitude release reentry) the maximum aeroshell temperatures were found to be over 7460°R. Plastic behavior of the FWPF carbon-carbon material was predicted at these temperatures. A possible compressive failure of the aeroshell due to axial stress early into the heat pulse was also predicted. However, the apparent compressive failure affected only a small area (one-tenth wall thickness) of the outer aeroshell wall near the stagnation point and would not cause a loss of the LWRHU internals. The compressive failure mechanism in the FWPF material is not believed to cause a catastrophic event, as would a tensile failure. At no time during the side-on reentry analysis was a tensile failure predicted in the aeroshell.

For the end-on stable thermo-structural analysis, in a worst case steep gamma angle low altitude release reentry, no failures were predicted in the LWRHU aeroshell. Maximum temperatures witnessed by the aeroshell were predicted to be about 7460°R. Compressive and tensile stress safety factors calculated for the end-on stable analysis show survival of the aeroshell through the heat pulse even for conservative linear elastic FWPF material properties. The less severe (from a thermal stress standpoint) medium and shallow angle VEEGA reentry configurations were examined at a cursory level, but as expected, showed little cause for alarm.

Conclusions to be drawn from the results of the side-on stable and the end-on stable thermo-structural analyses are as follows: (1) a catastrophic failure of the LWRHU aeroshell is not expected from the thermal stresses encountered during the predicted VEEGA reentry heat pulses, (2) release of the LWRHU internal components and cladded fuel pellet is not expected to result from the thermal stresses encountered during the predicted VEEGA reentry heat pulses. Stress analysis for the orbital decay scenarios are reported in Reference 11 and in Section 5.0 of this appendix.

7.3.2 Methodology and Assumptions - Several stress analyses have been conducted (with increasing exactness and complexity) to determine the thermo-structural response of the LWRHU aeroshell to the thermal environment predicted for the Galileo VEEGA inadvertent reentries. Common assumptions made in both the side-on and end-on thermo-structural analyses are detailed here. Only the aeroshell structure of the LWRHU was considered in the thermo-structural analyses.

Thermal stress analyses were conducted utilizing a finite element code called "Stress Analysis of Axisymmetric Solids" (SAAS III). This program is capable of plane strain, plane stress, axisymmetric, stress resultant boundary condition (SRBC) and gap element computations. SAAS III also has the capability of defining linear elastic and bi-linear elastic-plastic temperature dependent material properties.

Material properties for the AVCO Fine Weave Pierced Fabric (FWPF) carbon-carbon aeroshell material were also taken from the previous analyses by Waeber. The weave-form of the FWPF consists of stacked layers of woven fabric (in plane) pierced with graphite rods perpendicular to the plane of the fabric (axial). Accordingly, the in-plane orthotropic properties are assumed to be equal, while the axial material properties are different. Very little new material property information has been acquired concerning the FWPF material since Reference 21 was published. Material properties up to $5000^{o}R$ are based upon test data from the Air Force Pan Pilot Production Program. Above $5000^{o}R$, the material properties are based upon bulk graphite properties at 1% strain. This strain assumption is considered conservative as FWPF is believed to support loads at up to 5% compressive strain. Further FWPF material property assumptions shall be discussed in the analysis descriptions.

7.3.3 Results of Side-on Stable Analysis - Initial conditions for this side-on reentry configuration are an inertial velocity of 46,750 feet per second, an inertial flight path (gamma) angle of -90^{o} and a free release altitude of 271,000 feet. The approximate thermo-structural response of the aeroshell during the first 6.00 seconds of the reentry heat pulse was determined with the plane stress option of SAAS III. Symmetry in both geometry and thermal loading was assumed. A coarse finite element model, which consisted of 90 four-noded plane elements with five elements through the thickness of the aeroshell wall, was initially used to determine the time of maximum thermally-induced stresses during reentry. Figure G-26 shows the element and node layout of the coarse model in a rectangular (R-Z) coordinate system. All elastic material properties were used in this initial approximation.

Temperature distribution data at discrete time steps into the steep gamma angle reentry were obtained from the SHTP code. Figure G-27 is a color-coded plot of the nodal temperature distributions as interpolated by SAAS III from the SHTP data. (This

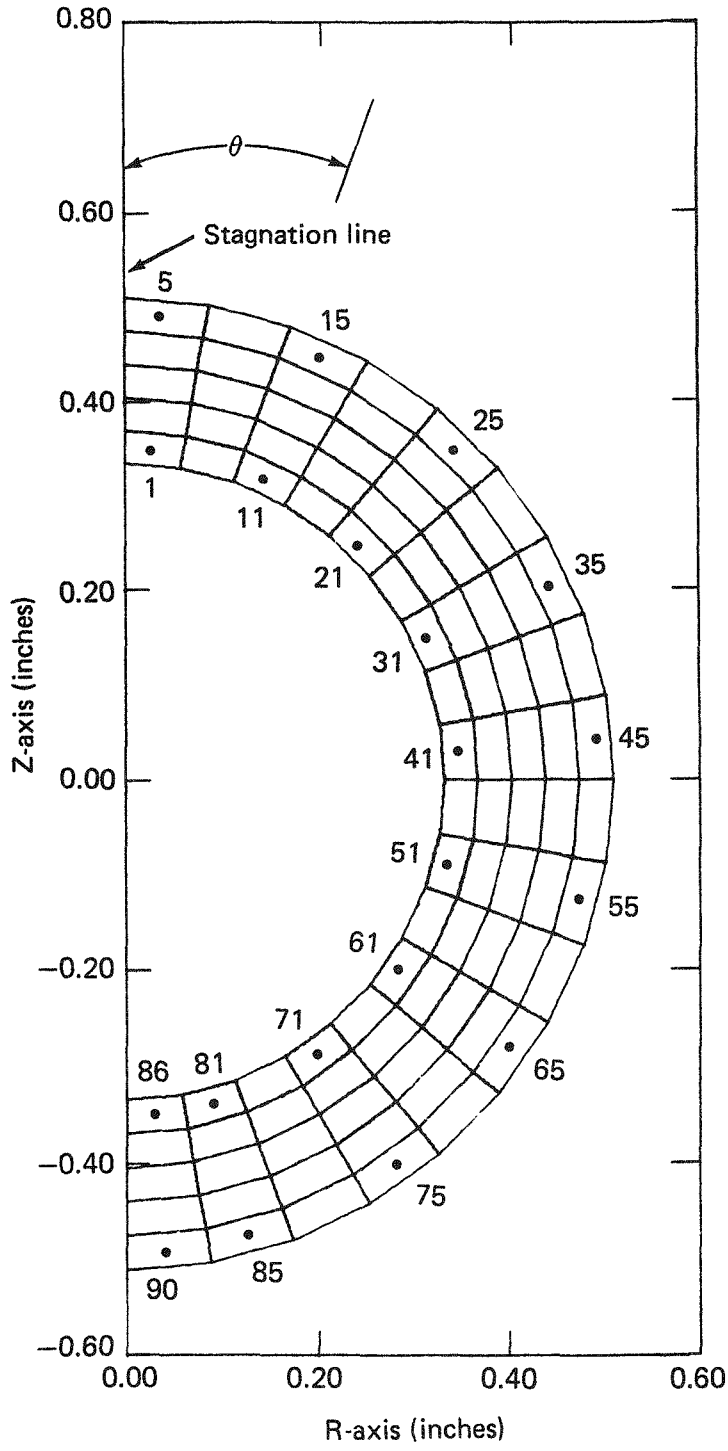

Figure G-26: **Coarse mesh planar cross section model for side-on reentry calculations.**

photograph was produced in the PDA-PATRAN finite element pre- and post-processing software on the Apollo computer system.) The time of maximum temperature was found to be 2.40 seconds with a maximum of 7600^{o}R on the outer wall surface near the stagnation point. Initially, the thermal gradient through the aeroshell wall near the stagnation point was most critical. As the reentry time progressed, the aeroshell increased in overall temperature and the through-wall gradient reduced in magnitude. The thermal gradient along the wall of the aeroshell then became the more important factor, although never as great a concern as the through-wall gradient. As the aeroshell increased in overall temperature, the along-wall thermal gradient progressed further along the aeroshell wall. Initially, the outer wall was at a higher temperature as expected, but after about 4.40 seconds, the outer wall temperature was lower than that of the inner wall. This led to a reversal of stress direction near the stagnation point at this time, as detailed in the stress analysis results below.

The maximum stresses were found to travel around the aeroshell in a manner similar to the temperatures. Initially, the maximums occurred near the stagnation point, as expected, due to the large thermal gradient through the wall. As reentry time progressed, the highest magnitude stresses began to move along the aeroshell wall. Stress results for each discrete time step of the reentry analysis were compared to determine time of maximum stress.

Those evaluated were major and minor principal, hoop, radial and calculated equivalent stresses. Hoop stress was considered to be the most likely mode of failure for the side-on reentry, as in the previous analyses by Waeber (Reference 6). This is a valid assumption as the major and minor principal and equivalent stresses followed the magnitudes of the hoop stress. Figure G-28 shows a hoop stress time history for the coarse analysis. Radial stress appeared to be of little concern. The largest tensile hoop stress was determined to occur at 1.40 seconds into the reentry heat pulse at the stagnation point inner wall. This is one full second before the time of maximum temperature. The safety factor for this stress was 4.24 (a safety factor less than 1.00 signifies failure). The maximum compressive hoop stress occurred at 1.00 second at the outer wall near the stagnation point. The safety factor for this stress was 3.21. The minimum safety factors for both tensile and compressive hoop stresses were found to occur at different times than the maximum magnitude

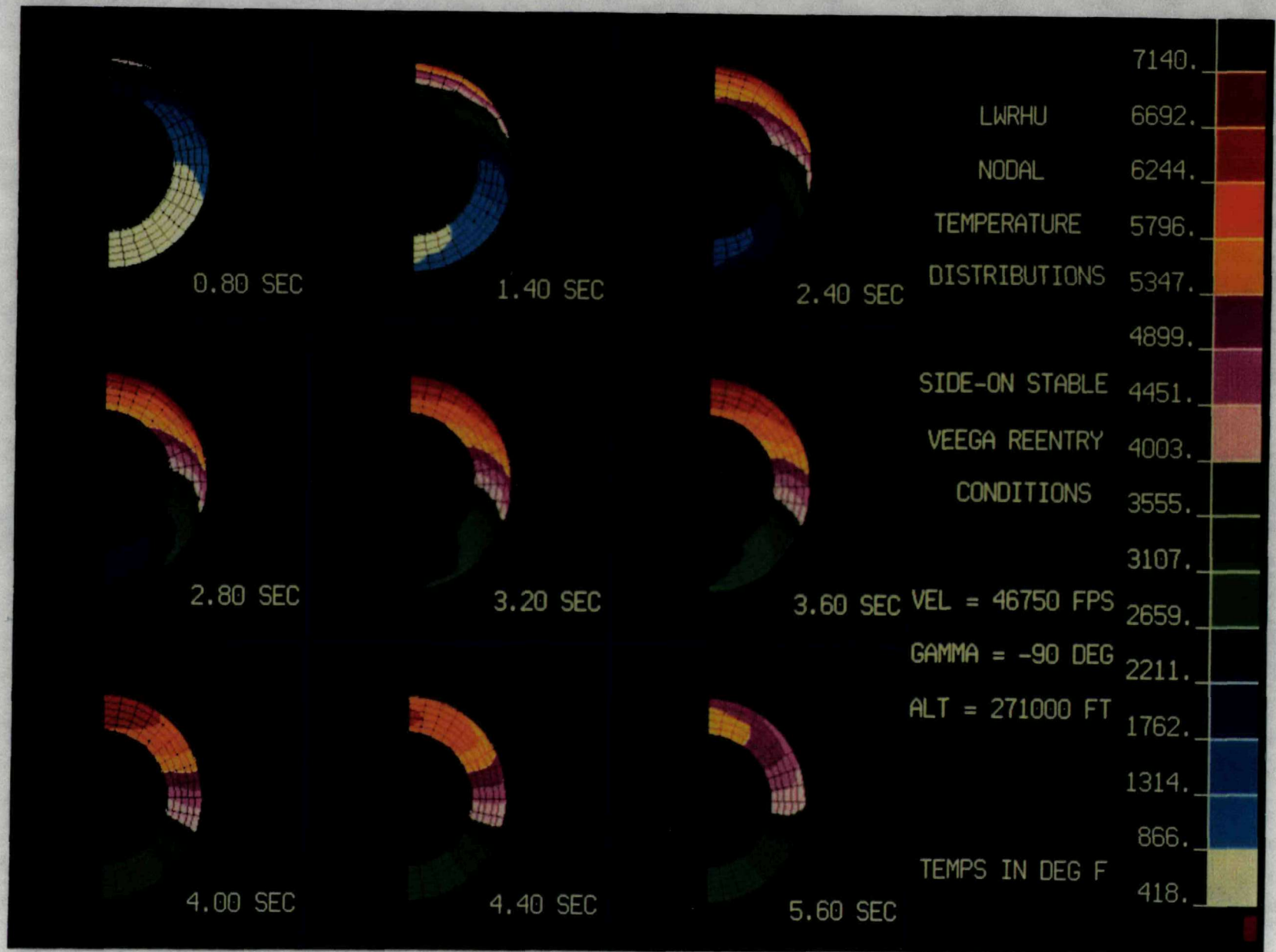

Fig. G-27: LWRHU nodal temperature distributions.

THE JOHNS HOPKINS UNIVERSITY
APPLIED PHYSICS LABORATORY
LAUREL, MARYLAND

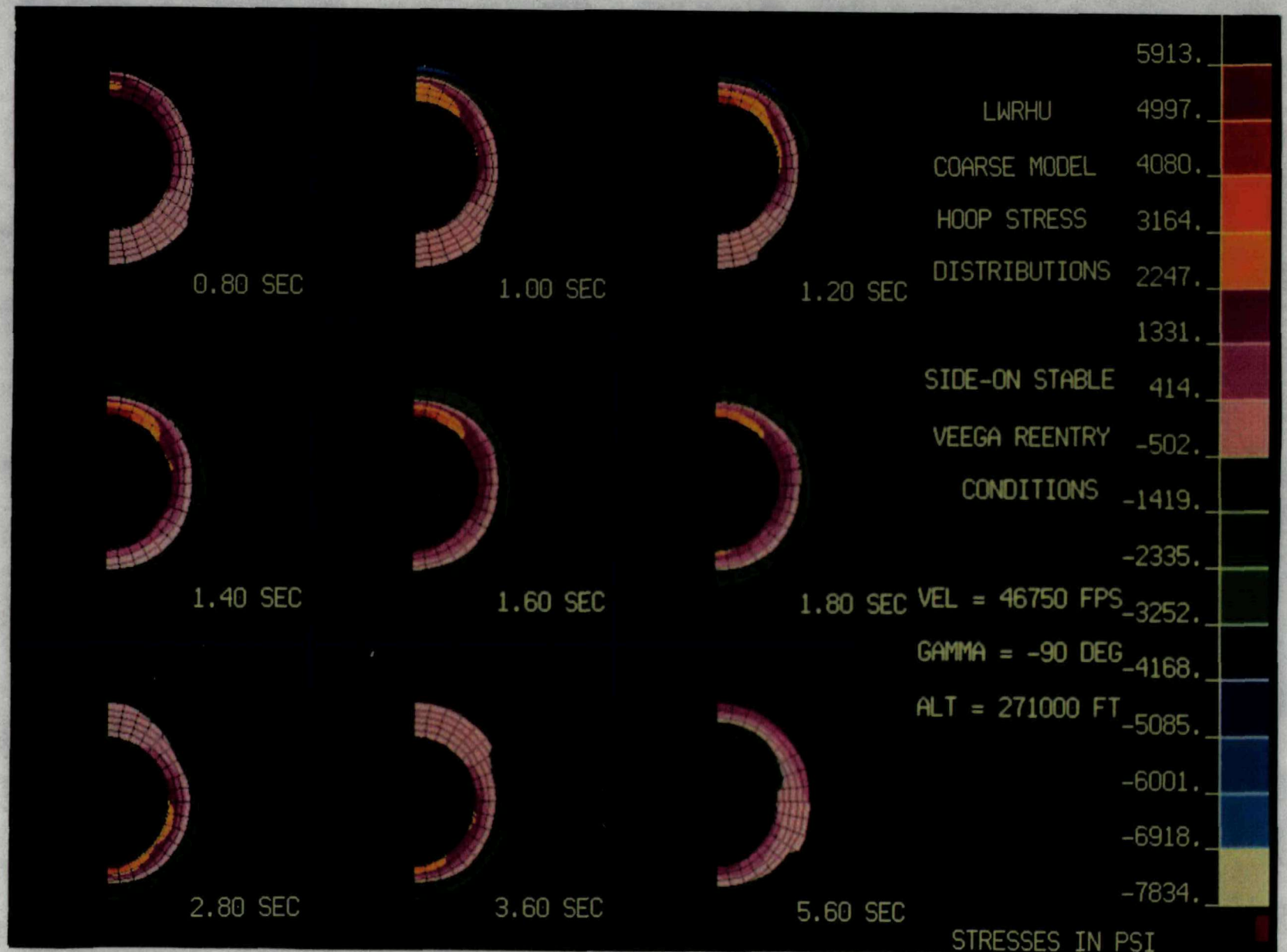

Fig. G-28: LWRHU coarse model hoop stress distributions.

THE JOHNS HOPKINS UNIVERSITY
APPLIED PHYSICS LABORATORY
LAUREL, MARYLAND

stresses. For tensile hoop stress, the minimum safety factor was 3.67 at 1.60 seconds. For compressive hoop stress, the minimum safety factor was 1.94 at 1.40 seconds. Table G-13 is a listing of both maximum stresses and minimum safety factors for the coarse elastic analysis.

A more refined analysis was performed only at 1.40 seconds based upon the above findings. This analysis consisted of several steps, each more complex. First, a similar plane stress elastic finite element analysis was run with a finer mesh of 360 four-noded elements with 10 elements through the thickness of the aeroshell wall. Figure G-29 shows the layout and element numbering scheme for the fine mesh model. The results of this analysis compared well with those of the coarse plane stress analysis.

Next, both the coarse elastic model and the fine elastic model were run with the Stress Resultant Boundary Condition (SRBC) option. The SRBC option of SAAS III is a two-dimensional iterative process which couples in-plane stresses and axial stresses normal to the plane, thereby accounting for axial end conditions of the model (i.e., end forces and moments are equal to zero). This is a highly conservative analysis approach, especially when the assumed physical constraints on the ends of the LWRHU aeroshell do not exist in the actual reentry. Comparison of the results for these two analyses with the plane stress executions shows a minor increase in hoop stress magnitudes due to the coupling effect. The maximum axial stresses calculated with the SRBC version of SAAS III were double the magnitude of the maximum hoop stresses. As with the previous comparison between coarse and fine models, the maximum fine model compressive stresses were somewhat higher in magnitude and the maximum fine model tensile stresses were slightly lower. These conservative analysis results also showed minimum safety factors for compressive axial stress which were below 1.00, thus indicating a possible compressive failure of the aeroshell. In both the coarse and the fine models, the apparent region of failure is at the outer wall surface from the stagnation point to approximately 45^{o} around the aeroshell. Table 10 contains a tabulation of the SRBC coarse analysis results. Both the plane stress and the SRBC fine elastic analysis results are tabulated in Table G-14.

Table G-13: LWRHU Side-On Stable Coarse Model VEEGA Steep Reentry Hoop and Axial Stresses and Safety Factors

		IN-PLANE						AXIAL						
		Elem ID #	Elem Centroid R(in)	Elem Centroid θ(deg)	Elem Temp(°F)	σ Hoop (psi)	σ Ult (psi)	SF	Elem ID #	Elem Centroid R(in)	Elem Centroid θ(deg)	Elem Temp(°F)	σ Axial (psi)	σ Ult (psi)	SF
MAXIMUM TENSILE STRESS	R1	1	0.3522	5.0	3527	5913	25071	4.24							
	TIME	1.40 SECONDS													
	R2	1	0.3522	5.0	3527	6523	25071	3.84	36	0.3522	75.0	2048	12937	24322	1.88
	TIME	1.40 SECONDS													
MINIMUM TENSILE SF	R1	1	0.3522	5.0	3995	5791	21253	3.67							
	TIME	1.60 SECONDS													
	R2	1	0.3522	5.0	3527	6523	25071	3.84	36	0.3522	75.0	2048	12937	24322	1.88
	TIME	1.40 SECONDS													
MAXIMUM COMP. STRESS	R1	5	0.4932	5.0	4724	-7834	-25147	3.21							
	TIME	1.00 SECONDS													
	R2	9	0.4580	15.0	4877	-5619	-22582	4.07	25	0.4932	45.0	5163	-17685	-16978	0.96
	TIME	1.40 SECONDS													
MINIMUM COMP. SF	R1	10	0.4932	15.0	6060	-1806	-3504	1.94							
	TIME	1.40 SECONDS													
	R2	10	0.4932	15.0	6060	-2082	-3504	1.68	15	0.4932	25.0	5739	-9501	-8171	0.86
	TIME	1.40 SECONDS													

Velocity = 46750 FPS, Gamma = -90°, Altitude = 271000 FT

R1 - Coarse Plane Stress Elastic Tensile R2 - Coarse SRBC Elastic Tensile

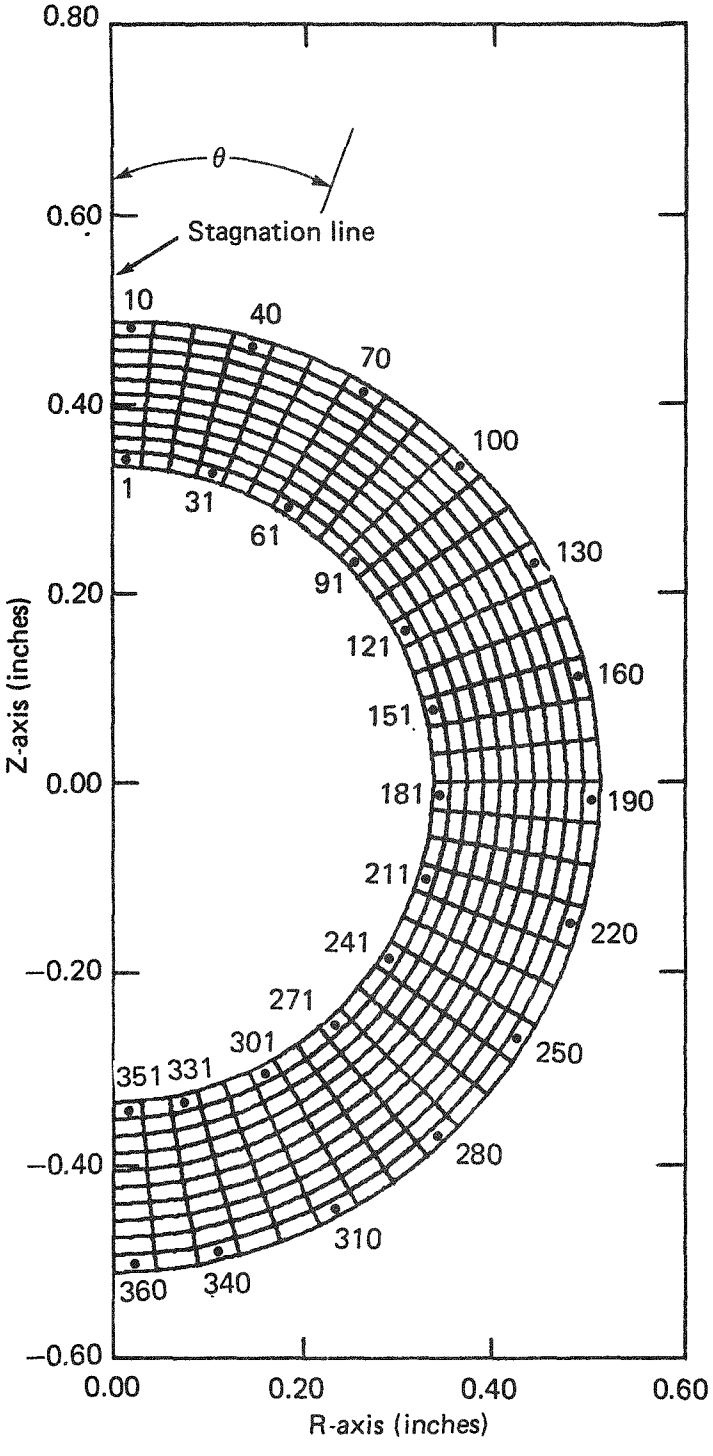

Figure G-29: **Fine mesh planar cross section model for side-on reentry calculations.**

Table G-14: LWRHU Side-On Stable Fine Model VEEGA Steep Reentry Hoop and Axial Stresses and Safety Factors at 1.40 Seconds (Basic Assumptions).

		IN-PLANE							AXIAL						
		Elem ID #	Elem Centroid R(in)	Elem Centroid θ(deg)	Elem Temp(°F)	σ Hoop (psi)	σ Ult (psi)	SF	Elem ID #	Elem Centroid R(in)	Elem Centroid θ(deg)	Elem Temp(°F)	σ Axial (psi)	σ Ult (psi)	SF
MAXIMUM TENSILE STRESS	R3	1	0.3334	2.5	3480	5166	25365	4.91							
	R4	1	0.3434	2.5	3480	5652	25365	3.48	131	0.3434	67.5	2216	12784	24290	1.90
MINIMUM TENSILE SF	R3	1	0.3434	2.5	3480	5166	25365	4.91							
	R4	1	0.3434	2.5	3480	5652	25365	4.48	131	0.3434	67.5	2216	12784	24290	1.90
MAXIMUM COMP. STRESS	R3	5	0.4844	37.5	5235	-5568	-16537	2.97							
	R4	9	0.4844	37.5	5235	-6252	-16537	2.64	140	0.5012	67.5	4302	-20007	-23808	1.19
MINIMUM COMP. SF	R3	10	0.5012	37.5	6034	-2131	-3495	1.64							
	R4	10	0.5012	37.5	6034	-2426	-3495	1.44	50	0.5012	22.5	6477	-4881	-3514	0.72

Velocity = 46750 FPS, Gamma = -90°, Altitude = 271000 FT

R3 - Fine Plane Stress Elastic Tensile

R4 - Fine SRBC Elastic Tensile

A further step involved the use of the fine elastic plane stress results to isolate regions of the model which were totally in tension or in compression. Both tensile and compressive material properties were used. This results in a more exact representation of the LWRHU aeroshell at the reentry time of this analysis. Only marginal change was observed between the results of the tensile only and the tensile-compressive SRBC elastic fine results.

The final step was the use of the bi-linear elastic-plastic material properties option of SAAS III for an even more exact representation. As would be expected at the temperatures predicted during the reentry, the material did exhibit yielding and underwent some plastic flow. Compressive yield strengths of the FWPF are substantially lower than the tensile yield strengths. The stress results did show a slight reduction in magnitude and the safety factors showed a minor increase. As in the previous analyses, an axial compressive failure was still predicted. A tabulation of the results from both of these analyses may be found in Table G-15.

The stress results for the most complex analysis conducted (fine SRBC- EPTC) showed only one small area of the aeroshell which possibly would fail under the subject VEEGA temperature loadings. The outer aeroshell wall near the stagnation point showed compressive axial stress safety factors of less than 1.00 at the 1.40 second time. Elements 10, 20, 30, 40, 50, 60, 70 and 80 of Figure 24 (a single outer wall element thickness from 0^{o} to 37.5^{o} for the fine model) were the only elements having axial compressive stress safety factors less than 1.00. A single element thickness is one-tenth of the total LWRHU wall thickness or approximately 0.018 inch. The elements deeper into the wall did not show failure at this reentry time, therefore, it is questionable whether the compressive failure of this row of outer wall elements would cause a catastrophic failure of the LWRHU aeroshell. Under compressive loading, the FWPF ultimate strengths used (based on 1% strain) should be taken not as an indicator of catastrophic failure, but only as a sign of increased compressive plastic deformation. The "failed" material would tend to remain intact and not allow a release of the insulators and the cladded fuel pellet.

In order to check for a compressive stress path which could lead to additional failure under compressive loadings, the subject elements were removed from the fine model and an analysis was performed at 1.60 seconds into the reentry. This analysis showed no

Table G-15: LWRHU Side-On Stable Fine Model VEEGA Steep Reentry Hoop and Axial Stresses and Safety Factors at 1.40 Seconds (Refined Assumptions).

		IN-PLANE							AXIAL						
		Elem ID #	Elem Centroid R(in)	Elem Centroid θ(deg)	Elem Temp(°F)	σ Hoop (psi)	σ Ult (psi)	SF	Elem ID #	Elem Centroid R(in)	Elem Centroid θ(deg)	Elem Temp(°F)	σ Axial (psi)	σ Ult (psi)	SF
MAXIMUM TENSILE STRESS	R5	1	0.3434	2.5	3480	5616	25365	4.51	131	0.3434	67.5	2216	11979	24290	2.03
	R6	1	0.3434	2.5	3480	5519	25365	4.59	131	0.3434	67.5	2216	11956	24290	2.05
MINIMUM TENSILE SF	R5	1	0.3434	2.5	3480	5616	25365	4.51	131	0.3434	67.5	2216	11979	24290	2.03
	R6	1	0.3434	2.5	3480	5519	25365	4.59	161	0.3434	82.5	1816	11842	24158	2.04
MAXIMUM COMP. STRESS	R5	79	0.4844	37.5	5235	-6099	-16537	2.71	140	0.5012	67.5	4302	-16827	-23808	1.42
	R6	79	0.4844	37.5	5235	-5677	-16537	2.81	140	0.5012	67.5	4302	-16283	-23808	1.46
MINIMUM COMP. SF	R5	80	0.5012	37.5	6034	-2428	-3495	1.44	50	0.5012	22.5	6477	-4928	-3514	0.71
	R6	80	0.5012	37.5	6034	-2303	-3495	1.52	50	0.5012	22.5	6477	-4403	-3514	0.79

Velocity = 46750 FPS, Gamma = -90°, Altitude = 271000 FT

R5 - Fine SRBC Elastic Tensile-Compressive

R6 - Fine SRBC Elastic-Plastic Tensile-Compressive

further failure of the underlying elements due to axial compressive stresses. All other compressive and tensile stresses at this time showed high safety factors. A further analysis was performed with the removed elements model at 5.60 seconds into the reentry heat pulse as this appeared to be the time of maximum tensile stresses in the critical region. The tensile stresses in this area never rise above 3000 psi and the temperatures at these later times are reduced substantially. Thus, safety factors at the time of peak tensile stress in the critical area were well above tensile stress ultimate limits. Results from these additional analyses show that such a compressive failure near the stagnation point would not cause a catastrophic failure of the LWRHU aeroshell. Therefore, no release of the internals of the LWRHU would be expected due to thermal stress for the side-on stable steep gamma reentry. The shallow gamma (-10^{o}) and medium gamma (-50^{o}) side-on stable temperature predictions were examined and compared to that of the steep gamma (-90^{o}) temperature predictions. Thermal gradients were lower for these additional analyses and are therefore considered less severe from a thermal stress standpoint. Thermo-structural analyses utilizing these inputs therefore were considered unnecessary. These reentries are more important in the ablation analyses.

7.3.4 Results of End-on Stable Analysis - The initial conditions for the steep gamma, end-on stable reentry configuration are the same as for the side-on stable: an inertial velocity of 46,750 feet per second, an inertial flight path (gamma) angle of -90^{o}, and a free release altitude of 271,000 feet.

The approximate thermo-structural response of the aeroshell during the first 6.00 seconds of the reentry heat pulse was determined with the axisymmetric option of SAAS III. Symmetry in the axial direction was assumed, thereby reducing the size and complexity of the model. This assumption is based upon the belief that boundary effects at the closed end of the aeroshell will not alter behavior at the end cap region.

A finite element model which consisted of 144 four-noded axisymmetric elements was used for the end-on case, Figure G-30. The axisymmetric option of SAAS III considers the geometry to be a solid rotated through 360^{o} about the Z-axis. The side-wall and the end cap of the aeroshell were considered a monolithic structure in the initial analysis executions. Also, all elastic material properties were used in the initial approximations. Use of these initial assumptions provided a quick and inexpensive

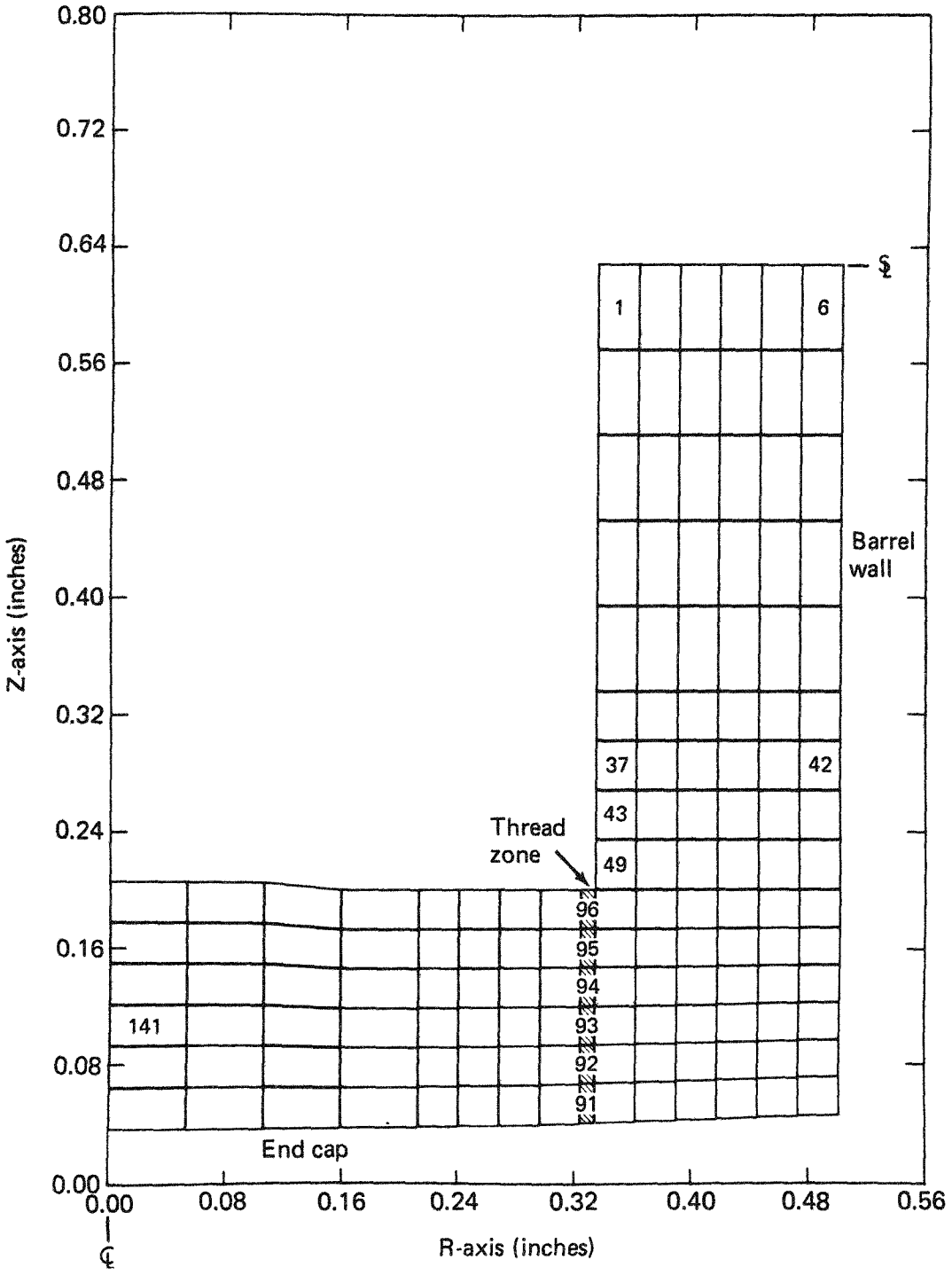

Figure G-30: **Axisymmetric model for end-on reentry calculations.**

method of determining the time of maximum thermally-induced stresses during the reentry.

The time of maximum temperature was found to be approximately 3.00 seconds with a maximum of 7460°R at the center of the outer surface of the end cap. Initially, very large thermal gradients through the wall of the end-cap caused high stresses in the surrounding region. These thermal gradients peaked at about 1.60 seconds into the reentry. A direction reversal of thermal gradient near the center of the end-cap occurred after approximately 4.50 seconds. At the edge of the aeroshell wall, however, this reversal did not occur. At the end of the 6.00 second study, elements in this region were nearly the same temperature.

Stresses were evaluated throughout the entire 6.00 seconds of the reentry for which were studied. Hoop stress appeared to be the most critical as in the side-on stable analysis. Radial stress was also considered important due to the rapid expansion of the constrained end cap as described above.

Table G-16 is a tabulation of the hoop and radial stresses and corresponding factors of safety for the end-on elastic analysis. The maximum compressive hoop stress occurred at 1.00 second at the leading edge of the aeroshell wall. The minimum safety factor for compressive hoop stress occurred at the time of maximum thermal gradient at 1.60 seconds. Magnitudes and safety factors for the compressive radial stresses follow closely with the compressive hoop stresses. Tensile radial stress safety factors never dropped below a value of 4.0. Axial stresses were of little concern never dropping below a 2.0 safety factor. Major and minor principal stress levels followed closely with those of the hoop and radial stresses. All safety factors for the end-on elastic material properties analysis showed a minimum margin of safety of at least 50 percent.

Two further analyses were conducted at the 1.60 second time of the reentry. The first was a SAAS III execution with elastic-plastic tensile and compressive material properties. Stress levels were little changed from the elastic tensile only run indicating a good initial representation of the material in this run. Very few of the elements werre in total compression and little, if any, plastic flow had occurred at this critical time of the reentry. Another SAAS III execution was run using gap elements to represent the thread openings of the end cap to aeroshell side wall interface. As expected, some shifting of

Table G-16: LWRHU End-On Stable VEEGA Steep Reentry Hoop and Radial Stresses and Safety Factors (Elastic Tensile Material Properties).

	HOOP STRESS							RADIAL STRESS						
	Elem ID #	Elem Centroid R(in)	Elem Centroid Z(in)	Elem Temp(°F)	σ Hoop (psi)	σ Ult (psi)	SF	Elem ID #	Elem Centroid R(in)	Elem Centroid Z(in)	Elem Temp(°F)	σ Radial (psi)	σ Ult (psi)	SF
MAXIMUM TENSILE STRESS	43	0.3493	0.2485	3563	14663	24780	1.69	141	0.0268	0.086	3126	5724	26044	4.55
TIME	2.90 SECONDS							1.20 SECONDS						
MINIMUM TENSILE SF	90	0.4961	0.018	4475	11479	17333	1.51	141	0.0268	0.086	3126	5724	26044	4.55
TIME	5.00 SECONDS							1.20 SECONDS						
MAXIMUM COMP. STRESS	90	0.4961	0.018	4587	-15138	-27250	1.80	121	0.1874	0.018	4749	-11019	-24793	2.25
TIME	1.00 SECOND							1.20 SECONDS						
MINIMUM COMP. SF	91	0.3212	0.018	5762	-4693	-7321	1.56	91	0.3212	0.018	5762	-4725	-7321	1.55
TIME	1.60 SECONDS							1.60 SECONDS						

Velocity = 46750 FPS, Gamma = -90°, Altitude = 271000 FT

stresses to structural elements in the thread area was encountered. Also evident was the reduction of stresses in the aeroshell wall past the end cap, indicating less bending of the aeroshell wall due to the uncoupling of the two pieces. However, no gap openings occurred during this analysis, indicating that the seal between the end cap and the aeroshell wall remained intact. Safety factors for both of the additional runs showed that maximum stresses did not exceed ultimate strengths of the FWPF material. Therefore, based on thermo-structural considerations, the LWRHU aeroshell is expected to survive an end-on stable steep gamma VEEGA reentry intact and without a release of the internal insulators or cladded fuel pellet.

As with the side-on stable analysis, the shallow gamma (-10^{o}) and medium gamma (-50^{o}) end-on stable temperature predictions were examined and compared to that of the steep gamma (-90^{o}) temperature predictions. Thermal gradients were lower for these additional analyses and are therefore considered less severe from a thermal stress standpoint. Thermo-structural analyses utilizing these less severe inputs therefore were considered unnecessary.

7.4 LWRHU Ablation Response Tests - A series of tests was successfully conducted to assess the full scale ablation response behavior of the General Purpose Heat Source (GPHS), the Graphite Impact Shell (GIS), and the LWRHU modules to simulated reentry environments. The LWRHU was tested in an end-on orientation to (a) eliminate the uncertainties in the aerodynamics and aerothermodynamics that would result from the interference generated by a side-mount, and (b) to minimize the shear load on the model holders. For these first tests, these were considered to be important considerations.

The tests were completed in April 1988 at the NASA/ARC 20 MW AHF facility. The experimental results are currently being reviewed and analyzed. Preliminary results show that the stagnation point recession of the GPHS (in a broadside orientation) and of the LWRHU (in an end-on orientation) is predicted within 10% by 1-D predictions for orbital decay conditions. The experimental results will be documented as a) a "quick look" report, where photographic coverage (still photographs) of the stagnation surface will be presented, and b) a final test report, where the information pertaining to the test and experimental data, as well as the data itself, will be presented.

The objective of the test program (Reference 22) is to assess the ablation response of the full scale, flight ready GPHS/GIS/LWRHU modules (with a fuel simulant in place of the nuclear fuel) for simulated conditions corresponding to orbital decay and/or minimum gamma type entries. Here, the ablation response is defined as the aeroshell material removal and associated surface temperature corresponding to the test conditions. Local aeroshell burnthrough and subsequent module behavior are also of interest and were intentionally programmed.

8.0 MOUND FUEL ABLATION ANALYSES

The two cases defined earlier in the Section 7.0 superorbital analyses identify the release of the integral LWRHU pellet following aeroshell failure and clad melting in Zones A and B. The behavior of this bare fuel pellet is defined in the following two subsections. Note that for Zone C aeroshell failure, the failure is so late in the reentry that the released clad does not acquire enough aerothermal heating to melt. Zone D reentry does not result in aeroshell failure nor clad melting so the subsequent earth impact is "normal".

8.1 Zone A Fuel Pellet Behavior - APL has provided plutonia fuel pellet surface temperatures as a function of time in this shallow reentry regime (4^{o} - 7.5^{o}). In order to calculate the recession, the erosion was assumed to be wholly due to plutonia sublimination from the front (stagnation) point area of the side-stable fuel pellet. The temperature was used to calculate the vapor pressure at each time increment from the expression (assume liquid plutonia, melting point = 2675 K):

$$\log P = 6.00 - 25210/T$$

where P = plutonia pressure in atmospheres

and T = stagnatation area temperature in kelvins.

Then one employs the Langmuir-type expression for weight loss:

$$\dot{m} = 44.33\ P\ (T/M)^{-1/2} \quad \text{(Reference 5)}$$

where $\dot{m}$ = weight loss (g) per cm^2 s

and M = vapor species molecular weight (assumed to be stoichiometric PuO_2 of 270/g/mole).

In order to determine how much of the pellet has eroded, it should be realized that the pellet is of 87.4% theoretical density (which is 11.46 g/cm^3). Therefore, for every gram per square centimeter of evaporated plutonia, the surface erodes 1 mm.

Figure G-31 for Zone A reentry shows these data as a function of time. As the total erosion thickness approaches the pellet diameter during this pulse, the pellet will be vaporized in this scenario.

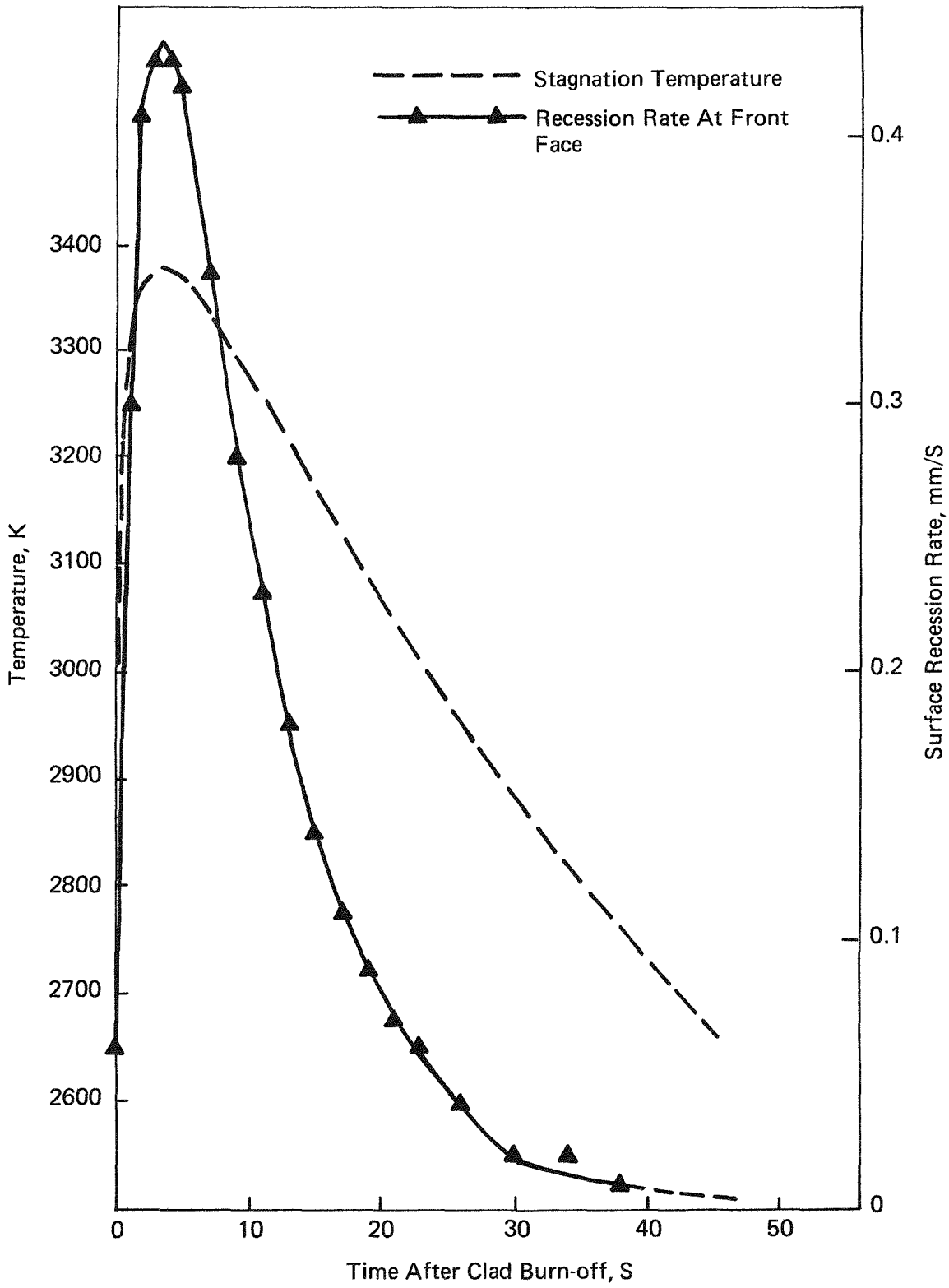

FIGURE G-31: For Zone A VEEGA reentry of the side-on stable LWRHU bare fuel pellet, the time-integrated surface recession shows virtually complete burn up (evaporation) after 50 S from clad disappearance.

It may be noted that all temperatures in Figure G-31 are in excess of the plutonia melting point of approximately 2670 K. The fuel pellet may spall into droplets during this reentry case but the ultimate dispersal would still be as vapor as these droplets would quickly evaporate at these high velocities.

8.2 Zone B Fuel Pellet Behavior - APL also provided time-temperature angular estimations for a side-on stable bare fuel pellet which reenters over the region $7.5^{o} < \gamma < 20^{o}$. Table G-17 provides these values over the two foremost segments defined in the calculations. In this assessment, it becomes readily obvious that the recession is well less than the pellet diameter so the weight loss per segment as a function of time above approximately 2600 K was calculated over the appropriate time increment. As each fuel pellet weighs 2.664 g initially and would loose 0.226 g in the reentry, the plutonia is released to the environment as high altitude vapor (0.085 fraction) and as a pellet of bare plutonia which impacts earth or water (0.915 fraction).

Note that the temperature regime in which significant evaporation occurs is again above the melting point of the fuel. However, in this case, much of the leading surface maintains its solid configuration and it was assumed that the liquid plutonia was not stripped from the front edge but escaped only via the evaporation process.

9.0 MOUND VEEGA REENTRY SCENARIOS

In the previous discussions regarding the ablation failures of LWRHUs, an aeroshell failure was identified when it had ablated to 50% of its original thickness. This value was chosen by APL to accommodate uncertainties in the reentry process.

The writer is choosing to accommodate the uncertainties surrounding the VEEGA reentries in a different yet structural manner. To address this, the APL-generated nominal stagnation recession values (Table G-10) are used to identify a 50% probability level. Further, it is assumed that the reentry uncertainties could, at a minimum case, result in only a 50% recession at a 3σ (0.005) probability level. Employing a log-normal plot as shown in Figure G-32, the probabilities of aeroshell failure (at 100% of the aeroshell thickness) is the intersection of the zone lines with the PASS/FAIL line.

TABLE G-17: The VEEGA bare fuel pellet reentry event for Zone B ($7.5^{o} < \gamma < 20^{o}$) shows that 8.5% of the plutonia will evaporate at high temperatures

	$\pm\ \theta = 15^{o}$			$\pm\ \theta = 15^{o} - 40^{o}$		
t, s	T, K	P, atm	$\dot{w}$, g/cm^2 s	T K	P atm	$\dot{w}$ g/cm^2 s
0	3165	0.011	0.14	2959	0.003	0.04
1	3261	0.019	0.24	3106	0.008	0.10
2	3114	0.008	0.11	2983	0.004	0.05
3	2944	0.003	0.04	2802	0.001	0.01
4	2772	0.001	0.01	2642(s)	<0.001	<0.01
5	2596(s)	<0.001	<<0.01	-		
Weight loss per square centimeter in reentry =			0.54 g			= 0.20
Weight lost per LWRHU Pellet - 0.165 g						= 0.061 g

Total weight lost per LWRHU pellet = 0.226 g
Weight fraction lost per LWRHU pellet = 0.085

Source: Reference 28

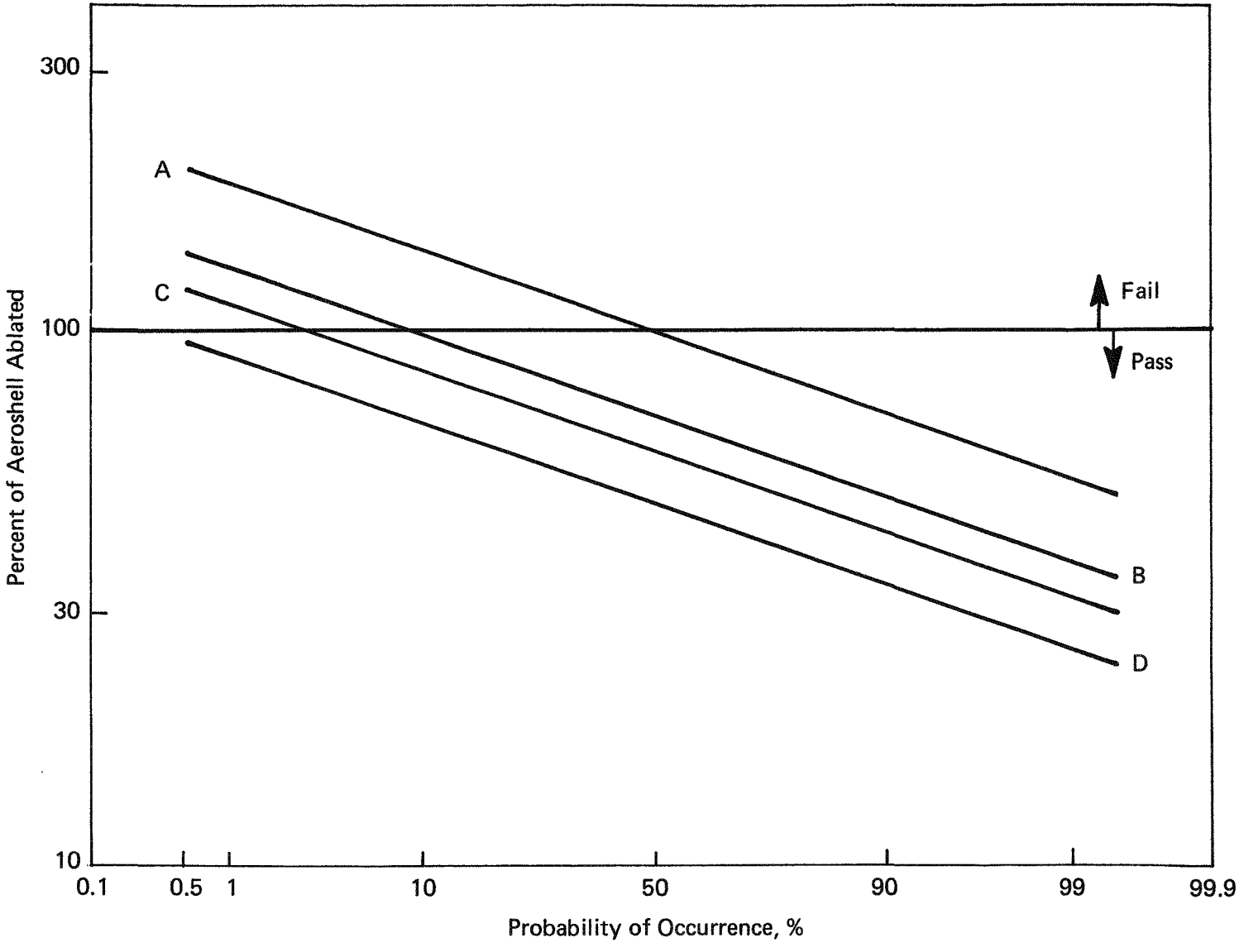

FIGURE G-32: By the use of a log-normal distribution about the nominal (50% probability) ablation values, a 3σ = 50% ablation curve provides an approximate failure (100% wall thickness erosion) percentage of occurrence.

9.1 Zone A

The Zone A curve in Figure G-32 shows that the inherent uncertainties associated with the assumed random nature of the reentry process result in a probability of aeroshell failure 50% of the time with fuel evaporation as discussed in Section 8.1. The PASS portion of the A curve does result in a clad temperature that exceeds the Pt-30Rh/C eutectic temperature (2033 K) and the melting point of the FAST for Zone A VEEGA reentry (Figure 19) shows the effect of this rationale on the release of plutonia.

9.2 Zone B

The Zone B VEEGA reentry "B" curve in Figure G-32 indicates a 10% probability that the aeroshell would be ablated at or exceeding the 100% level. The bare fuel pellet reentry is addressed in Section 8.2 and a branch with this 10% event given in Figure 20.

9.3 Zone C

A Zone C reentry will result in an intact reentry 98% of the time per the "C" curve in Figure G-32. The 2% "failures" occur so late in the reenetry process that aerothermal heating is minimal; thus, the FAST for Zone C in Figure 18 shows "LWRHUs/CLADS INTACT" as the result of reentry. As the terminal velocity impact of a bare clad (approximately 49 m/s) has been shown not to result in clad breaking, the consequence of a clad or an intact LWRHU impacting Earth's surface is the same.

9.4 Zone D

An inspection of the "D" curve in Figure G-32 shows that there is no LWRHU degradation even at the 3σ level. Therefore, the FAST for this reentry scenario results in ablated but intact LWRHUs impacting the Earth's surface with no failure resulting.

10.0 REFERENCES

1. Conn, D. W., "Final LWRHU End-On (Two-Dimensional) Thermal Analyses for Peak Clad Response," ANSP-201/EM-4985 (January 27, 1981).

2. Perini, L. L., "Impact Temperature of the Light Weight Radioisotope Heater Unit (LWRHU)," ANSP-225/BFD-4-82-016 (November 3, 1982).

3. Waeber, K. R., "Thermal Stress Analysis of the Light Weight Radioisotope Heater Unit Aeroshell," ANSP-206/BFD-4-81-008 (May 18, 1981).

4. Conn, D. W., "Compacted LWRHU Orbital Decay Reentry - A Proposed Consequence of a Centaur Explosion in a Parking Orbit," ANSP-276-EM5255 (August 21, 1985).

5. Draft of "Final Safety Report for the Galileo Mission and the Ulysses Mission - Volume I: Reference Design Document, Appendix A: General Purpose Heat Source Radioisotope Thermoelectric Genrator Program," General Electric, Valley Forge (May 1985).

6. Letter, J. C. Hagan/E. W. Johnson, ATD-RL-88-088, JCH-88-061 (August 18, 1988).

7. McRonald, A., Galileo VEEGA Earth Reentry Breakup Analysis, JPL D-4222 (Preliminary Release), Jet Propulsion Laboratory, Pasadena, CA, March, 1987.

8. Letter from McRonald, A., (Jet Propulsion Laboratory) to Hagen, J. C., (Applied Physics Laboratory), MS-301-165, August 17, 1987.

9. Conn, D. W., "Galileo-VEEGA Failure Boundaries and Related Computational Requirements", BFD-2-97-017, JHU/APL, Laurel, MD, September 21, 1987.

10. Hagan, J. C., JHU/APL, Letter to G. L. Bennett, DoE, "Planning for LWRHU/GPHS Reentry Analysis", ATD-RL-87-071 dated October 21, 1987.

11. Johnson, E. W., Light Weight Radioisotope Heater Unit Safety Analysis Report (LWRHU-SAR), Vol. II, Accident Model Document, Appendix G., Monsanto Research Corporation Report MLM-3293, Miamisburg, OH, October, 1985.

12. Lucero, E. F., "Estimated Continuum and Free Molecular Aerodynamics and Bridging Parameters for the LWRHU," JHU/APL BFD-2-88-004, March 2, 1988.

13. Lucero, E. F., "Estimated Subsonic Aerodynamics and Terminal Velocity of the RTG, GPHS Module, GIS, Fuel Clad and LWRHU," JHU/APL BFD-2-87-023, dated December 2, 1987.

14. Perini, L. L., "User's Manual for the 3DOF Trajectory Computer Program", ANSP-M-6, JHU/APL, Laurel, MD, September, 1973.

15. "Reentry Respnse of the Light Weight Radioisotope Heater Unit Resulting from a Venus-Earth-Earth-Gravity-Assist Launch Accident", ANSP-M-19, JHU/APL (to be published).

16. Hunter, L. W., "The Ablation Rate of Burning Carbon and In-Depth Heat Flux", ANSP-260, (BBP-84-153), JHU/APL, Laurel, MD, July 27, 1984.

17. Lundell, J. H. and Dickey, R. R., "Graphite Ablation at High Temperatures", AIAA Paper No. 71-418, AIAA 6th Thermophysics Conference, Tullahoma, TN, April 1971.

18. Dolton, T. A., et al, "Thermodynamic Performance of Carbon in Hyperthermal Environments", AIAA Paper No. 68-754, AIAA 3rd Thermophysics Conference, Los Angeles, CA, June 1968.

19. Perini, L. L., Review of Graphite Ablation Theory and Experimental Data, ANSP-M-1, JHU APL, Laurel, MD, December 1976.

20. Conn, D. W., "Perspective of the Fuel Reentry Problems - ANSP Planning", ANSP-282, JHU/APL, Laurel, MD, March 14, 1986.

21. March, E. B., Thermal and Ablation Response of Small Spherical Particles for Reentry -- Summary Report, SC-RR-68-547, Sandia Laboratories, Albuquerque, NM, October 1968.

22. Conn, D. W., "PuO2 Microsphere Reentry Studies: Thermal Properties", ANSP-275, JHU/APL, Laurel, MD, August 16, 1985.

23. Hampel, C. A., ed., Rare Metals Handbook, Robert Krieger Publishing Co., Inc., Huntington, NY., Tables 17.5 (p. 320) and 17.6 (p. 323), 1971.

24. Randall, J. D., SHTPE, A Computer Implementation of the Finite Difference Embedding Method of Ablation Analysis, CP 067, JHU/APL, Laurel, MD, May 1978.

25. Conn, D. W., "Final LWRHU End-on (Two Dimensional) Thermal Analysis for Peak Clad Response," ANSP-201/EM-4985, January 27, 1981.

26. Waeber, K. R., Thermal Stress Analysis of the Light Weight Radioisotope Heater Unit Aeroshell," JHU/APL ANSP-206 (BFD-4-81-008), May 18, 1981.

27. Lutz, S. A., "Test Plan for the GPHS/GIS/LWRHU Module Ablation Experiment for the NASA Ames Research Center 20 MW Aerodynamic Heating Facility," JHU/APL BBE/EM-5451/BFD-2-87-026, December 1987.

28. Telefax, D. W. Conn/E. W. Johnson, June 29, 1988.

APPENDIX H

IMPACT TEST PROGRAM RESULTS

1.0 LWRHU REENTRY IMPACT TEST PROGRAM

A series of tests was conducted at LANL to evaluate the normal response to the ablated LWRHU upon some reference earth surface as well as some bare clad impacts. Following is an excerpt from Reference 1, which summarizes this endeavor:

> Four units, LRF 021 through 024, were impacted "as built" shortly after their assembly. Two units, LRF 011 and 020, were stored at ambient temperature ($\sim$45°C) for about 2.5 yr and then impacted. The nominal impact velocity for all tests was 49 m/s (161 ft/s), which is 110% of the predicted reentry impact velocity at sea level, and the nominal temperature of the units just before impact was in the range of 25 to 50°C. The units were impacted in various orientations with respect to the vent end of the capsule. By convention, the angle is specified as the angle the flight trajectory makes with the cylindrical axis of the heat source; that is, the angle for a unit impacted on the vent end is 0°, on the side is 90°, and on the closure end is 180°. Before the actual impact test, each fueled capsule was removed from its graphite components and heated in an electron-beam furnace through a short duration thermal pulse to simulate the heating in a reentry event, The reentry impact conditions and results are summarized in Table H-1.
>
> The graphite components were significantly damaged, as might be expected. There was little or no damage or distortion to the fuel capsules because the graphite provides considerable protection. A small crack was observed in the interior of the closure weld zone of LRF 011, aged 2.5 years before impact, but the unit was not breached. No conclusion has been reached as to the cause of this small crack. During the engineering development of the LWRHU (Reference 2), capsules were impacted without graphite at 48 m/s (157 ft/s) in the 0°, 45°, and 90° orientations. They were also impacted in the 90° orientation as successively higher velocities (68, 88, 105, and 128 m/s) with substantial deformation but without failure. The development tests on the bare capsules and the safety analysis tests on capsules with graphite protection demonstrate that the ductile Pt-30 Rh alloy capsule provides excellent fuel containment capability under postulated impact conditions.

One impact test was performed at 105 m/s using an aeroshell machined to simulate the recession expected during an orbital decay reentry. This clad exhibited more distortion than those tested at the expected terminal velocity but suffered no failures; see Appendix D, Section 4.0 and Reference 2 for details. Table H-1 provides the LANL test program results.

TABLE H-1: Los Alamos National Laboratory-performed Reentry Impacts are documented below per Reference 1.

Unit ID	Test Conditions			Results
As Built	Angle	Velocity (m/s)	Temperature (^{o}C)	
023	45^{o}	49.3	47	Minimal capsule deformation
021	90^{o}	49.3	30	Minimal capsule deformation
022	135^{o}	49	51	Minimal capsule deformation
024	180^{o}	49.6	52	Minimal capsule deformation
Aged 2.5 yr				
011	135^{o}	49.9	24	Cracked weld/not breached
020	90^{o}	49.2	26	Minimal capsule deformation

2.0 LWRHU CLAD IMPACT ENGINEERING STUDIES

In Section 1.0 above, and in Reference 2, it was reported that a series of bare clad impacts were performed by LANL at 48 m/s at 0^{o}, 45^{o}, and 90^{o} orientations and at 90^{o} (side-on) at 68, 88, 105, and 128 m/s. In these tests, although substantial clad deformation occurred, failures that would result in fuel release were absent. As the terminal velocity of the bare LWRHU clad has been reported as 49 m/s (162 ft/s) (Reference 3), the impact of a bare clad on any land or water surface should not result in the release of plutonia.

3.0 FUEL PELLET IMPACT

No bare fuel LWRHU impacts have been performed so some assumptions will have to be made regarding the consequences of this event occurring. In general, three surfaces are generally considered: ocean, soil or rock. As the terminal velocity of a slightly ablated fuel pellet would be only 36 m/s (119 ft/s), ocean or solid impact would result in no significant added break-up (generation of particles less than 10 μm in diameter). However, if the pellet struck a hard surface, considerable comminution could occur. The resultant spectrum is assumed to be represented by the dashed line curve in Appendix J, Figure J-1.

4.0 REFERENCES

1. Tate, R. E., and Land, C. C., Environmental Safety Analysis Tests on the Light-Weight Radioisotope Heater Unit, LA-10352-MS, Los Alamos National Laboratory (May 1985).

2. Tate, R. E., The Light Weight Radioisotope Heater Unit (LWRHU): A Technical Description of the Reference Design, LA-9078-MS, Los Alamos National Laboratory (January 1982).

3. Lucero, E. F., Verbal Presentation at Gaithersburg, Maryland, March 30, 1988.

APPENDIX I

BURIAL THERMAL ANALYSIS

After certain abort situations, there is the potential that LWRHUs could become imbedded in earth media with the potential for release of plutonia to the soil. Earlier, it was noted that no earth impacts would result in clad breaching. Therefore, what must be assessed is the ability of the clad to withstand the conditions of earth burial.

The low quantity of heat emanating from a buried LWRHU would result in a modest temperature increase over normal ambient. The least favorable reported soil thermal conductivity was considered (Reference 1 cites 0.0346 W m^{-1} K^{-1} for diatomaceous earth). If a LWRHU clad is imbedded within an infinite diatomaceous earth medium, the temperature gradient would be:

$$\Delta T = \frac{Q}{4 \pi k r} = \frac{1 \text{ W}}{4 \pi (0.0346 \text{ W m}^{-1} \text{ k}^{-1}) (0.005 \text{ m})} = 460 \text{ K},$$

or the clad would be in the order of 775K (502°C) maximum. This assumes an average soil temperature of 315K (108°F). It would be less severe for any other burial media.

Platinum at this temperature* should last virtually forever, assuming these initial conditions. Vaporization of fuel through the vent would be insignificant; the vapor pressure of plutonia at this temperature is about 10^{-25} Pa. As all real conditions will be significantly less severe, soil burial will result in no release (<1 aCi or ~1 nBq/yr) of plutonia to the environment. This is significantly less than the allowable alpha residue after the decontamination process for most heat sources of ≤2000 dpm (33 Bq).

REFERENCES

1. Updated Safety Analysis Report for the Galileo Mission and the International Solar-Polar Mission, General Electric Co., GESP-7186, (April 1984).

2. Alcock, C. B., and Hooper, G. W., Proc. Royal Soc. A, 254, 551 (1960).

*Data from Alcock and Hooper (Reference 2) indicate an extrapolated oxidation rate of platinum at 500°C of about 1.3 fg/s·m^2. This corresponds to 0.2 nm/yr erosion. Rhodium is better by about an order of magnitude. As the temperature difference drops linearly with decreasing thermal output, an insignificant fraction of the LWRHU clad wall will be lost during soil burial.

APPENDIX J

SOURCE TERM EVALUATION

1.0 INTRODUCTION

Up to this point, for each of the vehicle conditions defined in the analysis, a sequence of adverse environments was defined and followed by an evaluation of the response of the LWRHU to each of the adverse environment sequences. As analyses of these extreme environments show that there is a potential for a fuel release, the occurrence probability was determined from the interrelation of the failure analysis and sequence tree construction.

To evaluate the consequences of these events, the analysis must define the source terms. Within the context of space nuclear safety, a source term is the quantity of fuel which may be uncontrolled and hence subject to dispersion into the environment. In describing a source term, one must consider its state (e.g., particle size distribution, chemical form if changed from its original form, and degree of containment) and its location (e.g., at high altitude, on land, or in water; latitude and longitude; or random deposition during reentry from a specified orbit).

When the first step of the risk analysis is completed, the analyst develops a series of specific nonnominal events that are postulated, with an associated probability of occurrence, to generate a known source term. The next step is to evaluate the consequences of the source terms. This will be addressed in Volume III, Nuclear Risk Analysis Document.

2.0 PLUTONIA PARTICLE SIZE SPECTRUM

In order to address the effect of the fuel particle size spectrum on the source term generated when the bare LWRHU fuel pellet impacts a rock surface, available data from various LWRHU tests were assessed. The comminution process as tested does not perfectly model the unconfined fuel impact on a hard surface but the small variance in particle size over a wide range of impact surfaces, velocities and protection implies that the use of this reference size spectrum is appropriate (the fuel pellet terminal velocity is 36 m/s.). The test descriptions are as follows:

A. Fines reported for impacted LWRHU (plutonia fueled) test assemblies: The two chosen were impacted at about 49 m/s at orientation angles of 45° (No. 023) and 90° (No. 021). The particle size data as shown in Figure J-1 were taken from Table III, Reference 1.

B. Some urania-fueled GPHS clads were subjected to overpressure environments only as reported in Reference 2. One case is shown plotted in Figure J-1 for the CST-1 unit.

C. LWRHU clads which had been struck by 1100 m/s flyer plates and then impacted the shuttle aluminum floor model were opened, and the fuel size distribution was characterized. The two analyses are also shown in Figure J-1 (data from Reference 3).

D. A high-velocity (approximately 600 m/s) impact of a clad containing a urania pellet fuel simulant resulted in severe fuel breakup. These data are provided on the log-probability plot, Figure J-1.

3.0 PLUTONIA VAPOR AND PELLETS

These forms are straight-forward. Appendix G addressed the partial or complete "burn-up" or vaporization of the side-on stable pellets in VEEGA Reentry Zones A and B. After a small ablation (8.4%), the still integral pellet would impact the Earth's surface. Thermal stressing was performed on fuel pellets during helium release studies up to about 17 K/s (Reference 4) with no reported breakup; APL reentry data for the bare LWRHU fuel pellet show up to 150 K/s heating rates in some locales, however. As no data exist which would indicate that LWRHU pellets fracture during normal or thermal stressed environments, for these analyses (other than evaporation loss of material from the liquid face of a reentering fuel pellet), the impacting item would be the integral fuel pellet.

4.0 SOURCE TERM SUMMARY

From Figures 19 and 20, which show the Phase 5A and 5B FASTs, the only plutonia releases from LWRHUs aboard the Galileo spacecraft are identified. These are:

Branch	Ci(TBq)	Form	Locale	Probability
5A	2935 (109)	Vapor	Upper Atmosphere	5×10^{-9}
5A	155 (5.74)	Particles	Land Surface	5×10^{-9}
5B	250 (9.25)	Vapor	Upper Atmosphere	1×10^{-8}
5B	1906 (70.5)	Pellets	Ocean Bed	1×10^{-8}
5B	644 (23.8)	Pellets	Land Surface	1×10^{-8}
5B	135 (5.00)	Particles	Land Surface	1×10^{-8}

Table J-1 provides the source term assessments for these releases when considered from maximum, most probable and expectation aspects. The methodology used to generate these data is provided in Volume III.

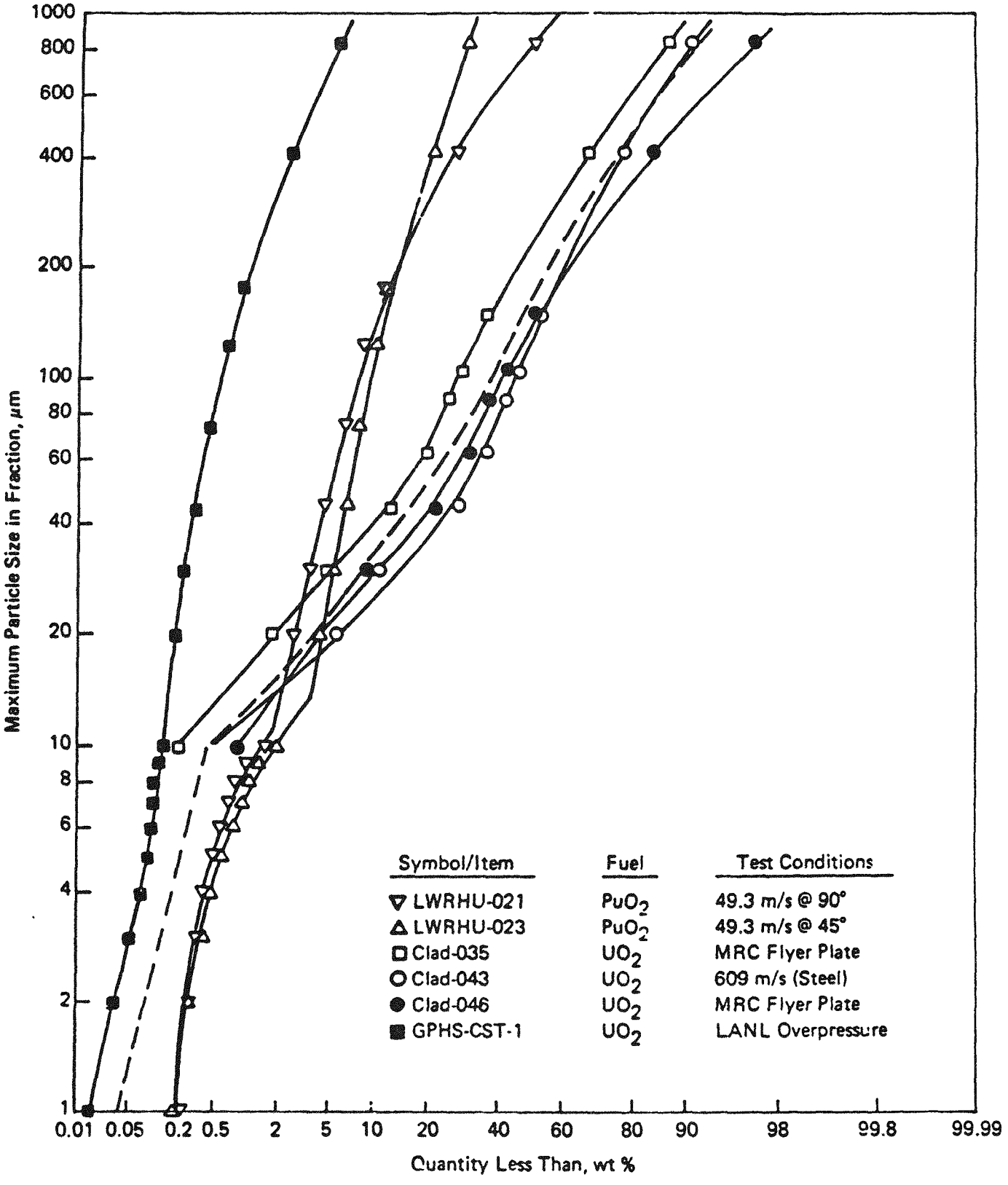

FIGURE J-1: Particle size distributions for various test cases are shown above. For the LWRHU cases in this document, the average released distribution is given by the dashed line. This is NUS "Code B" for size distribution (see Volume III).

Table J-1: Maximum, Most Probable and Expectation Release Cases are Provided below for the Galileo Mission Phase 5 accidents. Phases 0 through 4 have no LWRHU fuel releases identified and are thus not shown

Phase	Accident Type	Release Probability	Source Term, Ci (TBq)	Release Category	Description
			Most Probable Release Case		
5	Zone B VEEGA Reentry	1.00E-08	250 (9.3)	High Altitude	Vapor 0^{o} Latitude
			135 (5.0)	Ground Level	0^{o} Latitude
			Maximum Release Level		
5	Zone A VEEGA Reentry	5.00E-09	2935 (109)	High Altitude	Vapor 33^{o}N Latitude
			155 (5.7)	Ground Level	Rock Impact of Bare Fuel Pellets 33^{o}N Latitude
			Expectation Release Case		
5	VEEGA Reentry	1.50E-08	1145 (42.4)	High Altitude	Vapor 0^{o} Latitude
			142 (5.3)	Ground Level	Rock Impact of Bare Fuel Pellets 0^{o} Latitude

Note: 1 E-6 = 1 x 10^{-6}, etc.

5.0 REFERENCES

1. Tate, R. E., and Land, C. C., Environmental Safety Analysis Tests on the Light-Weight Radioisotope Heater Unit, LA-10352-MS, Los Alamos National Laboratory (May 1985).

2. Zocher, R. W., to Bradshaw, C. T., Telecommunication Message (April 29, 1985).

3. Johnson, E. W., Cryogenic Explosion Environment Modeling and Testing of Space Shuttle and Light-Weight Radioisotope Heater Unit Interactions, MLM-3303, Monsanto Research Corporation (October 1985).

4. Peterson, D. E., and Starzynski, J. S., Reentry Thermal Testing of Light-Weight Radioisotope Heater Units, LA-9226 (March 1982).

APPENDIX K

ABBREVIATIONS AND ACRONYMS

ABBREVIATION	DEFINITION	WHERE REFERENCED
AHF	Aerothermal Heating Facility	G.7.4
AMD	Accident Model Document	Title Page
APL	Applied Physics Laboratory	1.0.B
ATJ	Type of Polycrystalline Graphite	Figure G-18
C_D or CD	Drag Coefficient	Table G-5
D	Diffusion Coefficient	Table G-16
ΔPs	Static Overpressure	C.2.0
ΔV	Velocity Difference	D.5.1
ΔT	Temperature Differential	Figure G-11
E_D	Matting's Bridging Equation Exponent	Table G-5
EG&G-MAT	EG&G-Mound Applied Technologies	1.0.G
E	Emissivity	Figure G-16
EPTC	Elastic Plastic Tension Compression	G.7.3.3
EST	Estimated	Figure G-19
ET	External Tank	Table II
EUB	Experimental Upper Bound	E.2.0
F	Force, Heating Rate Factor	Figure G-19
FAST	Failure Abort Sequence Tree	1.0.C
FC	Convective Heat Transfer Conversion Factor	G.7.2.1.2
FSAR	Final Safety Analysis Report	Title Page
g	Gase Phase	G, p.9
G	Contact Conductance	G.2.1
γ	Reentry Angle	3.2.6
γ^*	Maximum Clad Temperature Reentry Angle	G.2.1
GE	General Electric Company	1.0.C
GIS	Graphite Impact Shell	G.7.4
GPHS	General Purpose Heat Source	G.7.4
h	Altitude	G.2.1
H	Enthalpy	Figure G-16
ID	Identification	Table G-13
I_D	Dynamic Pressure Impulse	C.2.0
IN	Inch	Table G-10
I_s	Static Overpressure Impulse	C.2.0
IUS	Inertial Upper Stage	G.7.2.3.1.2
JANAF	Joint Army Navy Air Force	G, p.9
JPL	Jet Propulsion Laboratory	1.0.E
JSC	Johnson Space Center	Figure G-16
k	Thermal Conductivity	G, Fig. 5
LANL	Los Alamos National Laboratory	1.0.A
LBA	Linear Boom Accutator	F.4.0

ABBREVIATIONS AND ACRONYMS - Continued

ABBREVIATION	DEFINITION	WHERE REFERENCED
LGA	Low Gain Antenna	D.3.1
LH_2	Liquid Hydrogen	C.2.1
LOX	Liquid Oxygen	C.2.1
LWRHU	Light Weight Radioisotopic Heater Unit	Title Page
m, $\dot{m}$	Mass, Mass per Unit Time per Unit Area	Figure G-17
M	Molecular Weight	G.7.2
m/C_DA	Ballistic Coefficient	C.3.0
MET	Mission Elapsed Time	D.4.0
MLP	Mobile Launch Pad	3.2.1.2.A
MMH	Monomethylhydrazine	C.2.4.a
MRC	Monsanto Research Corporation	1.0.F
1D	One Dimensional	G.6.0
OMS	Orbital Maneuvering Subsystem	C.2.4.a
P	Primary, Pressure	G.7.2
P_D	Dynamic Pressure	C.2.0
PG	Pyrolytic Graphite	C.3.0
Po	Atmospheric Pressure	C.3.0
P_R	Peak Reflected Pressure	C.2.0
PRSDS	Power Reactants Storage and Distribution Subsystem	C.2.4.e
P_s	Static Overpressure	C.3.0
psi	Pounds per Square Inch	D.5.1
PWS	Plasma Wave Subsystem	D.3.1
q, $\dot{q}$	Convective heating, Convective Heating Rate	G.2.1
r, R	Radius	Figure G-9
RCS	Reaction Control Subsystem	C.2.4.C
ρ	Density	C.3.0
RHU	Radioisotope Heater Unit	C.5.0.1
RPM	Retropulsion Module	C.2.4.b
RSS	Range Safety System Rotating Service Structure	Table II
RTG	Radioisotope Thermoelectric Generator	1.0.C
s	Solid Phase	G.7.2.3.1.2
S	Area, Secondary	G.7.1
SAAS II	Stress Analysis of Assymetric Solids	G.7.3.1
SHTPE	Types of Computer Code	G.7.2.5.2.2
σ	Stress, Stefan-Boltzmann Constant	T.5.0
SF	Safety Factor	Table G-1
6DOF	Six Degrees of Freedom	G.7.2.2.1
SRB	Solid Rocket Booster	3.2.1
SRBC	Stress Resultant Boundary Condition	G.7.3.2
SSME	Space Shuttle Main Engine	3.2.1
S/R	Surface Area/Radius	Figure G-2

ABBREVIATIONS AND ACRONYMS - Continued

ABBREVIATION	DEFINITION	WHERE REFERENCED
t, T	Time, Temperature	Figure G-6
θ	Angle	Table G-3
3D	Three Dimensional	Figure G-4
3DOF	Three Degrees of Freedom	G.7.1
TM	Thermochemical Model	E.2.0
2D	Two Dimensional	Figure G-5
UNK	Unknown	Figure G-18
V	Velocity	C.3.0
VEEGA	Venus-Earth-Earth Gravity Assist	2.0
W	Weight, Ablating Surface	Table G-6
X	Fraction	Figure G-7
Z	Altitude, Axis	F.5.0

APPENDIX L

UNCERTAINTY ANALYSIS

1.0 INTRODUCTION

In previous analyses in this document, no qualifications were assigned to the values presented. The numbers usually were conservative and, in areas where a significant data base existed, were nominal.

In generating the SAR, the ground rules were that no liberties were to be used with data provided in NSTS 08116 (Reference 1) nor was the use of unsubstantiated engineering judgment permitted. In this appendix, judgment is used freely: if data already existed, then there would not be uncertainties worth requiring an appendix such as this.

It is obviously very difficult (if not impossible) to place discrete limits on an engineering judgment when assessing these environments. The reader will note, therefore, that narrative assessments are provided oftentimes in lieu of statistically formal uncertainties.

2.0 EXPLOSION OVERPRESSURE RESPONSE UNCERTAINTY

2.1 Overpressure Aeroshell Failure Thresholds - The analysis performed by TES (Reference 2) indicated "lower bounds" of 570 psi (3.9 MPa) for end-on exposure and 800 psi (5.5 MPa) for side-on exposures of LWRHUs. Comments by APL (Reference 3) have been reviewed by TES and the effects deemed to be minor (Reference 4). The sole test of side-on and end-on exposures of an LWRHU to a 429 psi (2.96 MPa) indicated no aeroshell damage in either orientation; some PG cracking was noted however (Reference 5).

These data would indicate that the analytically defined lower aeroshell failure thresholds are probably valid.

2.2 Shielding - No attenuation credit was given due to intervening structures except for those LWRHUs within the probe. [The probe would receive a maximum (0.1% case) velocity of only about 70 m/s (230 ft/s) which would certainly not fail the LWRHU aeroshells. The energy thus absorbed by the LWRHUs in the probe is about 5% of the unattenuated incident energy.]

2.3 Summary - The defined threshold values appear conservative but it is difficult to quantitatively assess this conservatism. A good bit of overpressure lessening should be experienced but as no aeroshells are removed from about the clad regardless, the issue need not be belabored.

3.0 FRAGMENT IMPACT UNCERTAINTIES

3.1 LWRHU Velocity Errors - The velocity that LWRHUs receive from the various cryogenic fuel explosion environments were calculated using

methods discussed in Appendix D. In this assessment, it was assumed that the LWRHU was unsupported, uncanned and the ballistic coefficient was calculated based upon the end-on and side-on average areas. These errors are summarized as:

Weight: <1%,
Drag Coefficient: Approximately 10%,
Area: <2%,
Method: <5%,
or a total uncertainty of approximately ±11%.

As mentioned above, there would be considerable shock wave intensity attenuation due to intervening structures which would lower the calculated LWRHU velocity. These effects are uncharacterized. The attenuation effect due to bolt or hold-down failures is small. The effect of LWRHUs imbedded in structures or on sides opposite the blast wave would make for considerably lower velocities but of an unknown lowering amount.

3.2 LWRHU/Flyer Plate Encounters - Therefore, the worst-case LWRHU/flyer plate impact velocity uncertainties are:

±37 m/s for flame trench explosions
±35 m/s for on-pad explosions,
±12 m/s for aft compartment explosions and ±23 m/s for in-flight explosions.

4.0 CLAD TEMPERATURE RESPONSE

4.1 Fireball - The ten-second fireball clad responses were based upon clad temperature response during reentries with air-filled gaps. These uncertainties would be in the same order as those for reentry as summarized in Table L-1. A ±50 K uncertainty over the 10-s fireball duration is reasonable; this would not affect the conclusions of Appendix E as may be seen by referring to Figure E-1.

4.2 Solid-Rocket Fuel Fire Exposure - LANL test data have shown that with intact carbons about the clad, the Pt-30Rh does not melt, although the Pt-C eutectic and Pt melting temperatures are attained. As this was performed under what appears to be a worst-case scenario, no fuel releases would be experienced for this condition.

Note that this test is a severe overtest as the 1.9 m on edge cube burned on one side only. The 630-s burn would be at least halved (<315 s real burn time) so the reaction would be considerably below what was cited in Appendix E. Therefore, less than 30% of the Pt-30Rh clad wall would react with the PG to form the carbon/noble metal eutectic.

5.0 REENTRY ANALYSIS UNCERTAINTIES

5.1 General - The uncertainties associated with the reentry analyses are difficult to identify quantitatively. It should be pointed out that the analyses performed by APL are thought to be skewed to the maximum conservative end of the spectrum.

5.2 Clad Temperature, Orbital Reentry - Early in the program (Reference 6), some trade-off reentry analyses were performed by both APL and FI. As can be noted in Table L-1, these results are quite consistent when one considers the variables. The final three are particularly close among themselves and when compared to the temperature at which significant clad damage could occur (at the alloy/carbon eutectic-formation temperature of 2033 K), the minimum safety margin is over 170 K for this brief ($\sim$ seconds) excursion.

5.3 VEEGA Reentry Scenario - The APL-provided VEEGA reentry text (Reference 7) stated that due to extrapolations in the reentry theory, there is a large uncertainty in the VEEGA results to the LWRHU. However, as the ground rules for LWRHU are to be the same as for the GPHS as it would undergo a VEEGA reentry, Mound has elected to identify 100% wall thickness ablation as being the reentry failure point (Reference 8).

The random uncertainties were chosen to be addressed by employing a log-normal curve at the 50% probability and normal (calculated) aeroshell recession thickness. This was discussed earlier in Appendix G, Section 9.0. This treatment is of an *a priori* nature but, in the absence of calculated or measured values, would provide a truer representation of physical reality than an assumed 50% ablation = failure.

There are two non-random considerations which skew both the stated conclusions to the conservative:

A. A reentering LWRHU would very likely not assume a side-on stable configuration but take a 40° attitude (cylindrical axis tipped to the normal of the reentry direction). This would increase the effective aeroshell thickness, especially at the stagnation point (now the corner) and provide considerably more surface area (by about 15%) exposed to the thermal pulse.

B. The assumption that a single point or line aeroshell ablation at the 100% level immediately releases the clad to the aerothermal heating environments is extremely conservative. To disassemble the LWRHU, it would require 100% ablation about 50% of the way around the length of the aeroshell followed by some undefined forces which would cause the nested PG assembly to fly apart. This sort of assessment was not addressed in the APL analyses.

Figure L-1 illustrates these two effects.

Table L-1: Comparisons of Various Peak Clad Temperatures

for Reentering LWRHUs under Various Conditions

ANALYZER#	CONDITION†	GAP	MAXIMUM CLAD TEMPERATURE °F	K
APL	Gamma*	Vacuum	2500	1645
FI	Orbital Decay	Vacuum	2642	1723
FI	Orbital Decay	He @ 2000°F	2754	1785
FI	Orbital Decay	He @ 1500°F	2846	1836
APL	Gamma*	He @ ∿1500°F	2838	1832
APL	Gamma*	He @ ∿1500°F, Broken PGs	2880	1855

NOTE: Pt30Rh/C Eutectic ∿ 2033K; Pt30Rh melting Point = 2183K [ANSP-169, APL (October, 1969)]

Gamma* = -4.75° @ 11km/s velocity @ 122km altitude

FI = Fairchild Industries [at the LWRHU Final Design Meeting, August 28, 1980]

APL = Applied Physics Laboratory (as cited in Reference 5).

† All side stable.

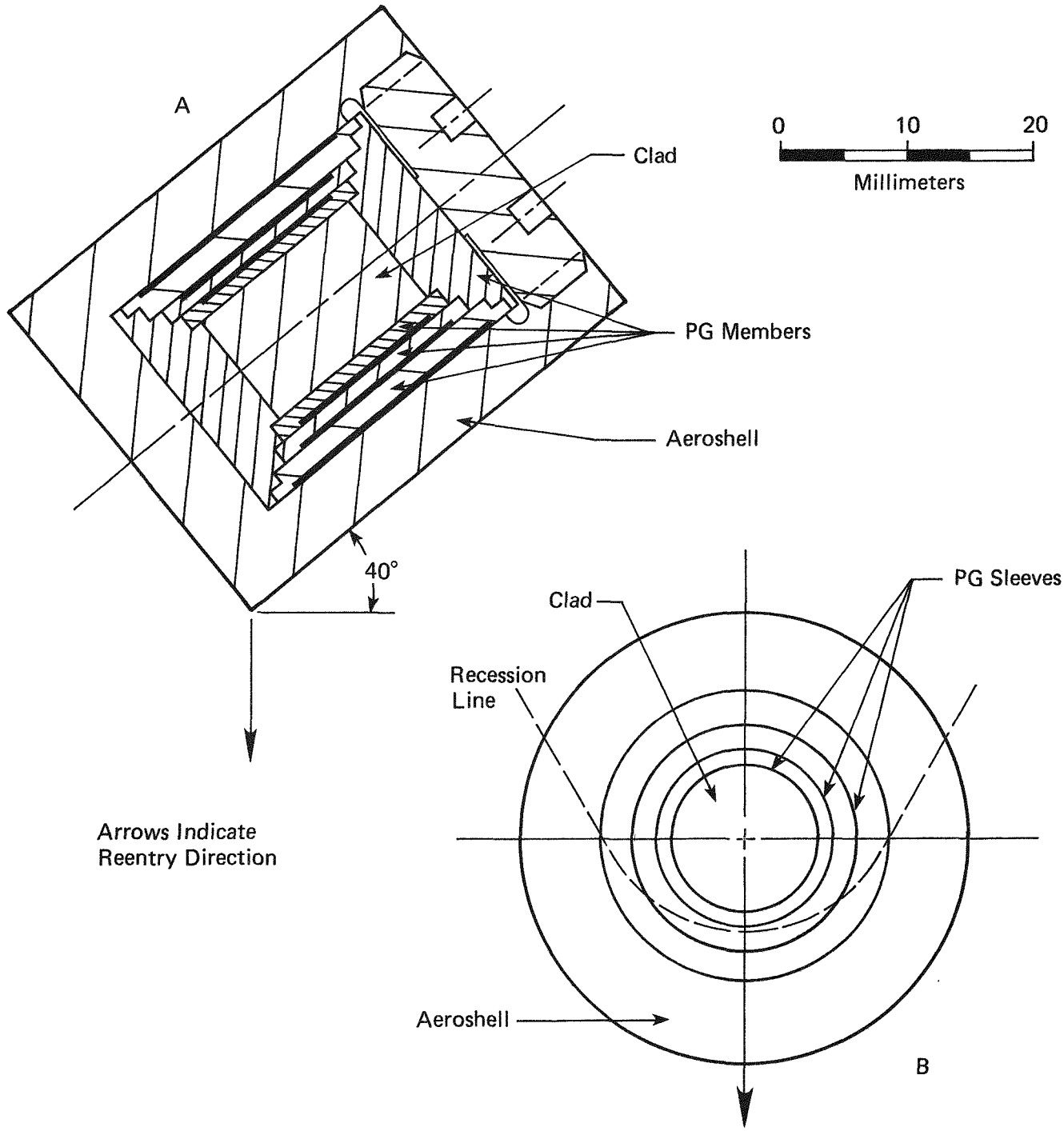

FIGURE L-1: A. The LWRHU will assume an attitude 40° to the cylindrical axis upon reentry. This will increase the wall thickness by about 1.55 times the normal "straight-through" value.
B. Schematic of how much aeroshell ablation would be required to release the PG/Clad assembly.

5.4 Fuel Fraction Evaporation - APL has performed some analytical modeling of the bare fuel pellet reentry case. In this analysis, the bare plutonia pellet (side-on stable superorbital reentry) achieves temperatures well beyond the melting point at the leading surface. The quantities of ablated material as calculated by APL was provided in Reference 7. Mound's calculations given in Appendix G were based upon evaporation only. These are as follows:

	% Ablated APL, Average	% Ablated APL, Worst	% Ablated MRC	Mean
Zone A	42	75	100	70 ± 30
Zone B	14	42	8.5	22 ± 20

This is a wide spread: about ±40 % for Zone A and about ±100 % for the Zone B calculations. Strangely enough, the shift in evaporated fractions is reversed for Zones A and B by the two agencies performing the estimations.

5.5 Conclusions - A hard number or series of uncertainty values relating to the various reentry scenarios cannot be obtained. However, the results appear to be toward the conservative, as pointed out in the first paragraph of this section. Good clad peak temperature margins exist for the intact and broken PG reentry cases. There is a large spread in the vaporization versus spallation cases for the bare fuel side-on stable superorbital reentries.

6.0 SOIL BURIAL ERRORS

6.1 Errors - The release values are so low and the margins so great that the analysis does not merit such an assessment.

7.0 SPACECRAFT BREAKUP

7.1 Errors - This required section really is not a contributor to uncertainties in the case of the LWRHUs. No unusual hardships over normal reentry conditions would be encountered by the LWRHUs regardless of spacecraft breakup variances.

8.0 PARTICLE SIZE UNCERTAINTIES

UO_2/PuO_2 Correlation - In the size range of <100 m, Figure E-4 implies that there seems to be fair agreement both for PuO_2/UO_2 and UO_2/UO_2 data populations. The norm would be ± 55% at 100 µm size range, ± 67% at the 10 m size area and ± 50% at the 1 µm limit. The PuO_2 data would make these bands conservative (fewer smaller particles) than the UO_2 tested items. Note that these are bare clad impacts; there are no clad failures associated with intact LWRHU impacts so the reentry impacts units are irrelevant in terms of PuO_2 comminution in case of LWRHUs.

9.0 REFERENCES

1. Space Shuttle Data for Planetary Mission Radioisotope Thermoelectric Generator (RTG) Safety Analysis, NSTS 08116.

2. Schumann, F. A., Study of the Blast Overpressure Capability for the RHU Heat Shield, TES-3203, Teledyne Energy Systems (June 3, 1985).

3. Letter, J. C. Hagan/G. L. Bennett, ATD-RL-85-069, ANSP-L-849 (August 26, 1985).

4. Telecon, E. W. Johnson/F. A. Schumann, October 7, 1985.

5. Johnson, E. W., Light-Weight Radioisotope Heater Unit Safety Analysis Report (LWRHU-SAR), MLM-3293, Volume II, Monsanto Research Corporation (October 1985).

6. Tate, R. E., Letter to Distribution, CMB-5-C-81-29 (March 11, 1981).

7. Letter, J. C. Hagan/E. W. Johnson, ATD-RL-88-088, JHC-88-061 (August 18, 1988).

8. Letter, E. W. Johnson/W. R. Amos, September 9, 1988.